Ministry of Forests, Lands, Natural Resource Operations and Rural Development

Emergency ManagementBC

Public Safety Canada | Sécurité publique Canada

BULLETIN 2020-2-RPFA

British Columbia Extreme Flood Project

Regional Precipitation-Frequency Analysis – Technical Report

PREFACE AND ACKNOWLEDGEMENTS

The British Columbia Extreme Flood Project was initiated by the Water Management Branch (WMB), Dam Safety Section, of the British Columbia Ministry of Forests, Lands, Natural Resource Operations & Rural Development (FLNRORD), the regulator of BC water dams. A large challenge hydrologists face when estimating the magnitude of extreme flood events is access to sufficient data and guidance on what regional data can be utilized in the catchment area of interest. Estimation of the magnitude of an extreme flood is a substantial task with multiple approaches available. When the design is for an engineered structure, a Professional Registrant of Engineers and Geoscientists BC requires specialized education and work experience. Standardization of relevant information is useful to a Professional Registrant as it reduces the level of effort, allows for a wider area of data to be considered in the analysis, provides a standardized approach for comparison with other studies, and provides an initial estimate to verify more detailed project-specific analyses.

It is recognized that there is considerable uncertainty with estimating the magnitude of floods and that decisions must be made involving considerable infrastructure dollars and public safety risk. The goals of the project were to supplement observed hydrology and hydrometeorological data in BC and improve the quality and confidence in baseline data pertaining to the magnitude and uncertainty of extreme flood events to support the design of hydrotechnical structures, such as: dams, spillways, dikes and river crossings (bridges and culverts). The guidance provided in the project documents is mostly limited to the use of the products developed as part of the current study.

The project is being released as a series of 5 technical bulletins, data portals, and GIS information. The bulletins and associated products have been developed and quality controlled by the consulting firms in consultation with the project technical advisors, who also proved technical support and review. The bulletins have not undergone detailed external review to date and do not provide all information or guidance necessary to complete a hydrotechnical study. It is anticipated these bulletins will be utilized by Professional Registrants who design dams and by qualified hydrologists tasked with calculating the magnitude of floods in BC. The uncertainties of climate cycles and climate change, the occurrence of future low probability events, and changes in land cover characteristics requires that the study be periodically updated, and that the Professional Registrant exercise judgement based on the information available for the specific analysis being completed.

The Province thanks the advisory committee for their provision of technical support and review. The committee consisted of Angela Duren, US Army Corps of Engineers; Edgar Watt, Professor Emeritus, Queen's University; and Zoran Micovic, BC Hydro. The Province also thanks the consulting firms who assembled a skilled team to respond to a complex task over a relatively short time frame and provided additional out of scope material to improve the final product. The project would not have been possible without the support of Scott Morgan, Jesal Shah, and Ted White of the WMB. Assistance was also provided by several staff within FLNRORD and other provincial ministries, as well as all those who responded to the project request for information. Funding for the project was provided by Emergency Management BC and the Public Safety Canada National Disaster Mitigation Program.

Robert K McLean, M.Sc, P.Eng.
FLNRORD Senior Dam Safety Engineer and Project Manager

Cover page photo credits clockwise from bottom left: BC Ministry of Forests, Lands, Natural Resource Operations, and Rural Development (Grand Forks, May 2018); BC Ministry of Transportation and Infrastructure, BC MoTI (Rocket Creek, Highway 97, June 2011); BC MoTI (Fisher Creek Bridge, June 2011); main photo: BC MoTI (Bridge No. 07146 Walper, June 2016).
Graphics designer: Christina Peressini, Piotr Kuraś.

Suggested citation:

DTN and MGS Engineering (2020). British Columbia Extreme Flood Project, Regional Precipitation-Frequency Analysis for British Columbia – Technical Report (Bulletin 2020-2-RPFA). Report prepared by DTN, LLC and MGS Engineering Consultants, Inc. for the British Columbia Ministry of Forests, Lands, Natural Resources Operations, and Rural Development. May 2020.

REGIONAL PRECIPITATION-FREQUENCY ANALYSIS FOR BRITISH COLUMBIA

BULLETIN 2020-2-RPFA

TECHNICAL REPORT

Prepared by:

DTN, LLC
3030 S. College Ave. Unit 207
Fort Collins, CO 80525
(970) 460-6401

MGS Engineering Consultants, Inc.
7326 Boston Harbor Road NE
Olympia, WA 98506
(360) 570-3450

Northwest Hydraulic Consultants, Ltd.
30 Gostick Place
North Vancouver, BC V7M 3G3
Canada
(604) 980-6011

Custom Climate Services, Inc.
3519 Queen Street
Regina, Saskatchewan S4S 2G1
Canada
(306) 586-5489

EXECUTIVE SUMMARY

The objective of this project was to develop gridded point precipitation-frequency estimates with uncertainty bounds across British Columbia for the 24-, 48-, 72-, and 96-hour durations at annual exceedance probabilities from 1:2 to 1:1,000,000 (average recurrence intervals from 2-year to one million-years).

The approach used to create the gridded point precipitation-frequency estimates was the Schaefer-Wallis-Taylor climate region method using L-Moments regional analysis (Schaefer et al., 2018). Regional analysis is a methodology to evaluate datasets comprised of measurements of the same phenomenon observed at multiple sites. The Schaefer-Wallis-Taylor climate region method reduces uncertainty in the regional analysis by using storm typing methods and optimizing spatial mapping procedures for estimating rare to extreme precipitation magnitudes.

The phenomenon considered was the mid-latitude cyclone storm type at the 24-, 48-, 72-, and 96-hour durations, each duration considered separately. Mid-latitude cyclones provide the chief mechanism by which precipitation is generated at the relatively high latitudes of British Columbia. This storm type is capable of producing large volumes of precipitation over one to several days over a large area. Examples of the mid-latitude storm type include incursions by the Aleutian Low (a large low-pressure feature that is often present in the Gulf of Alaska) and atmospheric rivers (equivalent to a river in the atmosphere that transports water vapor away from tropics).

Daily point precipitation data for the mid-latitude cyclone storm type were acquired from observation stations of various sources from across British Columbia and extending into portions of Alaska, Yukon, Northwest Territories, Alberta, Washington, Oregon, Idaho, Montana, northern California, northern Nevada, northern Utah, and western Wyoming. A large domain supports a larger sample size of precipitation gauges, and therefore a large sample of storm events needed to compute reliable precipitation-frequency estimates for rare to extreme annual exceedance probabilities. The large sample size provides for narrower uncertainty bounds in the final precipitation-frequency results and minimizes boundary effects in the spatial mapping of precipitation.

To complete the regional analysis, the annual maxima time-series at each of the precipitation observation stations was first compiled and subjected to rigorous quality control protocols to remove invalid data and false annual maxima. Climate Regions were delineated with similar climatology and physiography which were used to explore the spatial behavior and L-Moments at the stations. Homogeneous Sub-Regions were then formed as collections of stations within a narrow range of identified climatological and physiographic measures. Homogeneity was verified using regional L-Moment heterogeneity measures, and each Homogeneous Sub-Region produced a regional L-Coefficient of Variation (L-Cv) and L-Skewness value. The spatial behavior of the precipitation at-site mean and regional L-Cv and L-Skewness values were then analyzed, and predictor equations were developed to spatially map gridded values of each L-Moment statistic at all locations within the project domain. Lastly, a regional probability distribution was identified to compute precipitation magnitudes for selected annual exceedance probabilities. Specifically, the 4-parameter Kappa distribution was used to compute quantile estimates for each grid-cell using grid-cell specific values of the at-site mean, regional L-Cv, regional L-Skewness, and the regional shape parameter, Hondo.

Using this method, gridded maps of point precipitation-frequency estimates were not created by interpolation methods but rather by creating spatial grids of the statistical parameters. This approach provides for efficient use of both at-site and regional information to reduce statistical uncertainties in spatial mapping of point precipitation-frequency in the complex terrain of British Columbia. These characteristics are particularly important for providing robust precipitation estimates at rare annual exceedance probabilities.

The final point precipitation-frequency estimates with uncertainty bounds are available to view and download in a user-friendly format via the accompanying web-interface, MetPortal®. Guidance to access, interpret, and use these products is available in Bulletin 2020-5-PMP/RPFA: MetPortal User's Guide: Probable Maximum Precipitation and Regional Precipitation-Frequency Analysis for British Columbia.

The point precipitation-frequency estimates provide information for dam and spillway design as well as protection of critical infrastructure. Results may also be used in risk-informed analyses of extreme flood events.

TABLE OF CONTENTS

LIST OF FIGURES

LIST OF TABLES

ABBREVIATIONS AND ACRONYMS

AEP	Annual Exceedance Probability
AMS	Annual Maxima Time-Series
ARF	Areal Reduction Factor
ASM	At-Site Mean
CAPE	Convective Available Potential Energy
DDST	Database of Daily Storm Types
CDF	Cumulative Distribution Function
ECCC	Environment and Climate Change Canada
EIRL	Equivalent Independent Record Length
GEV	Generalized Extreme Value
GHCN	Global Historical Climatology Network
IDF	Intensity-Duration Frequency
L-Cv	L-Coefficient of Variation
LS	Local Storm
MAP	Mean Annual Precipitation
MEC	Mesoscale Storm with Embedded Convection
MCC	Mesoscale Convective Complex
MLC	Mid-Latitude Cyclones
NCEI	National Center of Environmental Information
NHC	Northwest Hydraulic Consultants, Ltd.
NOAA	National Oceanic and Atmospheric Administration
RMSE	Root-Mean-Square-Error
SWT	Schaefer-Wallis-Taylor

GLOSSARY

Term	Definition
Annual Exceedance Probability (AEP)	The probability associated with exceeding a given amount (of precipitation) in any given year; the inverse of AEP provides a measure of the average time between years (and not events) in which a particular amount (of precipitation) may be exceeded at least once.
Annual Maxima Time-Series (AMS)	List of the greatest precipitation magnitudes for a specific storm type (here, MLC) for a specified duration for each year in the period of record at a given station. Makes use of the seasonality of the storm type of interest, so may not extend to a full 12-month period in some of the Project Macro Regions.
At-site mean (ASM)	Mean of the annual maxima time-series at a precipitation station.
ASM Mapping Area	Group of Climate Regions in which the at-site means may be characterized by a single predictor equation that describes the regional behavior.
Automated algorithm	Procedure for assigning storm types and creating the DDST (Figure 17).
Climate Regions	Temporary constructs used to facilitate regional precipitation-frequency statistical analysis and mapping of the spatial behavior of L-Moment statistics for a storm type and duration. Climate Regions are contiguous geographical areas that exhibit similar characteristics, such as topography, meteorology, and climatology (Figure 4). However, there may be sufficient differences in the statistical behavior of site data such that collection of all sites within the Climate Region may not meet criteria for homogeneity.
Database of Daily Storm Types (DDST)	Listing of the dominant type of storm that produced each rainy day in the period 1851-2014 for each of the Storm Typing Zones.
Homogeneous Sub-Regions	Collections of stations within the larger Climate Regions that fall within a small range of selected climatic and/or location indices and satisfy statistical homogeneity criteria. May not necessarily be geographically contiguous.
Index stations	Set of high-quality stations with long periods of record and spatially well-distributed across the Project Domain (Figure 5). Used to examine storm seasonality and used in the manual storm typing procedures.
L-Cv Mapping Area	Grouping of Homogeneous Sub-Regions in which the regional L-Cv may be characterized by a single predictor equation that describes the regional behavior.
Local Storm (LS)	Storm type for relatively small-scale, isolated convective events (thunderstorms) which occur in the absence of any larger-scale atmospheric circulation. The areal coverage and duration of these storms are limited, typically less than a nominal 130-km^2 and one- to two-hours in duration.
L-Moments	Linear combinations of order statistics. Improvement over conventional product moment statistics for characterizing the shape of a probability distribution and estimating the distribution parameters, particularly for environmental data where data are highly variable and sample sizes are commonly small (definition from Schaefer and Barker, 2009).

Term	Definition
Mesoscale Storm with Embedded Convection (MEC)	Generic storm type intended to include mesoscale convective complexes and other mesoscale and sub-synoptic-scale storms with embedded convective cells (thunderstorms). MEC precipitation have spatial patterns indicative of short-duration (about 6-hours), localized heavy rainfall over a few hours within a larger area of lighter precipitation. Hydrologically, this storm type can produce floods on intermediate size watersheds (generally less than about 15,000-km^2) where peak discharge is the primary concern.
MetPortal®	Web-interface to access final products, including maps of point precipitation-frequency estimates for annual exceedance probabilities as rare as 1:1,000,000.
Mid-Latitude Cyclone (MLC)	Storm type for synoptic-scale, low pressure storm system with cyclonic circulation that potentially produces large volume of precipitation over one to several days. The spatial pattern of precipitation is relatively consistent and spatially coherent across the storm areas. MLCs are the chief mechanism by which precipitation is generated at the relatively high latitudes of the Project Domain. Hydrologically, these storms may result in floods with large volumes.
MLC/MEC Hybrid Storms	Storm type for situation when it is difficult to determine if the storm is an MLC or MEC. Treated as an MLC in this study.
Period of record	Time period from which data was collected: January 1851 – August 2019
Precipitation-frequency estimate	The magnitude of precipitation associated with a specific annual exceedance probability.
Project Domain	Region including the entire 944,735-km^2 area of the province of British Columbia. The Project Domain not only includes British Columbia but also extends into portions of Alaska, Yukon, Northwest Territories, Alberta, Washington, Oregon, Idaho, Montana, northern California, northern Nevada, northern Utah, and western Wyoming (Figure 1).
Project Macro Regions	Contiguous regions within the Project Domain where the seasonality of the MLC storm type was consistent (Figure 5). These include the Coastal region, the Lowland Interior region, the Interior Mountains region, and the Hybrid region.
Regional frequency analysis	Methodology to evaluate datasets comprised of measurements of the same phenomenon observed at multiple sites. The goal is to use the collective statistical information from all measurement sites to develop a mathematical model that represents the relationship between precipitation magnitudes and their frequency or occurrence that can be applied throughout the area.
Seasonality	Set of several months in which the storm type of interest predominately occurs. Seasonality typically includes the peak storm season and the "shoulder" season, when storms occurred but the frequency of occurrence was low.
Station	A location with meteorological instruments that report precipitation measurements and perhaps other meteorological variables. The terms station, precipitation gauge, and site are often used interchangeably.
Storm type	Categorization of storm based on the meteorological, temporal, and spatial characteristics of the storm. This includes MLC, MEC, LS, MLC/MEC hybrids, and dry days (Table 2).

Term	Definition
Storm typing procedures	Methodology in which the storm type of interest, here MLC, and associated data may be identified and extracted from the historical record, thus creating an input dataset that is nearly homogeneous regarding generating phenomenon. Split into manual procedures and automated methods.
Storm Typing Application	A graphical user interface that displayed several meteorological parameters for each Storm Typing Zone for the approximately 150 storms manually reviewed by meteorologists during the manual storm typing procedures.
Storm Typing Zones	Divisions of the Project Domain on which storm typing procedures was completed (Figure 10). The divisions allowed for different storm types to occur simultaneously across the Project Domain, and each Storm Typing Zone had its own unique DDST. The Storm Typing Zones had a spatial resolution of 2° latitude by 2°longitude, to coincide with the resolution of the 20th Century Reanalysis data used for examining the meteorological environment. In total, 88 Storm Typing Zones were considered in the storm typing procedures. The NOAA 20th Century Reanalysis data set is a comprehensive global atmospheric circulation analysis from 1850-2014.

DISCLAIMER

The services, data and equipment are provided by DTN "as is" except where such disclaimer is prohibited by applicable law. DTN disclaims all warranties, express or implied, including but not limited to any implied warranty of merchantability, accuracy, completeness, fitness for a particular purpose, or intellectual property infringement and DTN hereby expressly disclaims any of the foregoing. DTN does not represent or warrant that (i) the services or equipment will operate error free, (ii) customer's use of the equipment or services will be uninterrupted or (iii) all defects will be identified, reproducible or resolved. Such warranties shall not be enlarged, diminished or otherwise affected by the rendering of any advice or service by DTN in connection with the equipment or services or by any implied warranty arising out of any course of dealing, by statute, or by performance, custom or usage of trade. All third-party components, third-party content, third-party equipment and any information contained or obtained by you via any third-party website or other third-party information that you may access through the services are provided "as is" without any warranty or indemnity from DTN and any representation or warranty of or concerning the same is strictly between customer and the owner, licensor or distributor of such third-party components, third-party content, third-party equipment, third-party website or other third-party information.

SIGNATURE PAGE

Report prepared by:

March 27, 2020
Victoria Sankovich Bahls, Project Manager — Date
DTN, LLC

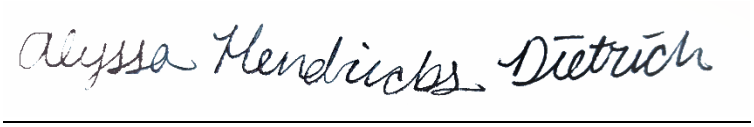

March 27, 2020
Alyssa Hendricks Dietrich, Senior Hydrometeorologist — Date
DTN, LLC

March 30, 2020
Mel Schaefer, Ph.D., P.Eng., Principal Engineer — Date
MGS Engineering, Inc.

Report peer-reviewed by:

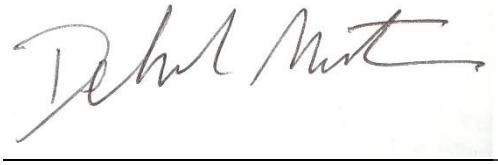

March 30, 2020
Debbie Martin, Senior Hydrometeorologist — Date
DTN, LLC

March 30, 2020
Tye Parzybok, CCM, Managing Director, Global Precipitation Services — Date
DTN, LLC

Technical Advisors:

Zoran Micovic, Ph.D., P.Eng.
Principal Engineer, BC Hydro

Angela Duren, P.Eng., P.H.
Senior Hydrologist, USACE Northwest Division

1. PURPOSE

The objective of this project was to develop gridded point precipitation-frequency estimates with uncertainty bounds across British Columbia for the 24-, 48-, 72-, and 96-hour durations at annual exceedance probabilities (AEPs) from 1:2 to 1:1,000,000 (average recurrence intervals from 2-year to one million-years). The point precipitation-frequency estimates will provide information for dam and spillway design as well as protection of critical infrastructure. Specifically, the 1:2 through 1:100 AEPs are of interest to the Ministry of Transportation for culvert and bridge design; the 1:100 through 1:200 AEPs are beneficial for dike elevation design; and the rare return periods are needed for dam design. Results may also be used in risk-informed analyses of extreme flood events. Furthermore, results will also increase the efficiency, improve the quality, and lower the cost of future hydrotechnical studies in British Columbia.

This analysis met these objectives by providing point precipitation-frequency estimates with uncertainty bounds for the 24-, 48-, 72-, and 96-hour durations in a user-friendly format via the accompanying web-interface, MetPortal®. Specifically, isopluvial gridded datasets were generated for the following AEPs and available to view and download in the MetPortal:

- 1:10
- 1:20
- 1:50
- 1:100
- 1:200
- 1:500
- 1:1,000
- 1:2,000
- 1:5,000
- 1:10,000
- 1:100,000
- 1:1,00,000

Bulletin 2020-5-PMP/RPFA: MetPortal User's Guide: Probable Maximum Precipitation and Regional Precipitation-Frequency Analysis for British Columbia provides guidance for the access, interpretation, and usage of these products.

This technical report provides a summary of the data, procedures employed, and the findings obtained from the regional precipitation-frequency analysis conducted for point precipitation for all locations within the province of British Columbia. Focus was placed on the mid-latitude cyclone (MLC) storm type since this is the chief meteorological mechanism by which precipitation is generated at the high latitudes of the Project Domain for long durations (24- through 96-hours).

2. APPROACH

Regional analysis is a methodology to evaluate datasets comprised of measurements of the same phenomenon observed at multiple sites (here, MLC storm precipitation at the 24-, 48-, 72-, and 96-hour durations, considered separately). The primary goal in a regional frequency analysis is to use the collective statistical information from all measurement sites within a project area to develop magnitude-frequency relationships that can be applied throughout the area. This essentially uses the concept of trading space for time sampling. This approach greatly reduces the sampling variability present at any one site and increases the reliability (i.e., narrows the uncertainty bands) of magnitude-frequency estimates throughout the region, particularly at ungauged locations.

The approach to create the gridded point precipitation-frequency estimates used here is the Schaefer-Wallis-Taylor (SWT) climate region method using L-Moments (Schaefer et al., 2018). The SWT climate region method reduces uncertainty in the regional analysis by using storm typing methods and optimizing spatial mapping procedures for estimating rare to extreme precipitation magnitudes. This method has been applied in several projects over the past 15 years, including the Tennessee Valley (MGS Engineering et al., 2015), along the Trinity River in Texas (MetStat and MGS Engineering, 2018a), above Mactaquac Dam on the Saint John River in New Brunswick (MetStat and MGS Engineering, 2019), for BC Hydro (MetStat and MGS Engineering, in draft), and in Colorado and New Mexico (MetStat and MGS Engineering, 2018a); the latter of which was evaluated by a Review Board that included participants from over ten local and federal U.S. government agencies.

Using this method, gridded maps of point precipitation-frequency estimates were created by mapping each of the regional L-Moment parameters then applying the four-parameter Kappa distribution to compute the point precipitation-frequency relationship (i.e., the AEP grids). In this manner, the point precipitation-frequency estimates were not directly interpolated between gauges but rather by creating spatial grids of the statistical parameters through predictor equations of geographically uniform and continuous base maps (explanatory variables). This state-of-the-practice technique offers considerable benefits, including reduction of uncertainty, improved representation of spatial variability of the L-Moment parameters, and high confidence in extrapolations beyond 1 in 1,000-year average recurrence interval (0.001 AEP).

The SWT climate region method may be subdivided into the following generalized elements:

1. Assemble and quality-check the input annual maxima dataset;
2. Delineate and verify the homogeneous sub-regions using regional L-Moment statistics;
3. Analyze the spatial behavior of the precipitation at-site mean and regional L-Moment ratios L-Cv and L-Skewness for use in spatial mapping;
4. Identify the regional probability distribution for computing precipitation AEPs;
5. Compute the Equivalent Independent Record Length (EIRL) to estimate the effective independent size of the regional dataset; and
6. Produce gridded datasets of point precipitation for selected AEPs from the median to at least 0.001 AEP and associated confidence intervals.

3. STORM TYPES OF INTEREST

Since regional analyses require the input dataset to be comprised of measurements of the same phenomenon, it is pertinent to have a clear definition of the phenomenon of interest. For regional point precipitation-frequency analyses, the phenomenon is a particular storm type. Different storm types exhibit different spatial and temporal characteristics, which produce differing flood characteristics in terms of flood peak discharge, duration, volume of runoff, and flood hydrograph shapes. Depending on the watershed size and location, one or more storm types may contribute to the flood hazard at a given dam.

Due to the relatively high latitude of the Project Domain, mid-latitude cyclones (MLCs) provide the chief mechanism by which precipitation is generated. These can be a hydrologic concern for high volume flooding. This storm type is capable of producing a large volume of precipitation over one to several days over a large area.

Other storm types are sub-daily and not considered in this project. These storm types have short bursts of very heavy rainfall over smaller areal extents that can lead to peak discharge concerns. They are Local Storms (LS), or thunderstorms, and Mesoscale storms with Embedded Convection (MECs), which have key durations of 2- and 6-hours, respectively. The LS and MEC storm types are considered in the storm typing procedures for the purpose of removing them from consideration as annual maxima.

3.1. Mid-Latitude Cyclone

MLCs are synoptic-scale, low pressure systems with cyclonic circulations that form in the mid-latitudes. The spatial pattern of precipitation from an MLC is relatively consistent and spatially coherent across the storm area. This is due to the atmospheric dynamics that are responsible for generating the precipitation associated with MLCs, which usually occur over broad areas and are somewhat uniform in space. They can produce precipitation from one to several days over very large areas and can occur during any season. Variations on precipitation are largely driven by orographic and other terrain features. This storm type includes frequent incursions by the Aleutian Low (a large low-pressure feature that is often present in the Gulf of Alaska), atmospheric rivers (equivalent to a river in the atmosphere that transports water vapor away from tropics), other storms that originate over the Pacific Ocean, and occasional sub-Arctic cyclones dropping south along the Rocky Mountains.

3.2. Other Storm Types

Although the following storm types were not explicitly analyzed as part of this project, descriptions of them are provided because they are considered in the storm typing procedures.

3.2.1. Mesoscale Storms with Embedded Convection

The Mesoscale storm with Embedded Convection (MEC) is a generic storm type that is intended to include Mesoscale Convective Complexes (MCCs) and other mesoscale and sub-synoptic scale storms. Most of the storms of the MEC storm type include clusters of convection cells (thunderstorms). MEC precipitation has spatial patterns indicative of short-duration, localized heavy rainfall over a few hours within a larger area of lighter precipitation. Spatial gradients in precipitation are often quite high, as the individual thunderstorms that comprise MECs may only be a few kilometers in spatial extent. MECs have a key duration of six-hours. Since MECs produce short bursts of very heavy rainfall, this is the storm type that can

produce floods on intermediate-sized watersheds (generally less than about 15,000-km^2) where peak discharge is the primary concern. The flood volume produced from this storm type is smaller than the MLC storm type.

Thus, these storms are identified in the historical record for purposes of removing them from the analysis. However, MEC storms that are heavily influenced by MLC events and take on MLC-like characteristics are grouped in an MLC/MEC hybrid category (see below) and are included in this project.

3.2.2. Local Storms

The Local Storm (LS) is the term given to relatively small-scale, isolated convective events (thunderstorms) which occur in the absence of any larger-scale atmospheric circulation. The areal coverage and duration of these storms are limited, typically less than a nominal 130-km^2 and one- to two-hours in duration. The key duration for LSs is two-hours. Like MECs, these storms are identified in the historical record for purposes of removing them from the analysis.

3.3. MLC/MEC Hybrid Storm

In some instances, the atmospheric dynamics do not fit tidily within a single storm type. For the case where it is difficult to determine if a storm is an MLC or MEC, then it may be classified as an MLC/MEC hybrid storm event. MLC/MEC hybrid storms are used in both the MLC and MEC storm analyses and are treated as MLC storms in this project.

In the Project Domain, such a classification is generally used for transition zones between instances of one storm type (e.g., MEC) occurring in one part of the domain while another type (e.g., MLC) occurs in another part of the domain. The areas that are heavily influenced by the MLC or have MLC-like characteristics are given the MLC/MEC hybrid designation. The part of the domain that is affected by the MLC storm is still typed as MLC, and the same for the area of the domain affected by the MEC. The storm typing process allows for such separation of storm events so to not have mixed events within the input dataset. In other cases, large areas may be typed “MLC/MEC hybrid” to denote events that consist of large, loosely organized areas of often-convective precipitation that appear to be neither precisely mesoscale nor synoptic in nature.

4. PROJECT DOMAIN

The region of focus for this analysis is the entire 944,735-km^2 area of the province of British Columbia. The Project Domain not only includes British Columbia but also extends into portions of Alaska, Yukon, Northwest Territories, Alberta, Washington, Oregon, Idaho, Montana, northern California, northern Nevada, northern Utah, and western Wyoming (Figure 1). A large domain supports a larger sample size of precipitation gauges, and therefore a large sample of storm events needed to compute reliable precipitation-frequency estimates for rare to extreme AEPs. The large sample size provides for narrower uncertainty bounds in the final precipitation-frequency results and minimizes boundary effects in the spatial mapping of precipitation.

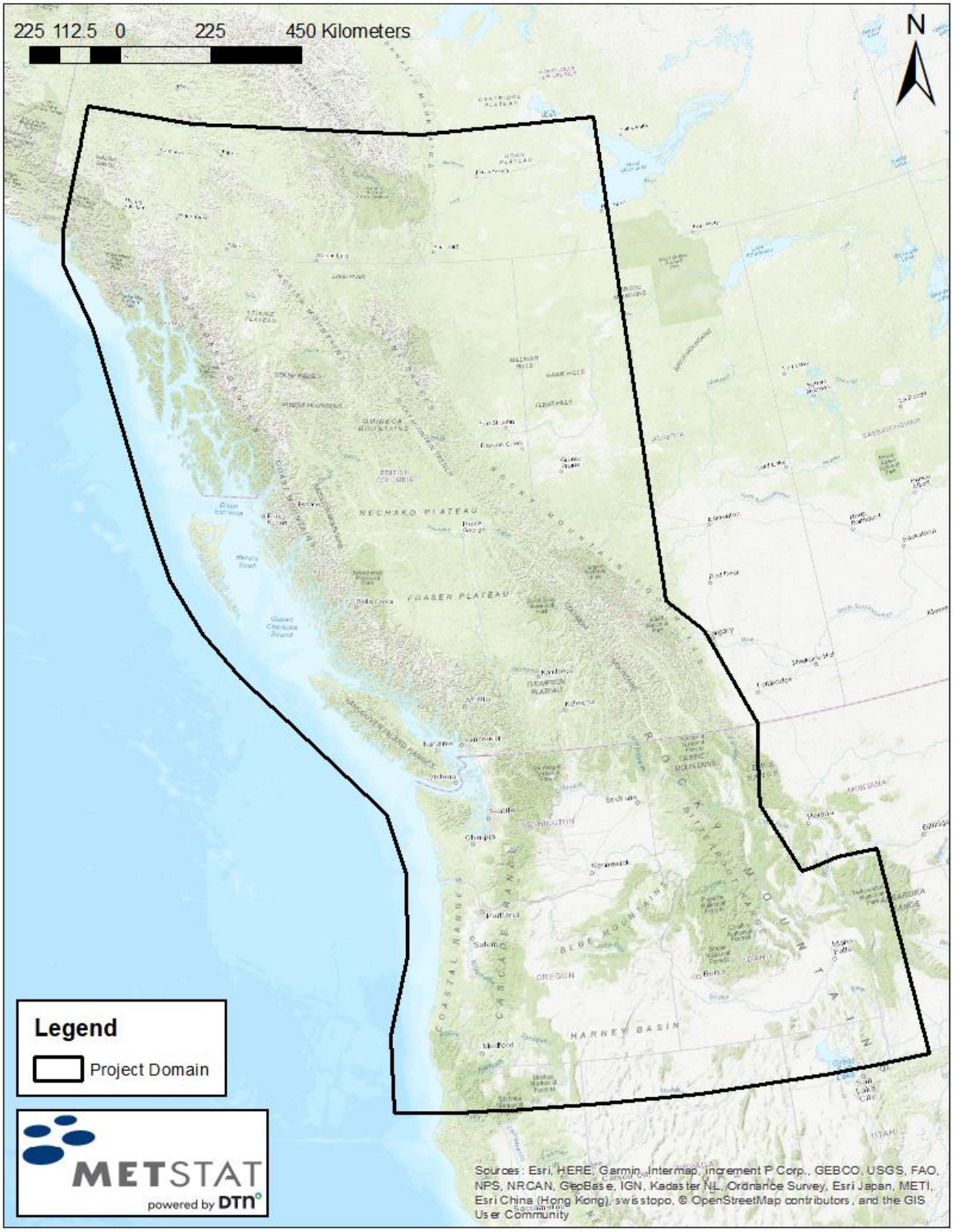

Figure 1: Project Domain.

4.1. Climatology of Project Domain

The climate of British Columbia is largely determined by two primary features: the Pacific Ocean and multiple large mountain ranges. The Pacific Ocean provides an ample supply of moisture that is carried across the Province by the predominant westerly flow of the atmosphere and by low pressure systems. Interaction of the moisture with the mountain ranges along the coast and in the interior result in areas of heavy orographic precipitation. Thus, the climatological distribution of precipitation closely mirrors the underlying topography of British Columbia, with very wet conditions along the coastal mountains and dry interior valleys (Figure 2).

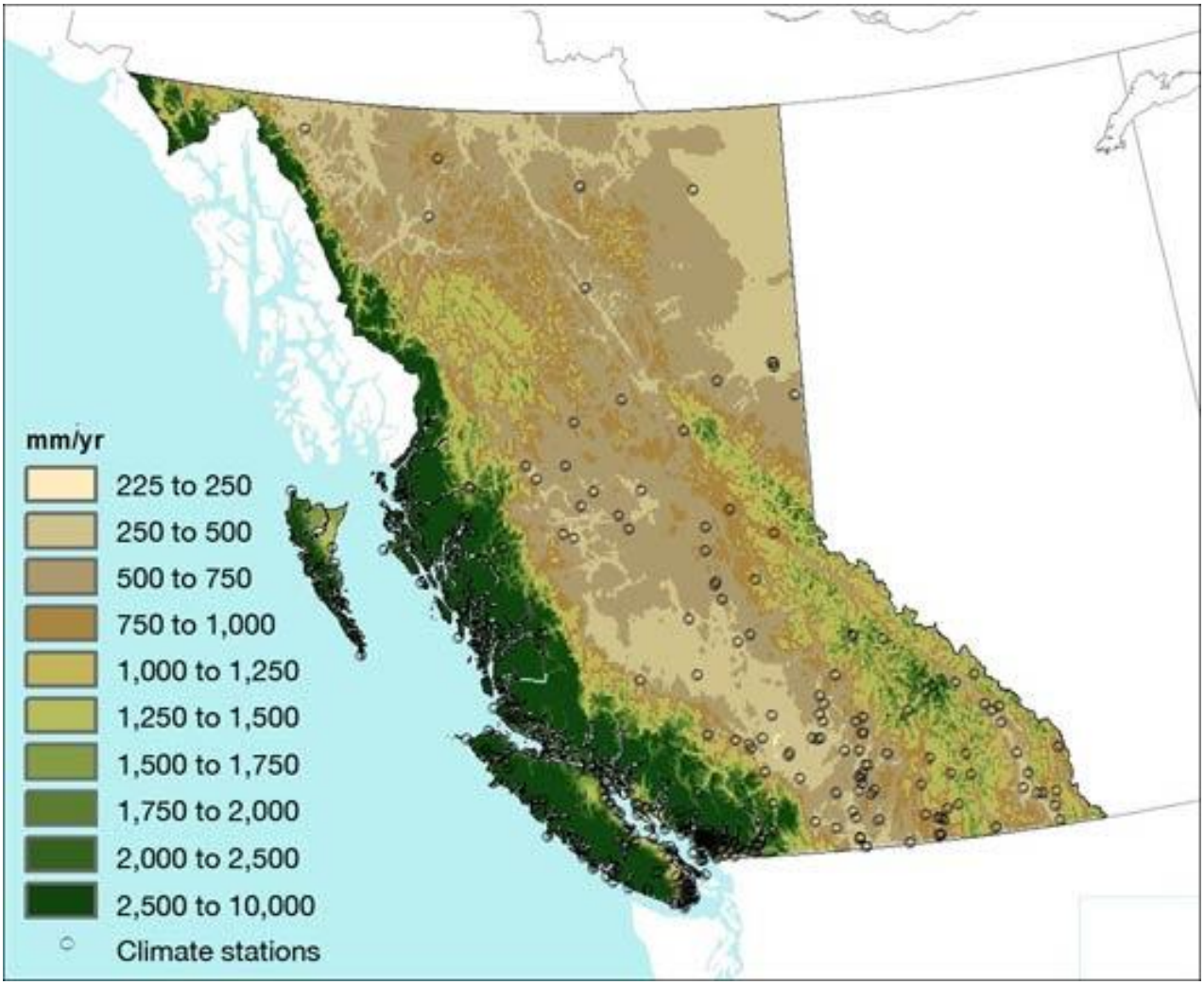

Figure 2: Mean annual precipitation across British Columbia.
Source: https://www.nrcan.gc.ca/environment/resources/publications/impacts-adaptation/reports/assessments/2008/ch8/10395

The mean annual precipitation map (Figure 2) likewise shows that a location's distance from the coast and elevation also heavily influence the amount of precipitation a location receives in a typical year. Conceptually, this is presented in Figure 3, which illustrates the modulating effects that the mountain ranges have on the maritime air masses that enter the region from the west. The mountain ranges act to both enhance stratiform precipitation when winds are favorably oriented (orthogonal) to the mountain ranges during MLC storm events and serve as focal points for generating convection during the summer months.

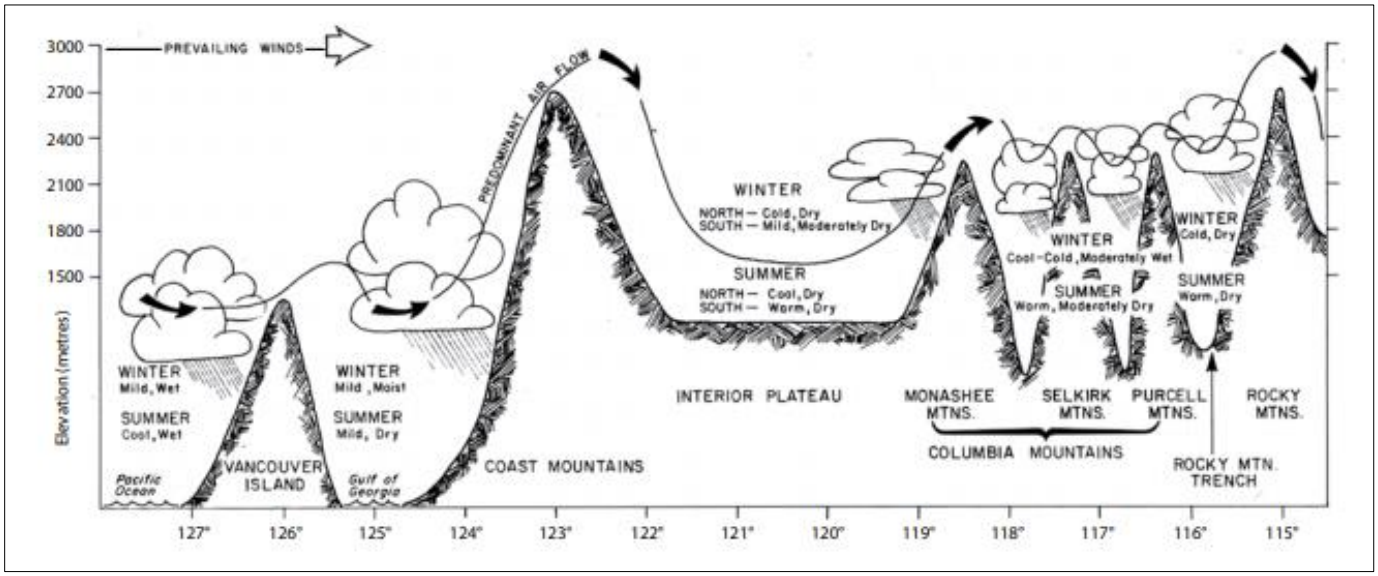

Figure 3: Schematic of topography of southern British Columbia and its effects on climate.
Source: https://www.for.gov.bc.ca/hfd/pubs/Docs/Lmh/Lmh66/LMH66_ch03.pdf

4.2. Climate Regions

Climate Regions are geographical areas that exhibit similar characteristics, such as similar topography, meteorology, and climatology. It is expected that the sources and tracks of atmospheric moisture and the predominant meteorological process will be the same throughout a Climate Region.

To delineate the Climate Regions, judgements were made based on meteorological, climatological, and topographical characteristics using the following sources and features:

- PRISM mean annual precipitation (PRISM Climate Group, 2015)
- Mean annual precipitation 1961-1990 from ClimateNA (Wang et al., 2016)
- Major mountain barriers and the Continental Divide
- Elevation (Digital Elevation Model, DEM) (USGS, 2015)
- NOAA's Northwest U.S. Climate Regions (Karl and Koss, 1984)
- Hydroclimatic regions used to describe and characterize extreme precipitation events in previous studies (Schaefer, 1997b; Schaefer et al., 2002, 2006, 2007; MetStat and MGS Engineering, in progress)
- British Columbia Hydrologic Zones (Coulson and Obedkoff, 1998)

Considering the above sources and features, the Climate Regions were largely delineated based on mean annual precipitation (MAP) while maintaining consistency with previous studies. Since the objective of this project concerns atmospheric processes, MAP is a favorable way to consider the distribution and gradient of atmospheric moisture across the Project Domain. MAP is preferred over topographic contours and stream/river boundaries. Figure 4 shows that the boundaries of the Climate Regions closely align with MAP. In total, 57 geographically contiguous Climate Regions were identified in the Project Domain. The Climate Regions were numbered with an integer consistent with previous studies.

Climate Regions are primarily used as temporary constructs to facilitate regional precipitation-frequency statistical analysis and mapping of the spatial behavior of L-Moment statistics for a storm type and duration. Since precipitation data within a Climate Region is expected to behave similarly, then the behavior of at-site means, L-Cv, and L-Skewness of the

precipitation annual maxima time-series (AMS) can also be expected to behave similarly. However, there may be sufficient differences in the statistical behavior of site data within the Climate Region so that the collection of all sites within the Climate Region may not meet criteria for homogeneity (e.g., the Climate Region may be too large).

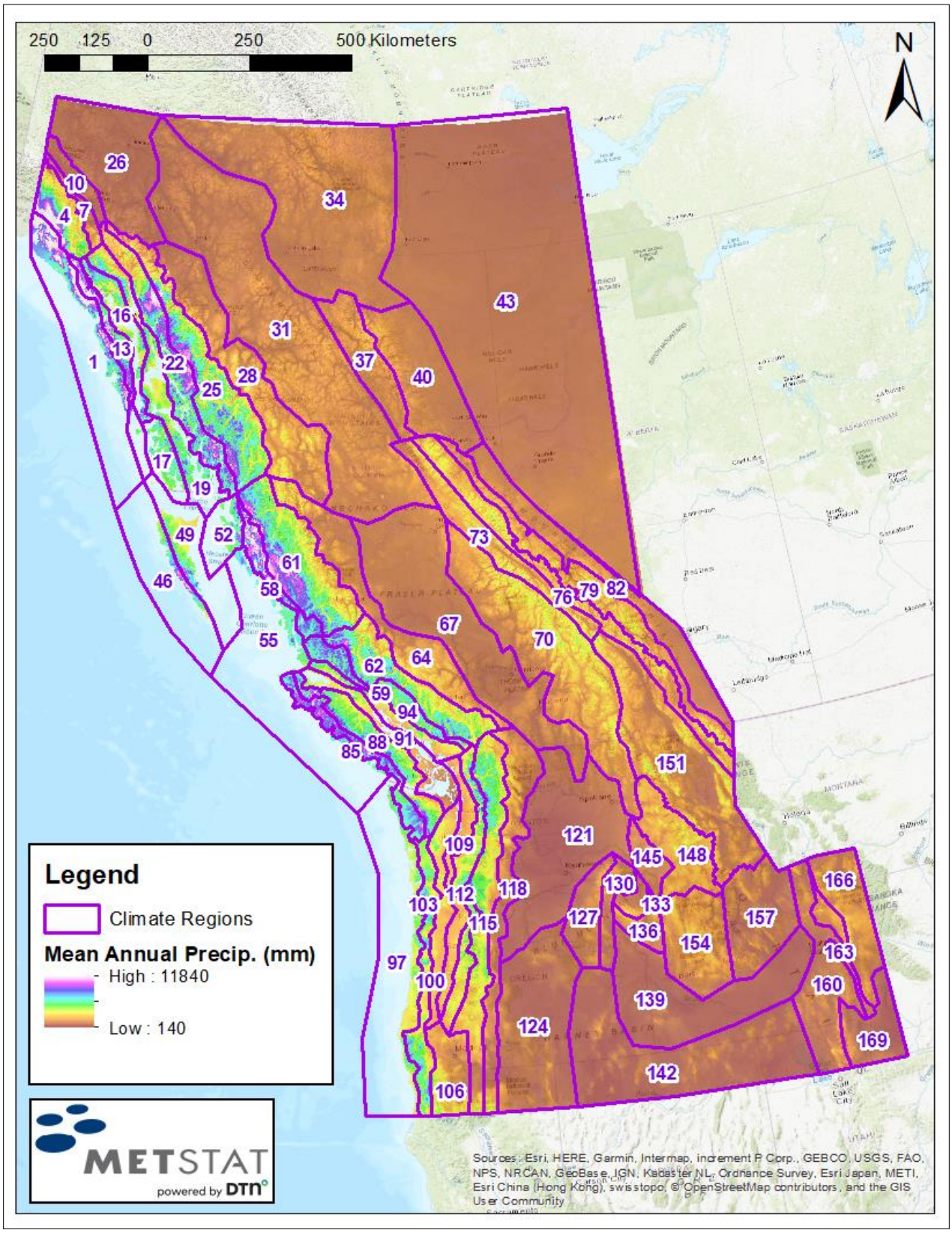

Figure 4: Climate Regions.

4.3. Seasonality and Project Macro Regions

The seasonality of the mid-latitude cyclone (MLC) storm type was needed to set the appropriate time period for the extraction of the precipitation AMS at all precipitation gauges within the Project Domain. Even though MLCs may occur during any month of the year, this storm type was more prominent in a set of several months (or "season") in regions within the Project Domain. So that while the terminology indicates 'annual' maxima time-series, the AMS for the MLCs may not extend to a full 12-month period in some of the Project Macro Regions.

An analysis of seasonality also provided a description of the likelihood for storms to occur at various times throughout the year. This information is important when conducting flood analyses because practitioners will want to link storm seasonality with soil moisture conditions and reservoir levels.

To determine the seasonality, a set of high-quality index stations in the Project Domain was identified (Figure 5). These stations had long periods of record and were spatially well-distributed across the Project Domain. For each index station, a 24-hour and 72-hour AMS was extracted from MetStat's existing precipitation database. These durations were selected to adequately represent the four durations (24-, 48-, 72-, and 96-hour) of this study. Cursory quality control measures were completed to remove any obvious incorrect precipitation magnitudes from the dataset. It should be noted that the dataset was comprised of all storm types (i.e., the dataset included MECs and LSs). Mostly, this could affect the 24-hour duration where a 24-hour precipitation total could result from a strong, short-duration thunderstorm event. This could also affect the 72-hour duration if the synoptic pattern was such that thunderstorms were occurring every afternoon for a few days in sequence. Otherwise, the assumption was used that long-duration high precipitation values are naturally associated with MLCs in this region. From the AMS data, histograms of storm events with precipitation 1.5 times greater than the at-site station median (which equates to about a 1-in-10-year event) were created to show the monthly frequency distribution of storms. Therefore, the seasonality results are based on the most significant, long-duration storm events.

Since the seasonality of storms differed across the Project Domain, the Project Domain was divided into smaller regions (i.e., Project Macro Regions) where the seasonality was consistent. The Project Macro Regions (also seen in Figure 5) were created using the Climate Regions (Figure 4) as a guide.

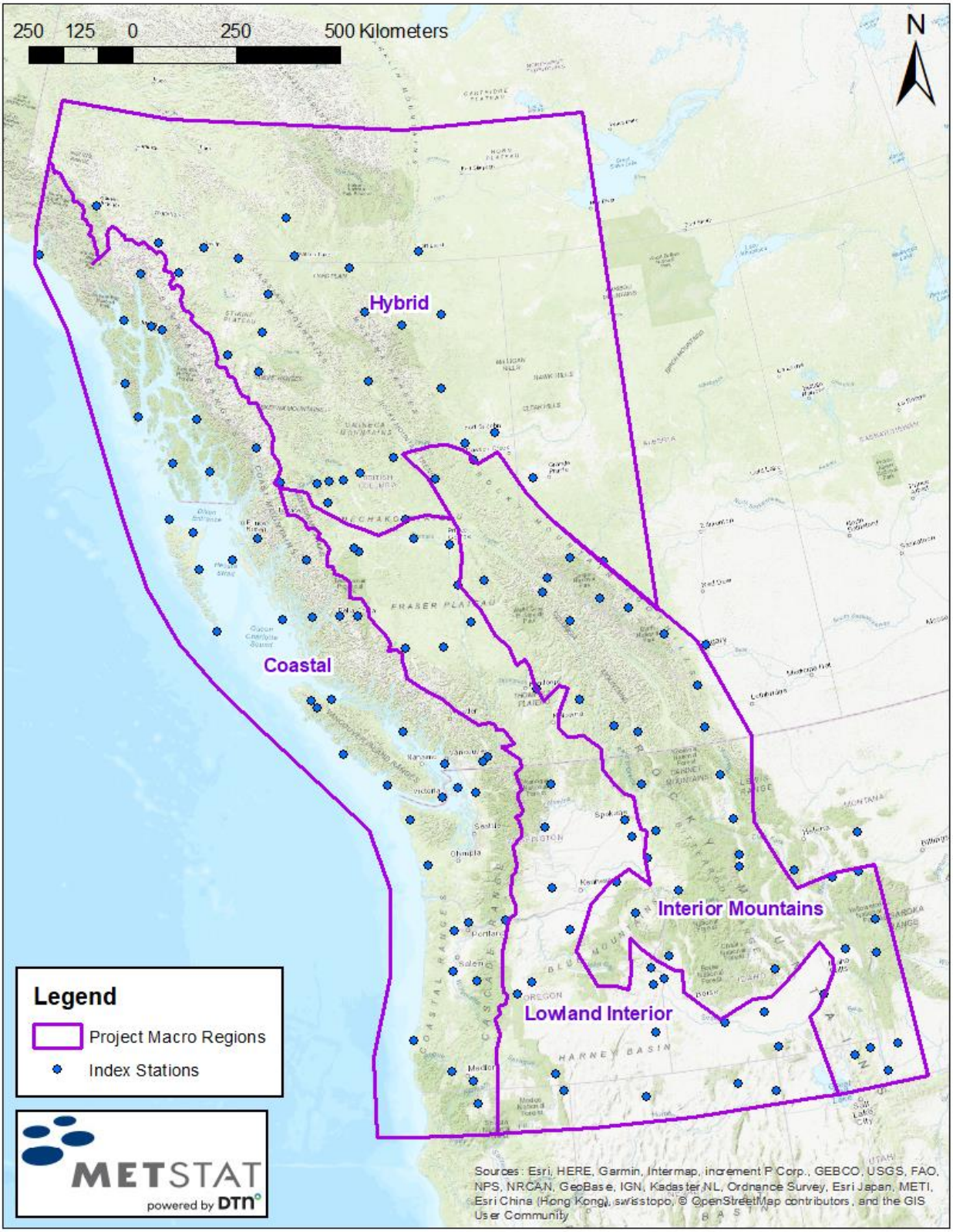

Figure 5: Project Macro Regions and index stations used for the seasonality analysis.

In the Coastal Macro Region, the peak of the storm season was from September to February for both the 24- and 72-hour durations (Figure 6). In this region, atmospheric river events dominated, and the polar jet had a heavy influence on the location where the atmospheric river events made landfall. The final seasonality was selected to be July 1 – April 30 for all durations (24-, 48-, 72-, and 96-hours; Table 1). The reason for expanding the season beyond the peak storm season was to fully capture any potential events occurring in the "shoulder" seasons (when storms occurred, but the frequency was low).

In the Lowland Interior Macro Region, the histograms depicted a more bi-modal pattern for both the 24-hour and 72-hour durations with a peak in late spring and another during winter (Figure 7). Here, MLC storms and frontal boundary systems could have interacted with moisture from the Pacific Ocean and perhaps from the Gulf of Mexico. Strong atmospheric river events could also penetrate through the Coast and Cascade Ranges and affect this area. Furthermore, there could be a mix of storm types included in this dataset since this is the only Project Macro Region where MECs and LSs are present. The final decision regarding seasonality (Table 1) for this Project Macro Region was to consider an all-season AMS.

In the Interior Mountain Macro Region, the peak of the storm season was May through June for both the 24-hour and 72-hour durations (Figure 8). The location of the polar jet has a strong influence here to siphon in moisture from the Pacific Ocean and/or the Gulf of Mexico, and atmospheric river events could affect this region during the winter months. The final seasonality was selected to be April 1 – October 31 to adequately capture the shoulder seasons yet remove the influence of atmospheric river events when the precipitation most likely fell as snowfall.

For the Hybrid Macro Region, storms most often occurred June through August and were most likely the result of MLCs and frontal boundaries coming off the Pacific Ocean. The final seasonality selected for this Project Macro Region was May 1 – October 31 (Figure 9).

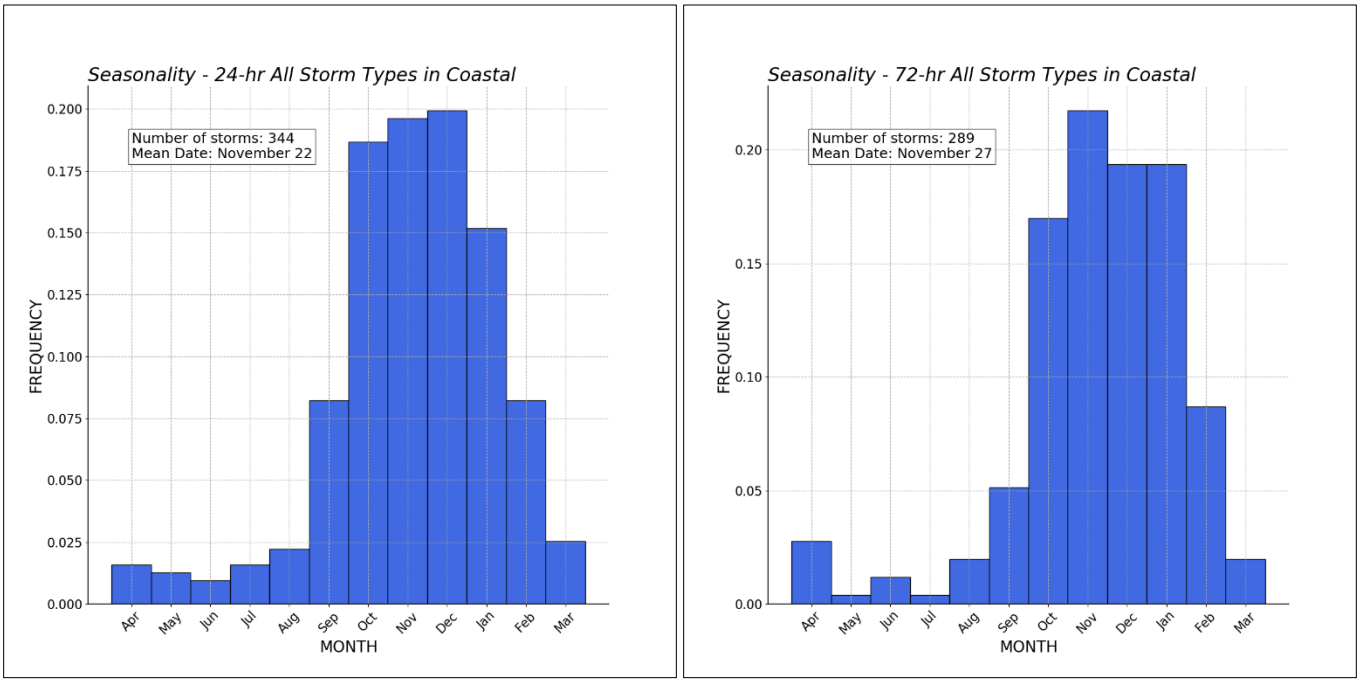

Figure 6: Coastal Macro Region histogram of storms for 24-hours (left) and 72-hours (right).

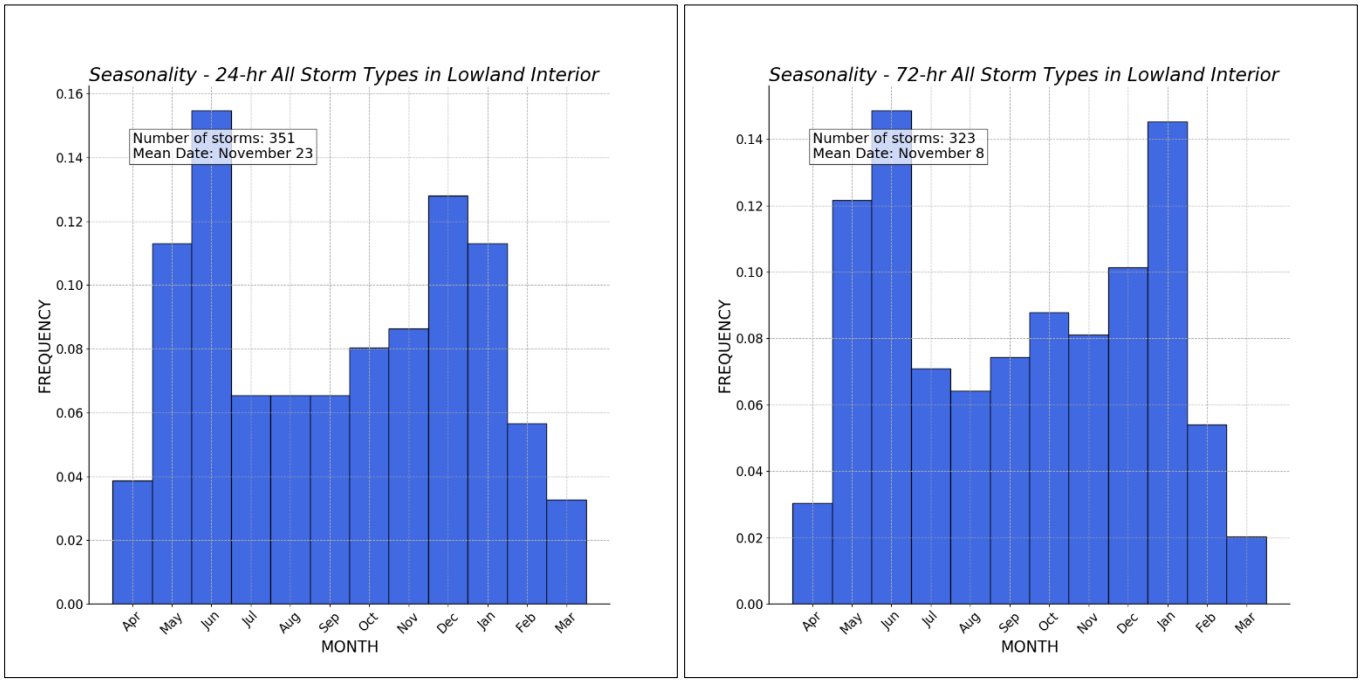

Figure 7: Lowland Interior Macro Region histogram of storms for 24-hours (left) and 72-hours (right).

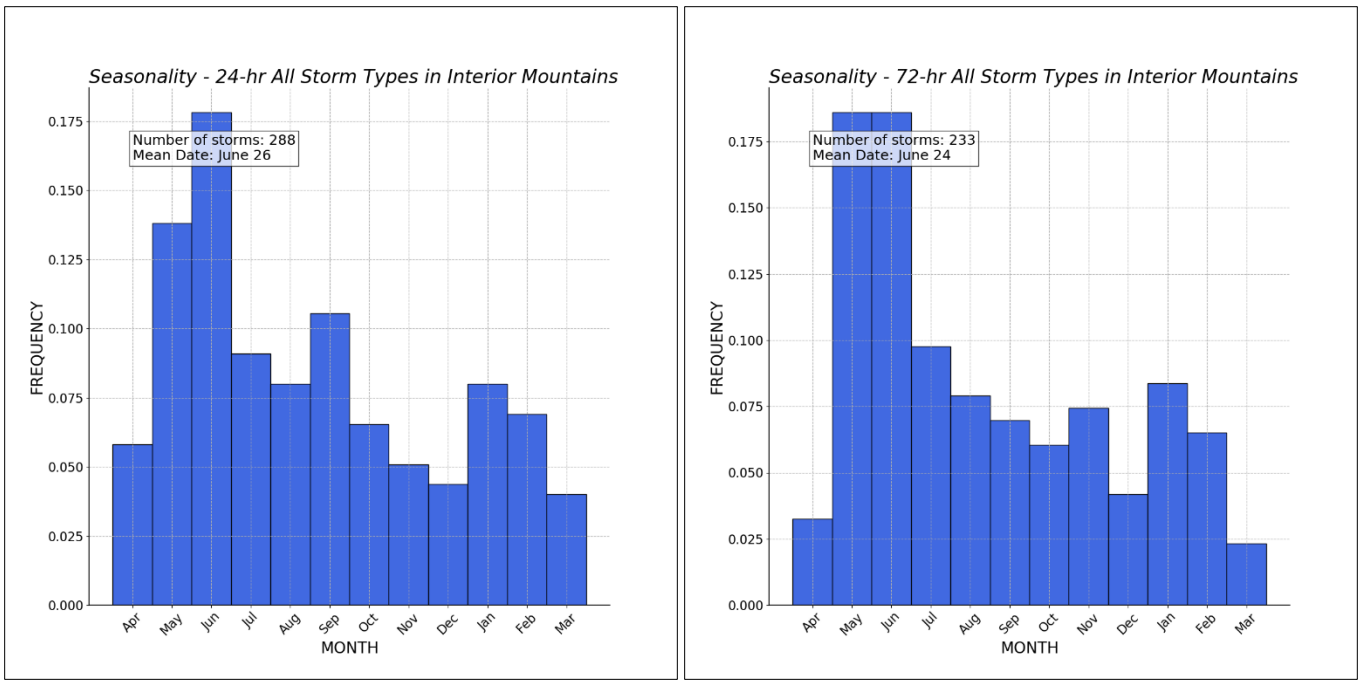

Figure 8: Interior Mountain Macro Region histogram of storms for 24-hours (left) and 72-hours (right).

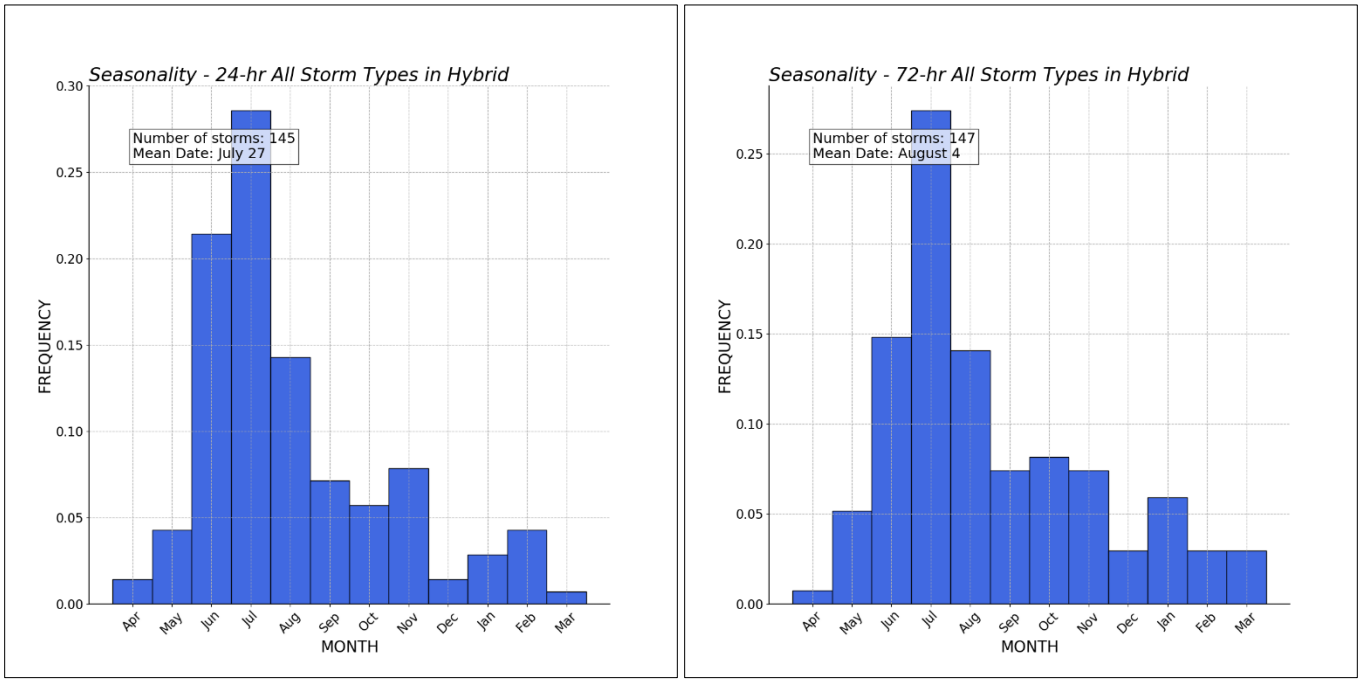

Figure 9: Hybrid Macro Region histogram of storms for 24-hours (left) and 72-hours (right).

Table 1: Seasonality by Project Macro Region (where gray shading indicates the months included).

Macro Region	Jan	Feb	Mar	Apr	May	Jun	Jul	Aug	Sept	Oct	Nov	Dec
Coastal												
Lowland Interior												
Interior Mountains												
Hybrid												

5. STORM TYPING PROCEDURES

5.1. Purpose

Since the focus of this project was a single storm type (MLC), it was necessary to conduct the precipitation-frequency analysis using only input data relating to this storm type. Storm typing procedures provide a methodology in which the MLC storm type and associated data may be identified and extracted from the historical period of record, thus creating an input dataset that is nearly homogeneous with regard to the generating phenomenon.

The storm typing approach coupled with regional precipitation-frequency analysis is a major advancement over traditional all-storm, all-season precipitation-frequency methods. In the traditional methods, the input datasets were comprised of a mixture of storms from various storm types (mixed distributions) leading to a flood-frequency analysis comprised of a mixture of flood events. This posed a problem for hydrologists since it's difficult to combine storm spatial and temporal patterns from different storm types into a plausible pattern for inflow design flood modeling.

The use of storm typing procedures and a nearly homogeneous dataset resulted in three notable outcomes: 1) separate precipitation-frequency relationships for each storm type were obtained; 2) spatial and temporal patterns specific to the storm type were created; and 3) greater insight into the statistical characteristics of the various storm types was gained. Thus, the storm typing approach provided the important direct link between a watershed precipitation-frequency relationship and the storm spatial, temporal, and seasonal characteristics of the storm type. Furthermore, due to the knowledge of the statistical characteristics of the storm types, the uncertainty bounds for estimation of extreme AEPs of precipitation can be more rigorously assessed and thus narrowed in extent.

The goal of the storm typing procedures is to produce a Database of Daily Storm Types (DDST). The DDST is a listing of the predominant type of storm that produced each rainy day in the period of record for Storm Typing Zones (Figure 10) across the Project Domain. This is a necessary step in the assembly of the homogeneous dataset with regard to the generating phenomenon (MLC storm type) for precipitation-frequency analysis. Specifically, the DDST will be referenced in the assembly of the precipitation AMS; at each precipitation gauge, the DDST provides the dates that the storm type of interest occurred from which precipitation annual maxima values may be selected.

Table 2 lists the storm types and the respective numerical codes that were used in the DDST. If a negligible amount of precipitation fell on a day in the period of record, then the day was marked with a 50, indicating a dry day.

Table 2: Storm Types and Numerical Codes.

Storm Type	Acronym	Numerical Code
Mid-Latitude Cyclone	MLC	10
Mesoscale Storm	MEC	30
Local Storm	LS	40
MLC/MEC Hybrid	-	60
Dry Day	-	50

5.2. Methods

To assign the type of storm that produced each rainy day in the period of record across the Project Domain (i.e., create the DDST), automated procedures were developed. Specifically, the methodology to create the DDST was accomplished in two steps:

1. Manually assign a storm type to a subset of storms to establish criteria; and
2. Apply those criteria in an algorithm to automatically assign a storm type to each day within the period of record.

5.2.1. Manual Storm Typing

Manual storm typing methods were performed to examine the meteorological environment of nearly 150 storm events. Since the spatial extent of the Project Domain was large enough that one storm could affect the northern or western portion of the domain and another could simultaneously affect the southern or eastern portion, the Project Domain was divided into Storm Typing Zones. The Storm Typing Zones had a spatial resolution of 2° latitude by 2° longitude, to coincide with the resolution of the 20th Century Reanalysis data used for examining the meteorological environment. In total, 88 Storm Typing Zones were considered in the manual storm typing methods (Figure 10). The Storm Typing Zones allowed for different storm types to occur simultaneously across the Province and ultimately result in a unique DDST for each.

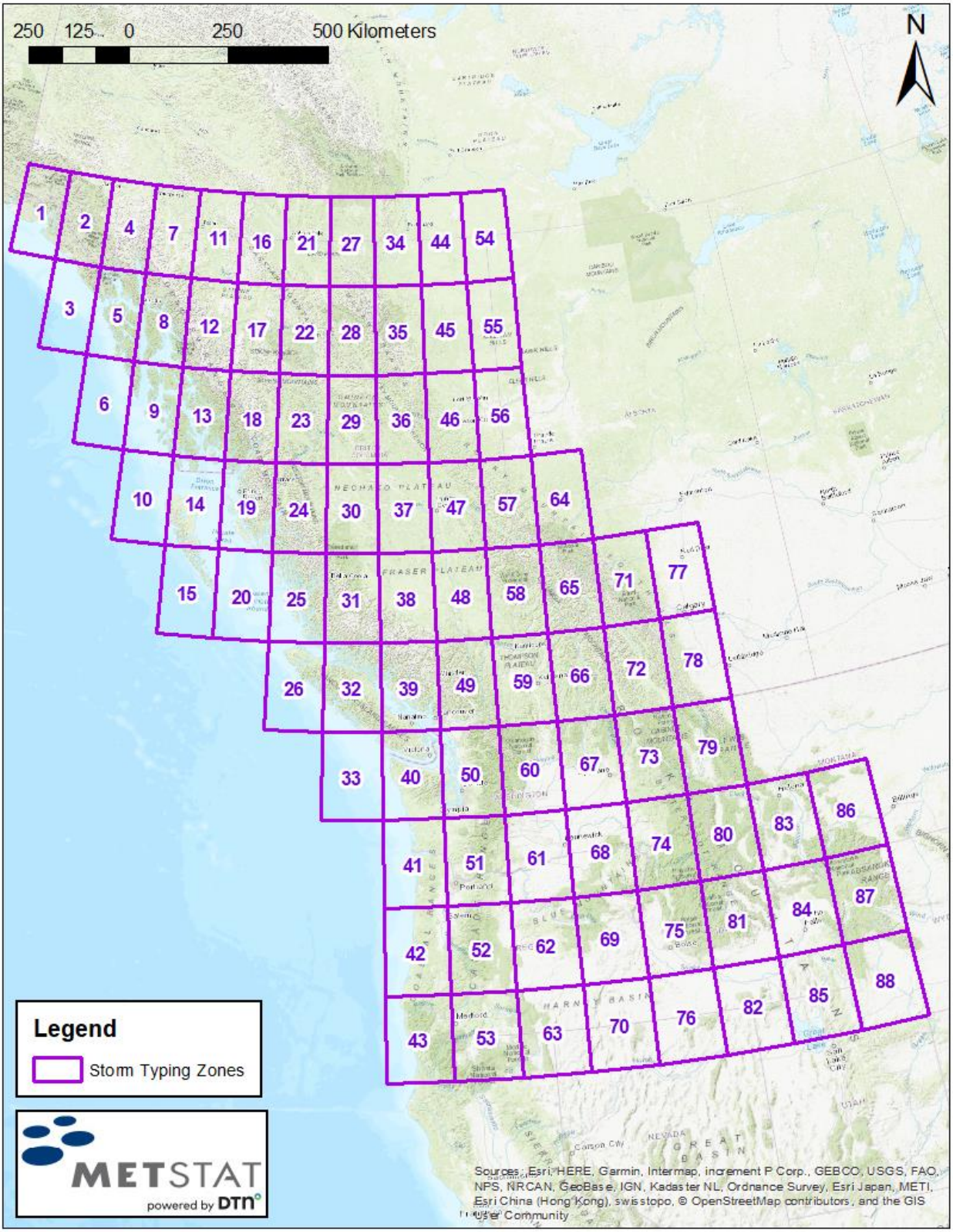

Figure 10: Storm Typing Zones.

5.2.1.1 Storm Subset Selection

To select the subset of storms for manual analysis, the all-season, all-type precipitation AMS for the index stations (Figure 5) was assembled. Next, a filtering process was applied to obtain a storm list that focused on the more extreme (rarer) precipitation events. This was important because the characteristics of the rare storm events needed to be identified and properly typed as they drive the upper tail of the probability distribution. The characteristics were also used to define the criteria for establishing thresholds of the automated storm typing algorithm. The first step in the filtering process was to compute the ratio of the observed storm amount to the at-site median (i.e., ratio-to-median) for each annual maximum to normalize the storm amounts and quantify the rareness of each storm (at the storm's respective point location). The list was then filtered to remove precipitation observations less than the 1.50 ratio-to-median threshold, which equates to about a 1-in-10-year event. Duplicate dates within the list were then also removed, saving only the largest ratio-to-median instance for a given date. This produced a list of 397 potential storm events. This list was manually sorted and examined to select storm events that matched the following criteria to ensure a wide selection of storms with different magnitudes and spatial and seasonal characteristics:

1. Top 50 storm events when sorted by the ratio-to-median
2. Top ~50 storm events when sorted by precipitation magnitude
3. Top ~75 storm events when sorted by number of stations recording significant precipitation for a given date
4. Bottom ~50 storm events when sorted by number of stations recording significant precipitation for a given date
5. ~40 storm events to ensure the following criteria were met:
    a. At least five storms from each decade 1900-2010
    b. At least five storms per each month of the year
    c. Removed consecutive dates as these are quite often the same storm event

Note that the totals in the above categories add up to more than 200 storm events, which is due to the overlap between the categories (e.g., a top 50 storm event by maximum precipitation magnitude is also likely to fall into the top 75 events by number of stations over threshold). In total, a subset of 147 representative storm events were selected for manual analysis (see APPENDIX A: Storms for Manual Storm Typing for storm list).

5.2.1.2 Storm Typing Application

The meteorological environment for the subset of nearly 150 storms was manually reviewed by meteorologists using a graphical user interface (GUI) Storm Typing Application (e.g., Figure 11 and Figure 12). The Storm Typing Application displayed several meteorological parameters for each Storm Typing Zone, including:

- three-day precipitation accumulation;
- maximum gradient in the 500-mb pressure field;
- convective available potential energy (CAPE);
- precipitable water; and
- maximum cloud cover fraction.

The two variables that were most beneficial to the manual storm typing methods are described in detail below:

- **Three-day precipitation accumulation –** A measure of the precipitation accumulation was needed to differentiate between MLCs, MECs, LSs, and dry days. If the three-day accumulation was negligible, then it was assumed that it was not raining in the Storm Typing Zone, and the grid cell was designated as a dry day. If the precipitation accumulation was minimal, then it was assumed that the precipitation within the Storm Typing Zone was not

spatially widespread, and the Storm Typing Zone was designated as a LS. Finally, if the three-day precipitation accumulation indicated that the precipitation was substantial, then the Storm Typing Zone was further investigated to determine if the storm type was either MLC or MEC. Definitive thresholds of three-day precipitation accumulation to distinguish storm type were established after the manual storm typing process was complete.

The three-day precipitation accumulation for each Storm Typing Zone was determined using the precipitation rate variable from the NOAA-CIRES Twentieth Century Global Reanalysis Version II dataset (Compo et al., 2011). The precipitation rate variable was re-gridded from a Gaussian grid to the 2° latitude by 2° longitude grid using bilinear interpolation to match the spatial resolution of the other 20th Century parameters. The temporal resolution was 3-hours (at 00Z, 03Z, 06Z, 09Z, 12Z, 15Z, 18Z, and 21Z), but to determine the three-day precipitation accumulation, the 3-hour precipitation rates were added over a three-day period. The data were available for the period 1851-2014.

- **Gradient in the 500-mb pressure field –** A measure of atmospheric pressure as geopotential height was reviewed to characterize the meteorological set up of a storm. Specifically, the 500-mb height in the upper atmosphere was considered. Gradients in space of the 500-mb heights across a Storm Typing Zone were indicative of large-scale synoptic storm events.

  The 500-mb heights were from the NOAA-CIRES Twentieth Century Global Reanalysis Version II dataset (Compo et al., 2011). The spatial resolution was 2° latitude by 2° longitude, matching the spatial resolution of the Storm Typing Zones. The temporal resolution was 6-hours (at 00Z, 06Z, 12Z, and 18Z), but to evaluate the storm at its peak, only the maximum 6-hour height over the storm duration (3 days) was considered. The data were available from 1851-2014.

The Storm Typing Application also showed contour maps of the large-scale precipitable water pattern, CAPE, 850-mb height pattern, 500-mb height pattern, and sea level pressure at 6-hour intervals for the duration of the 3-day MLC storm events. The contour maps provided insight into the spatial nature and evolution of the storm event.

5.2.1.3 Storm Typing Application Examples

To demonstrate the Storm Typing Application, below are three examples:

1. An atmospheric river (MLC) that affected part of the Project Domain;
2. An atmospheric river (MLC) that affected the majority of the Project Domain; and
3. An MLC/MEC hybrid storm event with origins in the continental interior.

5.2.1.3.1 An atmospheric river (MLC) that affected part of the Project Domain

On 21 Nov. 1909, a deep MLC developed in the north Pacific, directing a “Pineapple Express” moisture stream towards the southern Coastal and Lowland Interior regions. Upper level winds became more zonal (west-east orientation) throughout, trapping moisture to the south and inducing strong upslope flow along many of the Pacific Northwest mountain ranges. The storm event produced heavy precipitation across most of the western U.S., including California, coastal Washington and Oregon, and even interior mountain areas in Idaho and Nevada. Precipitation was prodigious because of the nearly stationary nature of the atmospheric river, resulting in very large precipitation totals over southern portions of the Project Domain and nearly dry weather conditions across the northern portion. Figure 11 and Figure 12 depict the various parameters from the Storm Typing Application that were available to the meteorologists when manually typing this event.

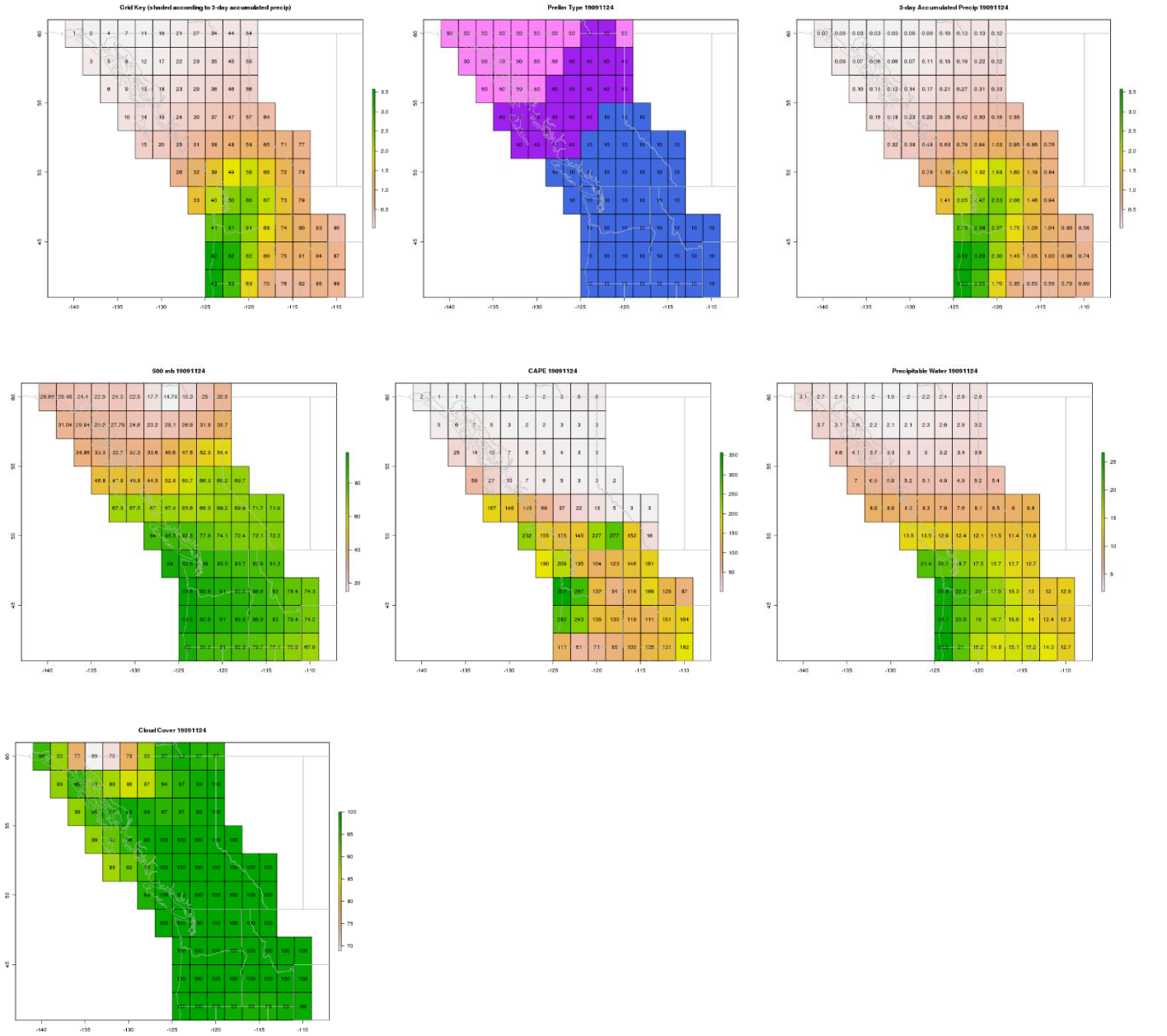

Figure 11: Maps available in the Storm Typing Application for the 21 Nov. 1909 storm event.
From top left to bottom right: Storm Typing Zone shaded by 3-day precipitation accumulation; first-guess automated algorithm storm type; 3-day precipitation accumulation; maximum 500-mb gradient, in meters per 2° of latitude/longitude; CAPE in j/kg; total column precipitable water (mm); maximum cloud cover fraction.

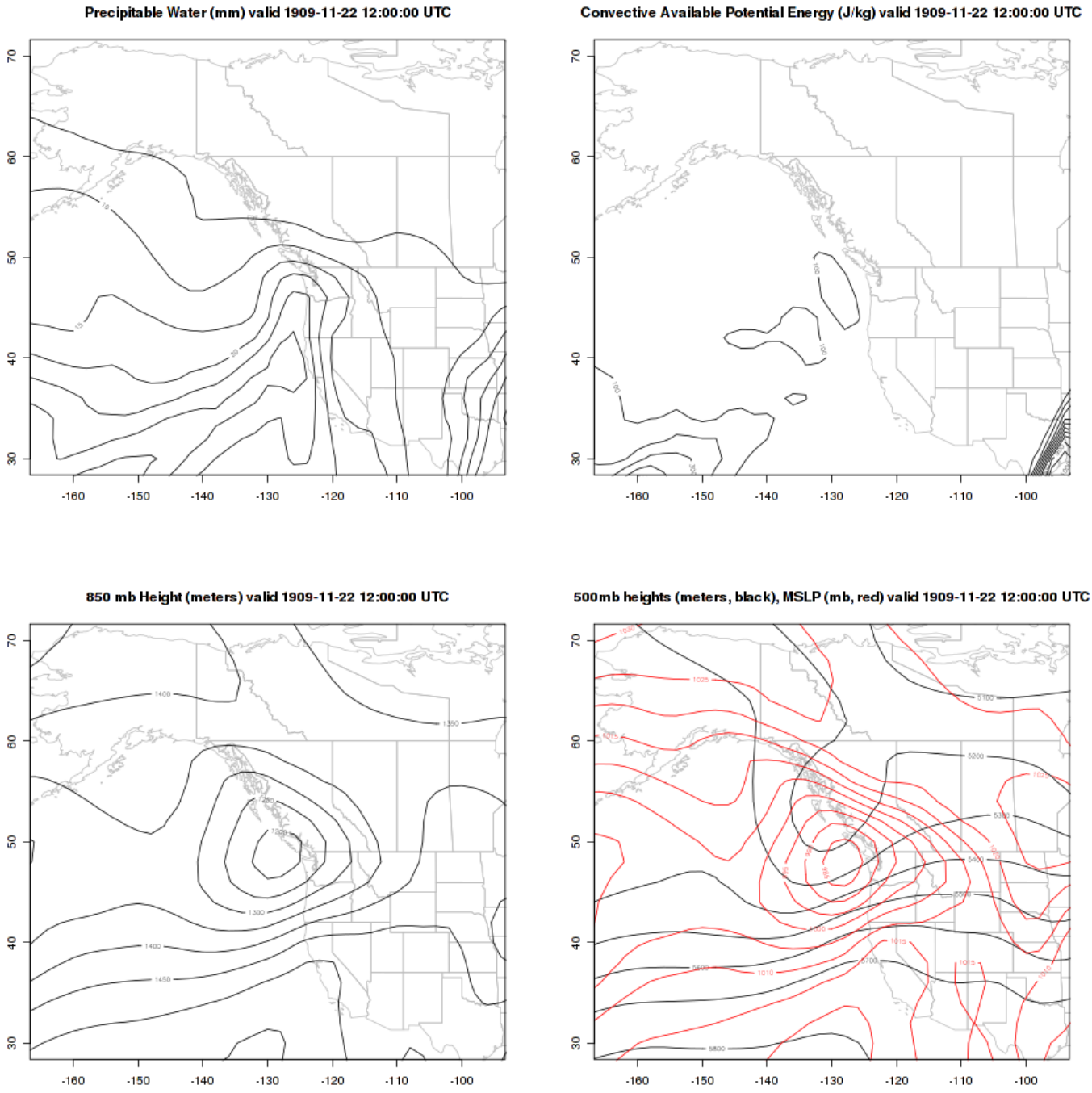

Figure 12: Four-panel plot available in the Storm Typing Application for the 21 Nov. 1909 storm event. From top left to bottom right: large-scale precipitable water pattern; CAPE; 850-mb height pattern; and 500-mb height pattern (black) overlaid on sea-level pressure (red).

5.2.1.3.2 An atmospheric river (MLC) that affected the majority of the Project Domain

A textbook example of a deep Aleutian Low occurred in late January 1959, directing a broad atmospheric river at much of the west coast of North America over a several-day period. The primary low remained well out to sea but directed strong, moisture-rich southwesterly flow at much of the coast. The focal point of the atmospheric river gradually shifted southward through the storm. Figure 13 and Figure 14 depict the various parameters from the Storm Typing Application that were available to the meteorologists when manually typing this event.

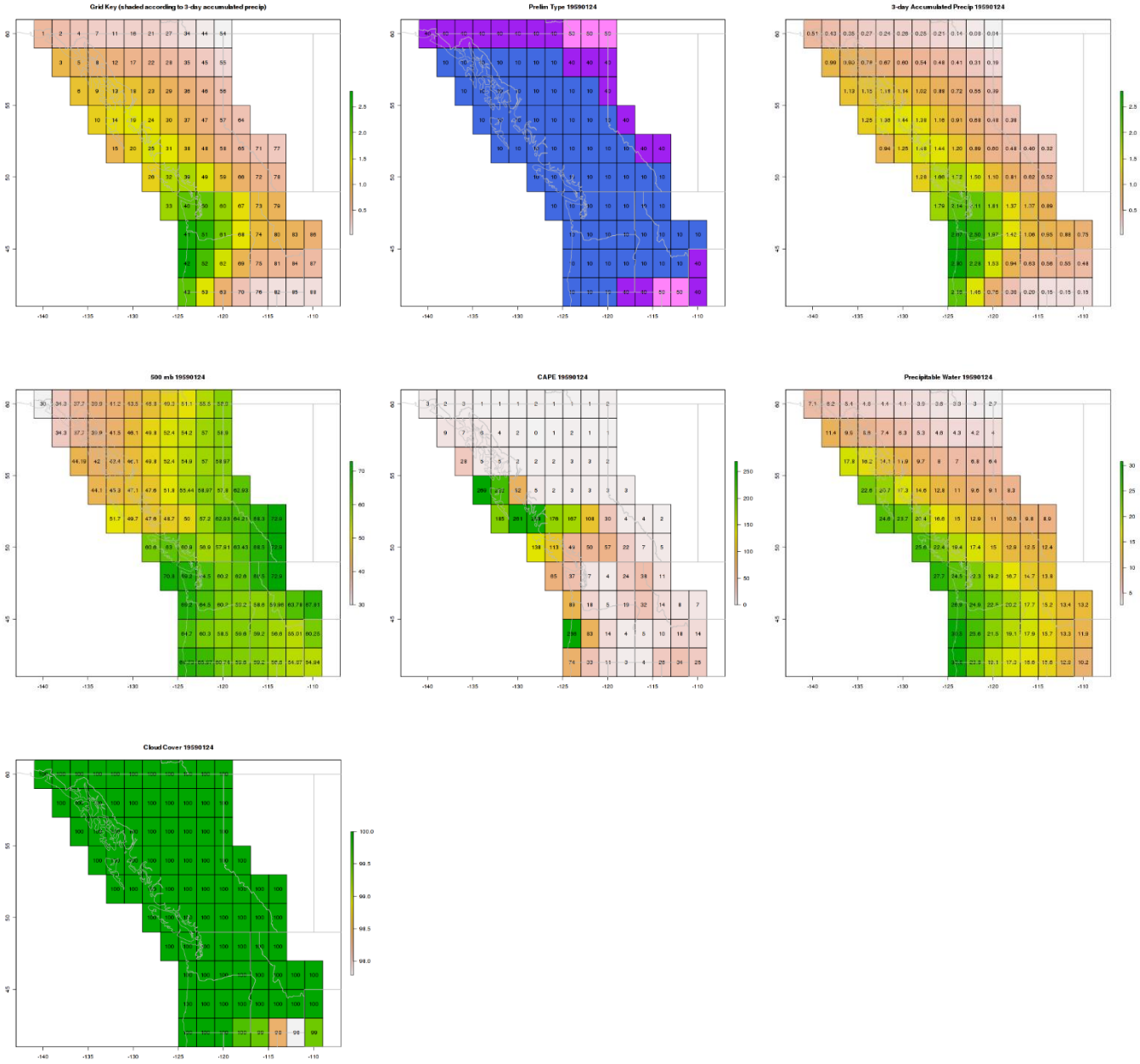

Figure 13: Maps available in the Storm Typing Application for the Jan. 1959 storm event.
From top left to bottom right: Storm Typing Zone shaded by 3-day precipitation accumulation; first-guess automated algorithm storm type; 3-day precipitation accumulation; maximum 500-mb gradient, in meters per 2° of latitude/longitude; CAPE in j/kg; total column precipitable water (mm); maximum cloud cover fraction.

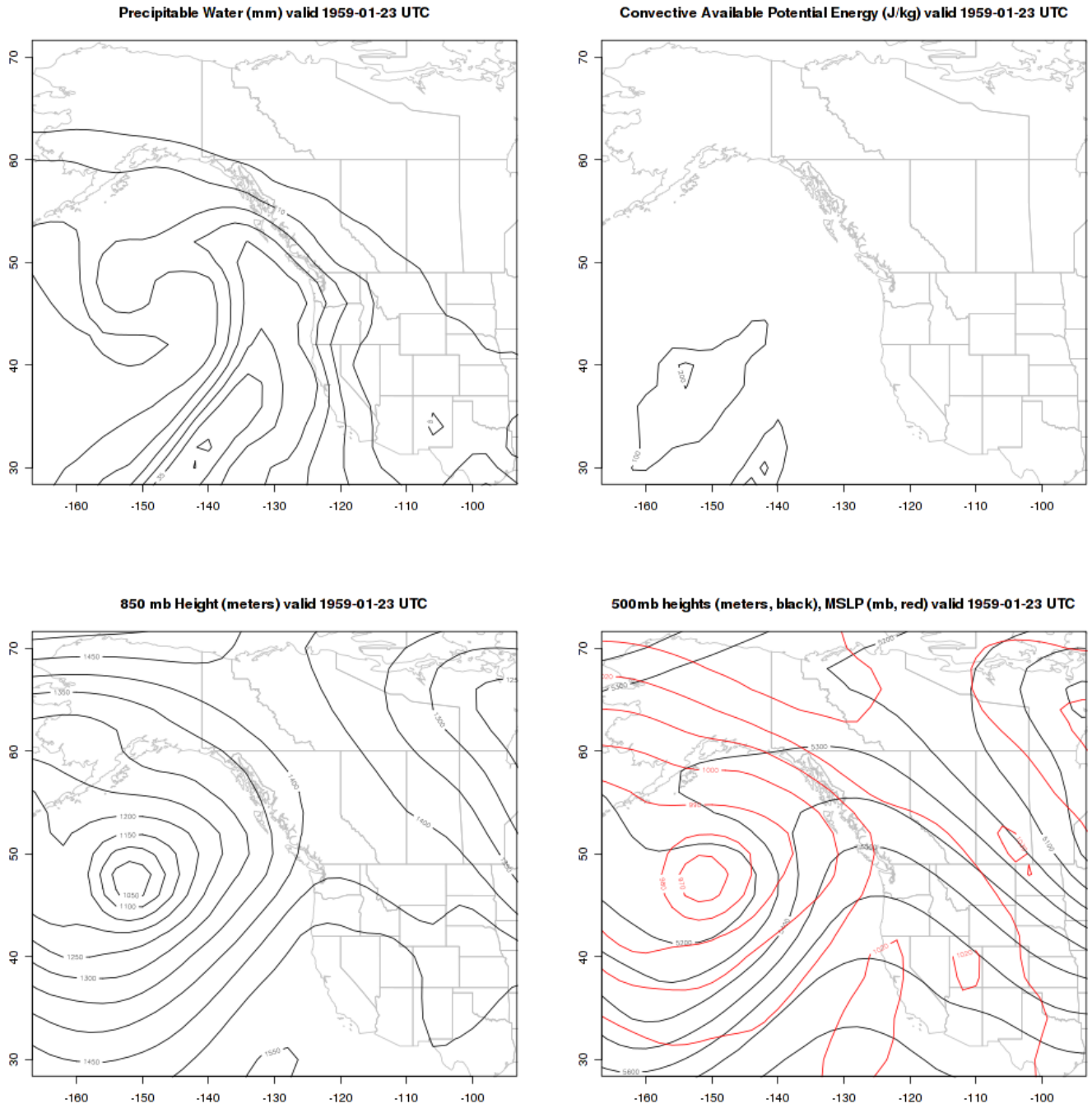

Figure 14: Four-panel plot available in the Storm Typing Application for the Jan. 1959 storm event. From top left to bottom right: large-scale precipitable water pattern; CAPE; 850-mb height pattern; and 500-mb height pattern (black) overlaid on sea-level pressure (red).

5.2.1.3.3 An MLC/MEC hybrid storm event with origins in the continental interior

Although atmospheric river events are the most common heavy precipitation producers in the Project Domain, notable storms that develop over continental regions and sweep southeastward also occur regularly, particularly during the warm season. A prime example of one of these events began to develop on 15 July 1962, when an upper-level low initially positioned over northwest British Columbia deepened and dropped southeastward. In response, surface pressures along the leeward side of the Canadian Rockies dropped, leading to lee cyclogenesis and upslope flow. This drew moisture westward from the prairies into the mountains, producing widespread showers and thunderstorms across much of northeastern British Columbia and far western Alberta. Figure 15 and Figure 16 depict the various parameters from the Storm Typing Application that were available to the meteorologists when manually typing this event.

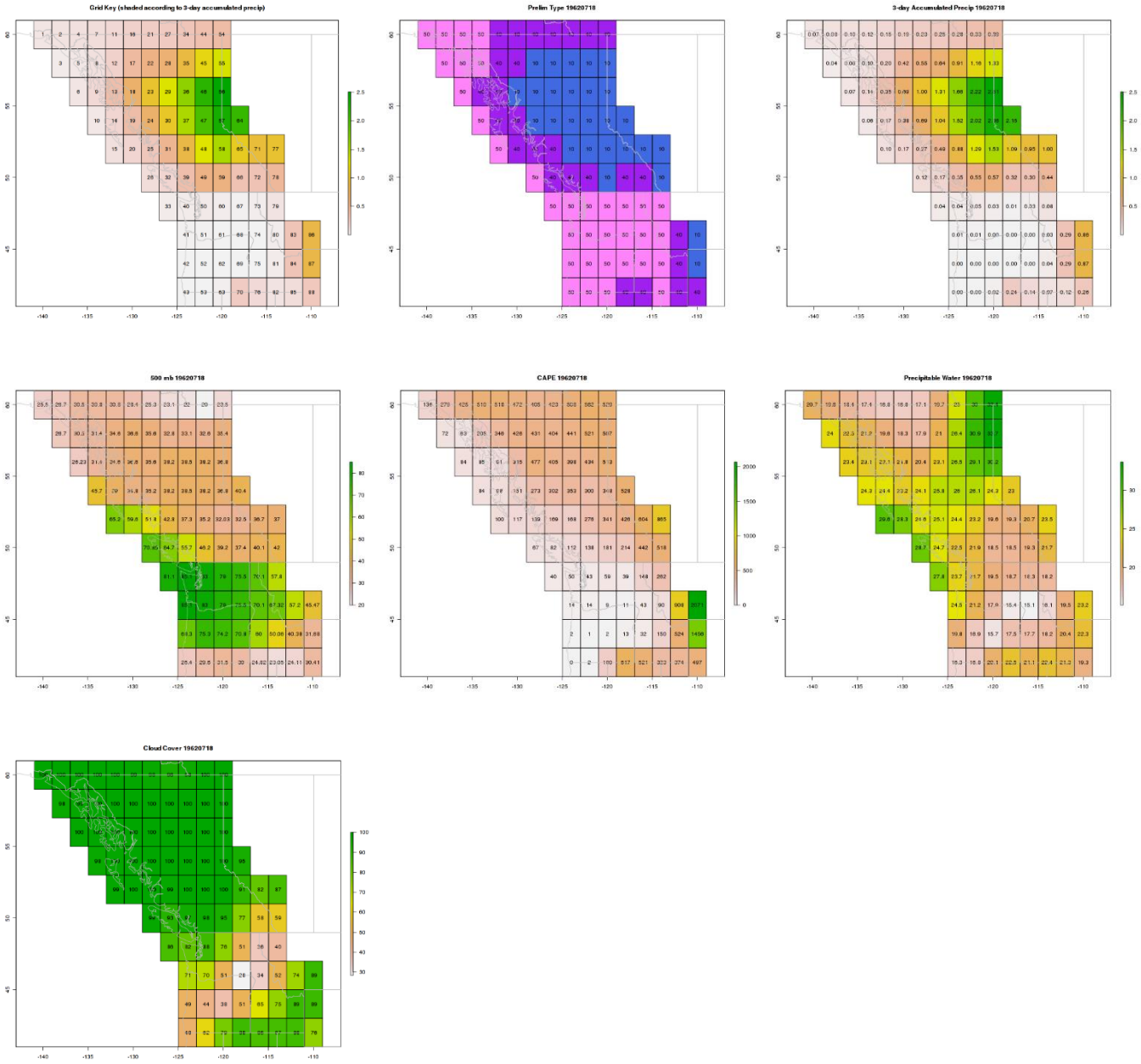

Figure 15: Maps available in the Storm Typing Application for the 15 July 1962 storm event.
From top left to bottom right: Storm Typing Zone shaded by 3-day precipitation accumulation; first-guess automated algorithm storm type; 3-day precipitation accumulation; maximum 500-mb gradient, in meters per 2° of latitude/longitude; CAPE in j/kg; total column precipitable water (mm); maximum cloud cover fraction.

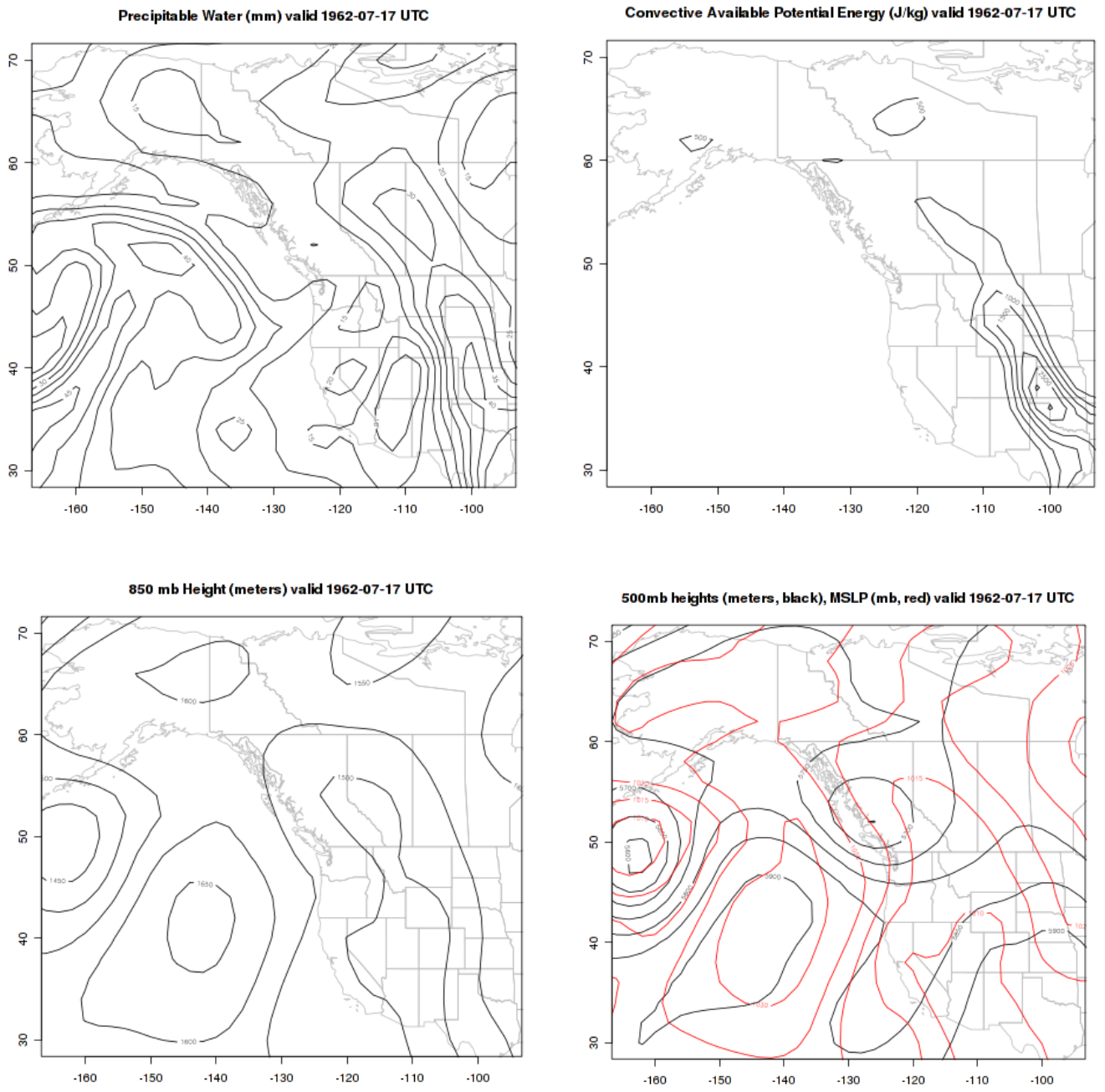

Figure 16: Four-panel plot available in the Storm Typing Application for the 15 July 1962 storm event. From top left to bottom right: large-scale precipitable water pattern; CAPE; 850-mb height pattern; and 500-mb height pattern (black) overlaid on sea-level pressure (red).

5.2.2. Automated Storm Typing Algorithm

There were approximately 59,500 days in the period of record (1851-2014) and 88 Storm Typing Zones that required a storm type, so it was necessary to develop automated procedures for assigning storm types and creating the DDST. To inform the automated algorithm, the key parameters and their respective thresholds identified in the manual storm typing methods were used in addition to knowledge gained from prior studies. Most notably, during the completion of the Colorado-New Mexico Regional Extreme Precipitation Study (MetStat and MGS Engineering, 2018a), it was found that gradients in the 500-mb height pattern provided a sense of the synoptic-scale organization of the atmosphere. The meteorologists that manually evaluated the approximately 150 MLC storms in this study found this to also be true of British Columbia. Additionally, the thresholds for the gradients in the 500-mb height pattern from the study completed for BC Hydro were tested and found to hold true for all British Columbia (MetStat and MGS Engineering, in draft). Ultimately, the key parameters used in the automated algorithm matched the parameters that were most beneficial for the manual storm typing methods, described above. The key parameters included 3-day precipitation accumulation and gradients in the height of the 500-mb pressure field.

An optimization algorithm used multiple combinations and permutations of each parameter. The upper and lower magnitude bounds for each parameter came from the minimum and maximum values from the manually typed subset of storms. The optimization algorithm then assessed magnitude values within the bounds at small, incremental intervals. The optimized, automated algorithm was compared against the storm type assigned to each Storm Typing Zone for the approximately 150 MLC storms in the manual storm typing method ("truth") to check for accuracy using a confusion matrix. The optimized, automated algorithm had an MLC sensitivity (the true positive rate) of 0.997, and a specificity (the true negative rate) of 0.987. The balanced accuracy (*[sensitivity + specificity]/2*) for MLC storm events was 0.992 (see Tharwat, 2018 for detailed descriptions of the sensitivity, specificity, and balanced accuracy tests).

The final thresholds for the key parameters were defined as follows:

- **Three-day precipitation accumulation –** As was described for the manual Storm Typing Application, the 3-hour precipitation rates from the NOAA-CIRES Twentieth Century Global Reanalysis Version II dataset (Compo et al., 2011) were added over the three-day storm period to calculate the three-day precipitation accumulation metric. Storm Typing Zones with 1-mm of precipitation or less over the three-day period were classified as a Dry Day (50). Storm Typing Zones with greater than 1-mm of precipitation but less than 20% of the mean annual 72-hour maximum precipitation of the Storm Typing Zone (approximately equivalent to the 2-year average recurrence interval) were classified as LS (40).

- **Gradient in the 500-mb pressure field –** The maximum gradient in the 500-mb pressure field from any direction was considered for classifying storm types. The 500-mb level resides near the middle of the atmosphere, largely removed from any direct influence from the surface. The presence of a strong maximum in the height gradient at 500-mb was a clear indication of synoptic organization, and thus would be typed as MLC (10). Conversely, a weak maximum in the height gradient at 500-mb indicated a lack of synoptic organization, resulting in an MEC designation (30). When the gradient was in between these thresholds, the MLC/MEC hybrid designation was used (60) since this mixed case was indicative of some larger-scale organization without a clear MLC being present. This categorization is summarized in Table 3.

Table 3: Storm type categorization using maximum gradient in 500-mb height.

	Weak Gradient in 500-mb	**Moderate Gradient in 500-mb**	**Strong Gradient in 500-mb**
Categorization	MEC	MLC/MEC Hybrid	MLC

The weak gradient threshold was found to be less than 31.0-m per 2°; whereas, the strong gradient threshold was found to be greater than or equal to 36.0-m per 2°. Due to the large geographical size of the Project Domain, the thresholds were adjusted to account for meridional (longitudinal) convergence based on latitudinal position. The thresholds are similar to those used in MetStat and MGS Engineering (in draft) for BC Hydro.

The decision tree for the automated algorithm may be found in Figure 17, where the thresholds are shown in blue boxes, and the storm type numeric codes (from Table 2) are shown as green circles.

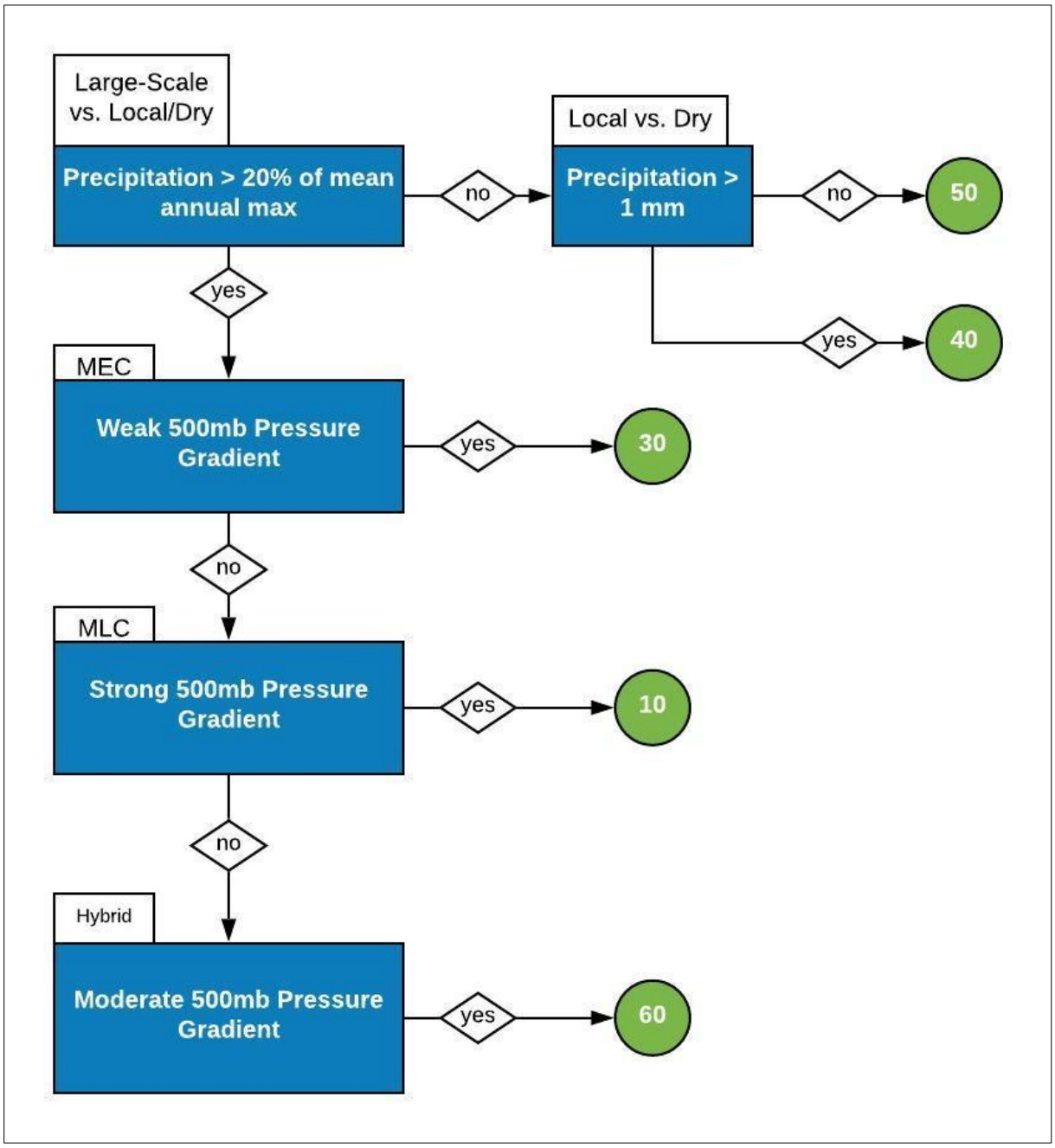

Figure 17: Decision tree for automated storm typing algorithm.

5.3. Database of Daily Storm Types

The DDST is a listing of the type of storm that produced each rainy day in the period of record for the Project Domain. This included a storm type for each of the 88 2° latitude by 2° longitude Storm Typing Zones for each day in the period 1851-2014. Note that the ending date for the DDST is Dec. 31, 2014, which coincides with the availability of the NOAA-CIRES Twentieth Century Global Reanalysis Version II dataset (Compo et al., 2011) that was referenced in the automated algorithm. The storm types that were included in the DDST were MLC, MEC, LS, MLC/MEC hybrids, and dry days (Table 2). However, the focus of this study was MLCs since this storm type is the chief meteorological mechanism by which precipitation is generated at the high latitudes of the Project Domain for long durations (24- through 96-hours). MLC/MEC hybrids were categorized as MLC storm events in the remainder of the analysis since there was synoptic organization associated with these storm events. The other storm types were identified in the historical record for purposes of removing them from the analysis to form a more homogeneous dataset of the generating phenomenon (MLC storm type).

The DDST will be referenced in the assembly of the precipitation annual maxima time-series at each precipitation gauge by providing the dates in which the MLC storm type occurred and thus providing a list from which precipitation annual maxima values may be selected.

The format of the DDST is a comma-delimited ASCII file with one date (month, day, year) per line followed by 88 columns presenting the storm type for each of the Storm Typing Zones.

6. POINT PRECIPITATION DATA

6.1. Sources of Point Precipitation Data

Point precipitation observation data measured at the daily time-step were acquired from gauges within the Project Domain from various sources. Focus was placed on the daily time-step since the MLC storm type and the four durations of interest were 24-hours or greater; storm types with sub-daily time-steps were not considered in this project. The sources of the daily precipitation data were as follows:

- NOAA's National Center of Environmental Information (NCEI) Global Historical Climatology Network (GHCN), which is an integrated database from a variety of observation networks
- Government of Canada's historical daily weather data provided by Environment and Climate Change Canada (ECCC)
- BC Hydro
- British Columbia Ministry of Agriculture
- Agriculture and Rural Development Act Network
- British Columbia Ministry of Environment – Air Quality Network
- British Columbia Ministry of Environment – Automated Snow Pillow Network
- Forest Ecosystems Research Network
- Wildfire Management Branch
- Forest Renewal BC
- Ministry of Transportation and Infrastructure
- Rio Tinto Alcan

For further information regarding data acquisition, please see APPENDIX B: Data Acquisition and Assembly Report from NHC.

Figure 18 shows all the daily precipitation gauges within the Project Domain. The data collection resulted in a total of 2,966 stations with daily data. The period of record began in January 1851 to coincide with the storm typing information found in the DDST. The end of the period of record was August 2019, even though the DDST ended in December 2014. Due to limitations in the NOAA-CIRES Twentieth Century Global Reanalysis Version II dataset (Compo et al., 2011), the years 2015 through 2019 were not explicitly separated by storm type, rather the long-duration annual maxima time-series for these years were assumed to consist of MLC storms.

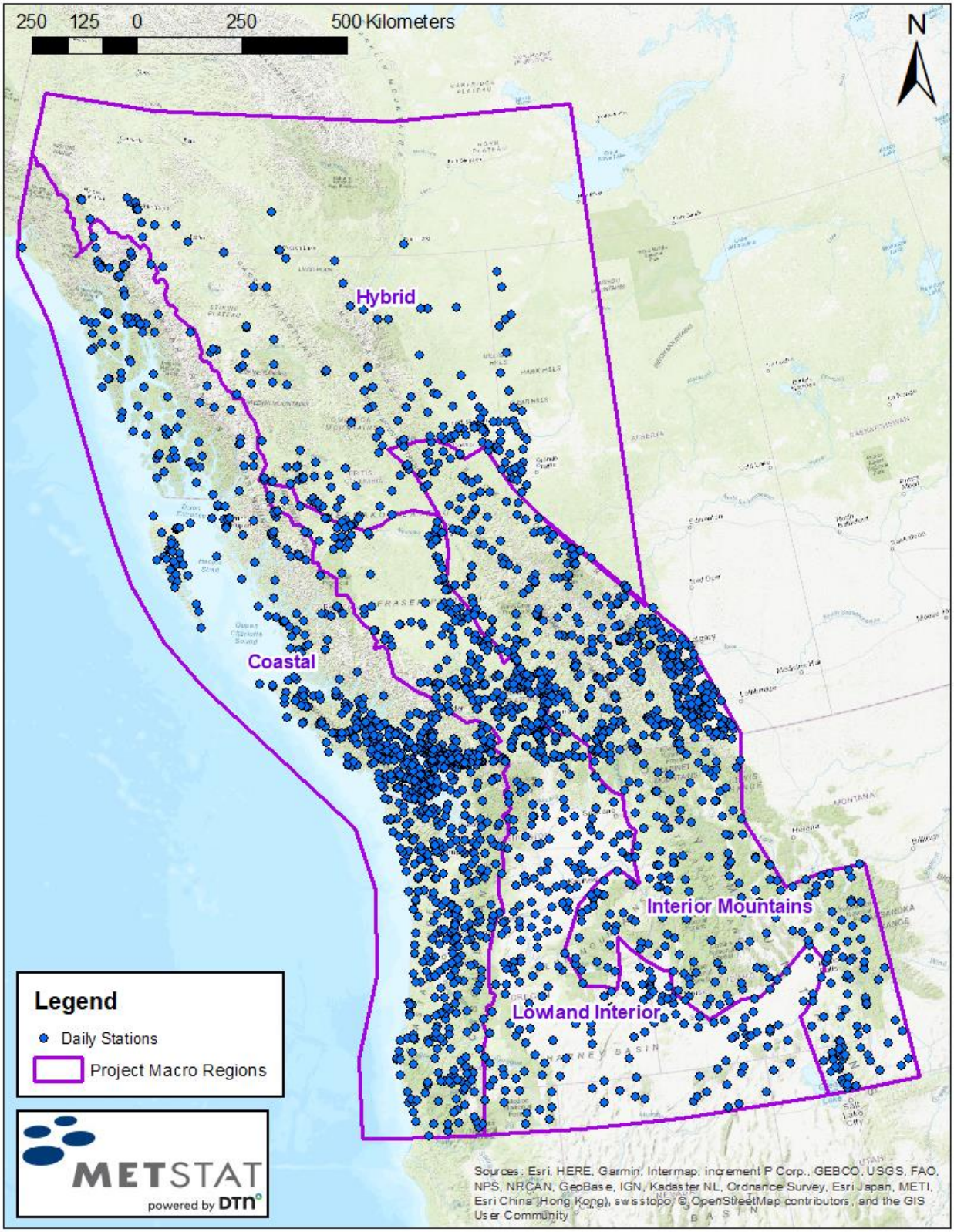

Figure 18: Map of all daily precipitation gauges in the Project Domain.

6.2. Quality Assurance and Quality Control of Point Precipitation Data

The quality assurance and quality control process of the point precipitation observation data was conducted in three phases:

- Phase 1: used automated data quality assurance/quality control software, developed by NHC, to test every station to flag data problems and suspected data problems.
- Phase 2: manually evaluated the validity of the precipitation outliers flagged in Phase 1, by checking the station's time-series and, in some cases, checking other stations' records for corroboration. (Due to time constraint, not all outliers were evaluated in Phase 2).
- Phase 3: summarized all quality control flags. This includes network supplied flags when available (ECCC only).

For detailed information about the three above phases, please see APPENDIX C: QA/QC of Precipitation Records Report from NHC.

6.3. Assembly of Precipitation Annual Maxima Time-Series

At each of the daily precipitation gauges in the Project Domain (Figure 18), a listing of the annual maxima time-series (AMS) for the MLC storm type for each of the four durations of interest was assembled. In this context, the term "annual maxima" refers to the greatest precipitation observation for the specific storm type (here, MLC) for each duration of interest for the appropriate season (Table 1) for each year in the period of record at each precipitation gauge. For the Lowland Interior Macro Region where the season is all-season, a "climatic year" was used to assemble the data. A "climatic year" was selected with consideration of the seasonal timing of the specified storm type so that the start and end of the climatic year occurred when that storm type was relatively dormant. For the Lowland Interior, the climatic year began on April 1 and ended on March 31, based on the seasonality analysis (Figure 7).

For the 48-hour duration, the highest 2-day aggregated amount of precipitation determined from a moving window was extracted for each appropriate season or climatic year (dependent upon the Project Macro Region; Table 1) and incorporated into a 2-day AMS for each daily precipitation gauge. Only data from the days typed as MLC in the DDST were considered; this is a critical step in the development of an input dataset comprised of homogeneous phenomena. Specifically, at least one of the two days within the 2-day aggregated window had to be classified in the DDST as an MLC. The exception to this rule were the years 2015-2019, after the end date of the DDST. As a reminder, each of the 88 Storm Typing Zones had an independent DDST that was applied to each daily precipitation gauge located within it.

Similar methods were used to create the AMS for the 24-, 72-, and 96-hour durations.

The AMS for each precipitation gauge was stored in the L-RAP ASCII Text format (Schaefer and Barker, 2009).

6.4. Quality Checking of Precipitation Annual Maxima Time-Series

In addition to the quality assurance and quality control process described above, the AMS for each precipitation gauge was subject to additional rigorous quality control protocols to remove invalid data and false annual maxima. Data quality checking was accomplished by examining the completeness of the record for each appropriate season or climatic year and scanning the AMS to identify anomalously small or large precipitation amounts using data quality checking software previously developed by MGS Engineering Consultants (Schaefer, 1997a). The software flagged observations with large

precipitation magnitudes that were not sufficiently corroborated by annual maxima at other nearby gauges. These observations were then considered by a storm analyst to determine if the observation was accurate. The software also identified, and subsequently accepted or rejected, low precipitation annual maxima for climatic years when data were missing for days, weeks, or months using a Bayesian-type approach.

6.4.1. Identification of Low Precipitation Annual Maxima

The Bayesian approach provides an estimate of the probability of a low precipitation annual maximum being the true season or climatic year annual maximum using conditional probabilities. The inputs into the software are: 1) completeness of record, which can be viewed directly as the probability that the true annual maxima were observed during the time period when measurements were taken/recorded; and 2) the non-exceedance probability of the annual maxima for that gauge computed using the ranked order of the annual maxima in the dataset. This is computed as *i/N*, where *i* is the rank of the annual maxima based on ordering from smallest to largest, and *N* is the total number of data elements. Heuristically, data near the upper end of observations (higher amounts of precipitation) are likely to be true annual maxima, and data ranked near the smaller end of observations (lower amounts of precipitation) are more suspect.

The Bayesian Probability of an annual maximum being a true seasonal or climatic year annual maximum is equal to:

$$\frac{P_C * P_r}{(P_c * P_r + (1 - P_c) * (1 - P_r))} \qquad \text{Equation 1}$$

where:

Pc = probability (evidence) of being true annual maximum based on completeness of record,
Pr = probability of being true annual maximum based on ranking, computed as (*i/N*) and ordered from smallest to largest.

This determines the Bayesian probability computed as evidence for being a true annual maximum divided by the combined probability of being true plus the probability of being false.

In short, if there are numerous observations missing from the record, and the annual maximum ranks near the low end of the dataset, it is likely to be a false annual maximum and should be rejected. Conversely, if the candidate is among the largest annual maxima, it should be accepted even if 50% of the record is missing.

Additionally, annual maxima were automatically accepted if the completeness was greater than a given threshold (usually 85%). This avoids too frequent rejections for the smallest annual maxima in the dataset which are true annual maxima. These values would otherwise need a very high level of completeness to avoid rejection from Bayesian computation.

In summary, the Bayesian computation brings a more quantitative and objective approach to quality control. It is followed by additional quality control measures during the precipitation-frequency analysis, including a measure of discordancy (Hosking and Wallis, 1997) which can identify stations whose sample statistics are markedly different from other gauges within a given region.

6.4.2. Identification of High Precipitation Annual Maxima

The largest annual maxima in the dataset were validated by corroboration with precipitation amounts and timing from nearby stations or by reviewing published data records. For the U.S. data, the data records were from the NCEI and included the original daily Observation Forms, Storm Data reports, Monthly Climatological Data publications, and other documents.

Similarly, Canadian data were checked by reviewing reports/tables available at ECCC's website and other in situ meteorological variables (e.g., snowfall and temperature).

Validating the largest annual maxima by corroboration with nearby stations was completed with the aid of a visualization tool (Figure 19). Here, the suspect xx-hour annual maximum is highlighted in the center of the map image, and stations within a radius of 100-miles (~161-km) are also depicted and labeled with their associated xx-hour accumulated precipitation observations from that time period.

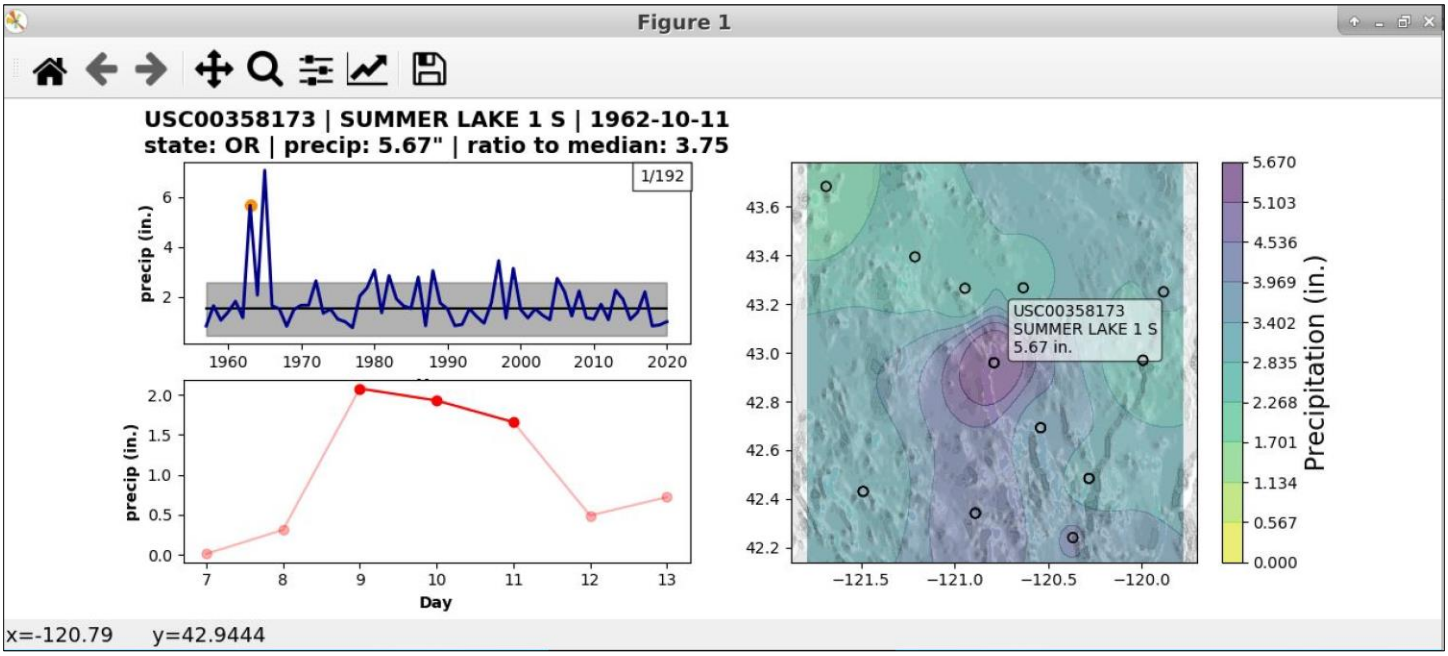

Figure 19: Visualization tool to view corroborating stations.

6.4.3. Other Adjustments to Annual Maxima Data

Several additional factors were considered during the quality control process, including:

1. **Identification of duplicate gauges** – Duplicate gauge is the term for the situation where two or more gauges are either co-located at a given site, closely located and have overlapping years of record, or when different sources report data from the same gauge. Gauges are considered to be "closely located" if they are within five miles (~8-km) of each other and within 500-ft. (~150-m) of elevation (increased to 1,000-ft. [~300-m] of elevation in the Coastal region to account for the steep terrain). Duplicate gauges are not considered in regional precipitation-frequency analysis to avoid double-counting.

2. **Merging of data from nearby gauges** – It is common for precipitation gauges to be moved short distances from time to time, primarily to accommodate a change in operator/observer. Some precipitation AMS were formed using data from two or more gauges in these situations. Gauges less than five miles apart (~8-km), within 500-ft. (~150-m) of elevation (or 1,000-ft. [~300-m] of elevation in the Coastal region), and with non-overlapping periods of record were merged into a single AMS to create a long-term record. Figure 20 shows an example of two gauge records (one in blue, another in orange) that were merged.

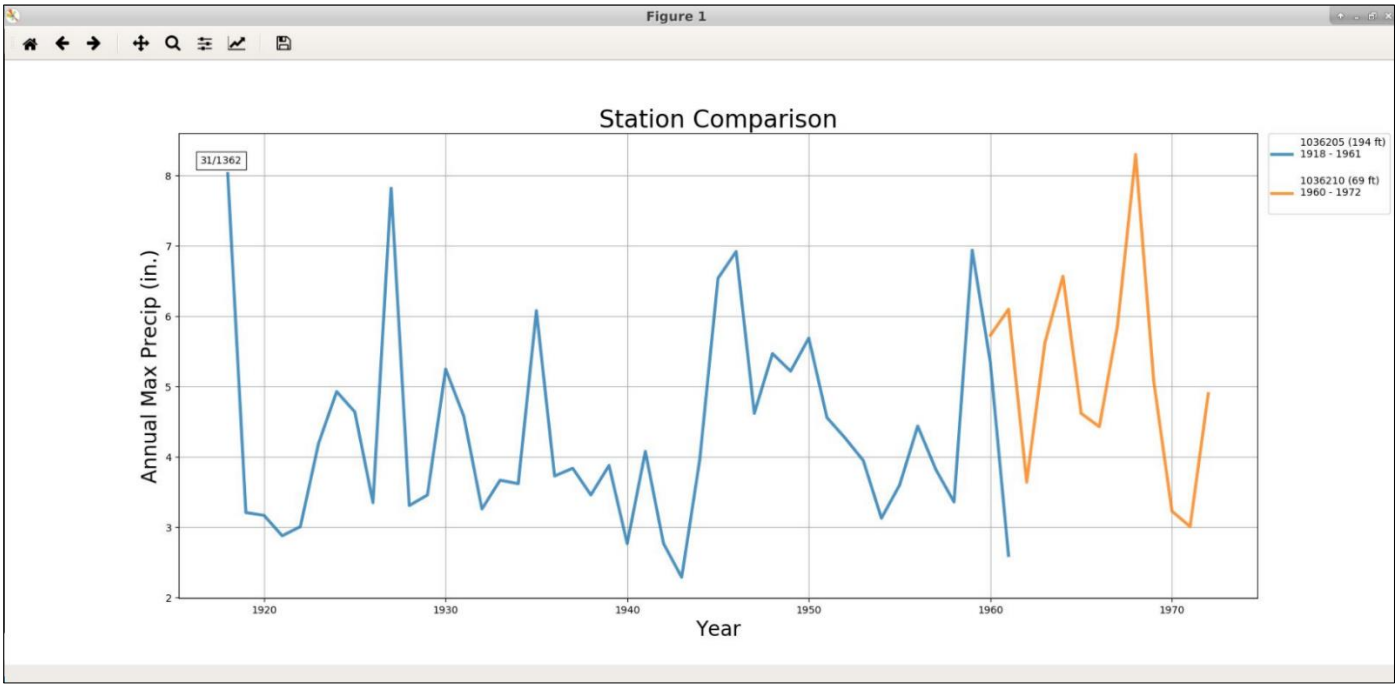

Figure 20: Example of AMS records that were merged.
Stations shown are Port Alberni (1036205) and Port Alberni Redford (1036210).

3. **Observation period adjustments** – Precipitation is reported on a fixed time interval and not on a continuous duration. For example, at a daily precipitation gauge where measurements are taken each day at 8 AM, part of a continuous 24-hour precipitation event may be reported on day 1, and the remainder on day 2. The maximum 1-day measurement therefore underestimates the continuous 24-hour measurement. In a similar way, a 2-day accumulation measurement can underestimate a 48-hour maximum. Standard practice is to use observational period adjustments to adjust the sample statistics for the mean and standard deviation from the fixed interval measurements to the representative continuous measurements (Weiss, 1964). Observational period adjustments were applied to the sample at-site-mean values at all precipitation gauges for each of the four durations of interest (Table 4).

Table 4: Observational period adjustments.

Duration	Observational Period Adjustment
24-hours	1.13
48-hours	1.04
72-hours	1.03
96-hours	1.02

6.5. Final AMS Datasets

After the quality control and merging measures were complete, the final AMS precipitation dataset of MLC storms consisted of 1,488 daily stations for 48-hours (Figure 21). For the other durations of interest (24-, 72-, and 96-hours), the final AMS dataset consisted of essentially the same set of stations, with minor differences.

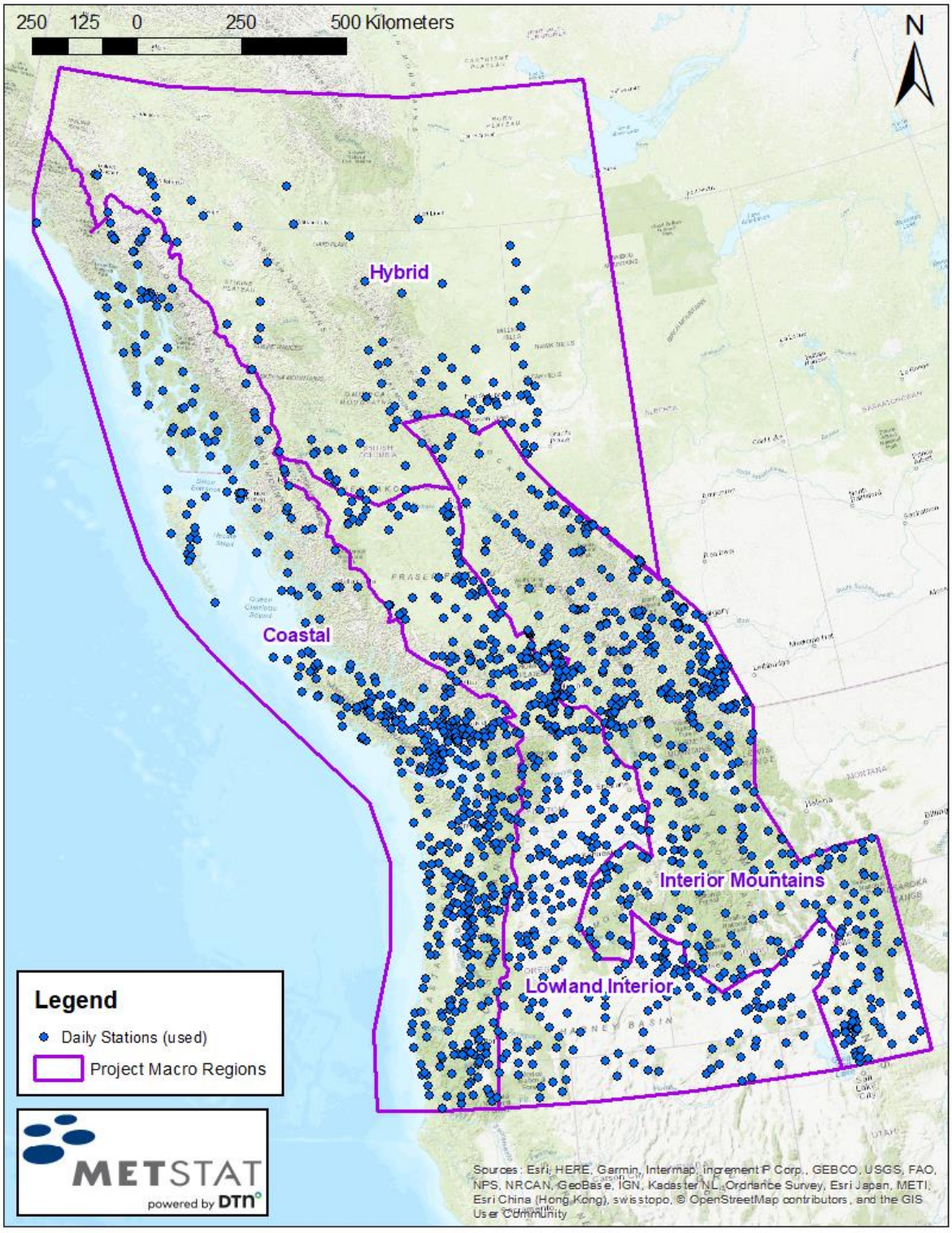

Figure 21: Map of daily precipitation gauges used in the precipitation-frequency analysis.

7. REGIONAL POINT PRECIPITATION-FREQUENCY ANALYSIS

With the completion of the final AMS datasets for each the four durations of interest, the regional point precipitation-frequency analysis may begin. This continues the path set forth by the SWT climate region method (See Section 2: Approach), repeated here:

1. Assemble and quality-check the input annual maxima dataset (Section 6.5);
2. Delineate and verify the homogeneous regions using regional L-Moment statistics (Section 7.1);
3. Analyze the spatial behavior of the precipitation at-site mean and regional L-Moment ratios L-Cv and L-Skewness for use in spatial mapping (Section 7.2);
4. Identify the regional probability distribution for computing precipitation AEPs (Section 7.3);
5. Compute the Equivalent Independent Record Length (EIRL) to estimate the effective independent size of the regional dataset (Section 7.4); and
6. Produce gridded datasets of precipitation for selected AEPs from the median to at least 0.001 AEP (Section **Error! R eference source not found.**).
7. Compute the uncertainty bounds at the 5^{th} and 95^{th} percentiles (Section 7.6).

7.1. Homogenous Sub-Regions

Using the Climate Regions (Section 4.2, Figure 4) as an initial guide, candidate Homogeneous Sub-Regions were constructed for each duration of interest. Homogeneous Sub-Regions are collections of stations within the larger Climate Regions that fall within a small range of selected climatic and/or location indices and satisfy statistical homogeneity criteria.

To form a candidate Homogeneous Sub-Region, 8-15 stations (more typically, 10-13 stations) in a Climate Region were grouped together by considering either the climatic index of mean annual precipitation (mm; from ClimateNA [Wang et al., 2016]) or the location index of latitude (decimal degrees). Each of the four Project Macro Regions were considered independently. The L-Moment heterogeneity measures H1 and H2 were used to assess the homogeneity of the candidate Homogeneous Sub-Regions (Hosking and Wallis, 1997). An H1 value of 1.0 was originally proposed by Hosking and Wallis (1997) to determine if a candidate sub-region was acceptably homogeneous. That criterion was based solely on statistical considerations of the sampling characteristics of L-Cv and L-Skewness. For this project, H1 and H2 less than 2.0 were used which also account for variability associated with machine- and human-induced aspects of precipitation measurement and recording. In some instances, H1 and H2 values greater than 2.0 were allowed due to the sampling variability of the precipitation measurements within that grouping of stations (marginal homogeneity). All H1 values were less than 3.0, which is sufficiently statistically homogeneous for the SWT climate region method. Table 5 lists the number of Homogeneous Sub-Regions created for each Project Macro Region for the 48-hour duration. Similar totals were established for the other durations of interest.

Table 5: Number of Homogeneous Sub-Regions by Project Macro Region for the 48-hour duration.

Project Macro Region	Total Number of Candidate Homogeneous Sub-Regions	Number of Candidate Homogeneous Sub-Regions with H1 and H2 less than 2.0	Number of Candidate Homogeneous Sub-Regions with H1 and H2 greater than 2.0 (marginal homogeneity)
Coastal	44	37	7
Lowland Interior	23	22	1
Interior Mountains	42	42	0
Hybrid	6	6	0
TOTAL	**115**	**107**	**8**

7.2. Spatial Mapping of L-Moments

Spatial mapping of the at-site mean, regional L-Cv, and regional L-Skewness for the four durations of interest was accomplished by developing predictor equations which relate the L-Moments to climatic and physiographic variables, such as mean annual precipitation (Schaefer and Barker, 2009; MGS et al., 2015). The following sections describe the mapping procedures for each of the regional L-Moment statistics. Once spatially mapped, these statistics were used to develop grids of precipitation magnitudes at various AEPs.

7.2.1. Spatial Mapping of At-Site Means

7.2.1.1 At-Site Means at the 48-Hour Duration

Spatial mapping of the at-site means at the 48-hour duration involved a three-step process:

1. Determine a predictor equation that describes the regional behavior of the at-site means for stations within a given at-site mean (ASM) Mapping Area, where an ASM Mapping Area is a grouping of Climate Regions that exhibit similar at-site mean behaviors;

2. Compute a best-estimate of the at-site mean at a given station using an empirical Bayes solution (Kuczera, 1982) which is essentially a weighted average of the regionally-predicted at-site mean (from Step 1) and the observed sample at-site mean, where the weights are a function of the unexplained variance for the predictor equation and the sampling variance for the station based on record length; and

3. Adjust the best-estimate at-site means to account for spatial coherence of the standardized error residuals from nearby stations (observed minus predicted /predicted) in a given locality.

For Step 1, a review of the behavior of the observed sample at-site means for several Climate Regions (Figure 4) allowed for the grouping of at-site mean data from adjacent Climate Regions to develop 18 ASM Mapping Areas at the 48-hour duration (Figure 22). This approach led to the formulation of a single predictor equation for each ASM Mapping Area. The candidate explanatory variables for the predictor equations had to be spatially continuous across the Project Domain (e.g., latitude, longitude, elevation, mean annual precipitation, etc.). The final explanatory variables used for the at-site mean predictor equations at the 48-hour duration were gridded values of mean annual precipitation (mm; normal from 1960-1991 from ClimateNA [Wang et al., 2016]) and latitude (decimal degrees). Generalized additive modeling methods were used to combine the explanatory variables into a single predictor equation for each ASM Mapping Area (Table 6).

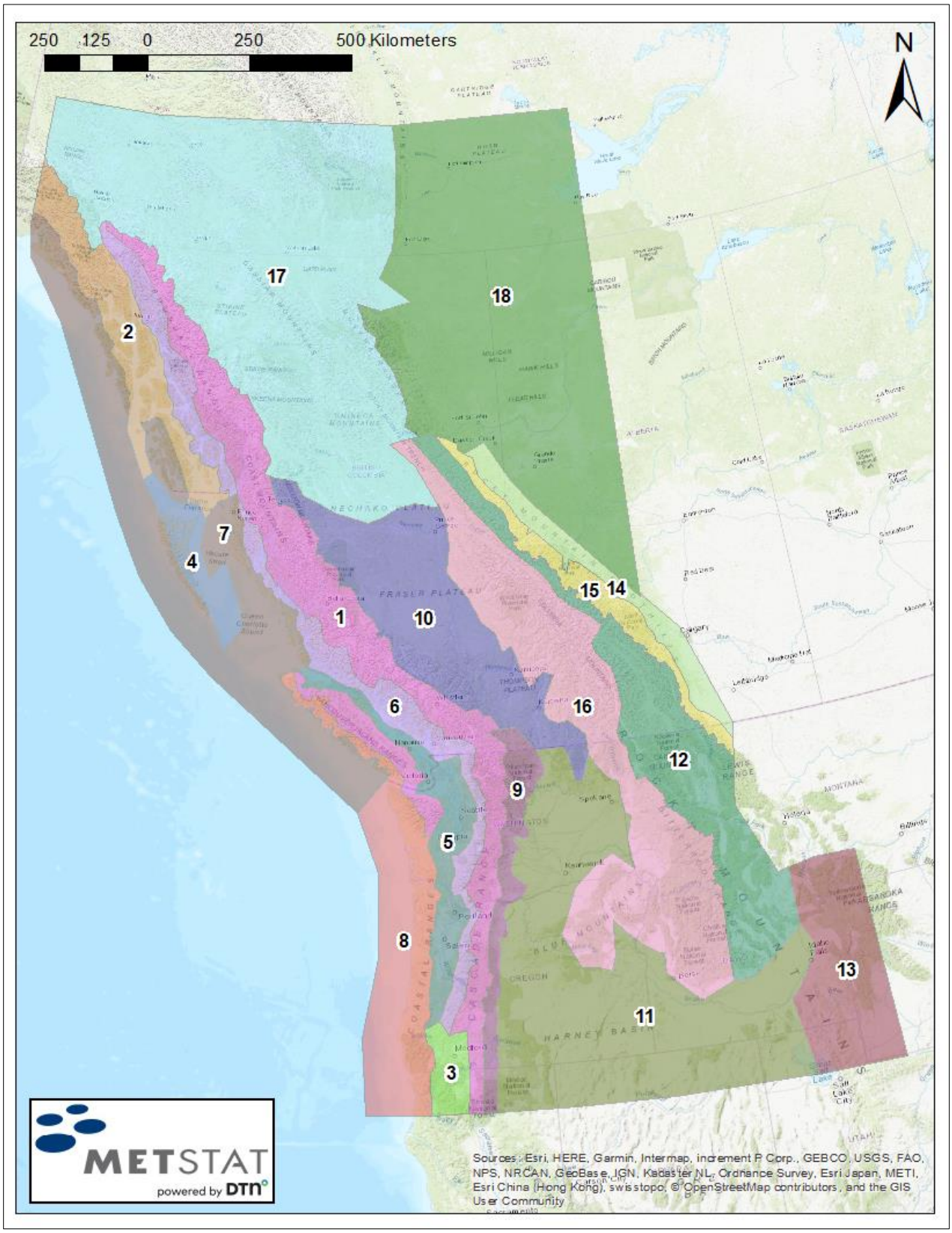

Figure 22: ASM Mapping Areas for the 48-hour duration.

Table 6: Predictor equations and resultant relative RMSE for the at-site means by ASM Mapping Area at the 48-hour duration. ASM Mapping Areas correspond to Figure 22.

ASM Mapping Area	Predictor Equations	Relative RMSE
1	$y = 0.6532a - 1.4526$	15.6%
2	$y = -0.3026a^2 + 3.1079a - 6.3830$	19.3%
3	$y = 0.7179a - 1.5798$	12.4%
4	$y = 0.6532a - 1.7630$	16.6%
5	$y = 0.81684a - 2.0163$	12.6%
6	$y = 0.7843a - 1.9478$	15.7%
7	$y = 0.8773a - 2.3184$	16.1%
8	$y = 0.6481a - 1.4066$	15.6%
9	$y = 0.7176a - 1.6223$	10.9%
10	$y = 0.6661a - 1.6369$	15.7%
11	$y = 0.5991a - 1.3985$	9.8%
12	$y = 0.4320a - 1.0140$	11.9%
13	$y = 0.3870a - 0.8725$	14.0%
14	$y = 0.2825a - 2.4513b + 3.7582$	12.4%
15	$y = 0.4846a - 1.0569$	25.1%
16	$y = 0.4846a - 1.2195$	9.7%
17	$y = 0.1269a^2 - 0.1967a - 0.2880$	11.4%
18	$y = 0.6884a - 1.5360$	12.8%

*y is the value of regional At-Site Mean;
a is the log10 transform of mean annual precipitation in (mm); and
b is the log10 transform latitude in decimal degrees.

The relative root-mean-square error (RMSE) for the regionally-predicted at-site mean values are also provided in Table 6. The relative RMSE values range from 9.7% to 25.1%. The ASM Mapping Areas with the largest RMSE were ASM Mapping Areas 2, 4, and 15:

- ASM Mapping Area 2 had a RMSE of 19.3% because it had only 17 stations in its domain, even though the domain was quite expansive. RMSE typically improves with increased amounts of data.

- ASM Mapping Area 4 had a RMSE of 16.6%. Again, this area had few stations (seven total). This ASM Mapping Area corresponded with Climate Region 49 on Haida Gwaii (Queen Charlotte Islands). Due to the unique topography and location of the islands, this ASM Mapping Area could not be combined with any other ASM Mapping Area.

- ASM Mapping Area 15 had a RMSE of 25.1%. This long, thin ASM Mapping Area had 27 stations and included the eastern foothills of the Canadian Rockies. Due to the varied elevation, identifying a trend in the station data was challenging. Nonetheless, there is confidence that the predictor equation for this ASM Mapping Area is sufficient given that it was ascertained by using the same slope as a nearby well-behaving ASM Mapping Area (ASM Mapping Area 16) and adjusting the slope for minimal bias.

For Step 2, the best-estimate of the at-site means at the stations were obtained using an Empirical Bayes Approach (Kuczera, 1982) as a weighted average of the regionally-predicted at-site mean value and the observed sample at-site mean. Greater weight was given to the observed sample at-site mean value as the record length at the station increased.

For Step 3, the standardized residuals were calculated as the difference between the observed sample at-site mean and the regionally-predicted at-site mean normalized by the regionally-predicted at-site mean. Adjustments were made to the best-estimate of the at-site means to account for coherence in the spatial distribution of residuals from nearby stations, where the standardized residuals in a given geographic area were not random, but rather systematically over-estimated or under-estimated the station at-site mean relative to the regionally-predicted at-site mean.

Figure 23 depicts a comparison of observed sample at-site mean values and mapped at-site mean values at the 48-hour duration. The observed station at-site mean values that are most distant from the red line of equality are mostly associated with stations with short record lengths.

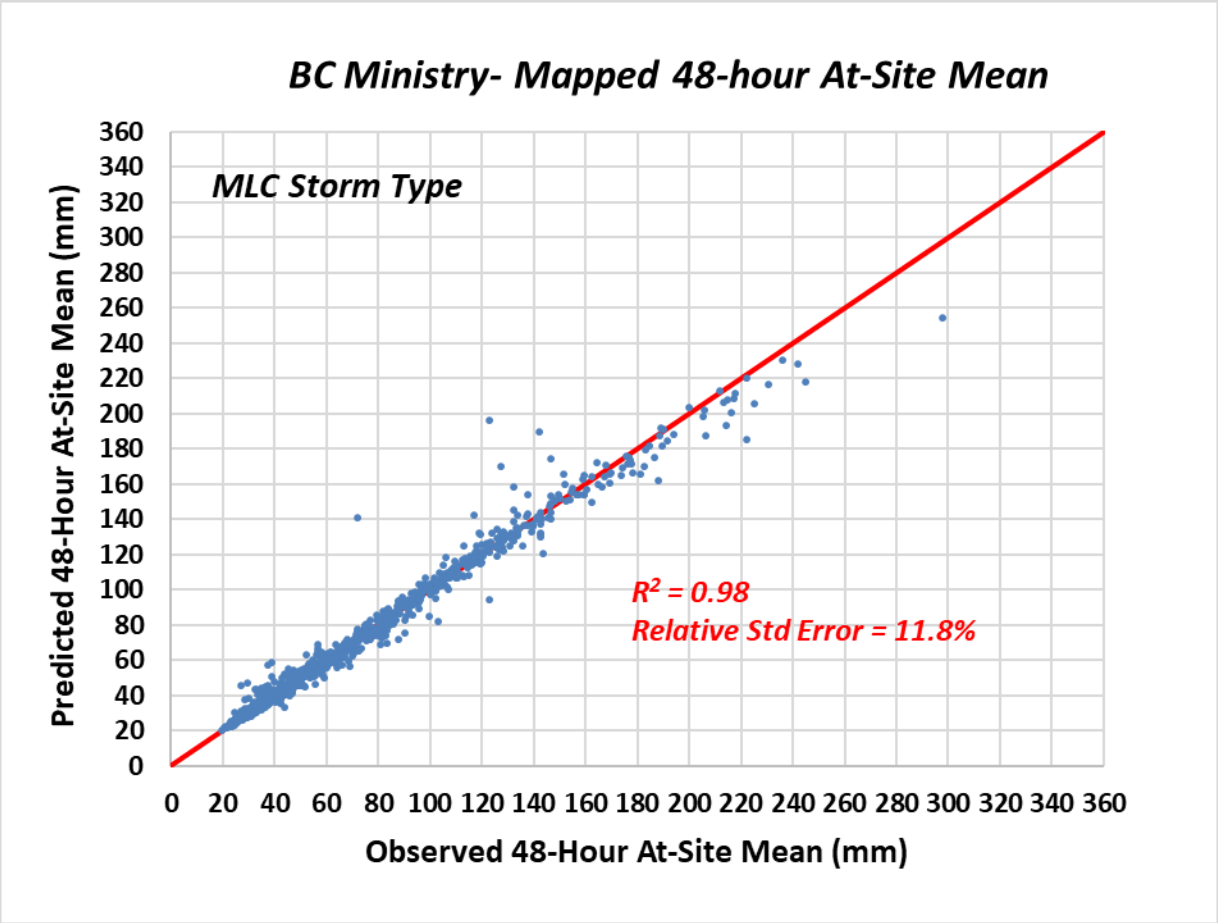

Figure 23: Comparison of observed and mapped at-site means at the 48-hour duration.

Due to the adoption of ASM Mapping Areas to define the predictor equations, it was inevitable that there would be some level of discontinuity at the boundaries between the ASM Mapping Areas. In fact, the boundaries exist because differences in spatial behavior of the observed sample at-site means between ASM Mapping Areas warranted separating the ASM Mapping Areas as opposed to combining them into a single region. Spatial smoothing occurred along the boundaries between the ASM Mapping Areas using a weighted matrix (15x23 grid cells, nominally 15-km) to determine the percent by which each ASM Mapping Area contributed to a given grid cell. Contributing predictor equations from each ASM Mapping Area were then applied to each grid cell, weighted by the percent contributed from each ASM Mapping Area. This resulted in smooth, natural transitions over limited areas between the ASM Mapping Areas.

The final spatial map of the at-site means at the 48-hour duration is shown in Figure 24. It should be noted that the area in northeast British Columbia has a limited number of stations and low population, so additional attention could be given to this area if needed in the future.

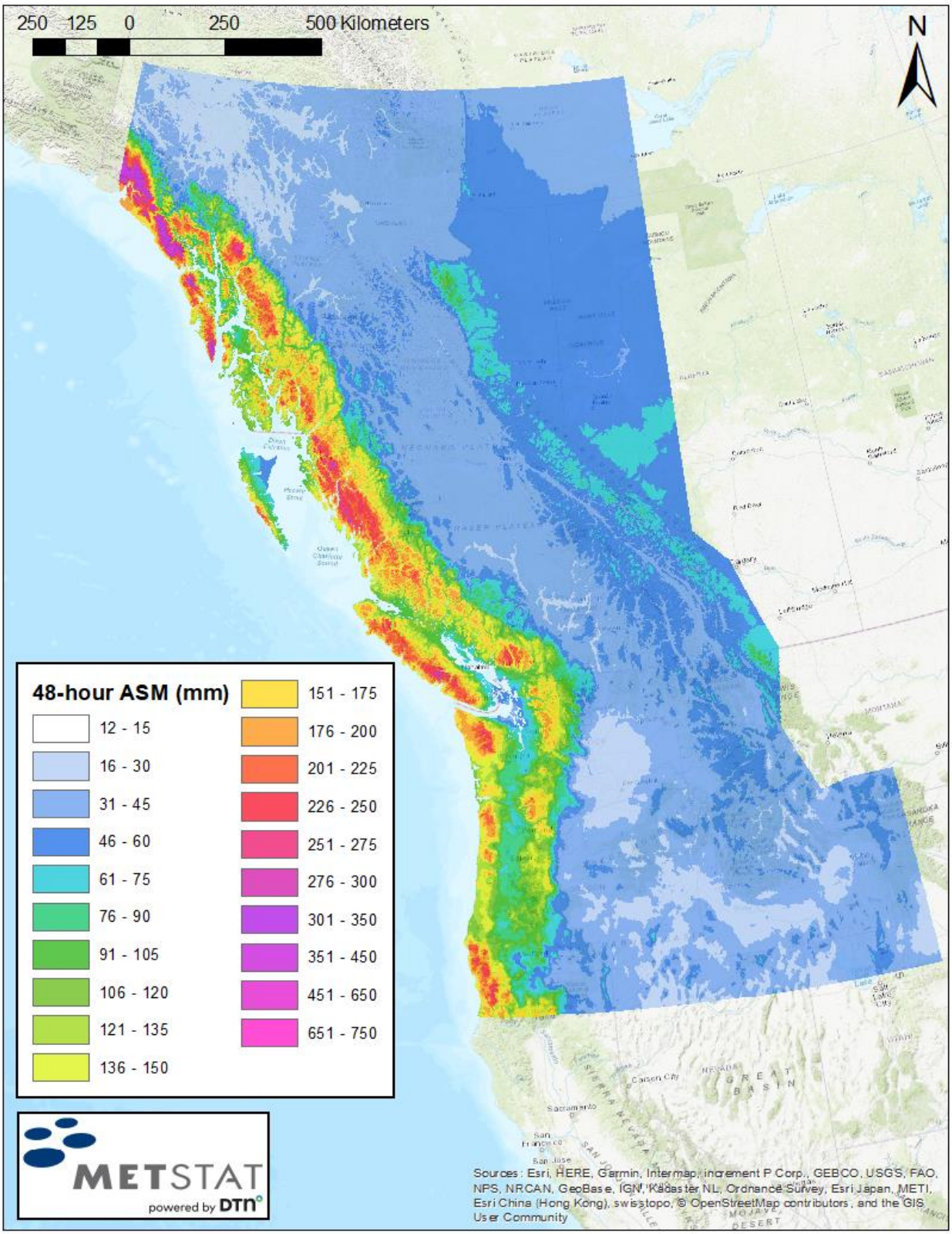

Figure 24: Map of the at-site means at the 48-hour duration.

7.2.1.2 At-Site Means at the 24-, 72-, and 96-Hour Durations

The computations for the gridded values of the at-site means at the 24-, 72-, and 96-hour durations relied on linear regressions between the observed sample at-site means at the 48-hour duration and the observed sample at-site means at the 24-hour (or 72- or 96-hour, as appropriate) duration. The linear regressions were calculated for each of the four Project Macro Regions independently, but with some modifications:

- For the 24-hour duration, the Interior Mountain region was divided into the Interior Mountains North, Climate Region 151, and Interior Mountains South for a total of six ASM Mapping Areas (Figure 25).
- For the 72- and 96-hour durations, the Interior Mountain region was divided into the Alberta mountains (Climate Regions 79 and 82 in Figure 4) and the British Columbia mountains (all other Climate Regions in the Interior Mountains Project Macro Region) for a total of five ASM Mapping Areas (Figure 26).

The modifications to the Project Macro Regions resulted in improved predictor relationships. The linear regression relationships for the 24-hour duration are found in Table 7, and the linear regression relationships for the 72-hour and 96-hour durations are found in Table 8 and Table 9, respectively.

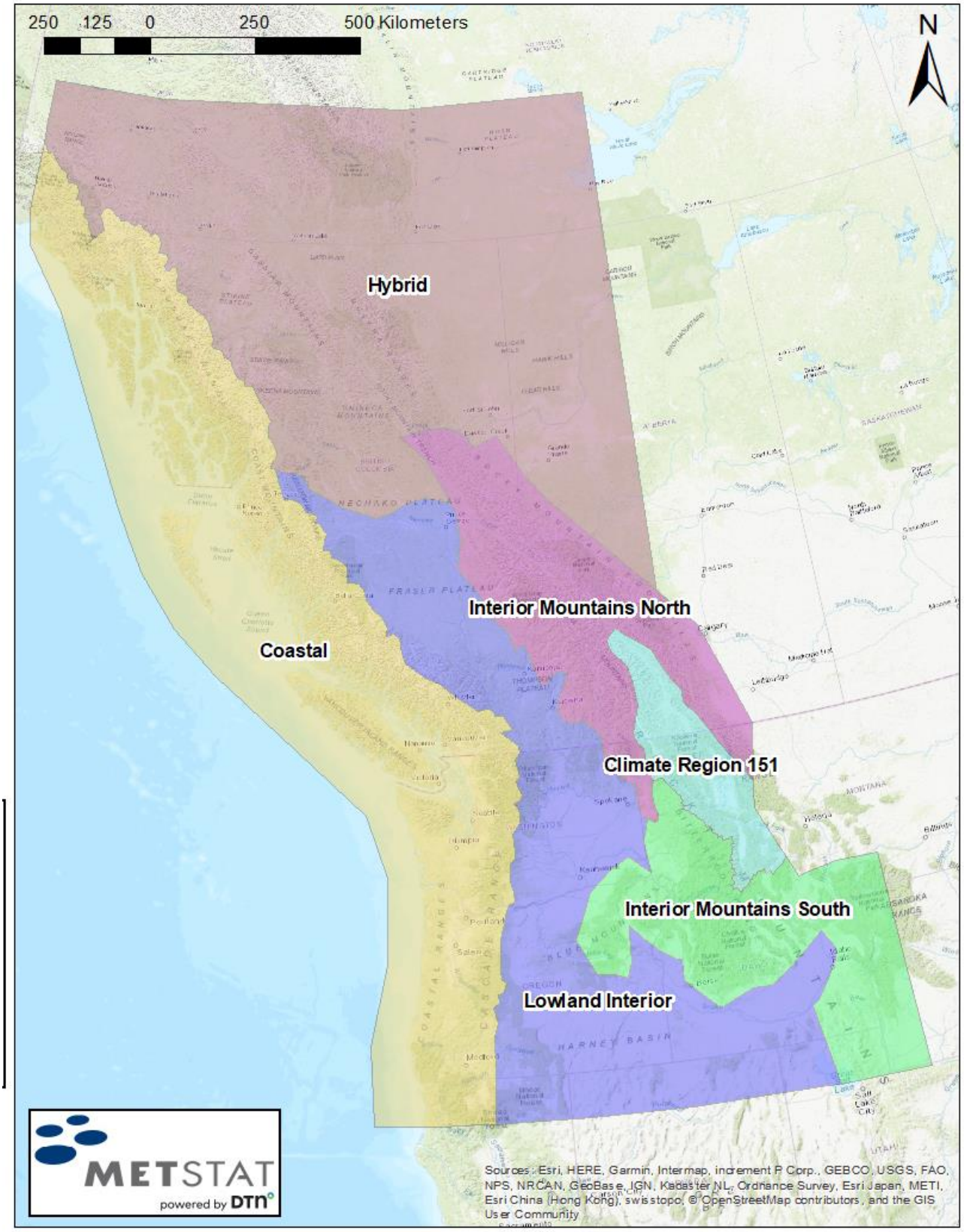

Figure 25. ASM Mapping Areas for the 24-hour duration.

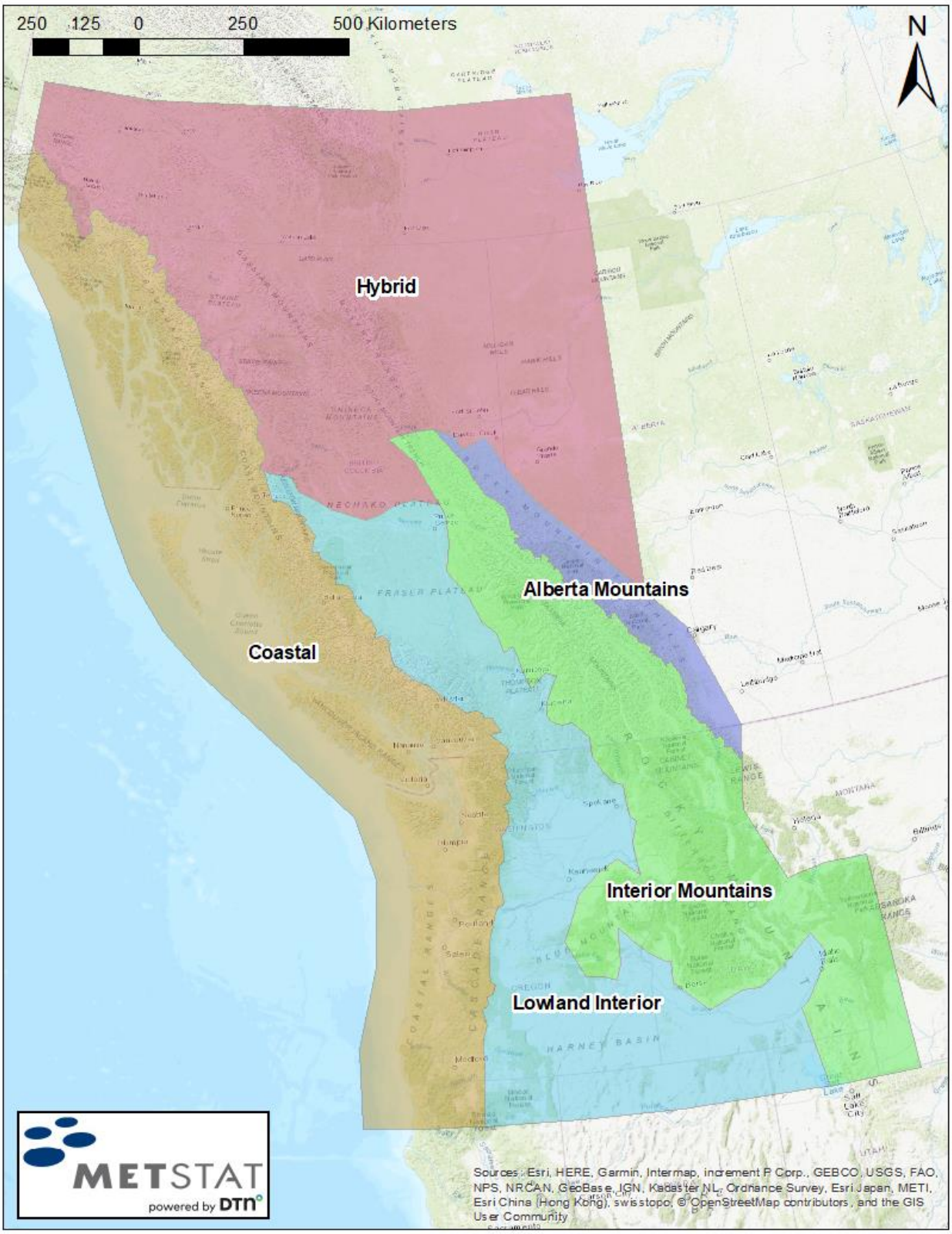

Figure 26: ASM Mapping Areas for the 72- and 96-hour durations.

Table 7: Linear regression equations for the at-site means at the 24-hour duration. The ASM Mapping Areas correspond to Figure 25.

ASM Mapping Area	Regression Equation	Constraint
Coastal	$y = 0.7249x + 0.1123$	none
Lowland Interior	$y = 0.7223x + 0.1682$	none
Interior Mountains South	$y_s = 0.7664x + 0.1138$	none
Hybrid	$y = 0.75848x + 0.07834$	none
Interior Mountains North	$y_n = 0.68783x + 0.04425$	none
Climate Region 151	$w = 1.00 - \frac{(z - 47.8)}{2}$ $y = w * y_s + (1 - w) * y_n$	if $z \geq 49.8$, then w= 1.00 if $z \leq 47.8$, then w=0.00

*where y is the observed sample at-site mean at the 24-hour duration; w is a weight function; x is the observed sample at-site mean at the 48-hour duration; and z is latitude.

Table 8: Linear regression equations for the at-site means at the 72-hour duration. The ASM Mapping Areas correspond to Figure 26.

ASM Mapping Area	Regression Equation
Coastal	$y = 1.21589x - 0.08303$
Lowland Interior	$y = 1.19440x - 0.10620$
British Columbia Mountains	$y = 1.15425x - 0.06065$
Alberta Mountains	$y = 1.08386x - 0.02691$
Hybrid	$y = 1.09917x + 0.02552$

*where y is the observed sample at-site mean at the 72-hour duration; and x is the observed sample at-site mean at the 48-hour duration.

Table 9: Linear regression equations for the at-site means at the 96-hour duration. The ASM Mapping Areas correspond to Figure 26.

ASM Mapping Area	Regression Equation
Coastal	$y = 1.3774x - 0.1703$
Lowland Interior	$y = 1.3360x - 0.1850$
British Columbia Mountains	$y = 1.3050x - 0.1454$
Alberta Mountains	$y = 1.1868x - 0.1143$
Hybrid	$y = 1.12350x + 0.08623$

*where *y* is the observed sample at-site mean at the 96-hour duration; and *x* is the observed sample at-site mean at the 48-hour duration.

The advantage of using linear regressions for the 24-, 72-, and 96-hour durations based on the observed sample at-site means from the 48-hour duration guaranteed that the final point precipitation-frequency relationships for each duration of interest would not cross one another at a location. The observed sample at-site means at the 48-hour duration were considered (as opposed to the mapped at-site means at the 48-hour duration from Figure 24) in the regression relationships to eliminate any adulteration from 1) the application of the standardized residuals or 2) smoothing at the ASM Mapping Area boundaries.

The linear regressions found in the above tables were then applied to the mapped at-site means at the 48-hour duration (Figure 24), such that the variable *x* is the at-site mean at the 48-hour duration from Figure 24, and the variable *y* is the predicted at-site mean at the duration of interest. This process allowed for all locations, not just the station locations, to feature an at-site mean value. Additionally, spatial smoothing occurred along the boundaries between the ASM Mapping Areas (Figure 25 and Figure 26) using a weighted matrix (15x23 grid cells, nominally 15-km), similar to the development of the map of the at-site means at the 48-hour duration The final spatial map of the at-site means at the 24-hour duration is shown in Figure 27, and the final spatial maps of the at-site means at the 72- and 96-hour durations are found in Figure 28 and Figure 29, respectively.

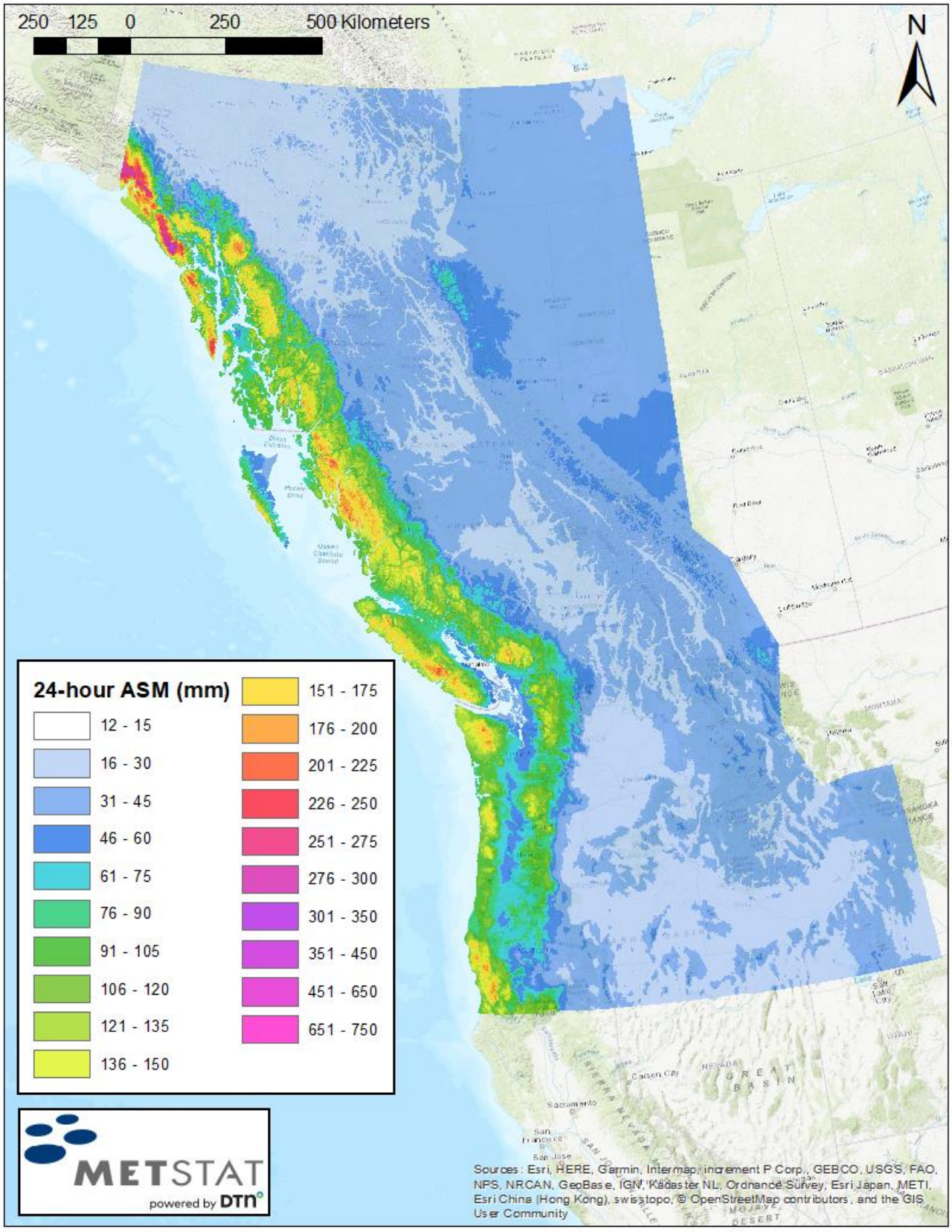

Figure 27: Map of the at-site means at the 24-hour duration.

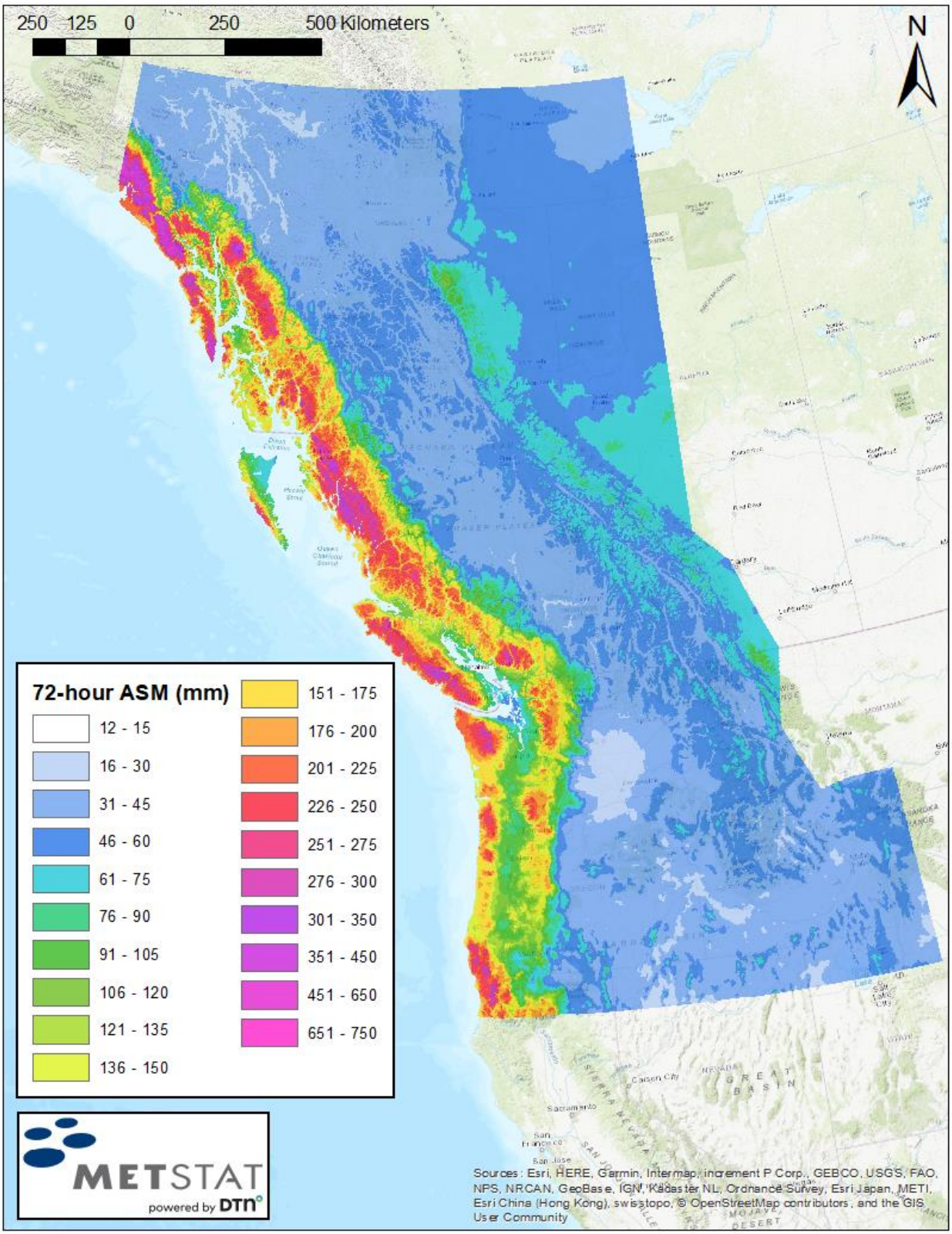

Figure 28: Map of the at-site means at the 72-hour duration.

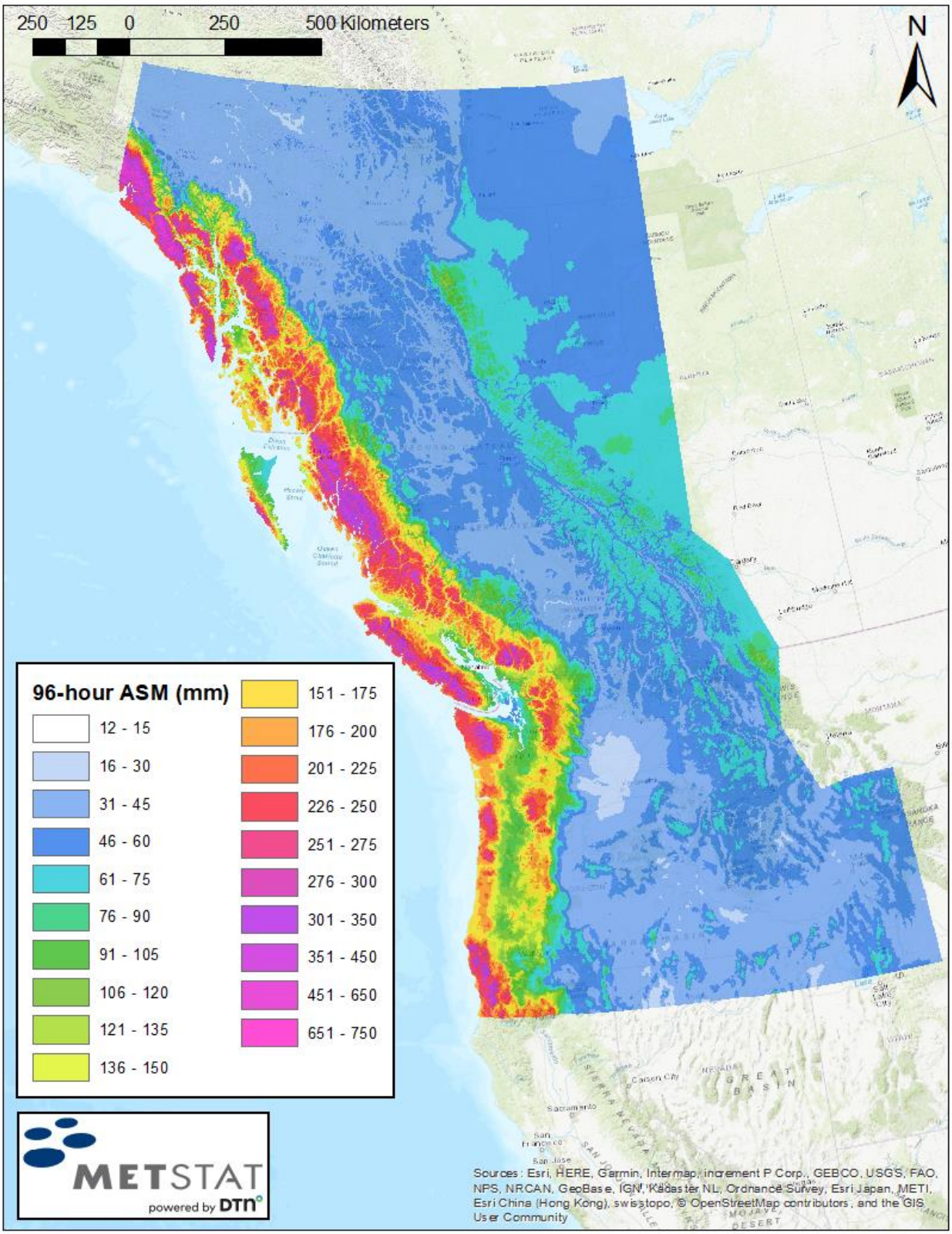

Figure 29: Map of the at-site means at the 96-hour duration.

7.2.2. Spatial Mapping of Regional L-Cv

Predictor equations to spatially map the L-Moment ratio L-Cv were developed based on the behavior of the regional values of L-Cv obtained from the 115 Homogeneous Sub-Regions (see Section 7.1). Each Homogeneous Sub-Region produced a regional L-Cv value associated with the group-average annual maxima precipitation weighted by the station record lengths.

7.2.2.1 L-Cv at the 48-Hour Duration

Similar to the methodology for calculating the at-site means at the 48-hour duration, a review of the behavior of the regional L-Cv values from the Homogeneous Sub-Regions allowed for the grouping of regional L-Cv values into L-Cv Mapping Areas. At the 48-hour duration, 17 L-Cv Mapping Areas were formed (Figure 30), and a single predictor equation for each L-Cv Mapping Area was determined. The explanatory variables used for the L-Cv predictor equations at the 48-hour duration were gridded values of mean annual precipitation (mm; normal from 1960-1991 from ClimateNA [Wang et al., 2016]) and latitude (decimal degrees). Generalized additive modeling methods were used to combine the explanatory variables into predictor equations. Specifically, combinations of second order polynomials in real space were found (Table 10). To limit the second order polynomials to a realistic range, constraints were added to the predictor equations (also found in Table 10).

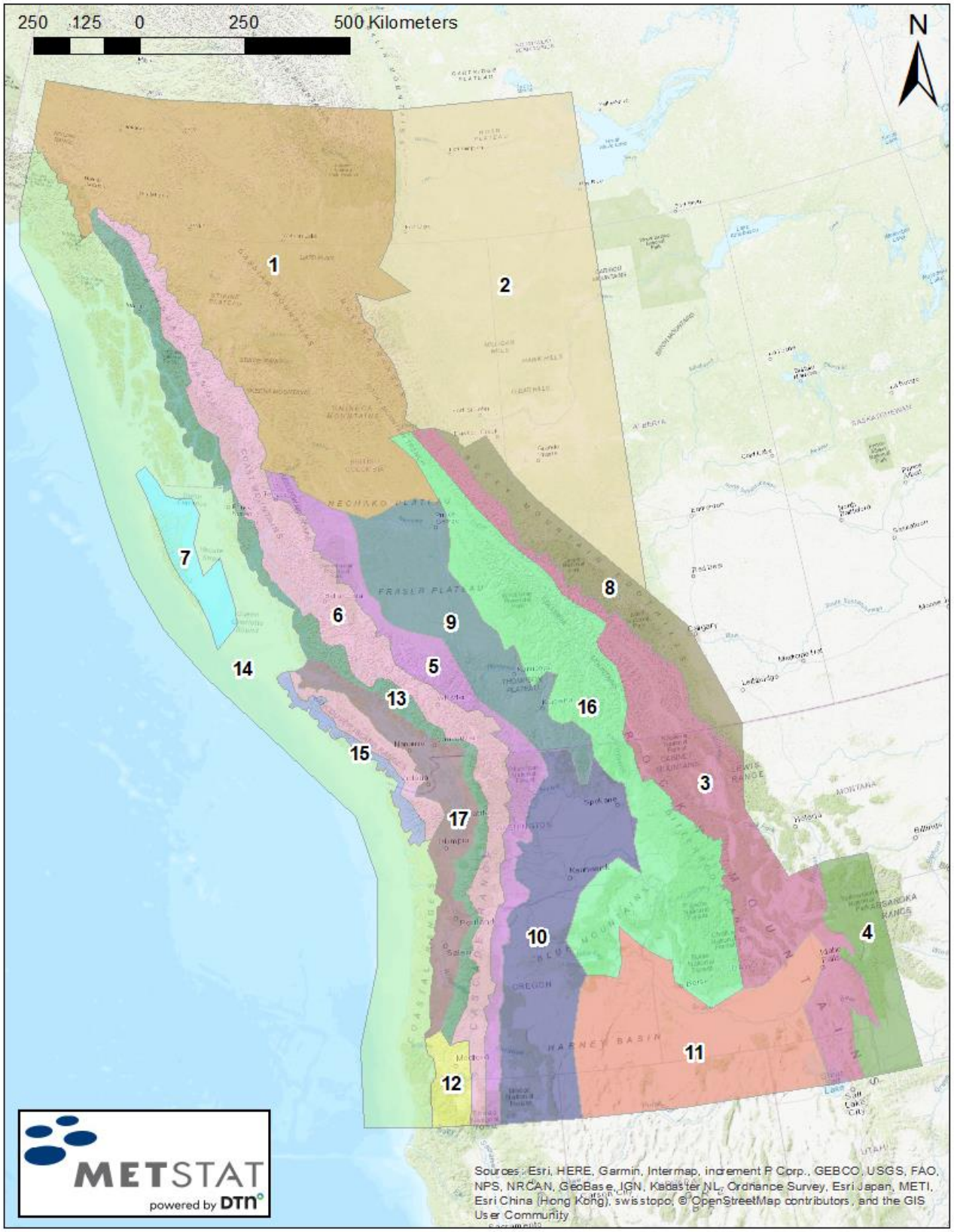

Figure 30: L-Cv (and L-Skewness) Mapping Areas for the 48-hour duration.

Table 10: Predictor equations for regional L-Cv by L-Cv Mapping Area at the 48-hour duration. L-Cv Mapping Areas correspond to Figure 30.

L-Cv Mapping Area	Predictor Equation	Constraint
1	$y = 0.02423a^2 - 0.0842a + 0.2341$	if $a \geq 1.6$, then $y = 0.1725$
2	$y = 0.0005833b^2 - 0.06548b + 2.0530$	if $b \geq 56.0$, then y=0.2150
3	$y = 0.02423a^2 - 0.0842a + 0.2335$	if $a \geq 1.7$, then $y = 0.1600$
4	$y = 0.02423a^2 - 0.0842a + 0.2190$	if $a \geq 1.7$, then $y = 0.1460$
5	$y = 0.007966a^2 - 0.05042a + 0.2335$	if $a \geq 2.6$, then $y = 0.1560$
6	$y = 0.007966a^2 - 0.05042a + 0.2300$	if $a \geq 2.6$, then $y = 0.1535$
7	$y = 0.007966a^2 - 0.05042a + 0.2100$	if $a \geq 2.6$, then $y = 0.1335$
8	$y = 0.0005833b^2 - 0.06548b + 2.0530$	if $b \geq 56.0$, then y=0.2150
9	$y = 0.007966a^2 - 0.05042a + 0.1935$	if $a \geq 2.6$, then $y = 0.1160$
10	$y = -0.0006004b^2 + 0.04544b - 0.07131a - 0.6047$	if $b \geq 41.0$, then y=0.2270
11	$y = 0.23225a^2 - 0.21125a + 0.2295$	if $a \geq 0.45$, then $y = 0.1818$
12	$y = 0.007966a^2 - 0.05042a + 0.2450$	if $a \geq 2.6$, then $y = 0.1685$
13	$y = 0.007966a^2 - 0.05042a + 0.2265$	if $a \geq 2.6$, then $y = 0.1500$
14	$y = 0.007966a^2 - 0.05042a + 0.2300$	if $a \geq 2.6$, then $y = 0.1535$
15	$y = 0.007966a^2 - 0.05042a + 0.2500$	if $a \geq 2.6$, then $y = 0.1735$
16	$y = 0.02423a^2 - 0.0842a + 0.2250$	if $a \geq 1.7$, then $y = 0.1520$
17	$y = 0.007966a^2 - 0.05042a + 0.2160$	if $a \geq 2.6$, then $y = 0.1395$

*y is the value of regional L-Cv;
a is mean annual precipitation in (mm/1000); and
b is latitude in decimal degrees.

The above predictor equations were applied to their respective L-Cv Mapping Area to produce gridded values of L-Cv. To alleviate any discontinuities at the boundaries between the 17 L-Cv Mapping Areas, spatial smoothing along the boundaries occurred using a weighted matrix (15x23 grid cells, nominally 15-km). The spatial smoothing resulted in smooth transitions over limited areas between the L-Cv Mapping Areas. The final spatial map of L-Cv values at the 48-hour duration is shown in Figure 31.

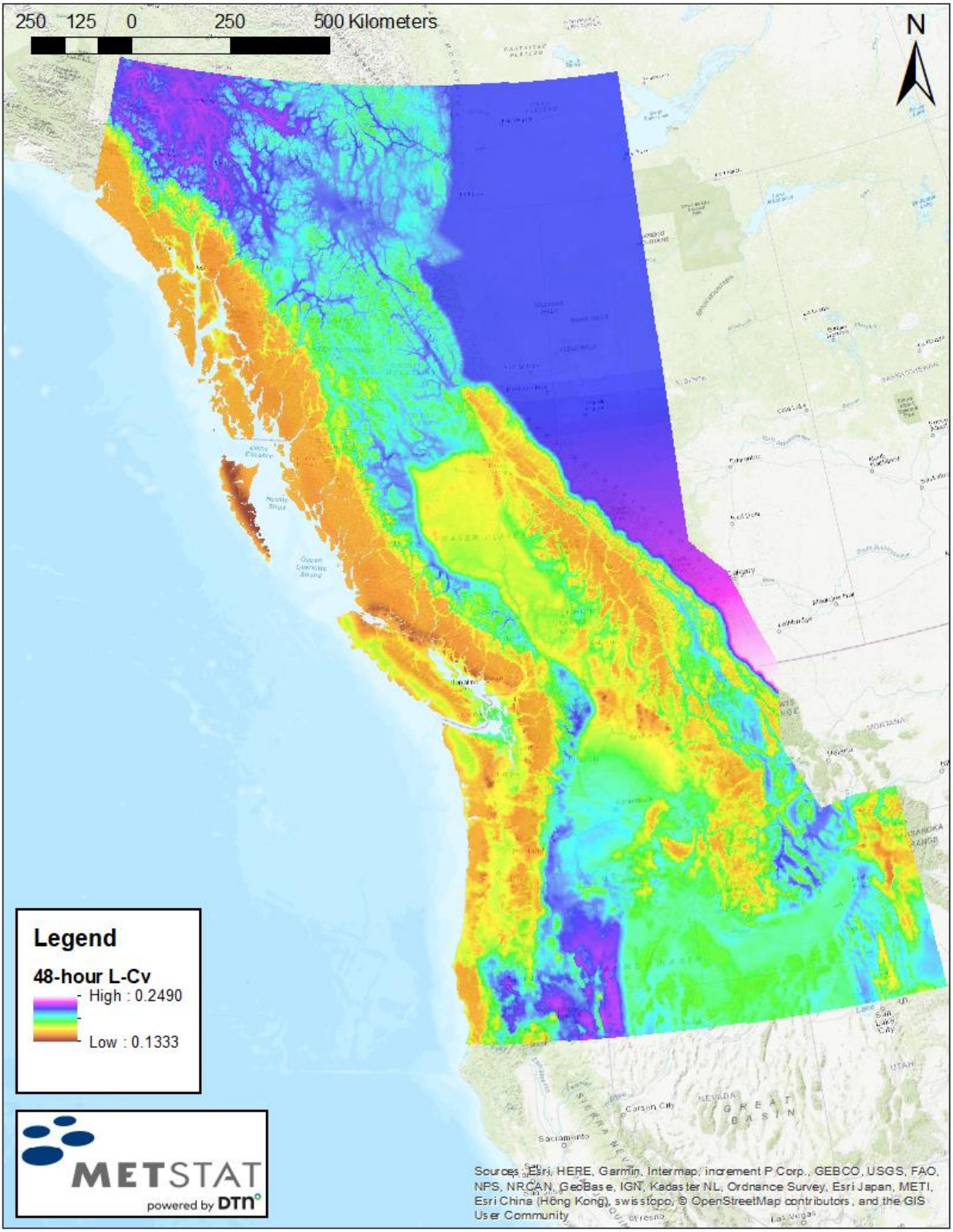

Figure 31: Map of L-Cv at the 48-hour duration.

7.2.2.2 L-Cv at the 24-, 72-, and 96-Hour Durations

The predictor equations to spatially map regional L-Cv at the 24-, 72-, and 96-hour durations used the gridded values of regional L-Cv at the 48-hour duration (Figure 31) as the explanatory variable. The predictor equations were calculated for each of the four Project Macro Regions independently, but with the Alberta mountains (Climate Regions 79 and 82 in Figure 4) moved from the Interior Mountains Macro Region to the Hybrid Macro Region. Statistically, the Alberta mountains exhibited behavior generally more aligned with the Hybrid Macro Region. Thus, there were four L-Cv Mapping Areas at the 24-, 72-, and 96-hour durations (Figure 32). The predictor equations for L-Cv at the 24-hour duration are found in Table 11, and the predictor equations for L-Cv at the 72- and 96-hour durations (same equations for both durations) are found in Table 12.

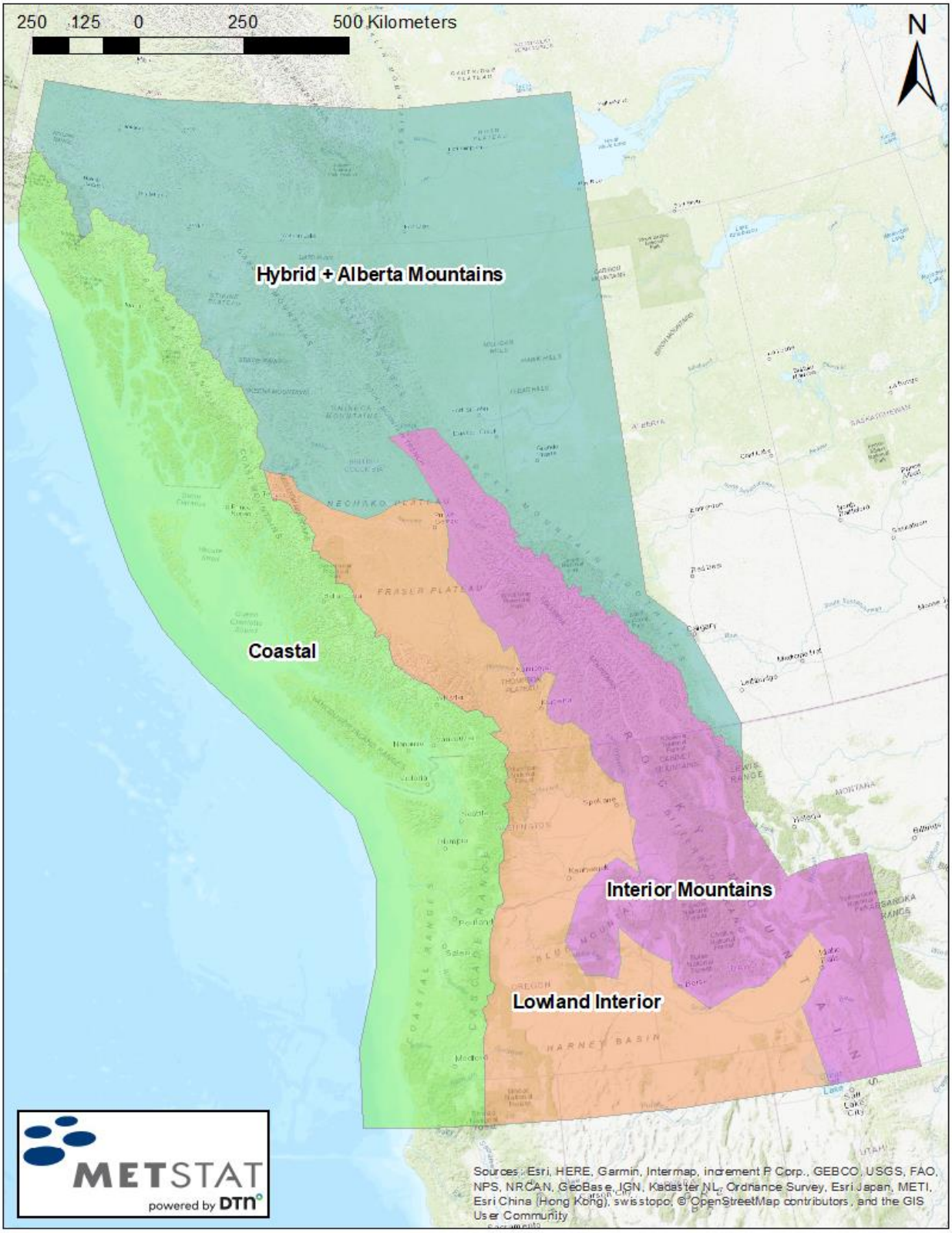

Figure 32: L-Cv (and L-Skewness) Mapping Areas for the 24-, 72- and 96-hour durations.

Table 11: Predictor equations for L-Cv at the 24-hour duration.
L-Cv Mapping Areas correspond to Figure 32.

L-Cv Mapping Area	Predictor Equation
Coastal	$y = 1.0000a + 0.0000$
Lowland Interior	$y = 1.0000a + 0.0000$
Interior Mountains	$y = 1.04a + 0.0013$
Hybrid + Alberta Mountains	$y = 1.04a + 0.0013$

**y* is the value of 24-hour regional L-Cv;
a is mapped 48-hour L-Cv

Table 12: Predictor equations for L-Cv at the 72- and 96-hour durations.
L-Cv Mapping Areas correspond to Figure 32.

L-Cv Mapping Area	Predictor Equation
Coastal	$y = 1.0986a - 0.0236$
Lowland Interior	$y = 1.0986a - 0.0236$
Interior Mountains	$y = 1.0000a + 0.0000$
Hybrid + Alberta Mountains	$y = 1.0000a + 0.0000$

**y* is the value of 72-hour/96-hour regional L-Cv;
a is mapped 48-hour L-Cv

The linear regressions found in the above tables were then applied to the gridded values of L-Cv at the 48-hour duration (Figure 31), such that the variable *a* is the mapped L-Cv at the 48-hour duration, and the variable *y* is the predicted L-Cv at the duration of interest. This resulted in L-Cv values at all locations within the Project Domain. Spatial smoothing occurred along the boundaries between the L-Cv Mapping Areas (Figure 32) using a weighted matrix (15x23 grid cells, nominally 15-km). The final spatial map of L-Cv at the 24-hour duration is found in Figure 33, and the final spatial map of L-Cv at the 72- and 96-hour durations (same equations for both durations) may be found in Figure 34.

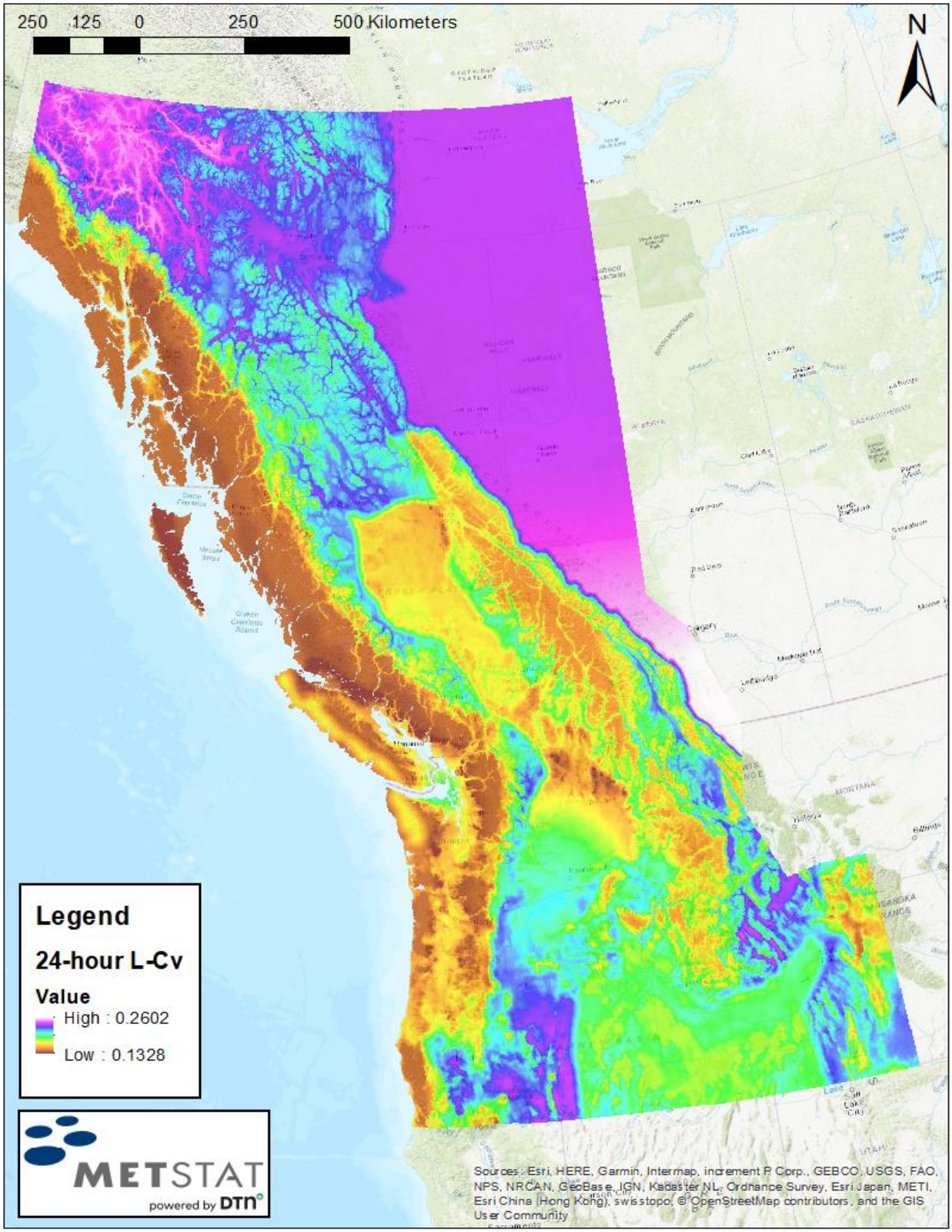

Figure 33: Map of L-Cv at the 24-hour duration.

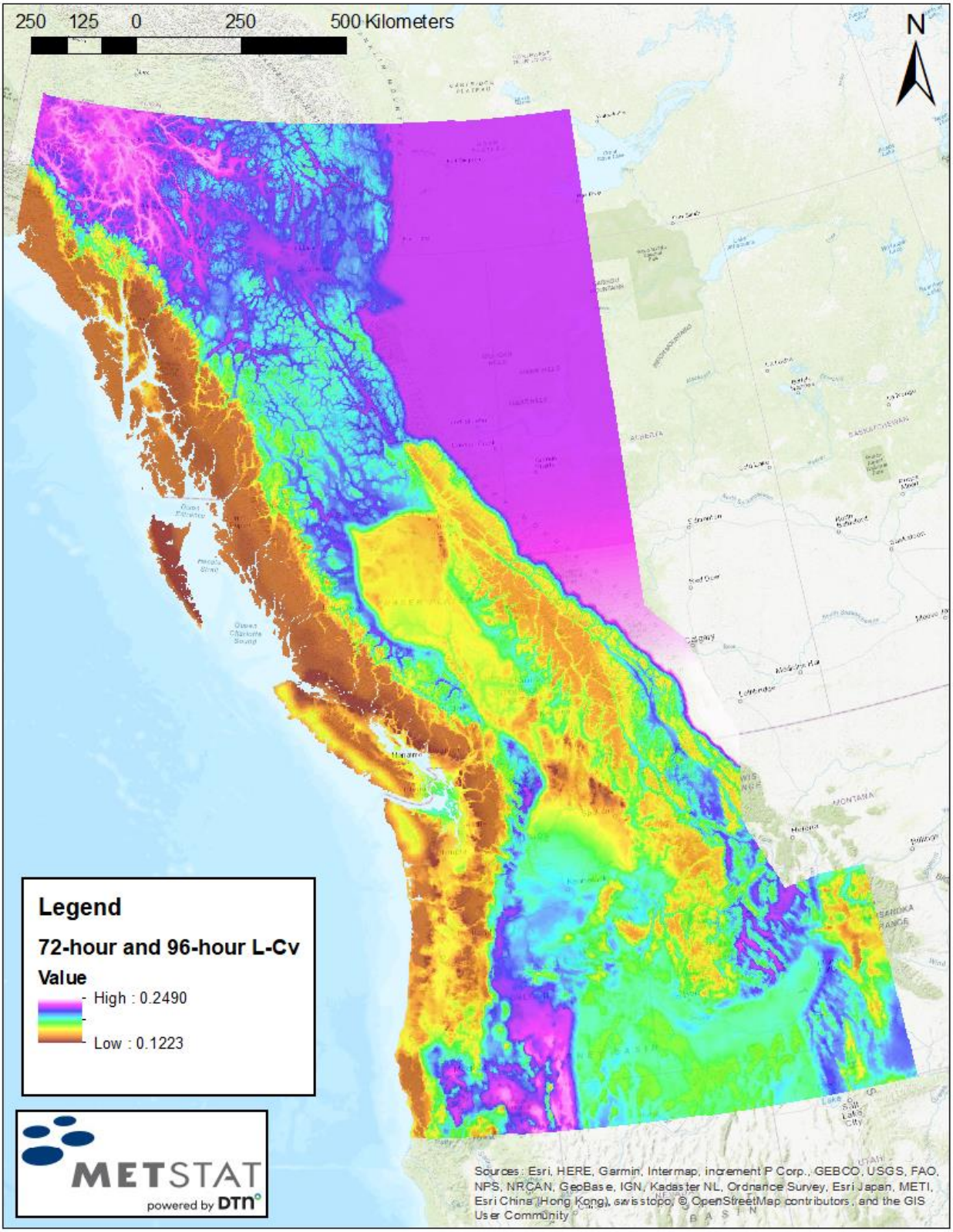

Figure 34: Map of L-Cv at the 72- and 96-hour durations.

7.2.3. Spatial Mapping of Regional L-Skewness

Similar to the L-Moment ratio L-Cv, predictor equations to spatially map the L-Moment ratio L-Skewness were developed based on the behavior of the regional values of L-Skewness obtained from the 115 Homogeneous Sub-Regions (see Section 7.1). Each Homogeneous Sub-Region produced a regional L-Skewness value associated with the group-average annual maxima precipitation weighted by the station record lengths.

7.2.3.1 L-Skewness at the 48-Hour Duration

Like the calculations for regional L-Cv at the 48-hour duration, a review of the behavior of the regional L-Skewness values from the Homogeneous Sub-Regions allowed for groupings of regional L-Skewness values into L-Skewness Mapping Areas. The L-Skewness Mapping Areas at the 48-hour duration were the same as the L-Cv Mapping Areas at the 48-hour duration (Figure 30). For each of the 17 L-Skewness Mapping Areas, a single predictor equation was found. The explanatory variables used for L-Skewness were gridded values of mean annual precipitation (mm; normal from 1960-1991 from ClimateNA [Wang et al., 2016]) and latitude (decimal degrees). Generalized additive modeling methods were used to combine the explanatory variables into predictor equations (Table 13). To limit the predictor equations to a realistic range, constraints were added to control the results at the tails of the equations (also found in Table 13).

Table 13: Predictor equations for regional L-Skewness by L-Skewness Mapping Area at the 48-hour duration. L-Skewness Mapping Areas correspond to Figure 30.

L-Skewness Mapping Area	Predictor Equation	Constraint
1	$y = 0.08446a^2 - 0.17475a + 0.2739$	if $a \geq 1.05$, then $y = 0.1835$
2	$y = 0.00039919b^2 - 0.048406b + 1.6657$	if $b \geq 58.2$, then $y = 0.2000$
3	$y = 0.08446a^2 - 0.17475a + 0.2564$	if $a \geq 1.05$, then $y = 0.1660$
4	$y = 0.08446a^2 - 0.17475a + 0.2450$	if $a \geq 1.05$, then $y = 0.1550$
5	$y = 0.003306a^2 - 0.023477a + 0.2335$	if $a \geq 3.4$, then $y = 0.1535$
6	$y = 0.003306a^2 - 0.023477a + 0.1950$	if $a \geq 3.4$, then $y = 0.1535$
7	$y = 0.003306a^2 - 0.023477a + 0.2070$	if $a \geq 3.4$, then $y = 0.1655$
8	$y = 0.00039919b^2 - 0.048406b + 1.6657$	if $b \geq 58.2$, then $y = 0.2000$
9	$y = 0.003306a^2 - 0.023477a + 0.1935$	if $a \geq 3.4$, then $y = 0.1135$
10	$y = -0.00072258b^2 + 0.056830b - 0.089904a - 0.83091$	none
11	$y = 0.01157a^2 - 0.05532a + 0.2130$	if $a \geq 1.64$, then $y = 0.1535$
12	$y = 0.003306a^2 - 0.023477a + 0.1950$	if $a \geq 3.4$, then $y = 0.1535$
13	$y = 0.003306a^2 - 0.023477a + 0.2065$	if $a \geq 3.4$, then $y = 0.1650$
14	$y = 0.003306a^2 - 0.023477a + 0.2170$	if $a \geq 3.4$, then $y = 0.1755$
15	$y = 0.003306a^2 - 0.023477a + 0.2300$	if $a \geq 3.4$, then $y = 0.1855$
16	$y = 0.0845a^2 - 0.1747a + 0.2679$	if $a \geq 1.05$, then $y = 0.1775$
17	$y = 0.003306a^2 - 0.023477a + 0.2090$	if $a \geq 3.4$, then $y = 0.1675$

*y is the value of regional L-Skewness;
a is mean annual precipitation in (mm/1000); and
b is latitude in decimal degrees.

The above predictor equations were applied to their respective L-Skewness Mapping area to produce gridded values of L-Skewness. To alleviate any discontinuities at the boundaries between the 17 L-Skewness Mapping Areas, spatial smoothing along the boundaries occurred using a weighted matrix (15x23 grid cells, nominally 15-km). The spatial smoothing resulted in smooth transitions over limited areas between the L-Skewness Mapping Areas. The final spatial map of L-Skewness values at the 48-hour duration is shown in Figure 35.

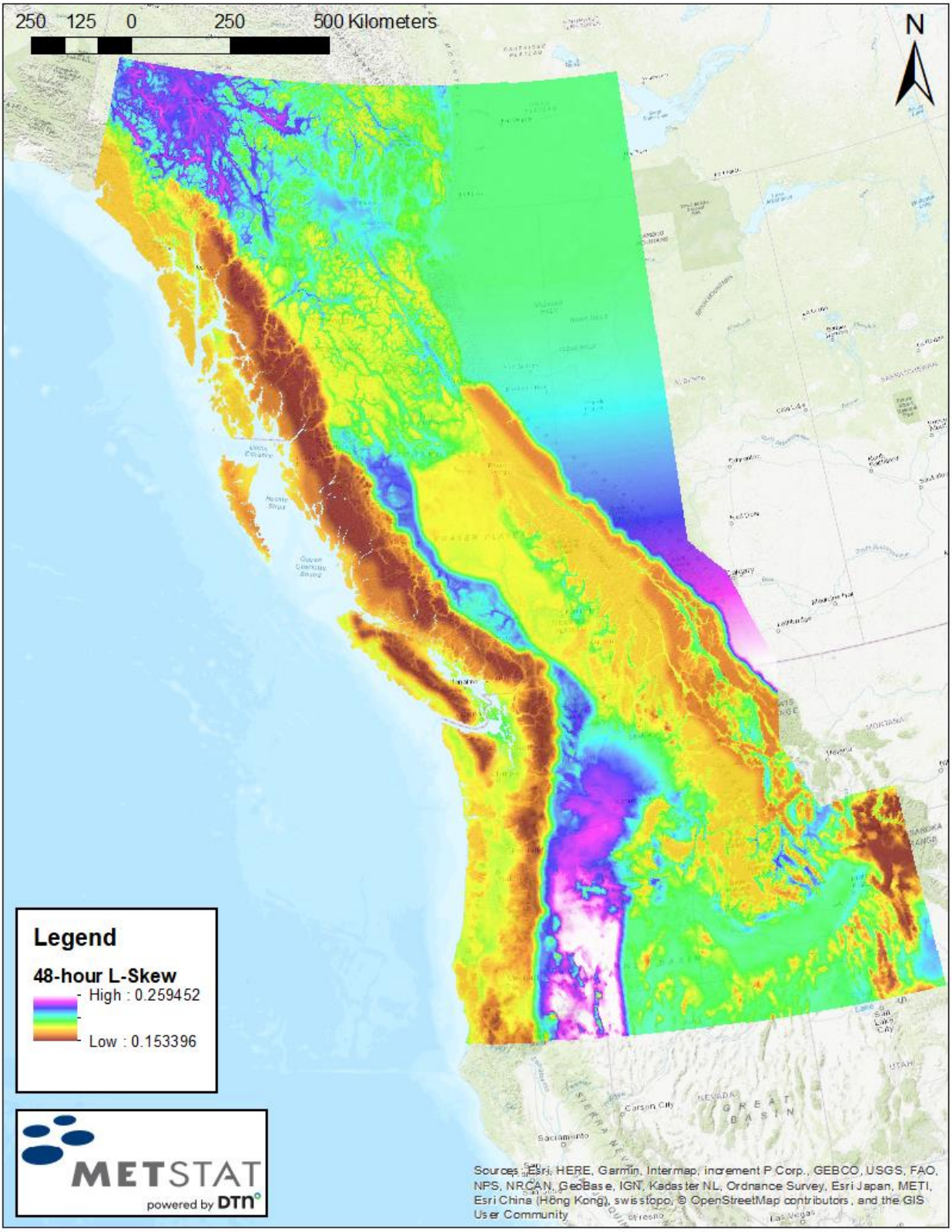

Figure 35: Map of L-Skewness at the 48-hour duration.

7.2.3.2 L-Skewness at the 24-, 72-, and 96-Hour Durations

Similar to the calculations for L-Cv, the predictor equations for gridded values of L-Skewness at the 24-, 72-, and 96-hour durations used the spatially mapped values of regional L-Skewness at the 48-hour duration (Figure 35) as the explanatory variable. The predictor equations were calculated for each of the four Project Macro Regions independently, but again with the Alberta mountains (Climate Regions 79 and 82 in Figure 4) moved from the Interior Mountains Macro Region to the Hybrid Macro Region (Figure 32). The predictor equations for the 24-hour duration are provided in Table 14, and the predictor equations for L-Skewness at the 72- and 96-hour durations are shown in Table 15 and Table 16, respectively.

Table 14: Predictor equations for L-Skewness at the 24-hour duration.
L-Skewness Mapping Areas correspond to Figure 32.

L-Skew Mapping Area	Predictor Equation
Coastal	$y = 0.7865a - 0.0459$
Lowland Interior	$y = 0.7865a - 0.0459$
Interior Mountains	$y = 0.7165a - 0.0690$
Hybrid + Alberta Mountains	$y = 0.7165a - 0.0690$

**y* is the value of 24-hour regional L-Skewness;
a is mapped 48-hour L-Skewness

Table 15: Predictor equations for L-Skewness at the 72-hour durations.
L-Skewness Mapping Areas correspond to Figure 32.

L-Skew Mapping Area	Predictor Equation
Coastal	$y = 0.6435a + 0.0654$
Lowland Interior	$y = 0.9232a + 0.0097$
Interior Mountains	$y = 0.9232a + 0.0097$
Hybrid + Alberta Mountains	$y = 0.9232a + 0.0097$

**y* is the value of 72-hour regional L-Skewness;
a is mapped 48-hour L-Skewness.

Table 16: Predictor equations for L-Skewness at the 96-hour durations.
L-Skewness Mapping Areas correspond to Figure 32.

L-Skew Mapping Area	Predictor Equation
Coastal	$y = 0.6435a + 0.0554$
Lowland Interior	$y = 8300a + 0.0217$
Interior Mountains	$y = 8300a + 0.0217$
Hybrid + Alberta Mountains	$y = 8300a + 0.0217$

*y is the value of 96-hour regional L-Skewness;
a is mapped 48-hour L-Skewness.

The linear regressions found in the above tables were applied to the spatially mapped values of L-Skewness at the 48-hour duration (Figure 35), such that the variable *a* is the mapped L-Skewness at the 48-hour duration, and the variable *y* is the predicted L-Skewness at the duration of interest. This resulted in L-Skewness values at all locations within the Project Domain. Spatial smoothing occurred along the boundaries between the L-Skewness Mapping Areas (Figure 32) using a weighted matrix (15x23 grid cells, nominally 15-km). The final spatial maps of L-Skewness at the 24-, 72- and 96-hour durations may be found in Figure 36, Figure 37, and Figure 38, respectively.

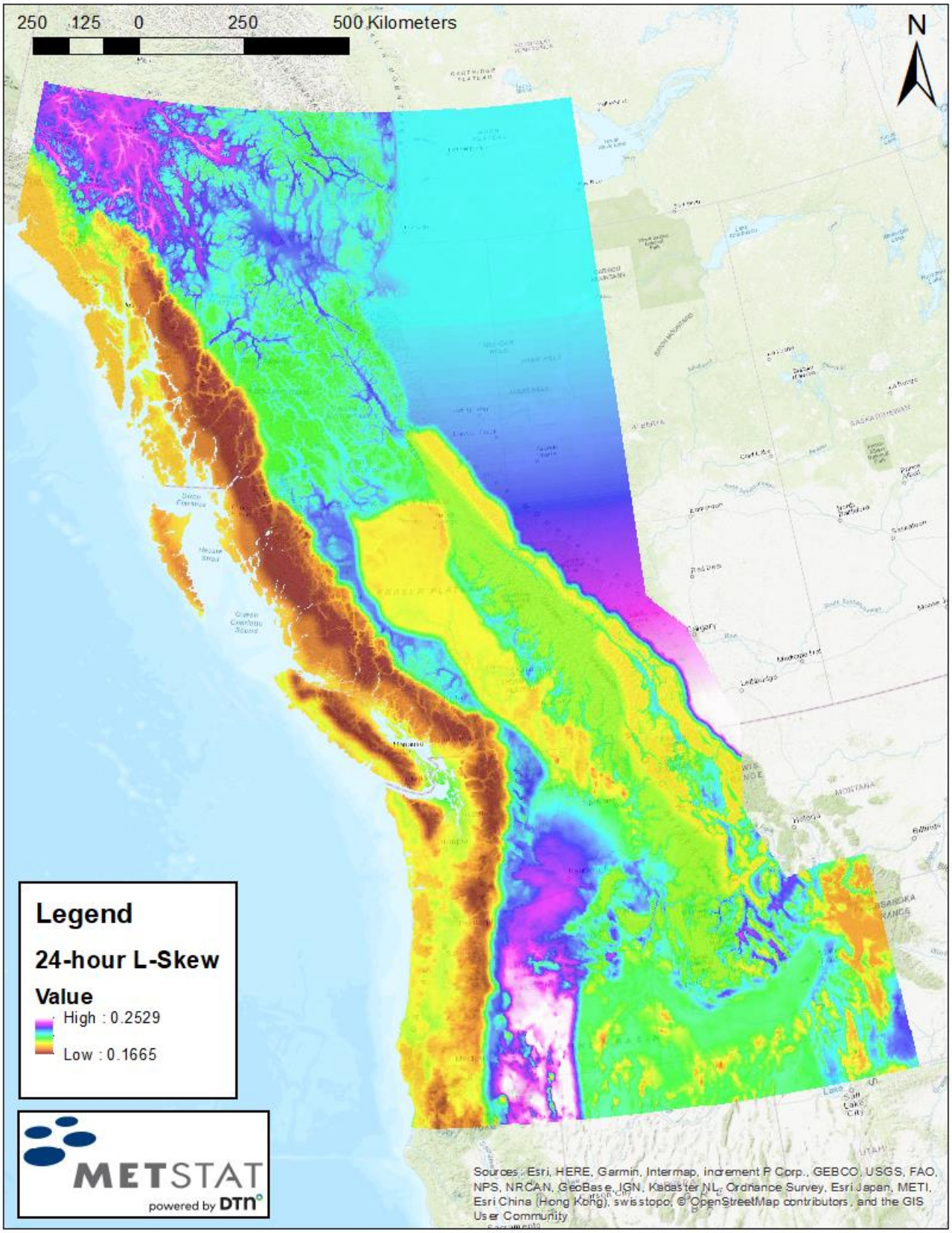

Figure 36: Map of L-Skewness at the 24-hour duration.

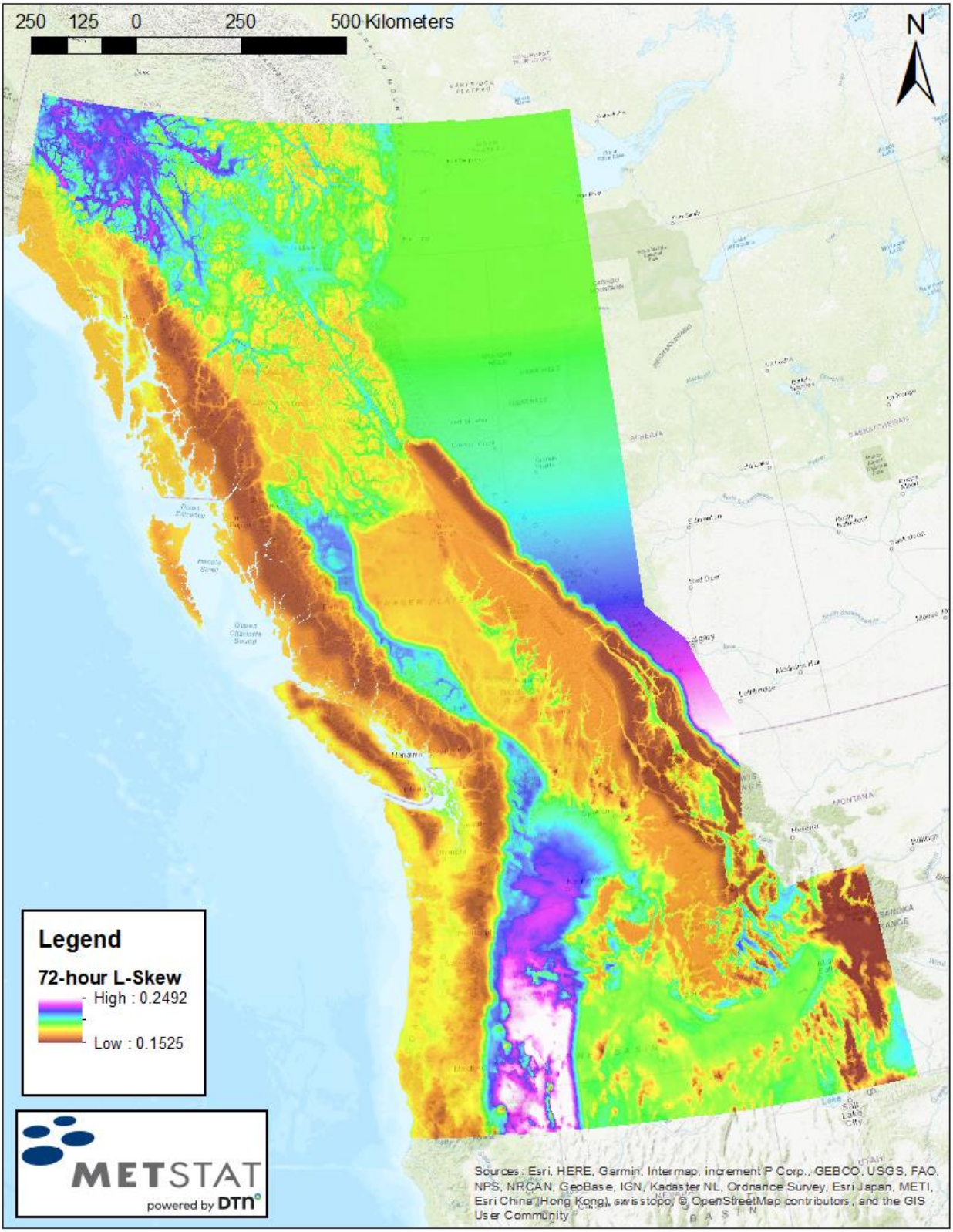

Figure 37: Map of L-Skewness at the 72-hour duration.

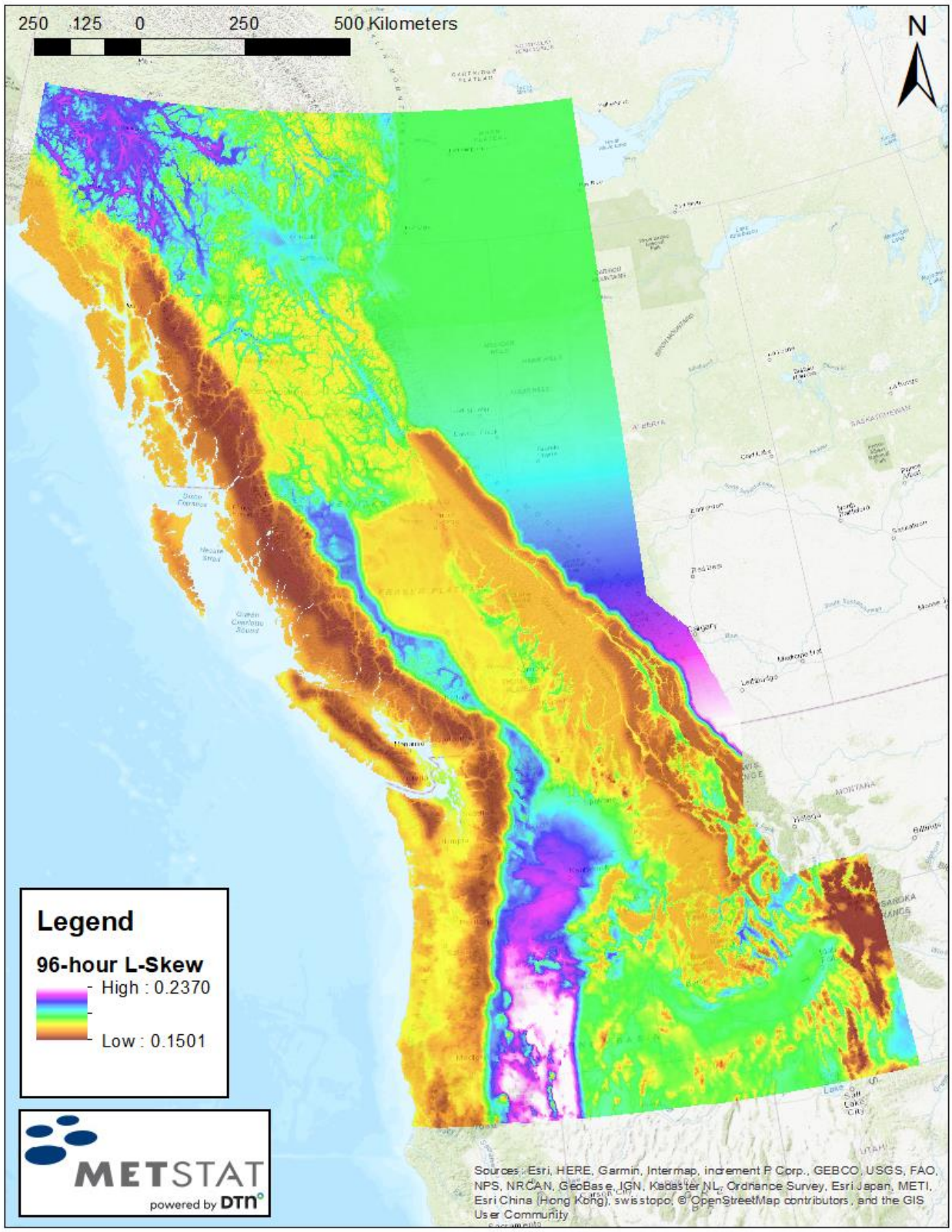

Figure 38: Map of L-Skewness at the 96-hour duration.

7.3. Regional Probability Distribution

7.3.1. L-Moment Goodness-of-Fit Tests

L-Moment goodness-of-fit tests (Hosking and Wallis, 1997) were used to identify a best-fit probability distribution. The L-Moment ratio diagram provides a graphical depiction of the goodness-of-fit tests by showing the nearness of regional L-Skewness and L-Kurtosis pairings to a number of 3-parameter probability distributions (e.g., Figure 39). This occurs because 3-parameter probability distributions have a fixed relationship between L-Skewness and L-Kurtosis. The centroid of the cluster of L-Skewness and L-Kurtosis pairings indicates the best-estimate 3-parameter probability distribution in the diagram, and the scattering of data in the cluster from the various Homogeneous Sub-Regions is due to the natural sampling variability of skewness and kurtosis measures that is inherent in real-world datasets.

L-Moment ratio diagrams were created for the four Project Macro Regions (Figure 39, Figure 40, Figure 41, and Figure 42). In each diagram, the centroid of the cluster of L-Skewness and L-Kurtosis pairings, shown as a black diamond, is very near to the Generalized Extreme Value (GEV) distribution.

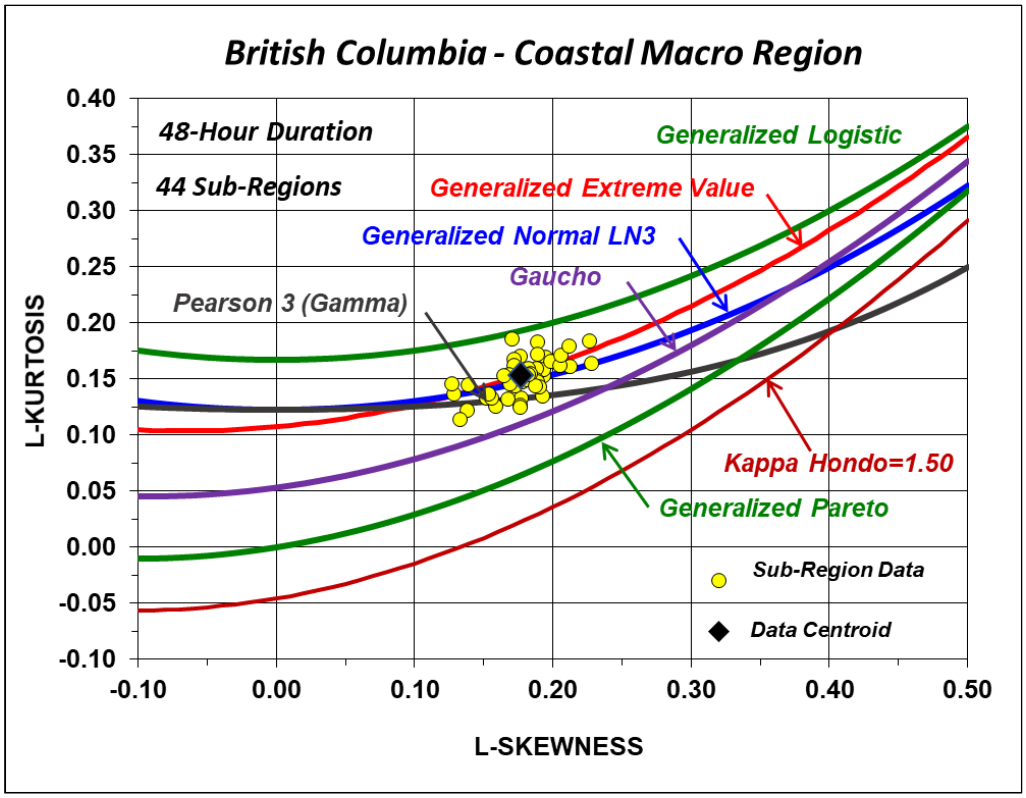

Figure 39: L-Moment ratio diagram for the Coastal Macro Region.

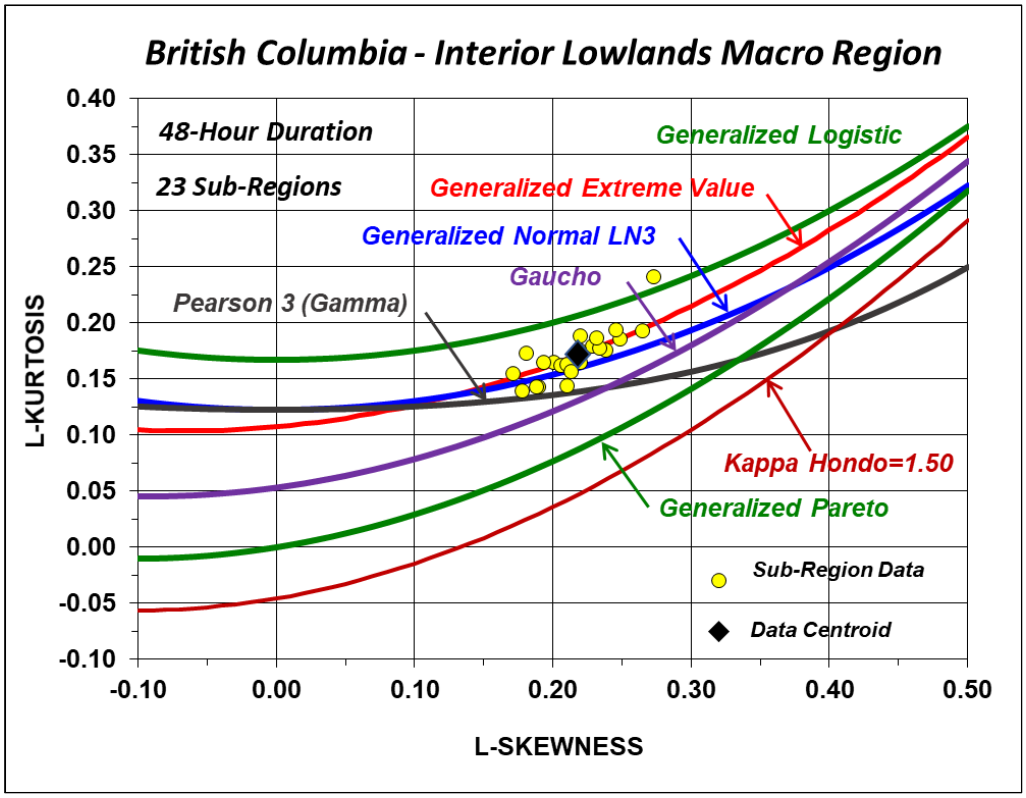

Figure 40: L-Moment ratio diagram for the Lowland Interior Macro Region.

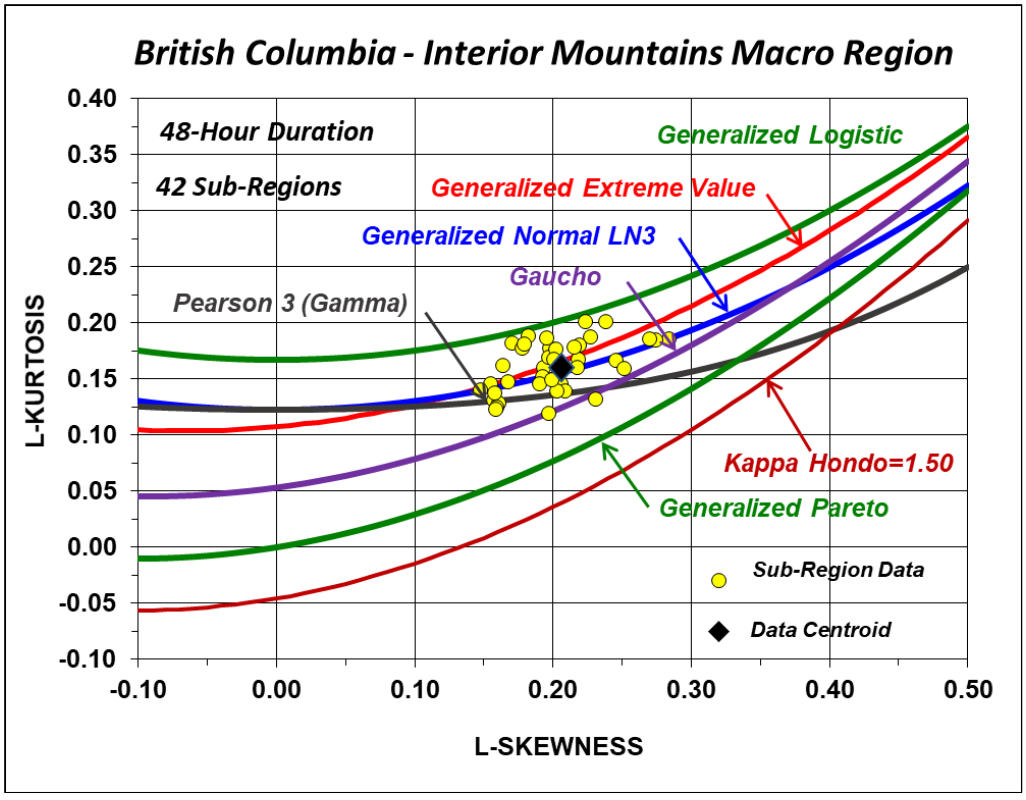

Figure 41: L-Moment ratio diagram for the Interior Mountains Macro region.

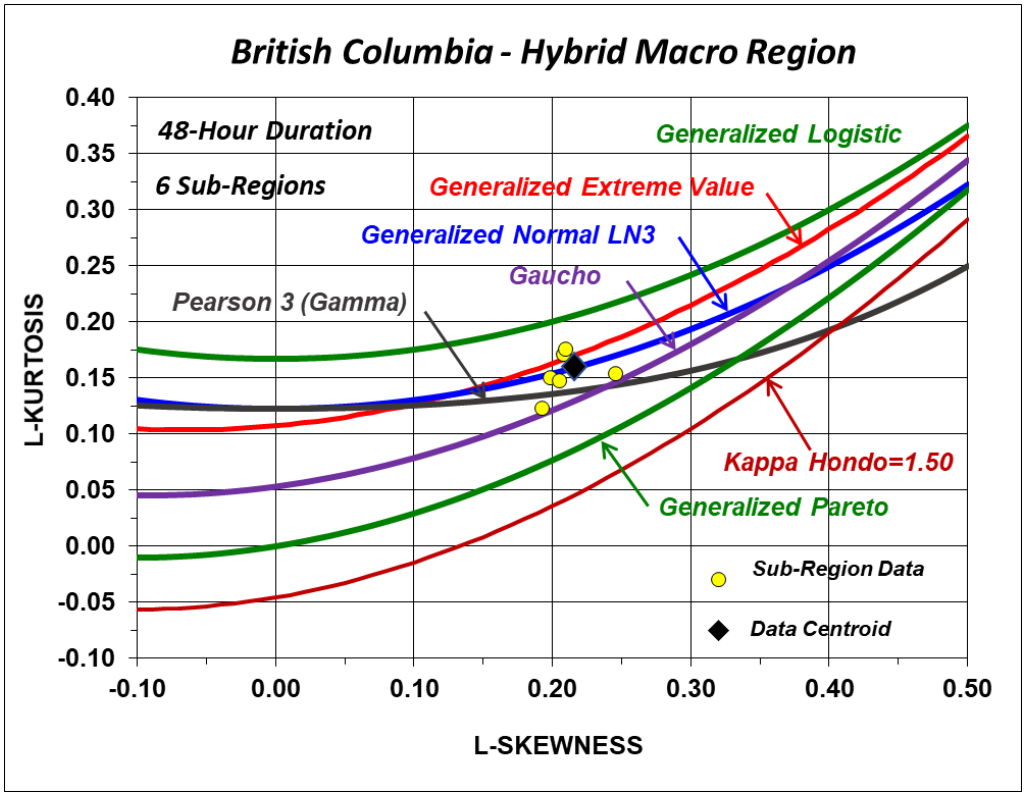

Figure 42: L-Moment ratio diagram for the Hybrid Macro Region.

The GEV distribution was identified as the best-fit 3-parameter probability distribution for each of the four Project Macro Regions. This is consistent with experience in analysis of precipitation annual maxima for durations of several days in the U.S. and western Canada where goodness-of-fit tests have shown the best-fit regional probability distribution to be near the GEV distribution (Schaefer and Barker, 1997; Schaefer et al., 2002; Schaefer and Barker, 2005; Schaefer et al., 2007).

7.3.2. Four-Parameter Kappa Distribution and Hondo

The 4-parameter Kappa distribution (Hosking and Wallis, 1997) is a very flexible distribution capable of emulating distributions near the GEV distribution, like the situations shown in Figure 39, Figure 40, Figure 41, and Figure 42, and thus was selected to describe the point precipitation-frequency relationships. The quantile function for the 4-parameter Kappa distribution is:

$$q(F) = \zeta + \frac{\alpha}{\kappa}\left\{1 - \left(\frac{1-F^h}{h}\right)^{\kappa}\right\} \qquad \text{Equation 2}$$

where ζ, α, κ, and h are location, scale, and two shape parameters, Kappa and Hondo, respectively. The distribution parameters (ζ, α, and κ) in Equation 2 were estimated by the method of L-Moments (Hosking and Wallis, 1997).

Hondo (h) is the second shape parameter of the 4-parameter Kappa distribution and is useful to describe the position of the Kappa distribution on the L-Moment ratio diagrams relative to the GEV (*h=0)* and the Generalized Pareto (*h=1)* 3-parameter probability distribution functions. Hondo is often a fixed value for a project area and storm type and was not found to systematically vary across the four Project Macro Regions with candidate explanatory variables. After analysis, it was determined that Hondo should be grouped into four mapping areas, similar to the L-Cv (and L-Skewness) Mapping Areas

for the 24-, 72- and 96-hour durations (Figure 32). Again, the Alberta mountains exhibited statistical behavior generally more aligned with the Hybrid Macro Region. The constants used for Hondo at all four durations of interest may be found in Table 17.

Table 17: Constants used for Hondo at the 24-, 48-, 72-, and 96-hour durations.

Mapping Areas	Constants
Coastal	0.05
Lowland Interior	0.05
Interior Mountains	0.05
Hybrid + Alberta Mountains	0.15

To produce a final map of Hondo, spatial smoothing using a weighted matrix (15x23 grid cells, nominally 15-km) was applied between the boundaries of the mapping areas. The final spatial map of Hondo for all four durations of interest may be found in Figure 43.

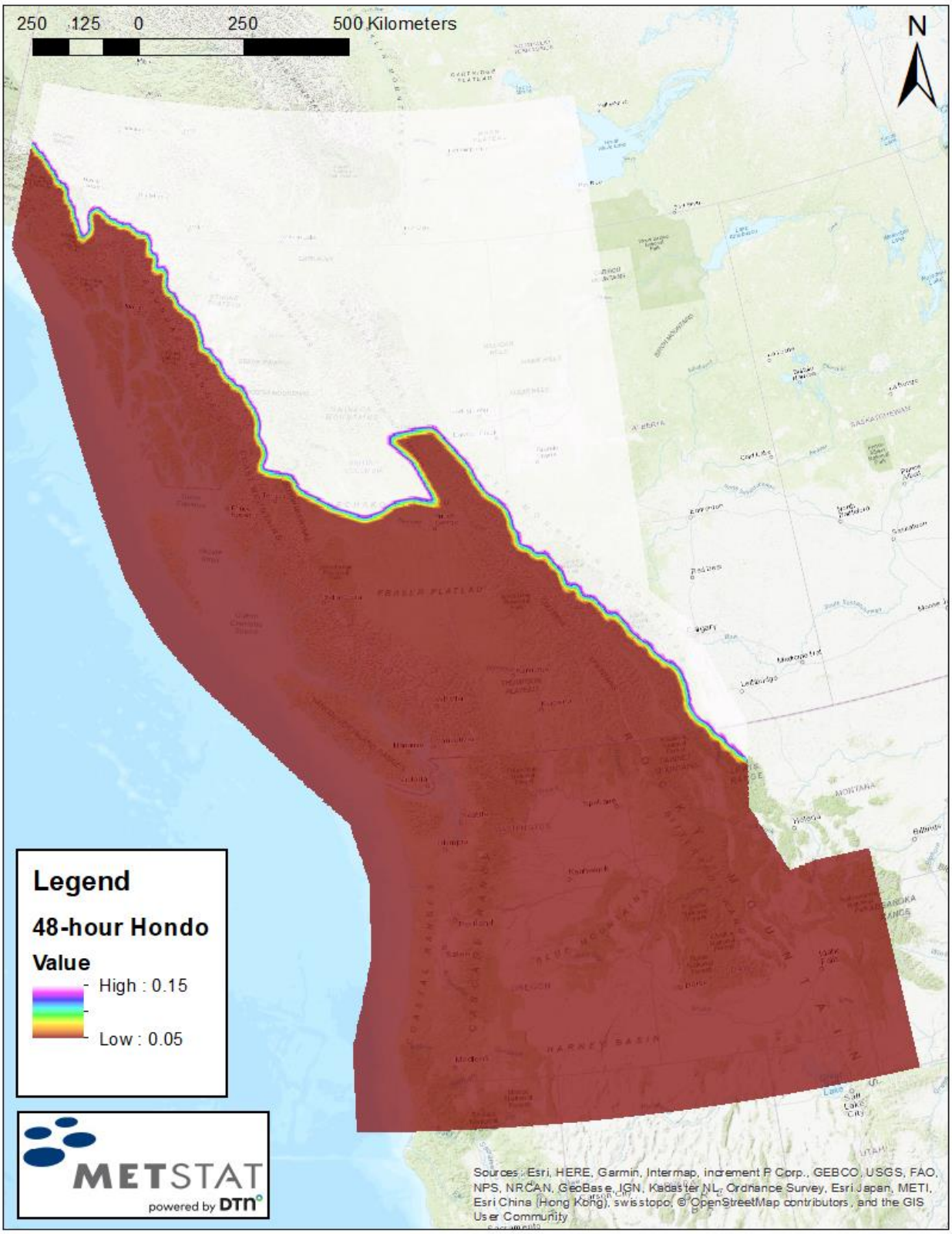

Figure 43: Map of Hondo at the 24-, 48-, 72-, and 96-hour durations.

7.4. Equivalent Independent Record Length

Equivalent Independent Record Length (EIRL) is a measure of the independent information contained in a regional dataset. When applied to the annual maxima time-series of MLC storms, EIRL provides a measure of the effective record length of the statistical information for the storms contained in the dataset. EIRL is a function of the size of the project area, the typical areal coverage of a storm, the density of precipitation stations, and the station-years of record.

For British Columbia, the MLC storm type has a large areal coverage relative to the density of the station network, so the EIRL is expected to be a relatively small fraction of the station-years of record. This occurs because the large areal coverage of a storm often produces annual maxima at many stations and results in greater correlation (statistical dependence) amongst the gauge records.

To estimate EIRL, the number of independent (separate) storm dates was found from all 48-hour precipitation annual maxima of the MLC storm type for stations with record lengths of 20 years or more. To be considered an independent storm/date, dates had to be separated by two or more non-MLC storm days. EIRL was calculated for each of the four Project Macro Regions independently, but similar to other statistical measures, the Alberta mountains (Climate Regions 79 and 82 in Figure 4) was moved from the Interior Mountains Macro Region to the Hybrid Macro Region. This is consistent with the L-Cv (and L-Skewness) Mapping Areas for the 24-, 72- and 96-hour durations (Figure 32). The number of stations with a record length of 20 years or more and the corresponding total station-years in each Project Macro Region is provided in Table 18. The EIRL, or number of independent storm dates/MLC events, is also provided in terms of station-years/MLC events and percentage of station-years (Table 18). As expected, the EIRL was a relatively small fraction of the station-years of record.

Table 18: Equivalent Independent Record Length.

Project Macro Region	Number of Stations	Station-Years	EIRL (years)	Percentage of Station-Years
Coastal	468	28,635	1,312	4.6%
Lowland Interior	341	21,919	1,421	6.5%
Interior Mountains	370	23,407	1,322	5.6%
Hybrid + Alberta Mountains	142	6,615	377	5.7%

7.5. AEP Grids

Point precipitation-frequency estimates at all point locations in the Project Domain for the four durations of interest were obtained from the spatially mapped L-Moment statistics. Specifically, for each duration, distribution parameters for the 4-parameter Kappa distribution were solved for each grid-cell using grid-cell specific values of the at-site mean (Section 7.2.1), regional L-Cv (Section 7.2.2), regional L-Skewness (Section 7.2.3), and regional Hondo (Section 7.3.2). This process was repeated for each grid cell, and the inverse cumulative distribution function (CDF) for the Kappa distribution (Equation 2) was used to compute the quantile estimates for selected AEPs.

Isopluvial gridded datasets were generated for the following AEPs and available to view and download in the online MetPortal® web-interface:

- 1:10
- 1:20
- 1:50
- 1:100
- 1:200
- 1:500
- 1:1,000
- 1:2,000
- 1:5,000
- 1:10,000
- 1:100,000
- 1:1,00,000

Example isopluvial maps for AEPs of 1:50 (0.02 AEP), 1:100 (10^{-2} AEP), 1:1,000 (10^{-3} AEP), and 1:10,000 (10^{-4} AEP) for each duration of interest may be found in the following appendices:

APPENDIX D: Maps of precipitation at select AEPs at the 24-hour duration
APPENDIX E: Maps of precipitation at select AEPs at the 48-hour duration
APPENDIX F: Maps of precipitation at select AEPs at the 72-hour duration
APPENDIX G: Maps of precipitation at select AEPs at the 96-hour duration

7.6. Uncertainty Bounds at the 5th and 95th Percentiles

The ability to characterize uncertainties in the development of point precipitation-frequency relationships is a major advantage of the SWT climate region method. Aleatoric uncertainties (chance occurrence) are inherent to all aspects of the natural processes of synoptic-scale MLC precipitation. Epistemic uncertainties (knowledge/understanding) exist regarding the meteorological processes and the statistical methods used to characterize those processes. Dimensionless uncertainty bounds were developed by characterizing epistemic uncertainties associated with estimating the at-site mean, regional L-Cv, regional L-Skewness, and the regional probability distribution when developing the point precipitation-frequency relationships. A multivariate Monte Carlo simulation using Latin-hypercube sampling (McKay et al., 1979) was used to characterize uncertainties associated with the L-Moment statistics.

The uncertainty simulations were conducted at the 48-hour duration for the Mapping Areas shown in Figure 30. The assumption was made that similar dimensionless uncertainty bounds would be applicable to the other three durations of interest (24-, 72-, and 96-hours).

Uncertainty bounds were computed using 60,000 computer simulations for each of the 200 Latin-hypercube sampling datasets for a total of 12 million simulations. This resulted in 200 separate plausible point precipitation-frequency relationships based on the magnitude of uncertainties in estimating the L-Moment statistics. Non-parametric ranking methods were used with the 200 generated point precipitation-frequency relationships to compute percentiles for the range of annual exceedance probabilities. Mid-range (mean) values of regional L-Cv and regional L-Skewness were used in all Mapping Areas to provide representative dimensionless uncertainty bounds. As an example, Table 19 and Table 20 list the

uncertainty characterizations for the L-Moment statistics for Mapping Area 13 (located in the Coastal Macro Region) and Mapping Area 9 (located in the Interior Mountains Macro Region), respectively.

Table 19:Uncertainty characteristics for computed precipitation-frequency relationships for Mapping Area 13 (Figure 30).

Uncertainty Characteristics					
Component	**Probability Model**	**Mean**	**Standard Deviation**		
At-Site Mean	Normal	1.0000	0.0650		
L-Cv	Normal	0.1535	0.0060		
L-Skewness	Normal	0.1670	0.0150		
Component	**Probability Model**			**Residuals**	
L-Kurtosis	L-Kurtosis functionally related to L-Skewness for Kappa Distribution with mean = 0.1453			**Probability Model**	**Standard Deviation**
				Normal	0.0097

Table 20: Uncertainty characteristics for computed precipitation-frequency relationships for Mapping Area 9 (Figure 30).

Uncertainty Characteristics					
Component	**Probability Model**	**Mean**	**Standard Deviation**		
At-Site Mean	Normal	1.0000	0.0500		
L-Cv	Normal	0.1705	0.0080		
L-Skewness	Normal	0.1835	0.0140		
Component	**Probability Model**			**Residuals**	
L-Kurtosis	L-Kurtosis functionally related to L-Skewness for Kappa Distribution with mean = 0.1520			**Probability Model**	**Standard Deviation**
				Normal	0.0101

Uncertainty bounds at the 5th and 95th percentiles for the range of the AEPs 1:10 through 1:10^6 for the Mapping Areas are found in Table 21 through Table 31. It is important to note that the uncertainty bounds varied with annual exceedance probability. Minor departures from the listed 5th and 95th percentile values in Table 21 through Table 31 can be expected for locations with regional L-Cv and regional L-Skewness markedly different than the mean values that were used in computing dimensionless uncertainty bounds for the Mapping Area.

Table 21: Dimensionless Uncertainty Bounds for Mapping Area 6 (Figure 30).

Dimensionless Uncertainty Bounds for Ratio to Best Estimate: Mapping Area 6 (Coastal region)												
1/AEP	**10**	**20**	**50**	**100**	**200**	**500**	**1,000**	**2,000**	**5,000**	**10,000**	**10^5**	**10^6**
5th Percentile	0.889	0.887	0.883	0.880	0.877	0.872	0.867	0.863	0.856	0.850	0.829	0.802
95th Percentile	1.101	1.105	1.112	1.118	1.124	1.133	1.140	1.148	1.159	1.168	1.202	1.242

Table 22: Dimensionless Uncertainty Bounds for Mapping Areas 7 and 13 (Figure 30).

Dimensionless Uncertainty Bounds for Ratio to Best Estimate: Mapping Areas 7 and 13 (Coastal region)												
1/AEP	**10**	**20**	**50**	**100**	**200**	**500**	**1,000**	**2,000**	**5,000**	**10,000**	**10^5**	**10^6**
5th Percentile	0.891	0.886	0.878	0.872	0.865	0.856	0.849	0.842	0.832	0.824	0.796	0.764
95th Percentile	1.102	1.108	1.116	1.123	1.130	1.139	1.147	1.156	1.167	1.176	1.209	1.247

Table 23: Dimensionless Uncertainty Bounds for Mapping Areas 14 and 17 (Figure 30).

Dimensionless Uncertainty Bounds for Ratio to Best Estimate: Mapping Areas 14 and 17 (Coastal region)												
1/AEP	**10**	**20**	**50**	**100**	**200**	**500**	**1,000**	**2,000**	**5,000**	**10,000**	**10^5**	**10^6**
5th Percentile	0.891	0.885	0.878	0.871	0.865	0.856	0.848	0.841	0.830	0.821	0.791	0.756
95th Percentile	1.101	1.107	1.116	1.123	1.130	1.141	1.149	1.158	1.170	1.180	1.217	1.258

Table 24: Dimensionless Uncertainty Bounds for Mapping Area 15 (Figure 30).

Dimensionless Uncertainty Bounds for Ratio to Best Estimate: Mapping Area 15 (Coastal region)												
1/AEP	**10**	**20**	**50**	**100**	**200**	**500**	**1,000**	**2,000**	**5,000**	**10,000**	**10^5**	**10^6**
5th Percentile	0.890	0.887	0.883	0.879	0.874	0.867	0.860	0.853	0.842	0.833	0.798	0.754
95th Percentile	1.101	1.109	1.120	1.128	1.137	1.149	1.159	1.169	1.182	1.193	1.231	1.273

Table 25: Dimensionless Uncertainty Bounds for Mapping Area 5 (Figure 30).

Dimensionless Uncertainty Bounds for Ratio to Best Estimate: Mapping Area 5 (Lowland Interior region)												
1/AEP	**10**	**20**	**50**	**100**	**200**	**500**	**1,000**	**2,000**	**5,000**	**10,000**	**10^5**	**10^6**
5th Percentile	0.914	0.910	0.902	0.896	0.888	0.877	0.867	0.857	0.842	0.829	0.781	0.723
95th Percentile	1.092	1.094	1.098	1.104	1.111	1.122	1.132	1.144	1.162	1.178	1.241	1.320

Table 26: Dimensionless Uncertainty Bounds for Mapping Area 9 (Figure 30).

Dimensionless Uncertainty Bounds for Ratio to Best Estimate: Mapping Area 9 (Lowland Interior region)												
1/AEP	**10**	**20**	**50**	**100**	**200**	**500**	**1,000**	**2,000**	**5,000**	**10,000**	**10^5**	**10^6**
5th Percentile	0.909	0.905	0.899	0.894	0.888	0.880	0.873	0.865	0.854	0.844	0.809	0.767
95th Percentile	1.084	1.090	1.098	1.106	1.113	1.125	1.134	1.144	1.158	1.170	1.213	1.262

Table 27: Dimensionless Uncertainty Bounds for Mapping Area 3 (Figure 30).

Dimensionless Uncertainty Bounds for Ratio to Best Estimate: Mapping Area 3 (Interior Mountains region)												
1/AEP	**10**	**20**	**50**	**100**	**200**	**500**	**1,000**	**2,000**	**5,000**	**10,000**	**10^5**	**10^6**
5th Percentile	0.894	0.889	0.882	0.875	0.868	0.859	0.850	0.842	0.829	0.819	0.782	0.738
95th Percentile	1.104	1.108	1.115	1.121	1.127	1.138	1.146	1.156	1.169	1.181	1.224	1.277

Table 28: Dimensionless Uncertainty Bounds for Mapping Area 16 (Figure 30).

Dimensionless Uncertainty Bounds for Ratio to Best Estimate: Mapping Area 16 (Interior Mountains region)												
1/AEP	**10**	**20**	**50**	**100**	**200**	**500**	**1,000**	**2,000**	**5,000**	**10,000**	**10^5**	**10^6**
5th Percentile	0.889	0.887	0.883	0.880	0.875	0.869	0.863	0.857	0.847	0.840	0.809	0.772
95th Percentile	1.100	1.107	1.118	1.127	1.137	1.151	1.162	1.174	1.192	1.206	1.258	1.319

Table 29: Dimensionless Uncertainty Bounds for Mapping Area 1 (Figure 30).

Dimensionless Uncertainty Bounds for Ratio to Best Estimate: Mapping Area 1 (Hybrid region)												
1/AEP	**10**	**20**	**50**	**100**	**200**	**500**	**1,000**	**2,000**	**5,000**	**10,000**	**10^5**	**10^6**
5th Percentile	0.889	0.881	0.868	0.858	0.847	0.832	0.819	0.805	0.785	0.769	0.710	0.641
95th Percentile	1.112	1.118	1.129	1.138	1.149	1.165	1.179	1.195	1.217	1.236	1.307	1.395

Table 30: Dimensionless Uncertainty Bounds for Mapping Area 2 (Figure 30).

Dimensionless Uncertainty Bounds for Ratio to Best Estimate: Mapping Area 2 (Hybrid region)												
1/AEP	**10**	**20**	**50**	**100**	**200**	**500**	**1,000**	**2,000**	**5,000**	**10,000**	**10^5**	**10^6**
5th Percentile	0.887	0.879	0.867	0.858	0.847	0.831	0.817	0.803	0.782	0.766	0.702	0.628
95th Percentile	1.107	1.112	1.121	1.130	1.141	1.157	1.172	1.188	1.213	1.233	1.314	1.414

Table 31: Dimensionless Uncertainty Bounds for Mapping Area 8 (Figure 30).

Dimensionless Uncertainty Bounds for Ratio to Best Estimate: Mapping Area 8 (Hybrid region)												
1/AEP	**10**	**20**	**50**	**100**	**200**	**500**	**1,000**	**2,000**	**5,000**	**10,000**	**10^5**	**10^6**
5^{th} Percentile	0.885	0.879	0.868	0.858	0.847	0.831	0.818	0.803	0.781	0.764	0.697	0.617
95^{th} Percentile	1.108	1.112	1.121	1.130	1.141	1.158	1.173	1.190	1.215	1.236	1.320	1.425

The uncertainty bounds are included in tabular and graphical format in the online MetPortal® web-interface to view and download. An example is shown in Figure 44.

Precipitation (mm) for 48hr Duration and Given AEP at 53.917N, 122.746W

	Lower Bound - 5% (mm)	Best Estimate (mm)	Upper Bound - 95% (mm)
AEP=1:10	50.35	55.39	60.04
AEP=1:20	56.35	62.27	67.87
AEP=1:50	64.00	71.19	78.17
AEP=1:100	69.62	77.88	86.14
AEP=1:200	75.09	84.56	94.12
AEP=1:500	82.17	93.38	105.05
AEP=1:1,000	87.33	100.04	113.45
AEP=1:2,000	92.31	106.72	122.09
AEP=1:5,000	98.67	115.54	133.80
AEP=1:10,000	103.15	122.22	143.00
AEP=1:100,000	116.87	144.46	175.23
AEP=1:1,000,000	127.90	166.75	210.44

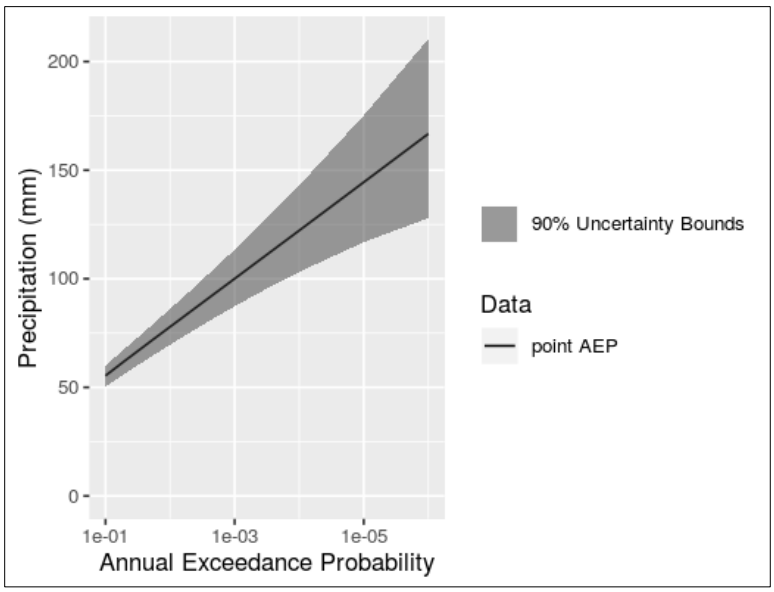

Figure 44: Example graphic of uncertainty bounds in tabular format (top) and graphical format (bottom) as shown in the MetPortal. Example is for Prince George, British Columbia.

8. SCALABLE TEMPORAL STORM PATTERNS

Scalable temporal storm patterns are needed in conjunction with point precipitation-frequency relationships to translate a point precipitation magnitude at a duration of interest and AEP into meaningful input for flood modeling. Historical temporal patterns are preferred to synthetic patterns so that the flood model may reflect natural storm behavior. There is great diversity in the shape of historical temporal storm patterns with variability resulting from:

- Single and multi-pulse temporal patterns;
- Timing of the high-intensity pulse: front-loaded, middle-loaded, and back-loaded temporal patterns; and
- Magnitude and sequencing of incremental precipitation.

Each of the components above can affect the shape of the flood hydrograph and the response of the reservoir to the inflow flood. Therefore, it is prudent to examine a suite of scalable temporal storm patterns in evaluating reservoir response and spillway performance for rare to extreme floods. To provide a range of possible flood outcomes, a wide variety of storm temporal patterns for each Project Macro Region was identified from historical storms that occurred within each Project Macro Region as listed in Bulletin 2020-3-PMP: Probable Maximum Precipitation Guidelines for British Columbia – Technical Report (Table 32).

Table 32: Suite of scalable temporal storm patterns for each Project Macro Region.
Storm Number is associated with the yyyy/mm/dd/storm center zone number of the storm.

Project Macro Region	Storm Number
Coastal	1950102820
	1990110920
	1993112410
	2007120310
	2006110610
Lowland Interior	1944062610
	1949021610
	1963102120
	1964122220
Interior Mountains	1955122010
	1984082610
	2004082210
	2005060510
	2012062210
	2013061710
Hybrid	1964062810
	1972072410
	1986061510
	1987080120
	2001061110

For additional information regarding the storms listed in Table 32, please refer to Bulletin 2020-4-PMP: MetStorm Reports Used for Determining the Probable Maximum Precipitation Guidelines for British Columbia.

The scalable temporal storm patterns are available for download in the online MetPortal® web-interface. The temporal storm patterns are presented as dimensionless temporal mass-curves (hyetographs) scaled by the point precipitation magnitude at the duration of interest and selected AEP as the indexing value. To reflect the storm as it occurred, the total storm duration is not limited to the duration of interest (24-, 48-, 72-, or 96-hours), so the total duration may differ from the duration selected. Guidance for application of the scalable temporal storm patterns is found in Bulletin 2020-5-PMP/RPFA: MetPortal User's Guide: Probable Maximum Precipitation and Regional Precipitation-Frequency Analysis for British Columbia.

9. FUTURE WORK

9.1. Areal Reduction Factors

Gridded *point* precipitation-frequency estimates were provided in this project. For very small watersheds (area size of 10-km^2 or less), the point precipitation-frequency values are applicable without any further adjustments. For watersheds larger that 10-km^2, the point precipitation-frequency estimates are not directly applicable. It must be stressed that it is not appropriate to average all the point precipitation-frequency estimates in a watershed; this will result in an overestimate of watershed precipitation, particularly for large watersheds. To estimate an appropriate watershed precipitation-frequency value from point precipitation-frequency information, an areal reduction factor (ARF) must be applied. This project did not calculate or update ARFs for British Columbia. Rather, guidance is provided to apply ARFs from previous studies in Bulletin 2020-5-PMP/RPFA: MetPortal User's Guide: Probable Maximum Precipitation and Regional Precipitation-Frequency Analysis for British Columbia. In the future, it may be decided that the previous ARFs should be revisited.

9.2. Shorter Duration Storms in the Lowland Interior Macro Region

Thunderstorms or local storms (LSs; key duration of 2-hours) and mesoscale storms with embedded convection (MECs; key duration of 6-hours) occur in the Lowland Interior Macro Region. These shorter-duration events can produce bursts of very heavy rainfall and produce large floods on small and intermediate-sized watersheds (generally less than about 1,000-km^2) where peak discharge may be the primary concern. However, these sub-daily storm types were not considered in this project. In the future, it may be decided that these storm types are important to small- and intermediate-sized watersheds in this Project Macro Region and require analysis. An analysis of this nature would also include short-duration scalable temporal storm patterns with granularity of 5- or 15-minute time-steps.

9.3. Climate Change

Potential future climate conditions were not considered in this study. The point precipitation-frequency estimates could be adjusted by potential future climate conditions from global climate model projections using a methodology similar to that developed by the U.S. Bureau of Reclamation (Bahls et al., 2014).

10. COMPARISONS OF METPORTAL POINT PRECIPITATION MAGNITUDES WITH OTHER STUDIES

Ron Hopkinson of Custom Climate Services compared the best-estimate point precipitation values from MetPortal with precipitation magnitudes from intensity-duration frequency (IDF) statistics computed from recording rain gauge data at 36 locations with long-term ECCC principal stations (https://climate.weather.gc.ca/prods_servs/engineering_e.html). The IDF analyses are updated by ECCC every couple of years. For this comparison, the 2014 version was used. The comparisons were completed at the 24-hour duration for the 1:10, 1:50, and 1:100 AEPs.

Additionally, the best-estimate point precipitation values from MetPortal were also compared with output from another ECCC product, Rain30. Rain30 was originally developed in the late 1980s by the Hydrometeorological Division of the Canadian Climate Centre and was assumed by the Climate Research Division of the ECCC in the 1990s (R. Hopkinson, personal communication). The Rain30 precipitation magnitudes were available at the 36 locations at all four durations of interest and for the 1:10, 1:50, and 1:100 AEPs.

Differences in the precipitation-frequency estimates between the three methodologies can vary depending on location. The differences may be attributed to the following:

- The IDF and Rain30 precipitation magnitudes were calculated solely on at-site station data, whereas the MetPortal values were computed using the regional analysis outlined above.
- The IDF and Rain30 precipitation magnitudes were calculated using a 2-parameter Gumbel distribution, whereas the MetPortal values were calculated from a 4-parameter Kappa distribution.
- The Rain30 program determined the AMS based on the calendar year, whereas the AMS for the MetPortal values was based on the appropriate season for the MLC storm type in each Project Macro Region.
- The MetPortal precipitation values were for a single storm type (MLCs) and the IDF and Rain30 precipitation magnitudes were calculated from a mixed population of storm types.
- The MetPortal values were based on rain gauge data collected through 2019, whereas the other studies had varying periods of record.

Figure 45 shows the comparison at Vancouver International Airport. For all four durations, the slopes of the curves are similar (out to 1:100 AEP), but the magnitudes from MetPortal are slightly greater by 10 to almost 20%.

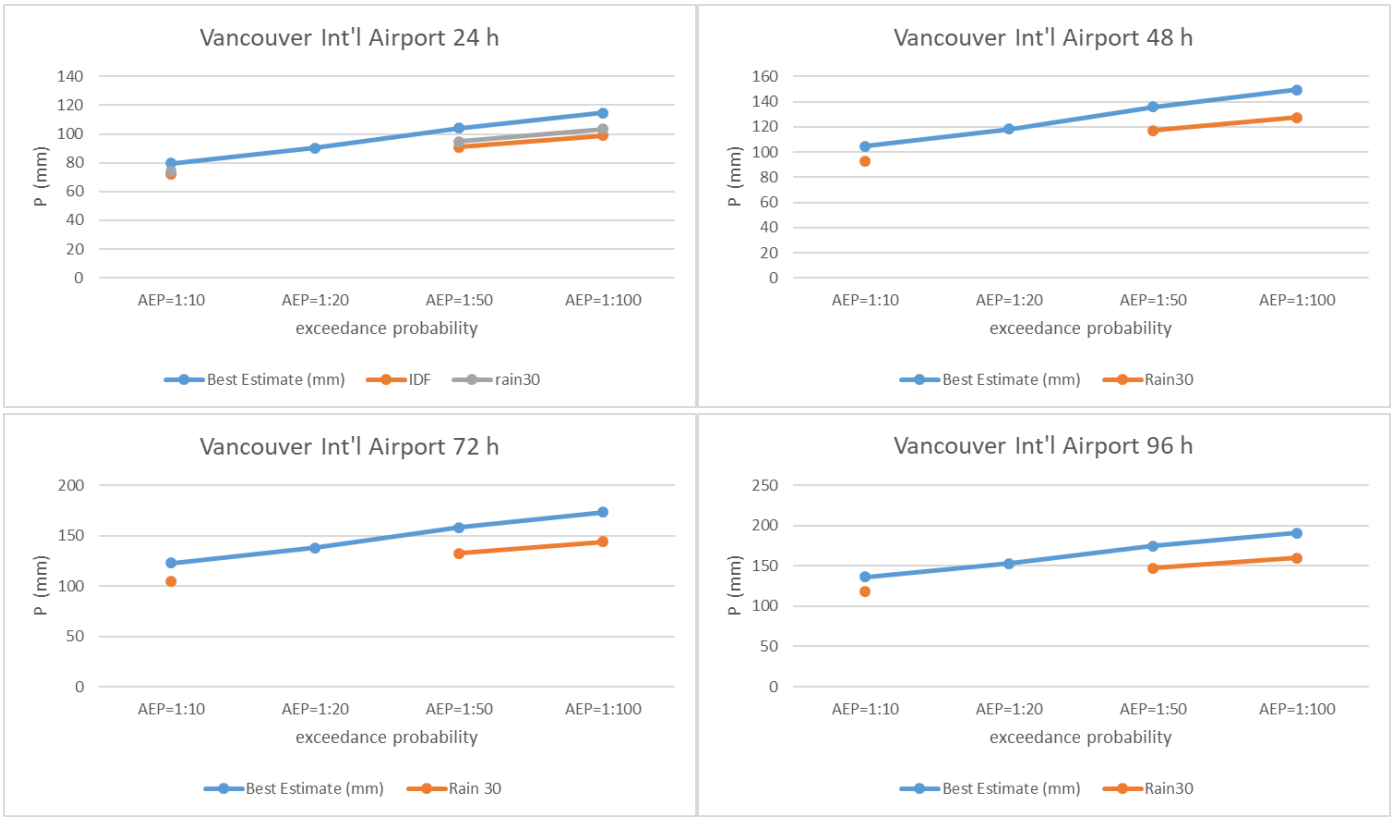

Figure 45: Comparison of point precipitation magnitudes for 1:10, 1:50, and 1:100 AEPs at the four durations of interest for Vancouver International Airport.

Figure 46 shows the comparison at Sandspit (53.253°N, 131.815°W). Here, the results from all three statistical methods were similar.

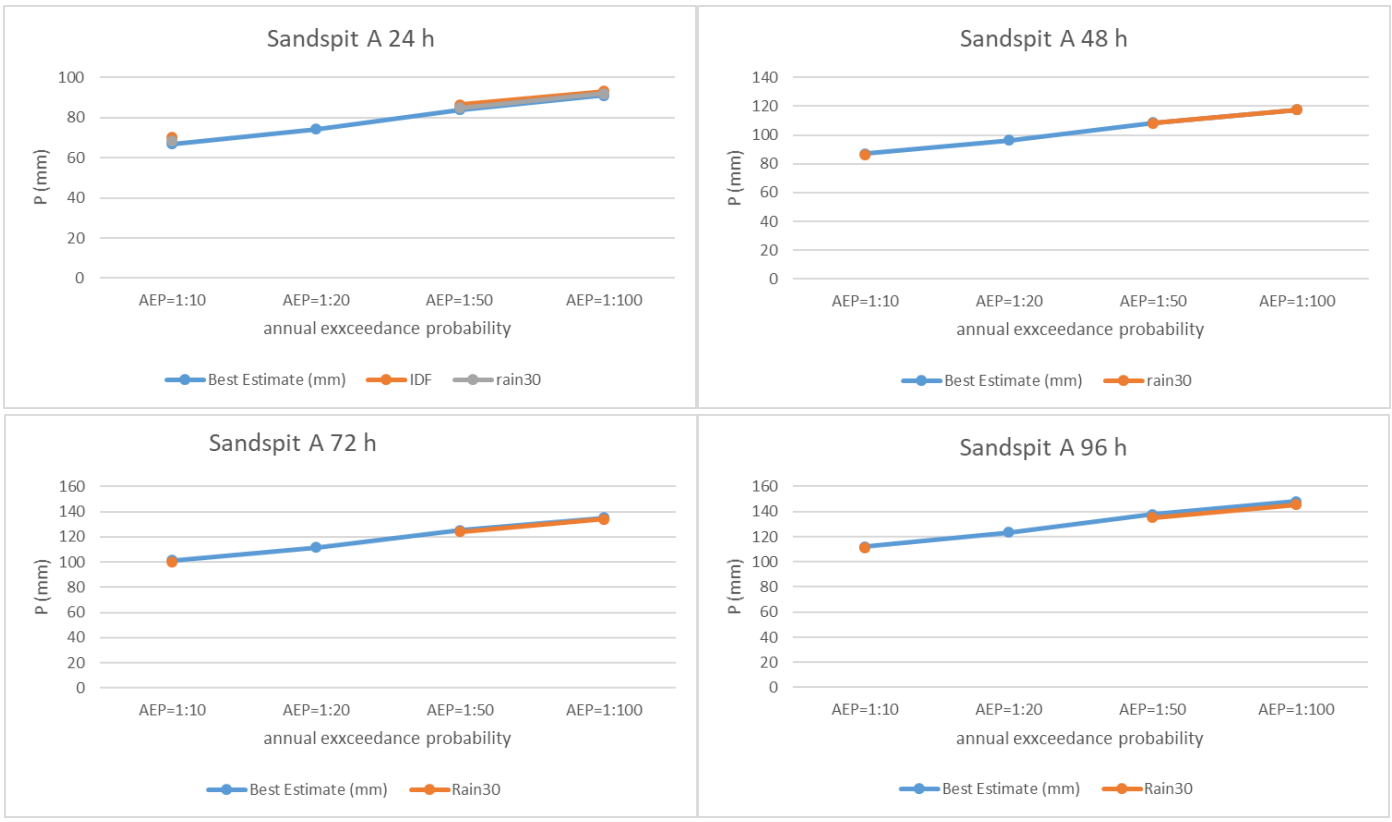

Figure 46: Comparison of point precipitation magnitudes for 1:10, 1:50, and 1:100 AEPs at the four durations of interest for Sandspit.

Figure 47 shows the comparison at Prince Rupert (52.292°N, 130.447°W). For the 24-hour duration, the precipitation values from MetPortal and the precipitation magnitudes from the IDF analysis at the 1:50 and 1:100 AEP are similar. The precipitation magnitudes from Rain30 at the 24-hour duration are slightly lower in magnitude but have the same slope. At the 48-, 72-, and 96-hour durations, the Rain30 precipitation magnitudes are all greater than the MetPortal precipitation values.

Figure 47: Comparison of point precipitation magnitudes for 1:10, 1:50, and 1:100 AEPs at the four durations of interest for Prince Rupert.

The comparisons at the remaining 33 locations may be found in APPENDIX H: Comparisons between MetPortal Point Precipitation Magnitudes with IDF and Rain30 Precipitation Magnitudes. Overall, the values from MetPortal for the 1:50 and 1:100 AEP are somewhat greater than the IDF and Rain 30 precipitation magnitudes. This can result from the use of different data and methodologies to calculate the statistics. The IDF and Rain 30 precipitation magnitudes would most likely fall within the 5th and 95th uncertainty bounds from MetPortal had they been plotted on the graphs.

REFERENCES

Bahls., V.S., K.D. Holman, and J.F. England, 2014: Climate Change in Hydrologic Hazard Analyses: Friant Dam Pilot Study. Part I: Hydrometeorological Model Inputs. Flood Hydrology and Consequences Group, Technical Service Center, Bureau of Reclamation.

Compo, G.P., J.S. Whitaker, P.D. Sardeshmukh, N. Matsui, R.J. Allan, X. Yin, B.E. Gleason, R.S. Vose, G. Rutledge, P. Bessemoulin, S. Brönnimann, M. Brunet, R.I. Crouthamel, A.N. Grant, P.Y. Groisman, P.D. Jones, M. Kruk, A.C. Kruger, G.J. Marshall, M. Maugeri, H.Y. Mok, Ø. Nordli, T.F. Ross, R.M. Trigo, X.L. Wang, S.D. Woodruff, and S.J. Worley, 2011: The Twentieth Century Reanalysis Project. Quarterly J. Roy. Meteorol. Soc., 137, 1-28. DOI: 10.1002/qj.776 Free and Open Access.

Coulson, C.H. and W. Obedkoff, 1998: British Columbia Streamflow Inventory. Province of British Columbia, Ministry of Environment, Lands and Parks.

Hosking, J.R.M., and J.R. Wallis, 1997: Regional Frequency Analysis - An Approach Based on L-Moments, Cambridge Press, 224 pp.

Kar, T.R. and W.J. Koss, 1984: "Regional and National Monthly, Seasonal, and Annual Temperature Weighted by Area, 1895-1983." Historical Climatology Series 4-3, National Climatic Data Center, Asheville, NC, 38 pp.

Kuczera, G., 1982: Combining Site-Specific and Regional Information: An Empirical Bayes Approach, *Water Resources Research*, 18, No. 2, 306-314.

McKay, M.D., W.J. Conover, and R.J. Beckman, 1979: A Comparison of Three Methods for Selecting Values of Input Variables in the Analysis of Output from a Computer Code, Technometrics, 221, pp239-245.

MetStat and MGS Engineering Consultants, 2019: Mactaquac Dam Risk-Informed Assessment of Spilling Capacity – Phase III, Stochastic Event Flood Model (SEFM) Meteorological Aspects, prepared for NB Power, July 2019.

MetStat and MGS Engineering Consultants, 2018a: Colorado-New Mexico Regional Extreme Precipitation Study, Summary Report Volume III, Regional Precipitation-Frequency Estimation, prepared for Colorado and New Mexico Dam Safety Programs, November 2018.

MetStat and MGS Engineering Consultants, 2018b: Trinity River Hydrologic Hazards Project Task 3 Report – Regional Extreme Precipitation-Frequency Analysis for the Trinity River Basin, prepared for US Army Corps of Engineers, Risk Management Center, May 2018.

MGS Engineering Consultants, MetStat, Applied Climate Services, and Riverside Technology, 2015: Regional Precipitation-Frequency Analyses for Mid-Latitude Cyclones, Mesoscale Storms with Embedded Convection, Local Storms and Tropical Storm Remnant Storm Types in the Tennessee Valley Watershed and Appendices, including Appendix E. Creating of the Database of Daily Storm Types by Manual and Automated Storm Typing Procedures, prepared for the Tennessee Valley Authority.
http://www.mgsengr.com/damsafetyfiles/TVA_Point%20Precipitation-Frequency_2015-03-02_Release.pdf

MetStat and MGS Engineering Consultants, in draft: Stochastic Modeling of Floods for Mica, Revelstoke, Arrow, Duncan, Sugar, Whatshan, and Kootenay Dams on the Upper Columbia River, Stochastic Event Flood Model (SEFM) – Meteorological Aspects: Regional Frequency Analysis, prepared for BCHydro.

PRISM Climate Group, Oregon State University, http://prism.oregonstate.edu, downloaded 2015.

Schaefer, M.G., 1997a: Data-Quality Checking Software for Precipitation Maxima. MGS Engineering Consultants.

Schaefer, M.G., 1997b: Magnitude Frequency Characteristics of Precipitation Annual Maxima in Southern British Columbia, MGS Engineering Consultants, Inc.

Schaefer, M., and B. Barker, 1997: Stochastic Modeling of Extreme Floods for A.R. Bowman Dam, MGS Engineering Consultants.

Schaefer, M., and B. Barker, 2005: Stochastic Modeling of Extreme Floods on the American River at Folsom Dam: Flood-Frequency Curve Extension. MGS Engineering Consultants for U.S. Army Corps of Engineers, Hydrologic Engineering Center, Davis, CA.

Schaefer, M.G. and B.L. Barker, 2009: L-Moments Regional Analysis Package (L-RAP). MGS Software LLC.

Schaefer, M.G., B.L Barker, G.H. Taylor, and J.R. Wallis, 2002: Regional Precipitation-Frequency Analysis and Spatial Mapping for 24-Hour and 2-Hour Durations for Western Washington, MGS Engineering Consultants and Oregon Climate Service for Washington State Dept. of Transportation, 93 pp.

Schaefer, M.G., B.L Barker, G.H. Taylor, and J.R. Wallis, 2006: Regional Precipitation-Frequency Analysis and Spatial Mapping for 24-Hour and 2-Hour Durations for Eastern Washington. MGS Engineering Consultants and Oregon Climate Service for Washington State Dept. of Transportation, 82 pp.

Schaefer, M.G., B.L Barker, G.H. Taylor, and J.R. Wallis, 2007: Regional Frequency Analysis and Spatial Mapping of 24-Hour Precipitation for Oregon. MGS Engineering Consultants and Oregon Climate Service for Oregon State Dept. of Transportation, 114 pp.

Schaefer, M.G., G.H. Taylor, and T.W. Parzybok, 2019: Technical Memorandum, Regional Precipitation-Frequency Analysis using the Climate Region Method (SWT) for application in Analyses of Extreme Precipitation and Floods, prepared for Colorado-New Mexico Regional Extreme Precipitation Study (REPS). https://metstat.com/papers_presentations/TM_RegionalPrecipAnalysis_ClimateRegionMethod_SWT_2019May07.pdf

Tharwat, A, 2018: Classification Assessment Methods, *Applied Computing and Informatics.* Available online at https://doi.org/10.1016/j.aci.2018.08.003

U.S. Geological Survey, 2015: USGS NED 1 arc-second n19w067 1 x 1 degree ArcGrid 2017: U.S. Geological Survey.

Wang, T., A. Hamann, D.L. Spittlehouse, and C. Carroll, 2016: Locally downscaled and spatially customizable climate data for historical and future periods for North America. *PLoS One* 11: e0156720. Available online at https://sites.ualberta.ca/~ahamann/data/climatena.html.

Weiss, L.L., 1964: Ratio of true to fixed-interval maximum rainfall: American Society of Civil Engineers, Journal of the Hydraulics Division, v. 90, HY–1, p. 77–82

APPENDIX A: Storms for Manual Storm Typing

Table 33: Storms used in the manual storm typing procedures, listed as storm start date (yyyy-mm-dd).

1893-10-08	1927-05-28	1953-01-18	1969-06-26	1984-01-27	1996-11-19
1896-11-15	1931-03-31	1955-05-17	1971-01-29	1986-01-09	1997-01-02
1902-07-04	1931-04-01	1955-11-04	1972-01-23	1986-01-26	1998-10-20
1906-03-13	1931-12-18	1955-12-23	1974-01-16	1986-02-19	1998-11-23
1906-05-30	1932-02-27	1956-12-10	1974-10-08	1986-07-03	2001-11-09
1908-05-28	1933-06-24	1957-11-23	1975-11-04	1986-10-16	2003-10-17
1908-07-15	1935-01-24	1959-01-24	1975-11-13	1987-08-01	2003-10-26
1908-10-16	1935-10-25	1959-04-29	1975-12-03	1987-10-29	2005-01-11
1909-11-24	1936-11-19	1959-12-06	1977-08-20	1987-12-04	2005-01-19
1913-07-26	1937-10-23	1961-02-11	1977-12-15	1988-07-13	2005-06-07
1914-01-06	1937-12-12	1961-08-14	1978-10-19	1989-11-09	2005-12-30
1916-03-09	1937-12-29	1961-10-14	1978-11-01	1990-04-28	2006-10-28
1917-11-19	1939-12-10	1961-11-24	1979-10-11	1990-06-12	2006-11-07
1917-12-29	1940-10-19	1962-01-28	1979-11-21	1990-11-10	2007-12-04
1920-01-14	1943-01-22	1962-07-18	1980-01-14	1990-12-04	2008-11-08
1920-01-18	1944-06-28	1962-10-12	1980-05-25	1991-05-19	2009-01-08
1920-08-06	1944-10-11	1963-01-06	1980-12-04	1991-10-10	2009-01-19
1921-11-22	1945-10-25	1963-02-01	1980-12-10	1992-09-29	2009-10-30
1921-12-12	1947-01-18	1963-12-23	1981-01-20	1993-01-26	2011-06-25
1922-10-26	1949-09-23	1964-10-19	1981-09-08	1993-02-27	2012-12-02
1923-01-07	1950-10-29	1964-12-24	1981-12-07	1993-11-26	2015-10-09
1923-10-01	1951-02-10	1965-06-27	1981-12-21	1994-10-26	2016-06-16
1924-02-12	1951-05-01	1965-10-21	1982-02-15	1995-06-07	
1924-12-12	1952-01-12	1966-08-28	1982-09-28	1996-02-08	
1927-02-20	1952-12-13	1969-01-21	1982-10-31	1996-09-25	

APPENDIX B: Data Acquisition and Assembly Report from NHC

1. Data Acquisition and Assembly

All available station data, at daily and hourly time steps, were acquired for British Columbia (BC). Precipitation data from long term stations within a defined band region of surrounding provinces was also acquired. In cases when temperature data was also available for the station, we obtained this data as well in order to flag when the temperature was above or below freezing.

There are two major sources of available data (Environment and Climate Change Canada, ECCC and the Pacific Climate Impacts Consortium, PCIC) and both were used, as summarized in sections 1.1 and 1.2. Additional data was collected from the BC Ministry of Environment and Climate Change Strategy (BC MoECCS) Data Catalogue (section 1.3). Data assembly is summarized in section 1.4.

1.1. Data Acquired from ECCC

All BC, Alberta (AB), Yukon (YT), and offshore (OT) stations were acquired in ECCC archive format, consisting of individual files by year and type, for the following data:

- (HLY01) – hourly total precipitation (P_{tot}) from a principal or autostations
- (HLY21) – hourly P_{tot} from the Fischer/Porter gauge, which has a coarser resolution
- (HLY03) – hourly rainfall
- (DLY02) – daily T_{max}, T_{min}, T_{ave}, P_{tot} from automated stations. Data is not qc'd.
- (DLY04) – daily T_{max}, T_{min}, T_{ave}, P_{tot}. Data is qc'd.
- (DLY44) – daily T_{max}, T_{min}, T_{ave}, P_{tot} from COOLTAP and manual stations, not qc'd.
- (DLY21) – daily total precipitation from Fischer/Porter gauges.

The archive file formats provided by ECCC include all stations and variable types in a fixed width format. A full explanation of data types can be found on the Environment Canada site[1]

1.2. Data Acquired from the PCIC Data Portal

PCIC has collected daily and hourly meteorological data from different sources and makes these available through their data portal: https://data.pacificclimate.org/portal/pcds/map/

The PCIC data portal includes the following networks:

- BC Ministry of Agriculture
- Agriculture and Rural Development Act Network
- BC Hydro
- Environment Canada Hourly

[1] ftp://client_climate@ftp.tor.ec.gc.ca/Pub/Documentation_Technical/Technical_Documentation.pdf

- BC Ministry of Environment – Air Quality Network
- BC Ministry of Environment – Automated Snow Pillow Network
- Forest Ecosystems Research Network
- Wildfire Management Branch
- Forest Renewal BC
- Ministry of Transportation and Infrastructure
- Rio Tinto Alcan

The above network data were downloaded from the PCIC data portal and meta data was compared between networks. ECCC data contained in the PCIC source was not used in preference to data provided directly from ECCC.

1.3. Data Acquired from the BC Data Catalogue (BCASWS)

BC MoECCS publishes data from the Automated Snow Weather Station (BCASWS) network on a daily basis to the BC Data Catalogue:
https://catalogue.data.gov.bc.ca/dataset/current-season-automated-snow-weather-station-data
https://catalogue.data.gov.bc.ca/dataset/archive-automated-snow-weather-station-data

This data includes hourly precipitation from BC Hydro stations that are part of the snow weather network. The data is near real-time and not subject to QA/QC prior to publishing but provides supplemental hourly data to the daily BC Hydro data contained in the PCIC BC Hydro network.

1.4. Data Assembly

Data assembly included the following:

- ECCC station data was assembled from the various source files, combining temperature and precipitation files when both existed for a station.
- PCIC station data was trimmed to precipitation and temperature. Data known to be provided in an accumulated format was processed to incremental precipitation.
- BCASWS station precipitation data was processed from accumulated to incremental and combined with temperature (when available for a station) for analysis.
- All data was processed into a flat file format.
- Station ID’s were made unique by network/source according to guidelines provided by MetStat.
- Meta data records were created organized by data source and network, and were formatted to match the example provided by MetStat.

Network names and abbreviations are provided in Table 34 on the following page.

Table 34: Source network names and abbreviations.
MFLNRORD = Ministry of Forests, Lands, Natural Resource Operations, and Rural Development.

Network/Source	Abbreviation
Environment and Climate Change Canada	ECCC
Pacific Climate Impacts Consortium	PCIC
BC Ministry of Agriculture	AGRI
Agriculture and Rural Development Act Network	ARDA
BC Hydro	BCH
BC Ministry of Environment - Air Quality Network	AQN
BC Ministry of Environment - Automated Snow Pillow Network	ASP
BC MFLNRORD - Forest Ecosystems Research Network	FERN
BC MFLNRORD - Wild Fire Management Branch	WMB
Forest Renewal British Columbia	FRBC
Ministry of Transportation and Infrastructure (electronic)	MoTI
Rio Tinto Alcan	RTA
BC Data Catalogue (BC Automated Snow and Weather Stations)	BCASWS

APPENDIX C: QA/QC of Precipitation Records Report from NHC

2. QA/QC of Precipitation Records

The QA/QC process was conducted in three phases:

- Phase 1: Used automated data QA/QC software, developed by NHC in the 'R' programming language (Hornik, 2016), to test every station to flag data problems and suspected data problems
- Phase 2: Manually evaluated the validity of the precipitation outliers flagged in Phase 1, by checking the station's time series and, in some cases, checking other stations' records for corroboration. Due to time constraint, not all outliers were evaluated in Phase 2.
- Phase 3: Summarized all flags into qcfl1 and qcfl3. This includes network supplied flags when available (ECCC only)

Each of these phases is described in Sections 2.1 - 2.4.

2.1. Test every station to flag suspected data problems (Phase 1)

NHC code QAQC_Functions.R (which is called by LoopMetadata.R to run for every station) performs the tests listed in Table 35 for each data entry, whether daily or hourly data.

Table 35: Tests performed for every entry in every station by program QAQC_functions.R

Test		Flag	Flag values	
			Yes	No
1	Precipitation missing?	qcfl1	M	
2	$\frac{T_{min}+T_{max}}{2} > 0°C$?	qcfl2	A	B
3	$Precip < 0$?	qcfl_neg_precip	TRUE	FALSE
4	$T_{min} \geq T_{max}$? or $T_{max} - T_{min} > 40°C$?	qcfl_Tmin_Tmax	TRUE	FALSE
5	Repeated precip values (≥6 times) ?	qcfl_rep	TRUE	FALSE
6	Long sequences of zero precipitation (28 days +) ?	qcfl_long_zeros	TRUE	FALSE
7	If $\sqrt[3]{precip}$ (the cubic-root of the precipitation value) deviates from its mean by more than 7 standard deviations, set flag to "TRUE".	qcfl_outlier	TRUE	FALSE
8	If T_{min} or T_{max} deviates from the seasonal (monthly) mean by more than 6 standard deviations, assume it is in error and set flag to "TRUE"	qcfl_outlier_Tmin qcfl_outlier_Tmax	TRUE TRUE	FALSE FALSE

Test 4 and Test 8 were applied for use in quality control of daily air temperature records. The QA/QC'd temperature records were then used (Test 2) to assign flag qcfl2 to precipitation records to indicate temperatures above or below freezing.

In the case of Test 7 in Table 35, precipitation values are transformed by taking their cubic root, before testing for their deviation from the mean, because this transformed variable (at daily time scale) has been shown to be approximately normally distributed[2] and can be used for screening for precipitation outliers[3]. In this work, this transformation was used for both daily and hourly data.

2.2. Phase 2: Check precipitation outliers

Once Phase 1 was completed, data entries which had been flagged with $qcfl_{outlier} = TRUE$ (from test 7 in Table 35) were checked manually. Due to time constraints, not all outliers could be checked (146 of the 448 stations with outliers were checked), and network sources were prioritized, starting with the ECCC hourly data. Metstat's qcfl3 was assigned the value "O", "W", or "V", using the methodology described below and represented in Figure 48 further below:

Step 1: Automated procedure, applied to every outlier precipitation value
Whenever the outlier precipitation value surpassed the established ***hard thresholds*** (which are 500 mm/24hr and 100 mm/hr), the value was assigned the flag $qcfl3 = W$, which is meant to indicate that the outlier value is in error and should not be used in statistical analyses. Daily data were checked for the 500 mm/24hr threshold. Hourly data were checked against the 100 mm/hr hourly threshold and also against the 500 mm/24hr daily threshold using a rolling sum of 24 hours. Outlier precipitation values below these hard thresholds were assigned the flag $qcfl3 = O$.

Step 2: Manual procedure, applied to outlier precipitation values that in Step 1 were assigned $qcfl3 = O$. Conducted for priority networks only.
a) Inspection of the time series graph. The principal method for manually checking and judging the validity of precipitation outliers was to inspect the time series graphs. A value which is part of a cluster, i.e., belonging to a precipitation event, and not accompanied by any clear data quality problems, was assumed valid and assigned $qcfl3 = V$. However, if the value is the highest in the station's record, seems excessively high, or is located near other data quality problems, then its validity could not be determined, and it was left as $qcfl3 = O$.
b) Seeking corroboration from other stations. In some cases, daily outliers were checked against the values reported by individual neighbouring stations; or by displaying in a map layout the 3-day total precipitation (centred on the day of the outlier) reported by other stations.
Examples of (a) and (b) are provided later in this section.

[2] Stidd, C. K. (1953). Cube-Root-Normal Precipitation Distributions. *Transaction, American Geophysical Union*, 34(1)

[3] Peterson, T. C. (2013). *Introduction to Quality Control of Daily Climate Data*. conference presentation. NOAA, Nanjing Workshop. [online] Available from: https://www.wmo.int/pages/prog/wcp/ccl/opace/opace2/documents/Peterson-Nanjing-2013-Introduction-to-quality-control.pdf.

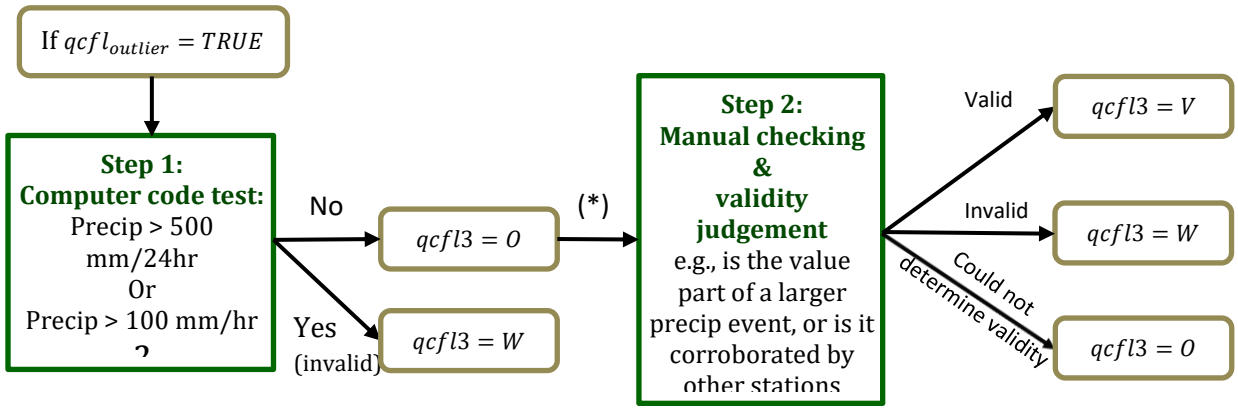

Figure 48: Methodology used for checking the validity of precipitation outliers. (*)
Many outliers with $\boldsymbol{qcfl3 = 0}$ *went through manual checking (step 2), but time constraints prevented checking all of them.*

2.3. Examples of how precipitation outliers were manually checked by inspection of the time series graph

The graphs provided by the auto-generated reports were inspected in Phase 2 to evaluate the validity of precipitation outliers flagged in Phase 1. As noted previously, due to time constraints, not all outliers could be checked, and network sources were prioritized, starting with the ECCC hourly data.

Example 1: Validation of an outlier in ECCC hourly station 116FRMN (Salmon Arm CS)

Figure 49 shows the entire station record (top panel) and a zoom-in around the outlier of January 7, 2015 (bottom panel). The outlier is seen to belong to a multi-hour precipitation event and, while this outlier value (26.3 mm in 1hr) is the highest observed in this station, the second highest outlier in January 8, 2016 (21.8 mm in 1hr), which also belongs to a multi-hour precipitation event, is not far behind in value. Both outliers were judged to be valid and assigned the flag $qcfl3 = V$.

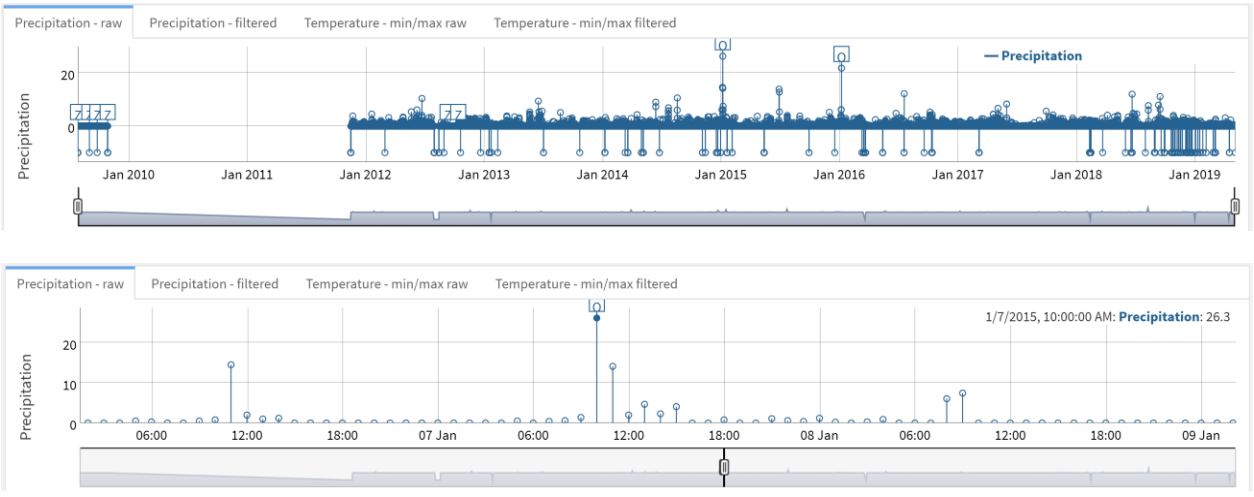

Figure 49: Time series graphs for EC hourly station 116FRMN (Salmon Arm CS) produced by the station's report. Top panel: Graph for the entire period of record. Bottom panel: Zoom-in for the outlier of January 7, 2015. The data are displayed in millimeters.

Example 2: Uncertain validity of an outlier in ECCC hourly station 1145M29 (Nelson CS)

Figure 50 shows the entire station record (top panel) and a zoom-in around the outlier of June 29, 2015 (bottom panel). The outlier is seen to be an isolated value surrounded by zeros, and represents the highest value recorded by the station (18.6 mm in 1hr). The validity of this outlier could not be determined with confidence, hence it was assigned the flag $qcfl3 = O$. Given more time, checking of neighbouring stations would have been pursued, but it was possible to do so for only a few stations.

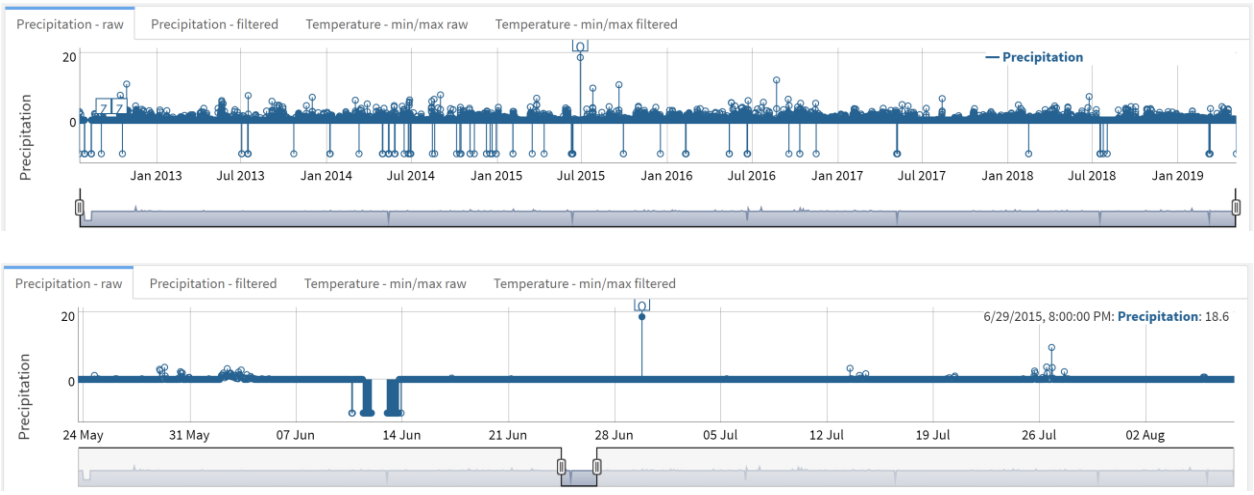

Figure 50: Time series graphs for EC hourly station 1145M29 (Nelson CS) produced by the station's report. Top panel: Graph for the entire period of record. Bottom panel: Zoom-in for the outlier of June 29, 2015.

Examples of how precipitation outliers were manually checked using corroboration from other stations

Precipitation outliers are especially important for intensity-duration-frequency (IDF) studies. Outliers were checked by hand using maps that indicate 3-day precipitation totals at all stations. The 3-day totals are centred on the day where the outlier value was detected. Whenever a clear spatial pattern was found, the outlier was validated with $qcfl3 = V$.

Example 3: January 3, 2003

On this date, several stations had values detected as outliers. This is one of several similar examples of a large-scale precipitation event. An interactive map for this date was studied and is reproduced below as a still image. The map displays, in the color scale shown, the precipitation total in the 3 days January 2-4, 2003. The presence of a coherent spatial pattern reassures us that these are true outlier values. Checking the North American Regional Reanalysis (NARR) daily data (https://www.esrl.noaa.gov/psd/cgi-bin/data/narr/plotday.pl/) reveals a similar spatial pattern of precipitation intensity, and the maps of integrated moisture flux show the arrival of an atmospheric river.

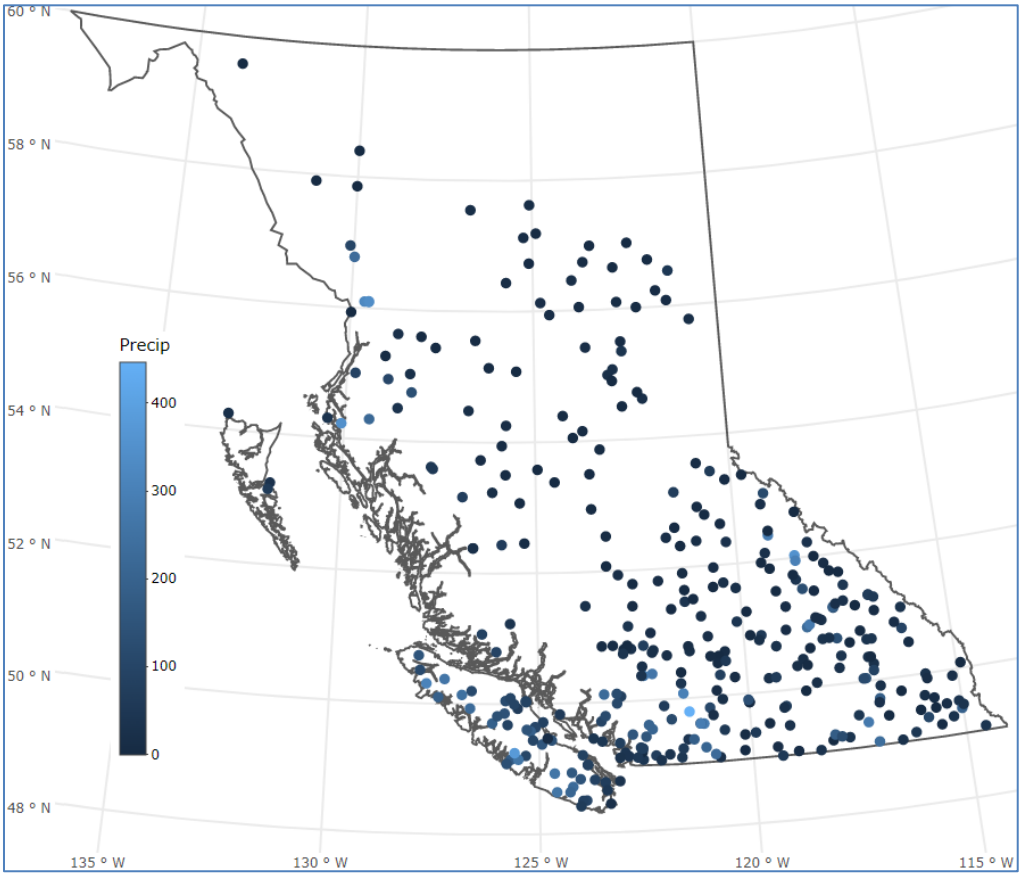

Figure 51: Example 3 of checking outliers. Map of 3-day precipitation for January 2-4, 2003, showing a spatially coherent, large-scale event. See also the NARR maps in the next figure.

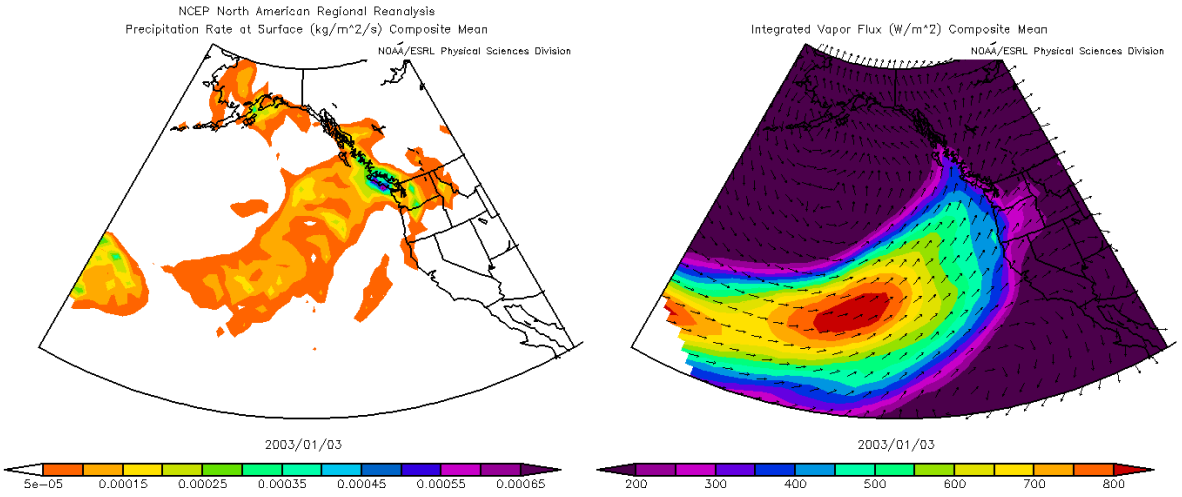

Figure 52: Example 3 of checking outliers. Maps of NARR precipitation (left panel) and integrated vapour flux (right panel) for January 3, 2003. Compare against the precipitation map in the previous figure.

2.4. Phase 3: Summarize Results in a Single Flag: qcfl3

The QAQC code issues values for several quality flags listed in Table 36 (qcfl_outlier, qcfl_rep, etc.). These flags are represented by a single flag – qcfl3 – for MetStat's subsequent review. Table 36 below and Table 37 on the following page summarize the values that may be taken by the flag qcfl3. Possible qcfl3 values are the single letter characters V, W, O, R, X, Y, Z, or F. When no quality issues are identified with the data entry, qcfl3 is left blank ("").

When two or more problems are detected by the different qcfl_ flags, the most relevant one is recorded in qcfl3. The exception to this is when data is missing; a qcfl1 value of 'M' overrides all other flags. When there are problems with both precipitation and temperature, it is the precipitation problem which is recorded in qcfl3. For example, if we have qcfl_outlier = TRUE and qcfl_Tmin_Tmax = TRUE, this leads to qcfl3 = V, W, or O (see Table 37), while qcfl2 will be blank.

A negative precipitation value always leads to qcfl1 = M, with qcfl3 = "" (blank).

Table 36: Converting multiple quality flags into a single flag, qcfl1 or qcfl3. This table contemplates cases where only one of the flags is TRUE. In those cases where two or more flags are TRUE, it is the most relevant flag which is recorded in qcfl3 (see text).

	qcfl3 = $\begin{cases} \boldsymbol{V}\ (validated) \\ \boldsymbol{W}\ (wrong) \\ \boldsymbol{O}\ (unknown\ validity) \end{cases}$	**qcfl3 = *R***	**qcfl3** $= \begin{cases} \boldsymbol{X}\ (validated) \\ \boldsymbol{Y}\ (wrong) \\ \boldsymbol{Z}\ (unknown\ validity) \end{cases}$	***qcfl1* = *M***
qcfl_outlier	**TRUE**	FALSE	FALSE	FALSE
qcfl_rep	FALSE	**TRUE**	FALSE	FALSE
qcfl_long_zeros	FALSE	FALSE	**TRUE**	FALSE
qcfl_neg_precip	FALSE	FALSE	FALSE	**TRUE**

Table 37: Additional qcfl3 values used (in blue) and their meaning.

qcfl3	Meaning
V	$qcfl3 = V$ indicates a precipitation outlier which has been validated (i.e. corroborated) by neighbouring meteo stations, as in "example 1" shown in section 2.3.
W	$qcfl3 = W$ indicates a precipitation outlier which is clearly in error. This includes daily precipitation values larger than 500 mm, hourly values larger than 100 mm, rolling sums over 24 consecutive hours larger than 500 mm.
O	$qcfl3 = O$ indicates a precipitation outlier of unknown validity. This includes outliers for which agreement from neighbouring meteo stations was unclear, as well as outliers which have not been checked manually. The outlier may or not be in error (undetermined).
R	$qcfl3 = R$ indicates a precipitation value belonging to a sequence of 6 or more repeated (non-zero) values.
X	$qcfl3 = X$ (validated zero) indicates a zero precipitation value belonging to a sequence of 28 days[1] or more of consecutive zeros, when it has been checked that neighbouring meteo stations also show a long sequence of zeros (hence the long sequence of zeros is believed to not be in error).
Y	$qcfl3 = Y$ (invalid zero) indicates a zero precipitation value belonging to a sequence of 28 days or more of consecutive zeros, when it has been checked that neighbouring meteo stations do not show a long sequence of zeros (hence the long sequence of zeros is believed to be in error).
Z	$qcfl3 = Z$ indicates a zero precipitation value belonging to a sequence of 28 days or more of consecutive zeros, when no checking against neighbouring meteo stations has been done – either because of station sparsity for the dates in question, or because checking was not conducted; or when checking was done but the results were inconclusive. The long sequence of zeros may or not be in error (undetermined).
F	The precipitation value is immediately preceded by a missing value. Therefore, it could possibly represent an unreported accumulation.

1. 28 days was selected considering the possibility of a complete month of data missing but represented as zeros.

Finally, absent any NHC flags, the network provided flags were recorded (mostly in qcfl3). Only ECCC provided precipitation quality flags; we mapped these flags to digits in qcfl3 in order to distinguish from the NHC QC letter flags. The definition of ECCC network flags, when available, are shown in Table 38 on the following page. Some flags (e.g. missing and accumulated) provided by ECCC could be mapped to qcfl1 flags currently used by MetStat.

Table 38: ECCC network-provided flag definitions.

ECCC Network Flag	NHC Flag	Network Description	Column
A	A	Accumulated amount; previous value C or L for elements 010, 011, 012.	qcfl1
C	1	Precipitation occurred, amount uncertain; value is 0	qcfl3
E	2	Estimated	qcfl3
F	A	Accumulated and estimated	qcfl1
H	3	Freezing	qcfl3
I	4	Unadjusted	qcfl3
J	5	Freezing and unadjusted	qcfl3
L	7	Precipitation may or may not have occurred; value is 0 or 0.1	qcfl3
M	M	Missing	qcfl1
T	8	Trace; value is zero	qcfl3

1. ECCC data flags were mapped to a unique digit where required in order to maintain NHC flags as outlined above.
2. The network flag was placed in qcfl1 or qcfl3 as required.

3. Deliverables

An interactive map was created for MetStat (Precipitation_Map.html). The map links individual QC reports for each station and provides station metadata. Station metadata is searchable. An image capture is given in Figure 53 on the following page.

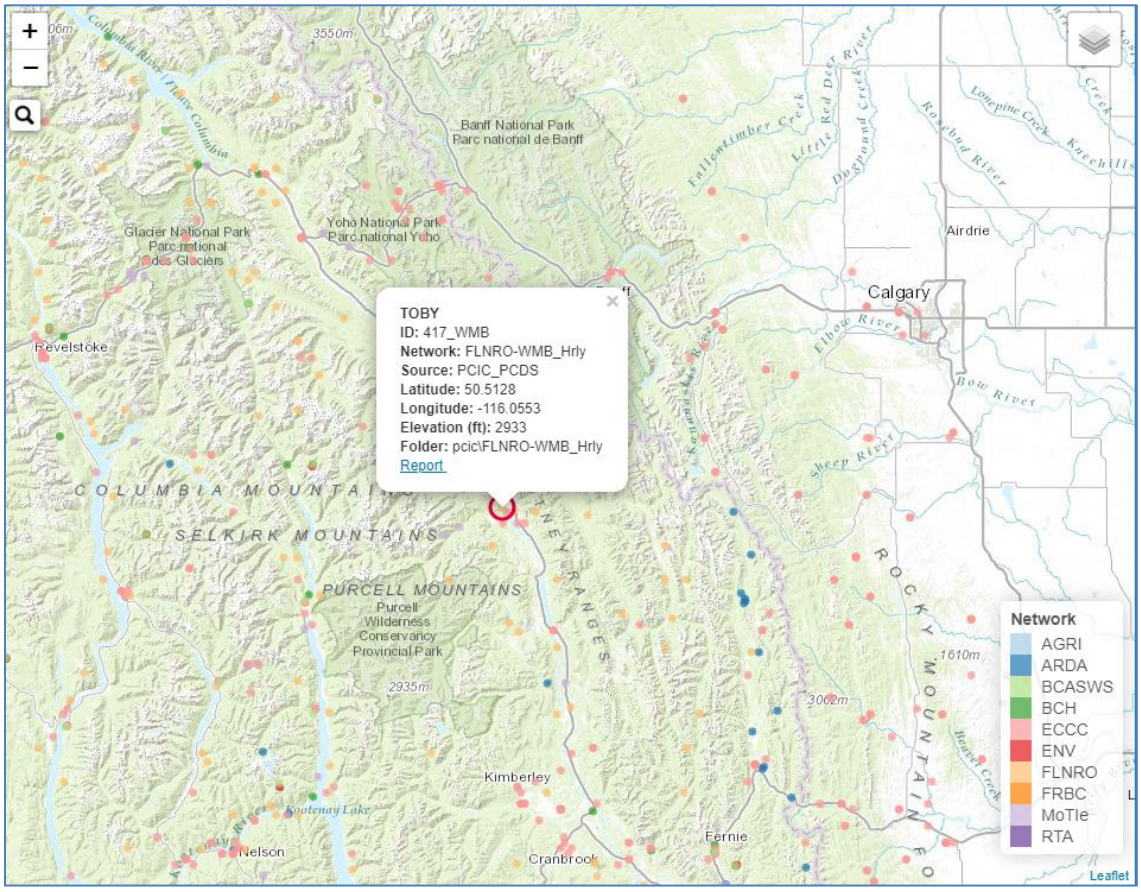

Figure 53: Image capture of the interactive visual application.

Along with the map, three sub-folders of deliverables have been provided: ‘csv_output/’, ‘non_QC_EC_AB/’, and ‘reports/’.

The reports folder stores all of the html reports that are linked by the map. The map expects this subdirectory to be located in the same folder as the html map file (i.e. links are relative to the map location). The csv_output folder contains the actual processed precipitation data, organized in the same structure as the reports folder, with metadata supplied by network. The non_QC_EC_AB are the ECCC data for Alberta stations with short records along the Rocky Mountain crest. These stations are parsed into timestamps the same way as the QC’d data, but no reports are generated, and quality control was not performed. They are not shown on the map.

Metadata shows the Province of the station in Metstat’s ‘state’ column. The state ‘OT’ indicates offshore weather buoys from the ECCC network.

As a whole, we recommend that Metstat place the highest priority on ECCC stations, as these are collected with the greatest rigour, and are likely to be of the highest quality. The poorest quality records are likely to be hourly records from the non-ECCC networks.

4. Notes

This section provides notes on several issues that may be of interest to MetStat in their interpretation and evaluation of the data. Individual station notes from manual station checking (when available) are also supplied in the document '20190712 3004871 Station Notes.R0.pdf'.

4.1. Observation Time and Climate Day

Observation times and definitions of climate day for daily precipitation data vary amongst networks and have changed over time. Data submitted to MetStat have been shifted in time as necessary to follow the current US definition of climate day (where the timestamp is at the end of the observation interval). Observation times shown in records submitted to MetStat have been adjusted to Local Standard Time using readily available information.

Table 39 below summarizes observation times and date shifts applied to adjust to US climate day definitions for daily ECCC data (based on personal communication with R. Hopkinson, CCS, 2019). "Ordinary" stations are those which report daily data only as opposed to "First Order" stations which report both hourly and daily data. There are no fully reliable network-wide records of observation time. It is understood that the majority of Ordinary stations have an 0800 LST observation time. However, some stations are believed to have a 1700 LST observation time and the observation time may have changed over time. In situations where the timestamp date shift rolled forward (creating a gap day), a missing data flag for the gap day was included. When the timestamp date shifts backwards, the first of the two observations was kept.

Absent any other information, non-ECCC daily data were assumed to have an observation time of 00. If the observation time for a particular station in any network needs to be known with greater certainty, then the data provider should be contacted for that information.

Table 39: Observation times and date shifts applied to adjust to US climate day definition for ECCC daily data.

Station Type	From Date	To Date	UTC Offset	Date Shift[1]	Observation Time
Ordinary	any	1932 Dec 31	any	0	8:00
Ordinary	1933 Jan 01	2019 Dec 31	any	1	8:00
First Order	any	1932 Dec 31	any	0	7:00
First Order	1933 Jan 01	1940 Dec 31	any	1	7:00
First Order	1941 Jan 01	1957 May 31	-7	1	6:00
First Order	1957 Jun 01	1961 Jun 30	-7	1	5:00
First Order	1961 Jul 01	2019 Dec 31	-7	0	23:00
First Order	1941 Jan 01	1957 May 31	-8	1	5:00
First Order	1957 Jun 01	1961 Jun 30	-8	1	4:00
First Order	1961 Jul 01	2019 Dec 31	-8	0	22:00

[1] Shift (days) applied to original data to adjust to US climate day definition

4.2. Potential timestamp problems

Throughout this analysis, a number of potential timestamp problems were identified. We will communicate information from the data provided if it becomes available

- The BCASWS hourly data was reportedly supplied as UTC, but may switch between UTC and local time zone in the period around the time of 2009-2010. We have contacted the data provider about this issue, but it has not been resolved.
- The MOTI data supplied by PCIC was reportedly supplied as UTC, but we suspected that the data is actually in local time. After discussions with PCIC (pers. communication, C. Ballantyne, 2019) we assumed that MoTI data was supplied in local time.

4.3. Known data problems

Some unique data issues were identified that were not expected to be handled by the automated QC process:

- Hourly data from the BCASWS network appeared to have diel temperature effects (i.e. daily wave pattern) in the accumulated data. This can lead to small amounts of precipitation being recorded on dry days. We expect that this effect is not as great during extreme precipitation events, but estimates of total precipitation volumes over long periods are not likely to be accurate from this network.
- In various networks, accumulated precipitation data appears to be erroneously input into the supplied incremental data. We identified some of these issues through the manual, spatial, validation step, and some summary notes are provided in file 'Station_notes.pdf'. However, it is likely that not all of these issues have been identified.

4.4. Coincident stations

There were many cases with multiple stations at the same location. The majority of these situations are when the same location provided multiple station types from ECCC, or are situations when multiple stations are actually near each other (for example in urban areas). However, other situations also occur. The two most common are:

- Coarse station location metadata. For example, for the 'ZZ' named stations in the BC MFLNRORD-WMB sites, the metadata is only down to the nearest 0.1 degree or even degree.
- Snow pillow data comes in daily form from PCIC and hourly form from BCASWS for the same stations.

After removing the coincident stations where both are ECCC stations, 186 situations occur where two stations are either within 500 m of each other, or have the same station ID. These names of coincident stations are supplied in the file '20190712 3004871 Station_duplicates.R0.xlsx'.

DISCLAIMER

This document has been prepared by **Northwest Hydraulic Consultants Ltd.** for the benefit of **MetStat, Inc.** for specific application to the **British Columbia Regional Precipitation Frequency Analysis Project**. The information and data contained herein represent **Northwest Hydraulic Consultants Ltd.** best professional judgment in light of the knowledge and information available to **Northwest Hydraulic Consultants Ltd.** at the time of preparation, and was prepared in accordance with generally accepted engineering practices.

Except as required by law, this report and the information and data contained herein are to be treated as confidential and may be used and relied upon only by **MetStat, Inc.** and **British Columbia Ministry of Forests, Lands, Natural Resource Operations and Rural Development**, and their officers and employees. **Northwest Hydraulic Consultants Ltd.** denies any liability whatsoever to other parties who may obtain access to this report for any injury, loss or damage suffered by such parties arising from their use of, or reliance upon, this report or any of its contents.

APPENDIX D: Maps of precipitation at select AEPs at the 24-hour duration

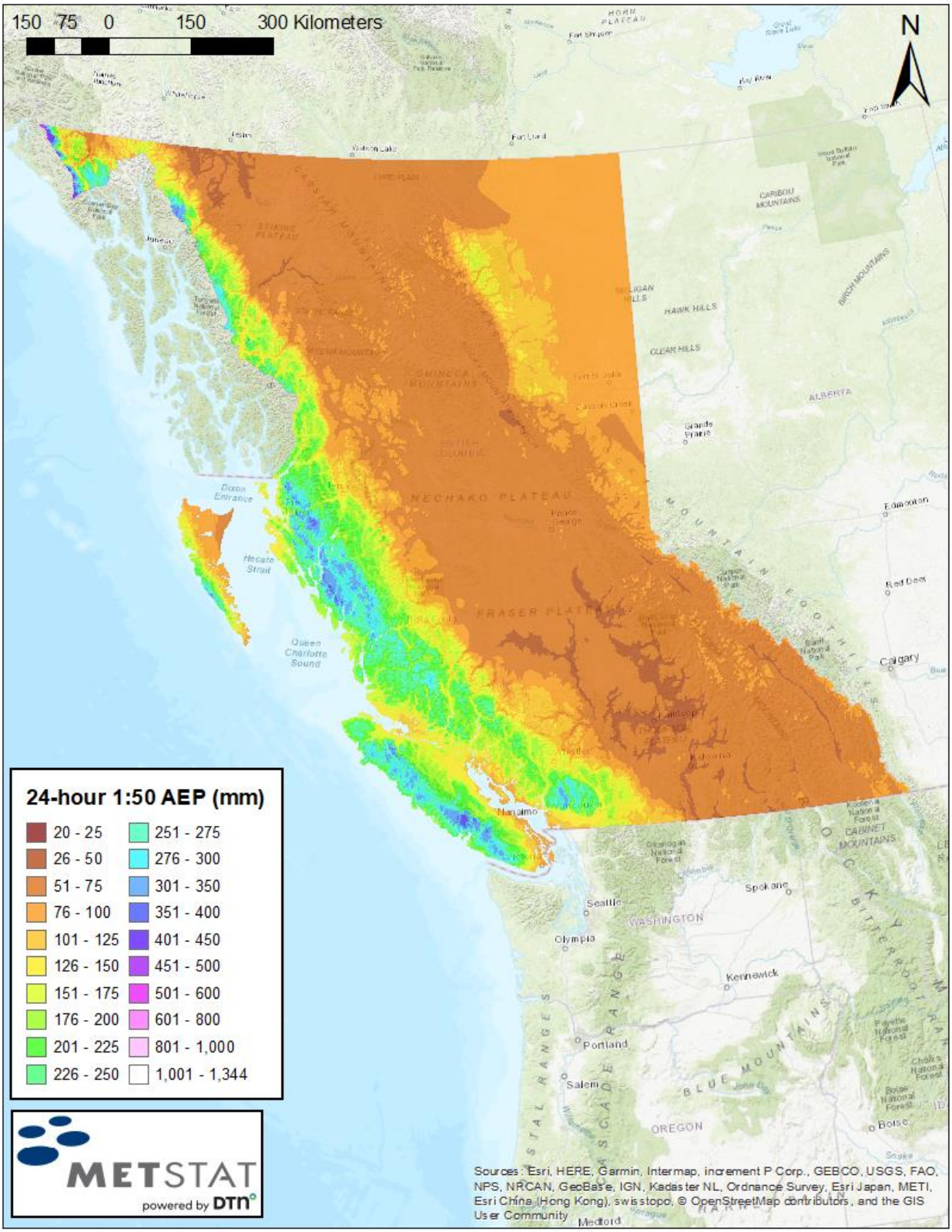

Figure 54: Map of precipitation (mm) for 24-hour 1:50 AEP.

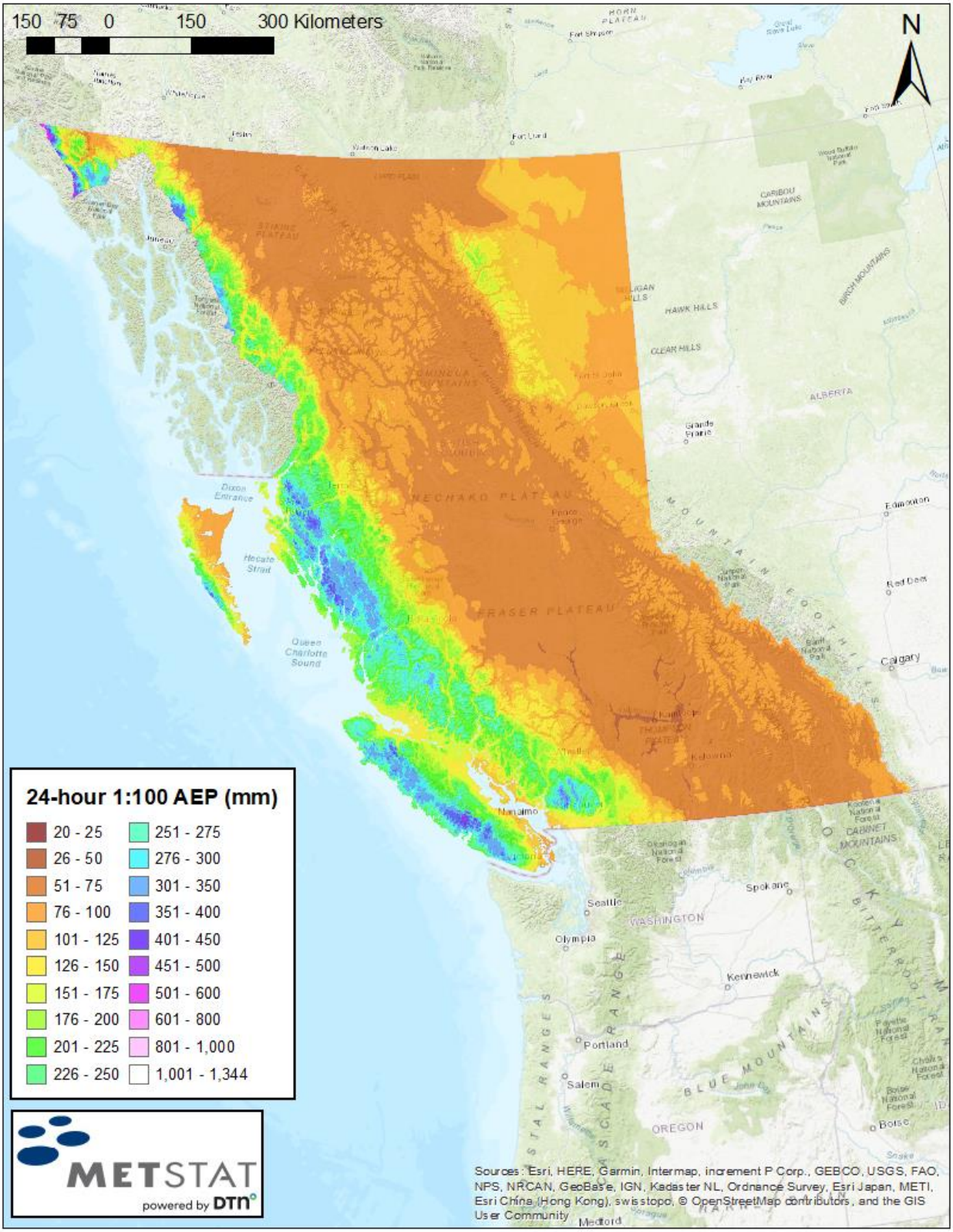

Figure 55: Map of precipitation (mm) for 24-hour 1:100 AEP.

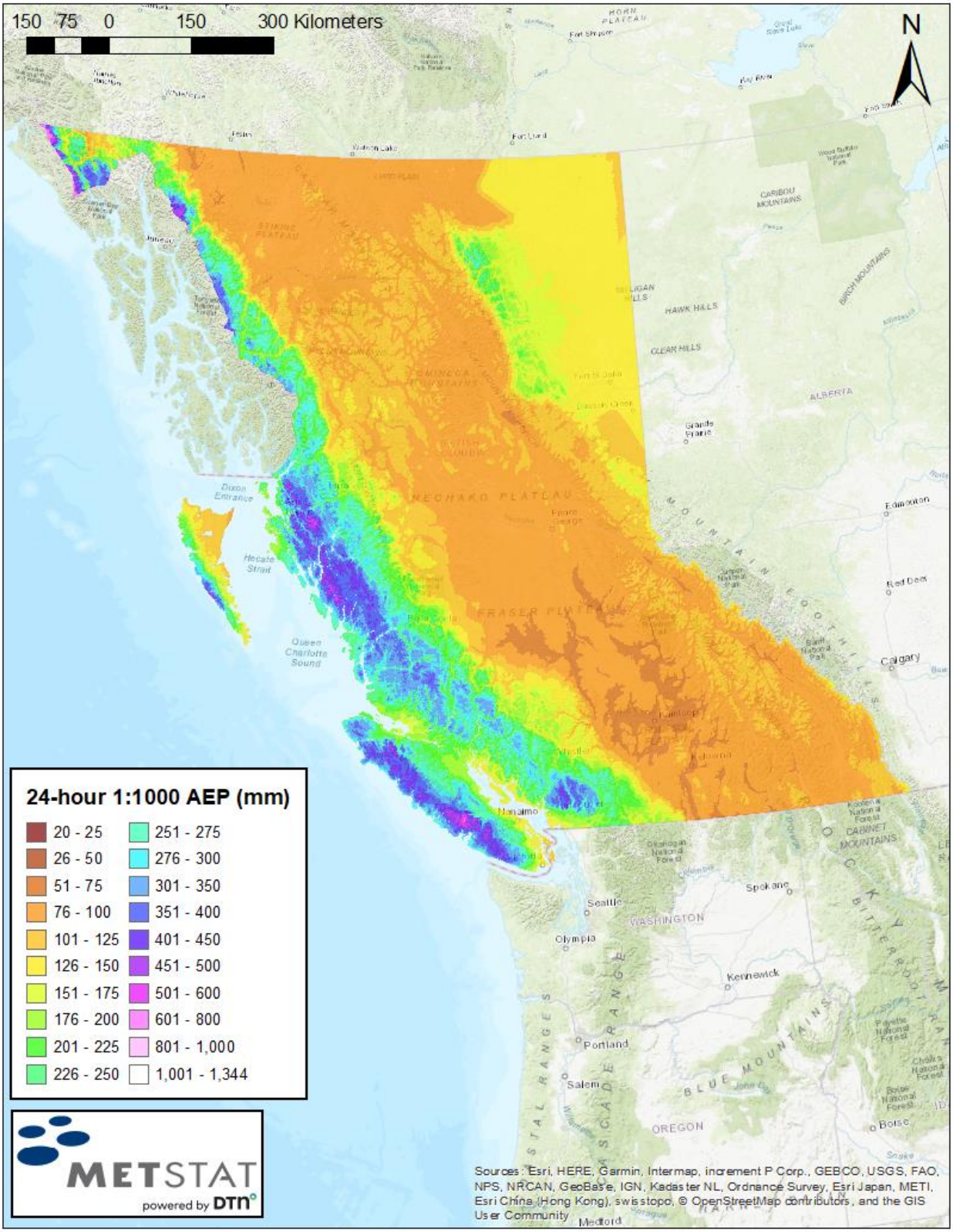

Figure 56: Map of precipitation (mm) for 24-hour 1:1,000 AEP.

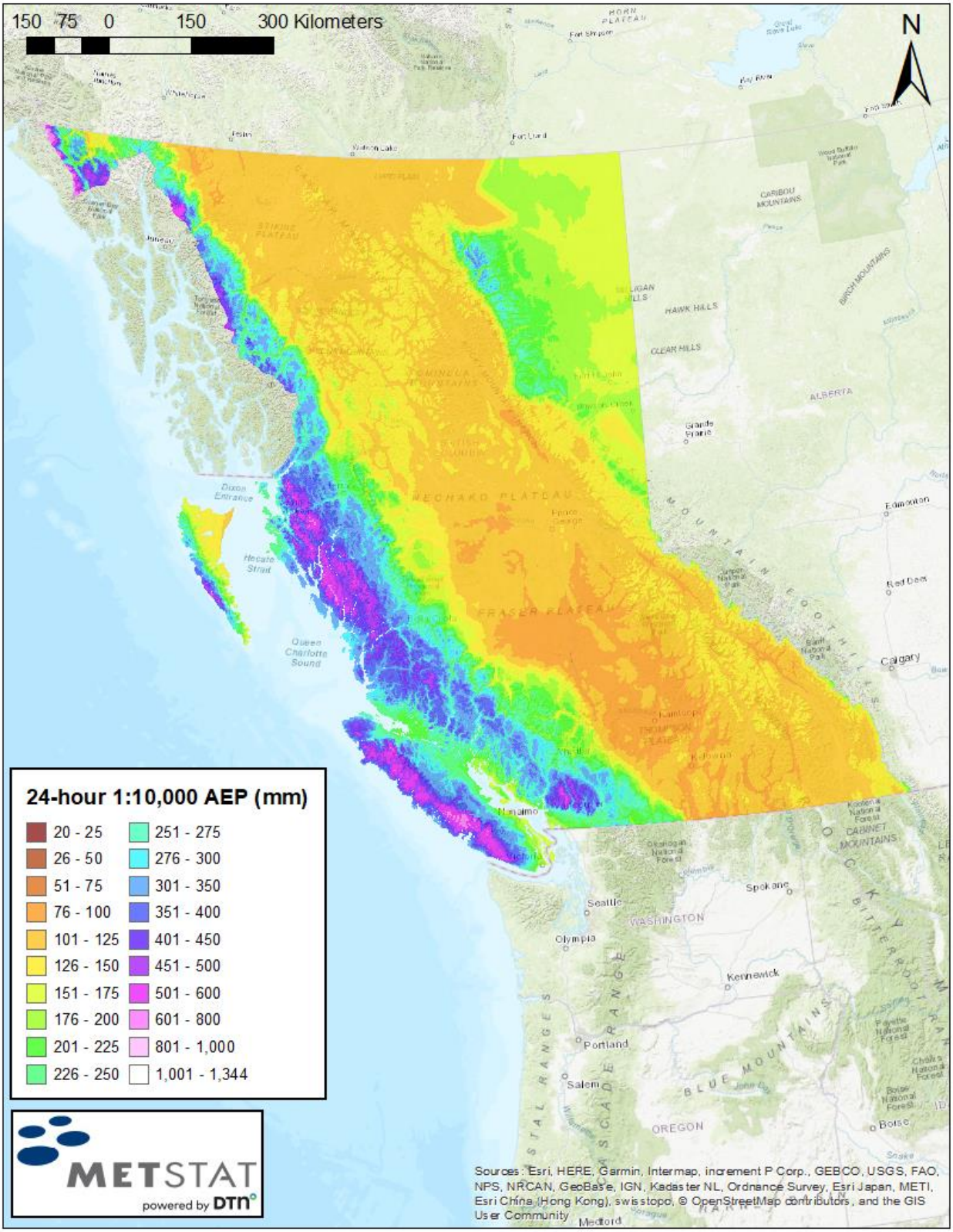

Figure 57: Map of precipitation (mm) for 24-hour 1:10,000 AEP.

APPENDIX E: Maps of precipitation at select AEPs at the 48-hour duration

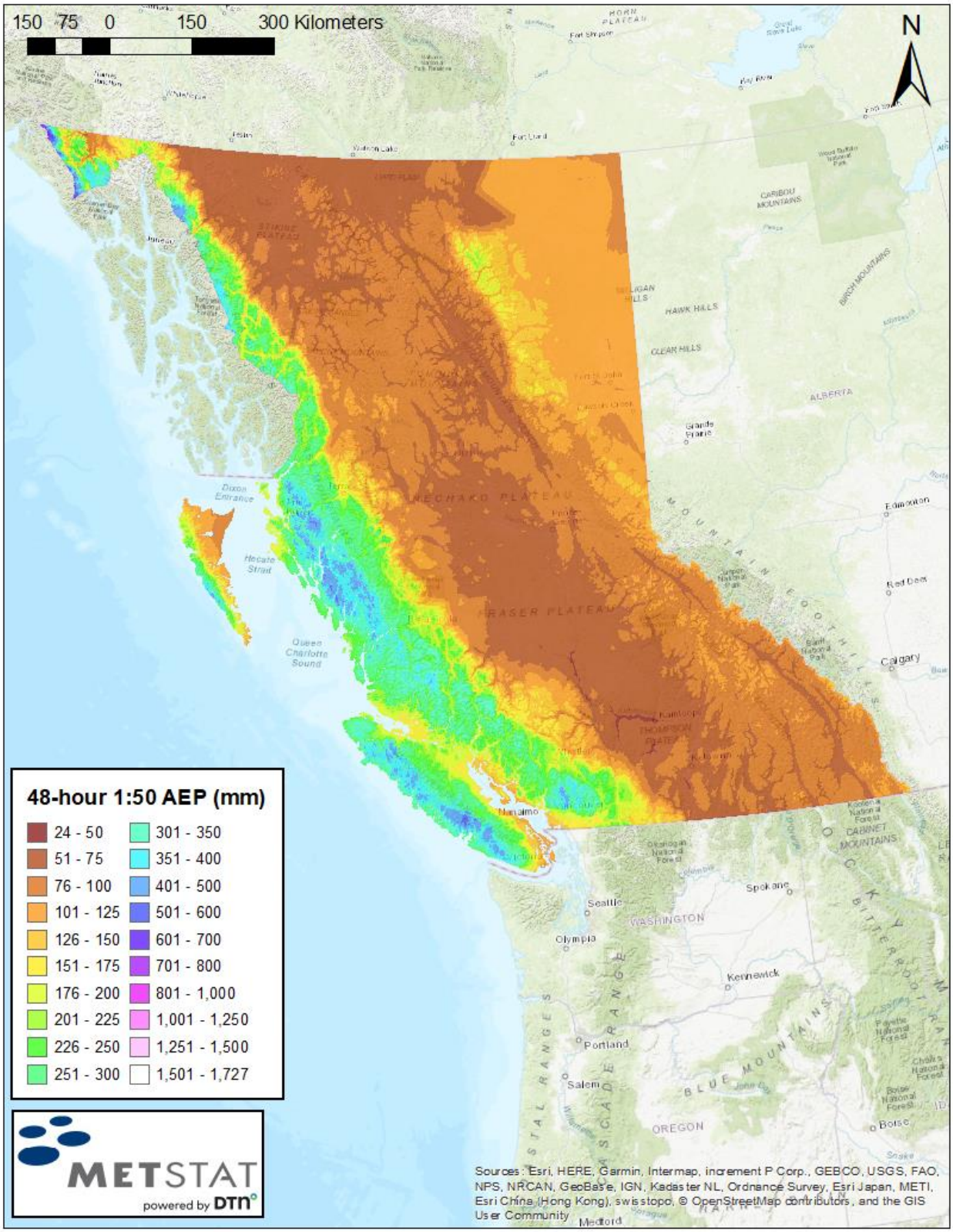

Figure 58: Map of precipitation (mm) for 48-hour 1:50 AEP.

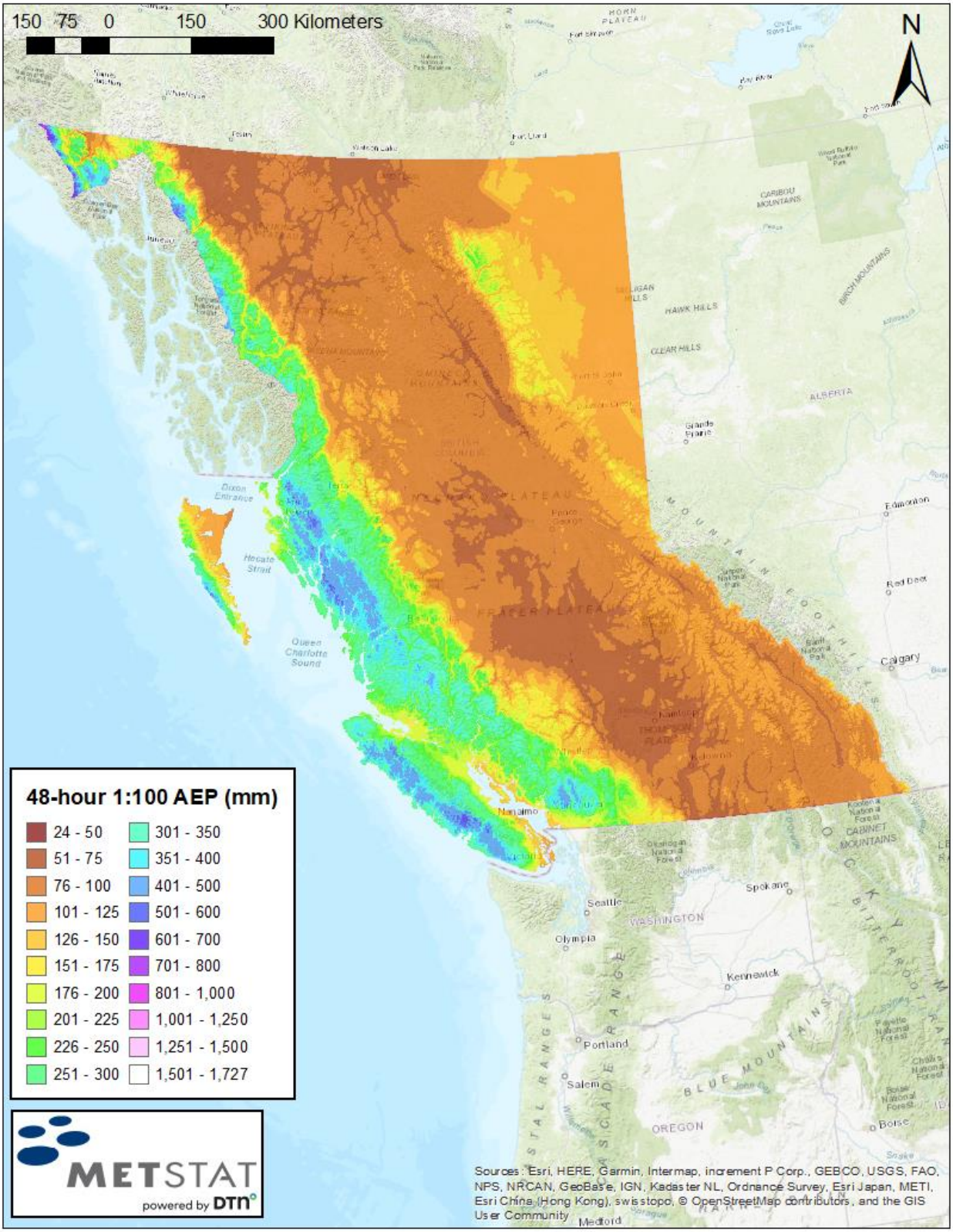

Figure 59: Map of precipitation (mm) for 48-hour 1:100 AEP.

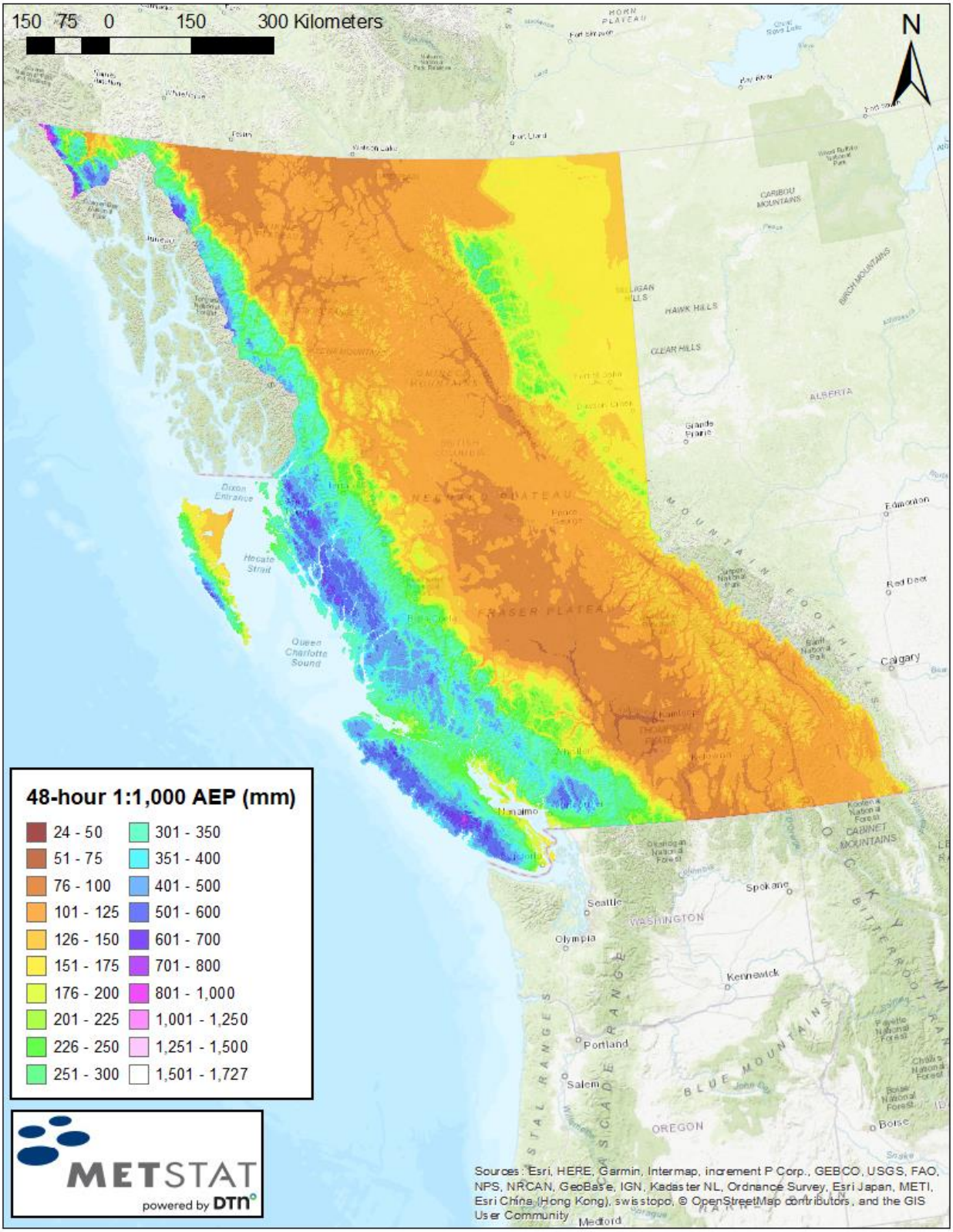

Figure 60: Map of precipitation (mm) for 48-hour 1:1,000 AEP.

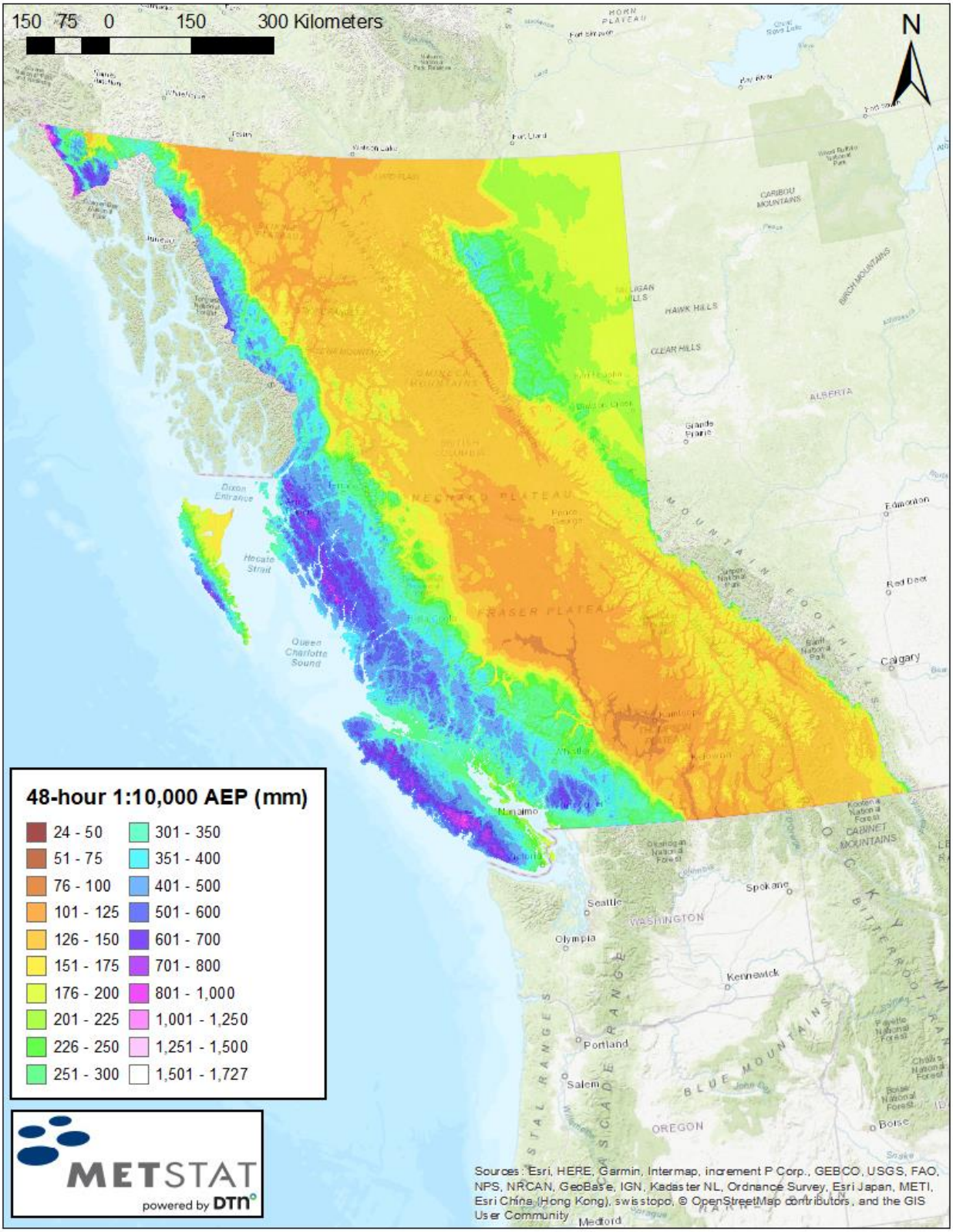

Figure 61: Map of precipitation (mm) for 48-hour 1:10,000 AEP.

APPENDIX F: Maps of precipitation at select AEPs at the 72-hour duration

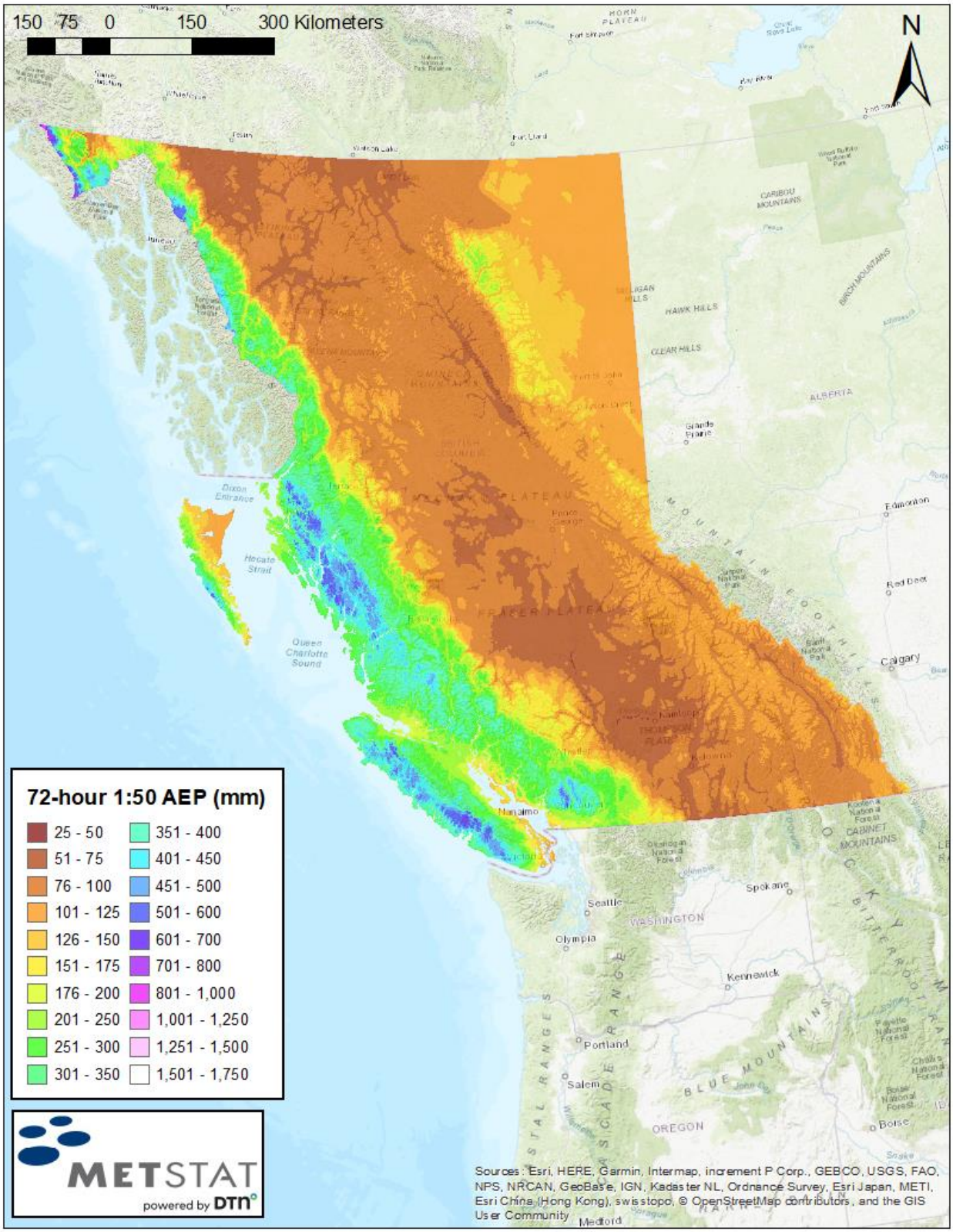

Figure 62: Map of precipitation (mm) for 72-hour 1:50 AEP

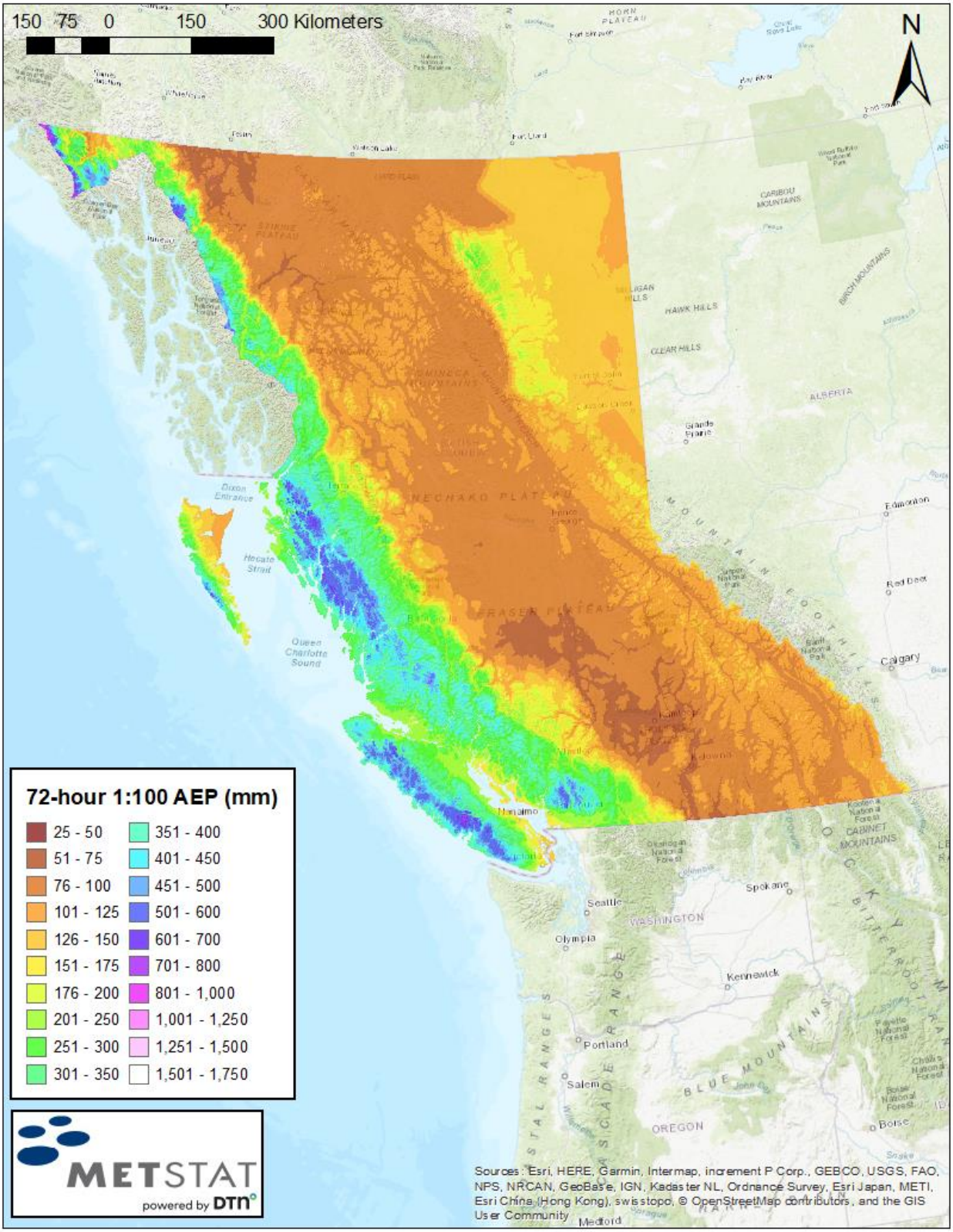

Figure 63: Map of precipitation (mm) for 72-hour 1:100 AEP.

.

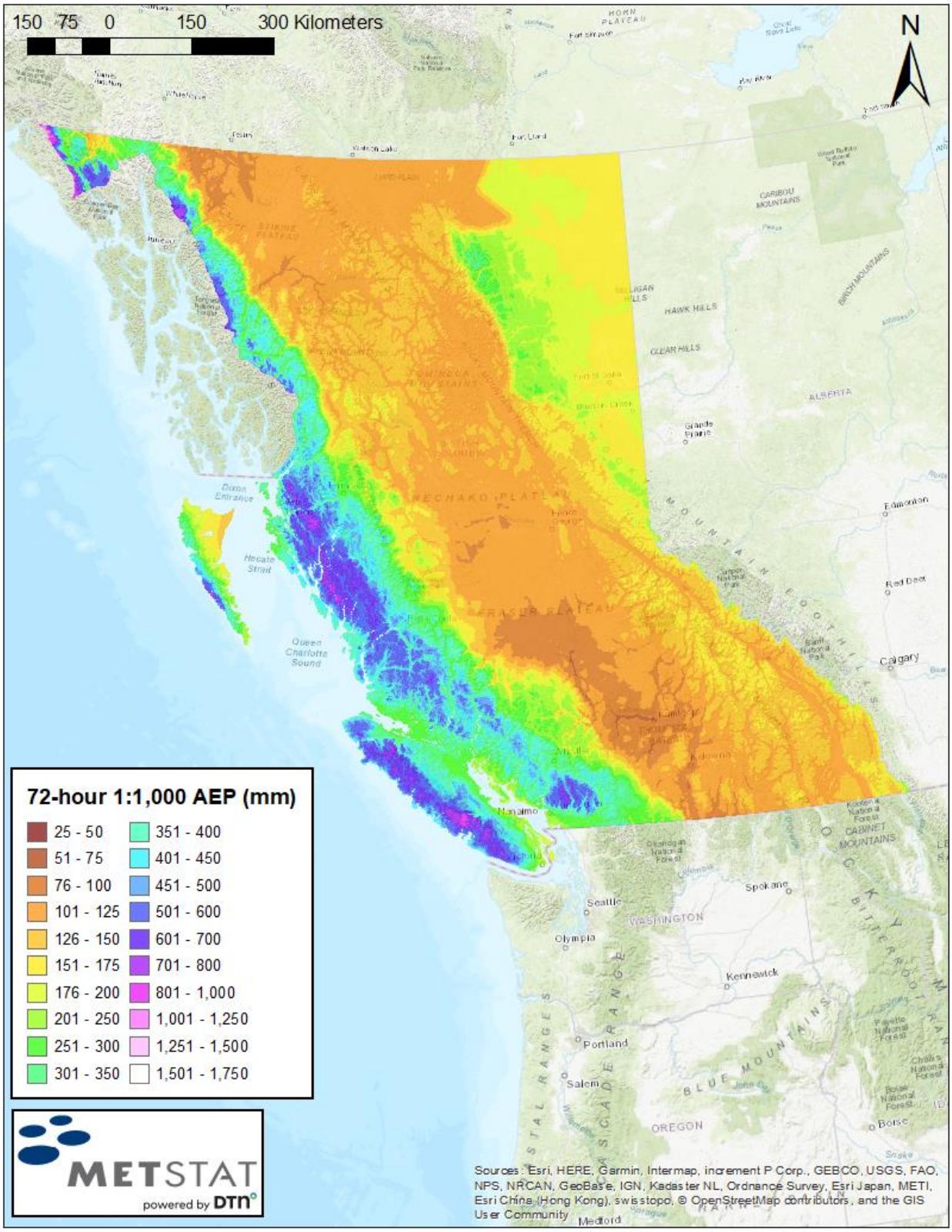

Figure 64: Map of precipitation (mm) for 72-hour 1:1,000 AEP.

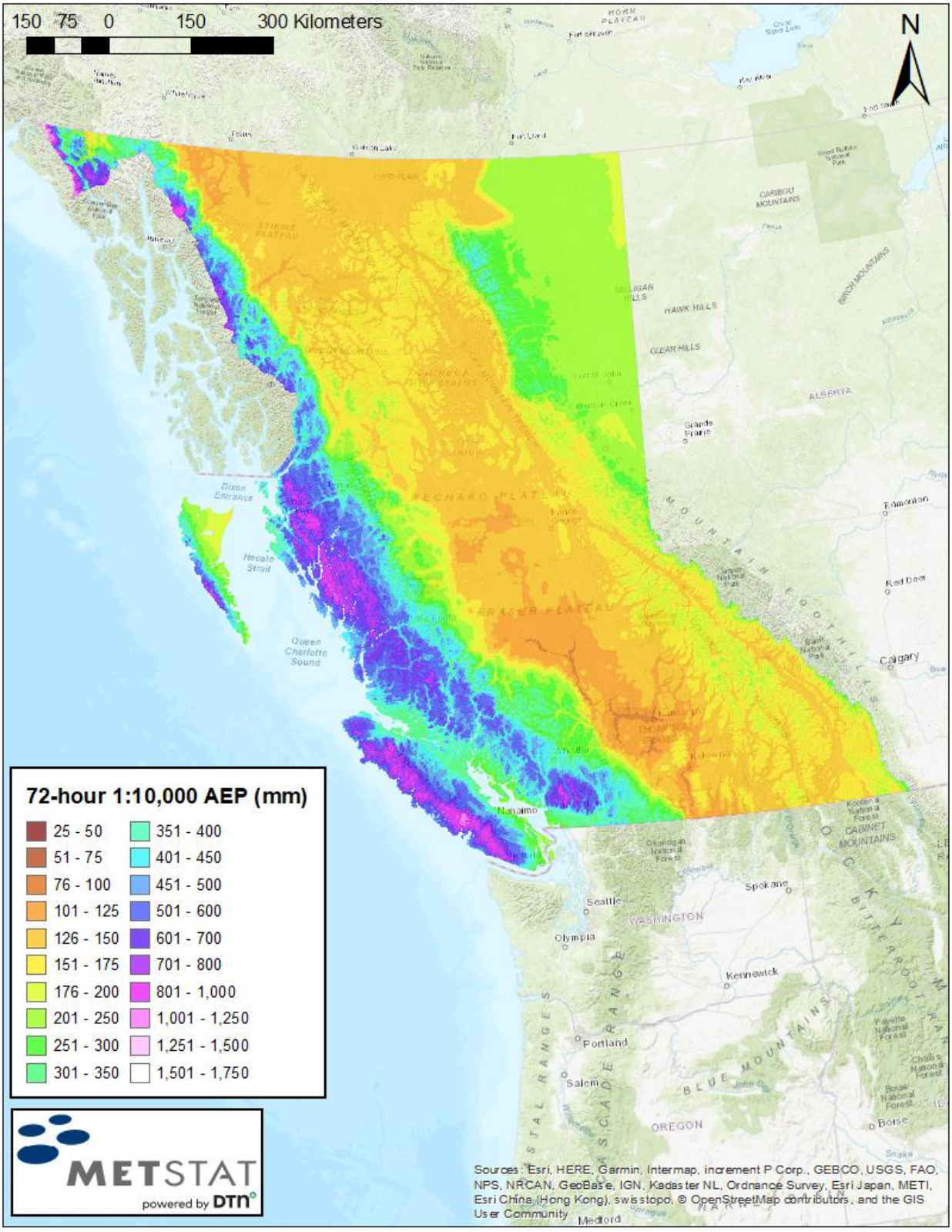

Figure 65: Map of precipitation (mm) for 72-hour 1:10,000 AEP.

APPENDIX G: Maps of precipitation at select AEPs at the 96-hour duration

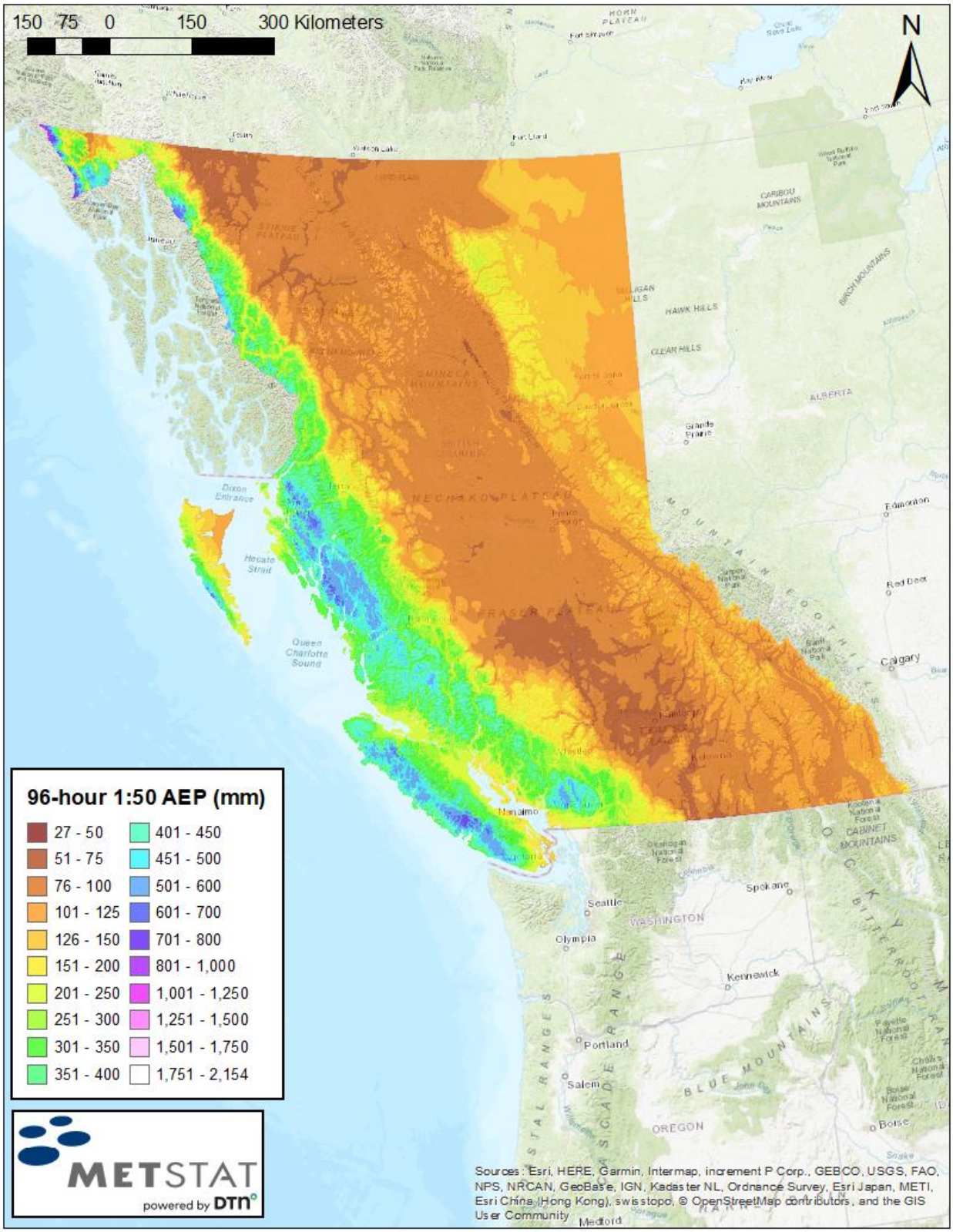

Figure 66: Map of precipitation (mm) for 96-hour 1:50 AEP.

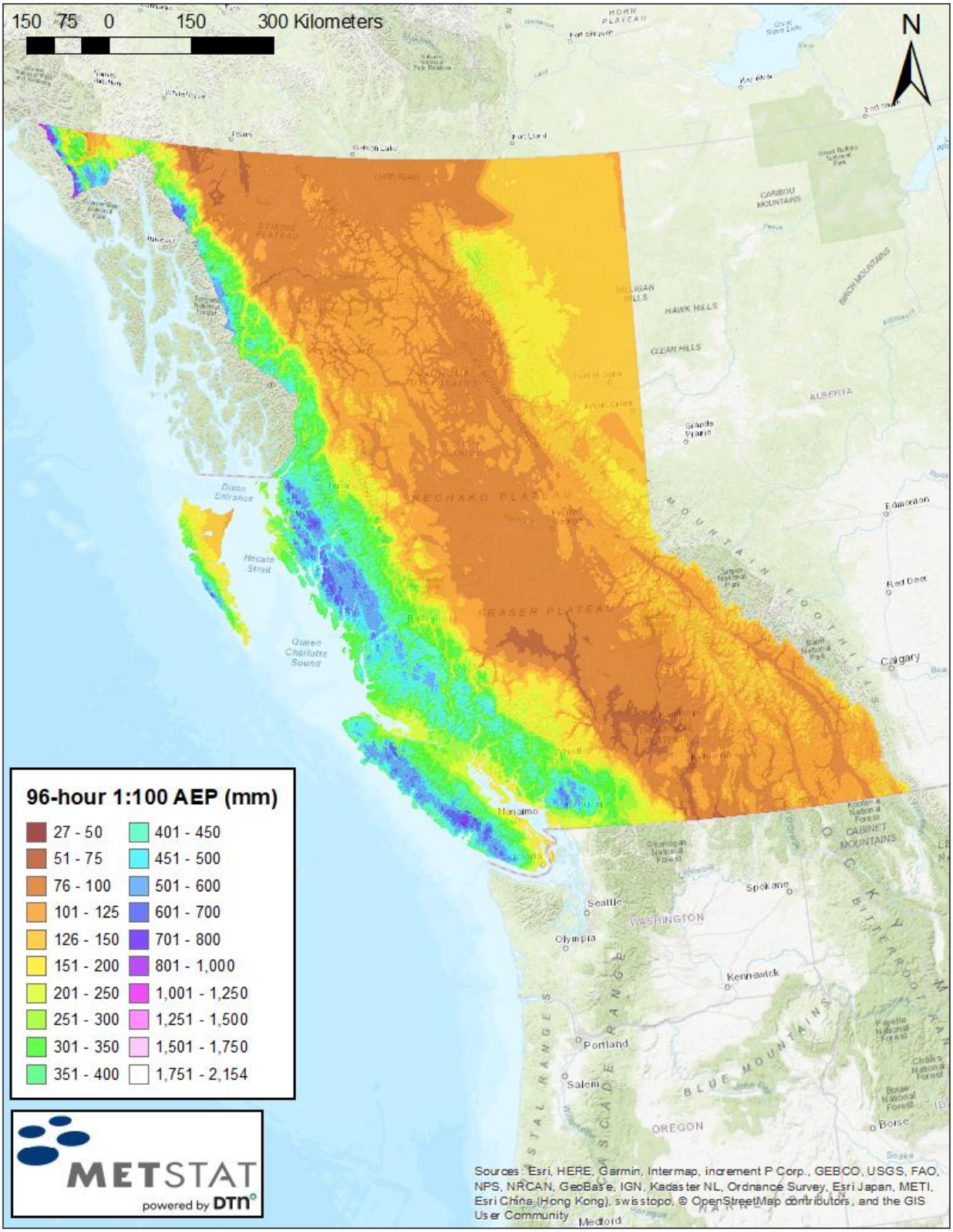

Figure 67: Map of precipitation (mm) for 96-hour 1:100 AEP.

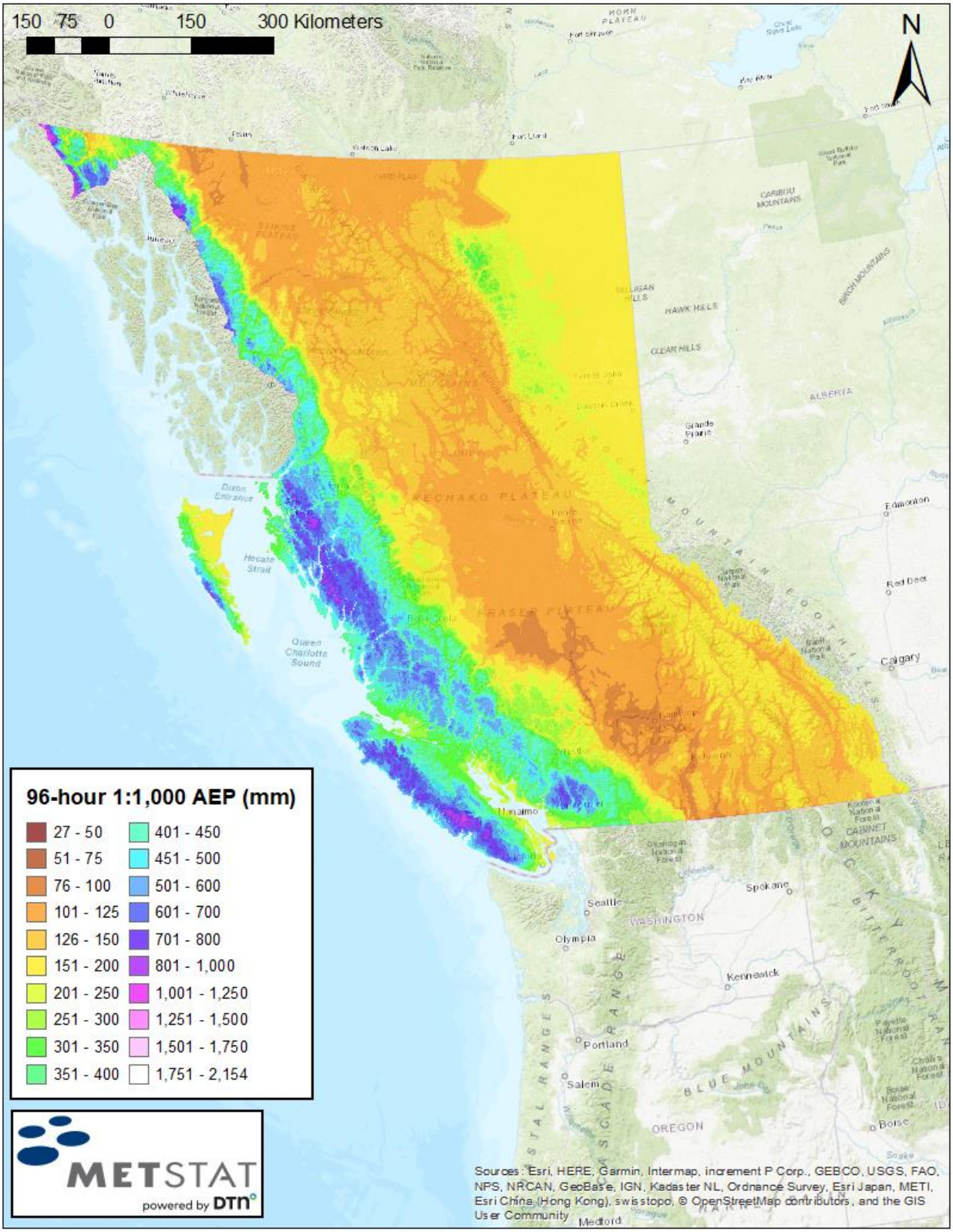

Figure 68: Map of precipitation (mm) for 96-hour 1:1,000 AEP.

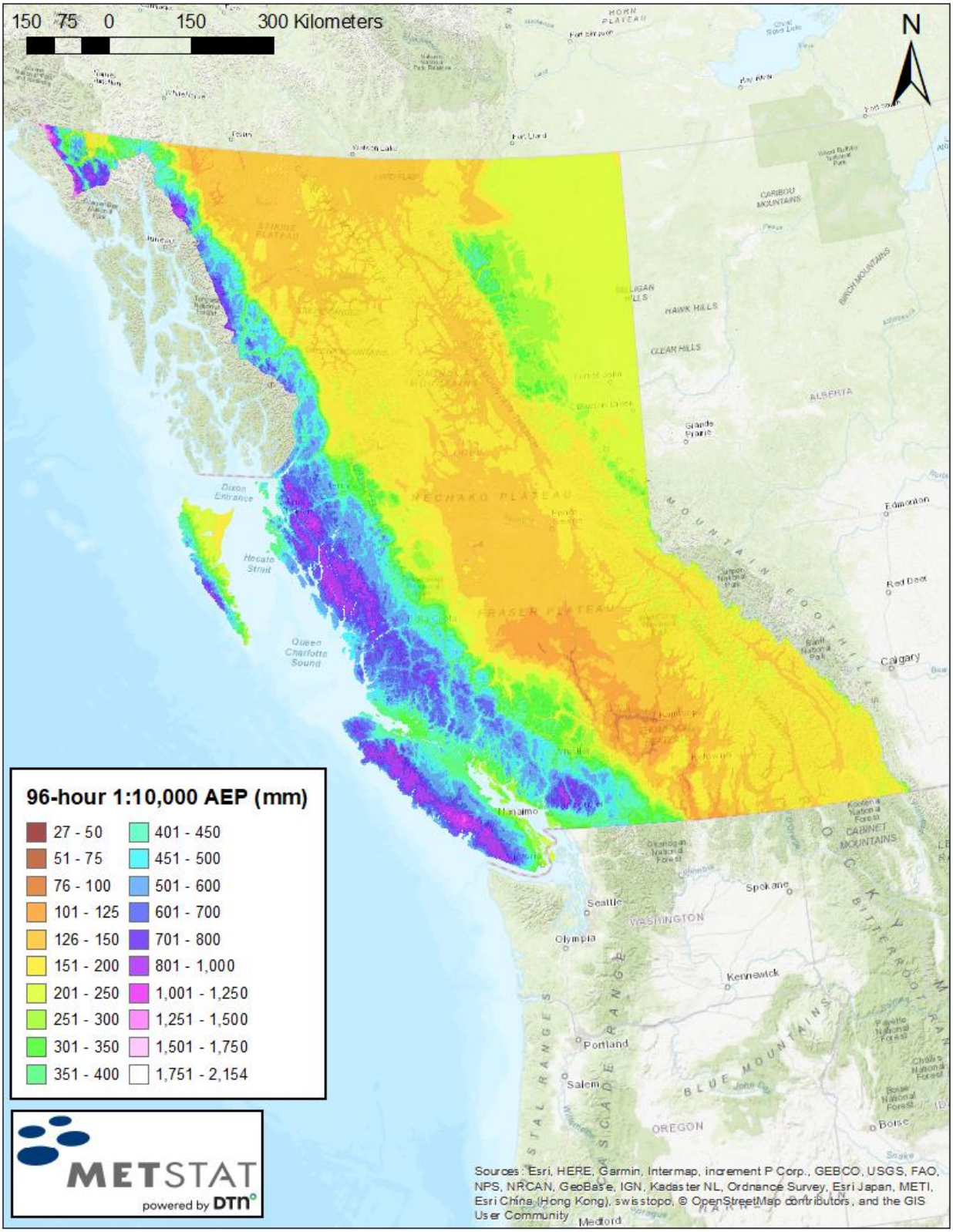

Figure 69: Map of precipitation (mm) for 96-hour 1:10,000 AEP.

APPENDIX H: Comparisons between MetPortal Point Precipitation Magnitudes with IDF and Rain30 Precipitation Magnitudes

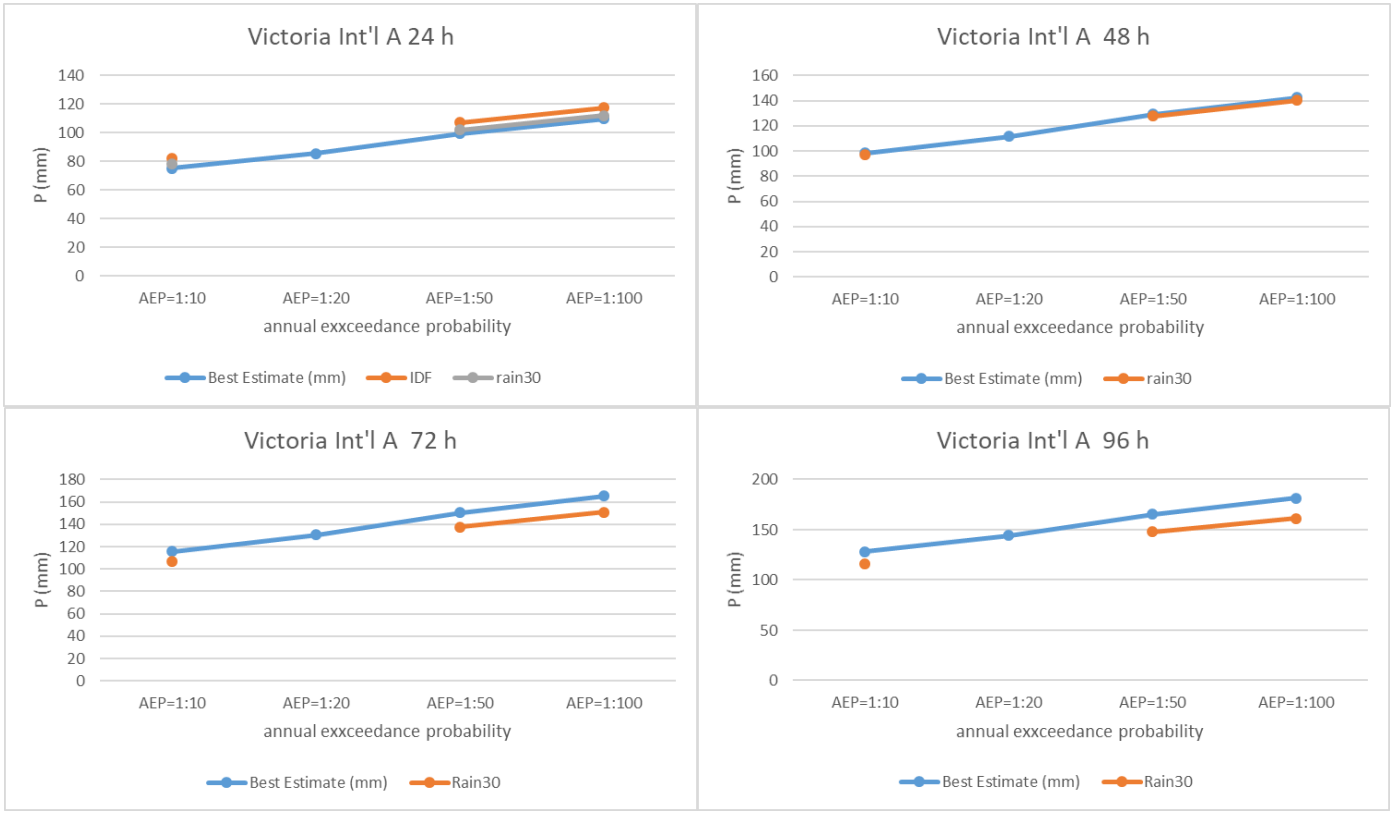

Figure 70: Comparison of point precipitation magnitudes for 1:10, 1:50, and 1:100 AEPs at the four durations of interest at Victoria International Airport (48.645°N, 123.429°W).

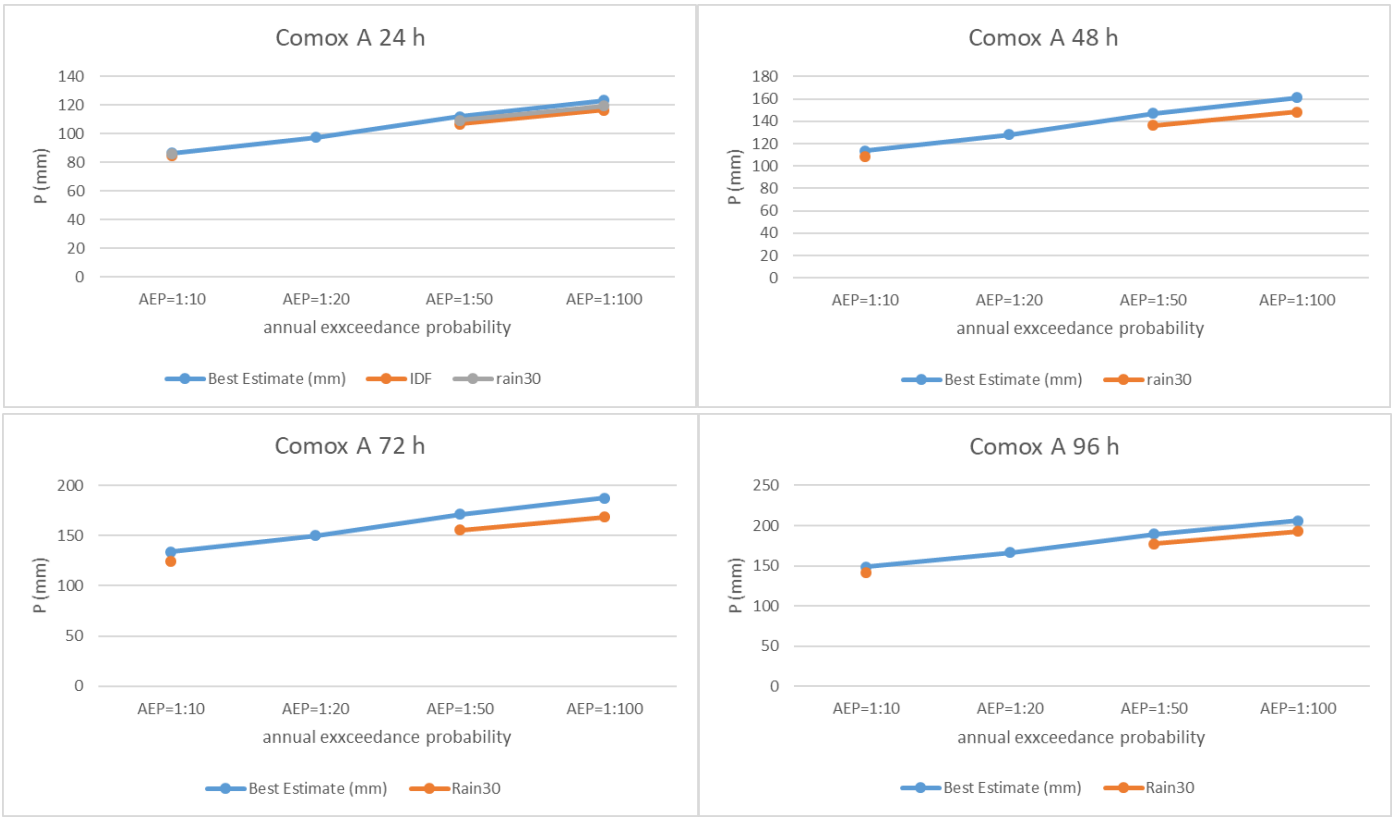

Figure 71: Comparison of point precipitation magnitudes for 1:10, 1:50, and 1:100 AEPs at the four durations of interest at Comox (49.711°N, 124.896°W).

Figure 72: Comparison of point precipitation magnitudes for 1:10, 1:50, and 1:100 AEPs at the four durations of interest at Tofino (49.152°N, 125.907°W).

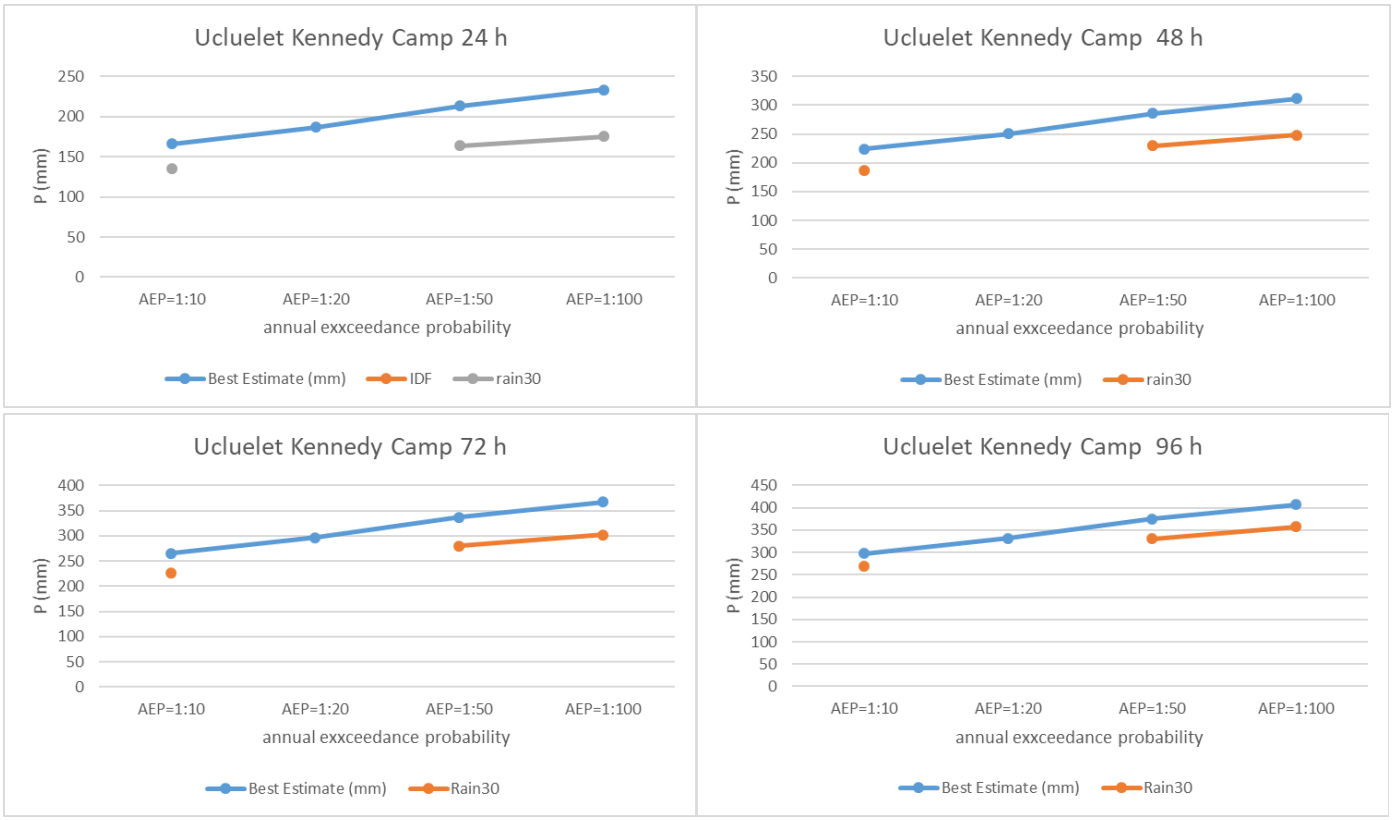

Figure 73: Comparison of point precipitation magnitudes for 1:10, 1:50, and 1:100 AEPs at the four durations of interest at Ucluelet Kennedy Camp (48.937°N, 125.54°W).

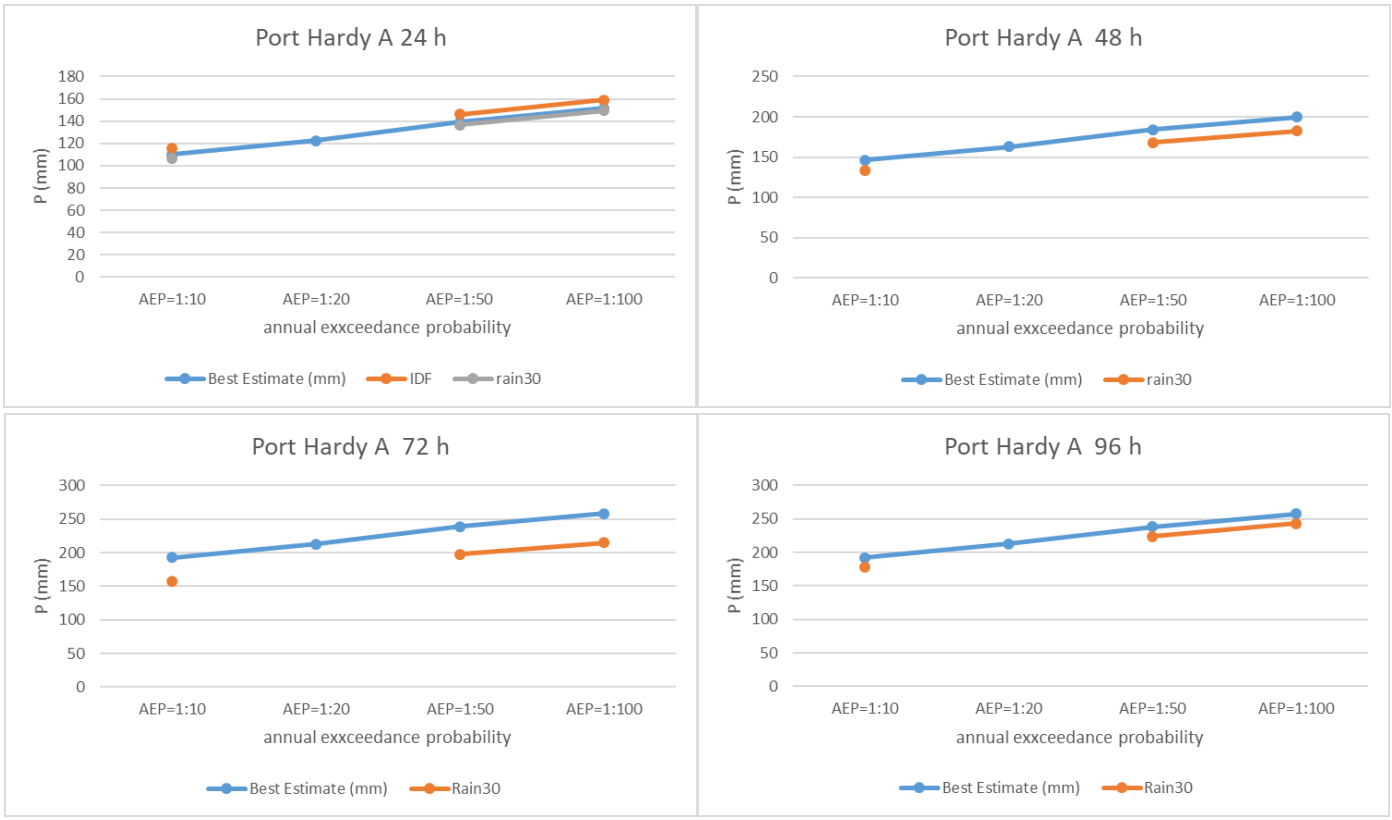

Figure 74: Comparison of point precipitation magnitudes for 1:10, 1:50, and 1:100 AEPs at the four durations of interest at Port Hardy (50.683°N, 127.374°W).

Figure 75: Comparison of point precipitation magnitudes for 1:10, 1:50, and 1:100 AEPs at the four durations of interest at Langara (54.246°N, 133.049°W).

Figure 76: Comparison of point precipitation magnitudes for 1:10, 1:50, and 1:100 AEPs at the four durations of interest at Kitamat Townsite (50.057°N, 128.631°W).

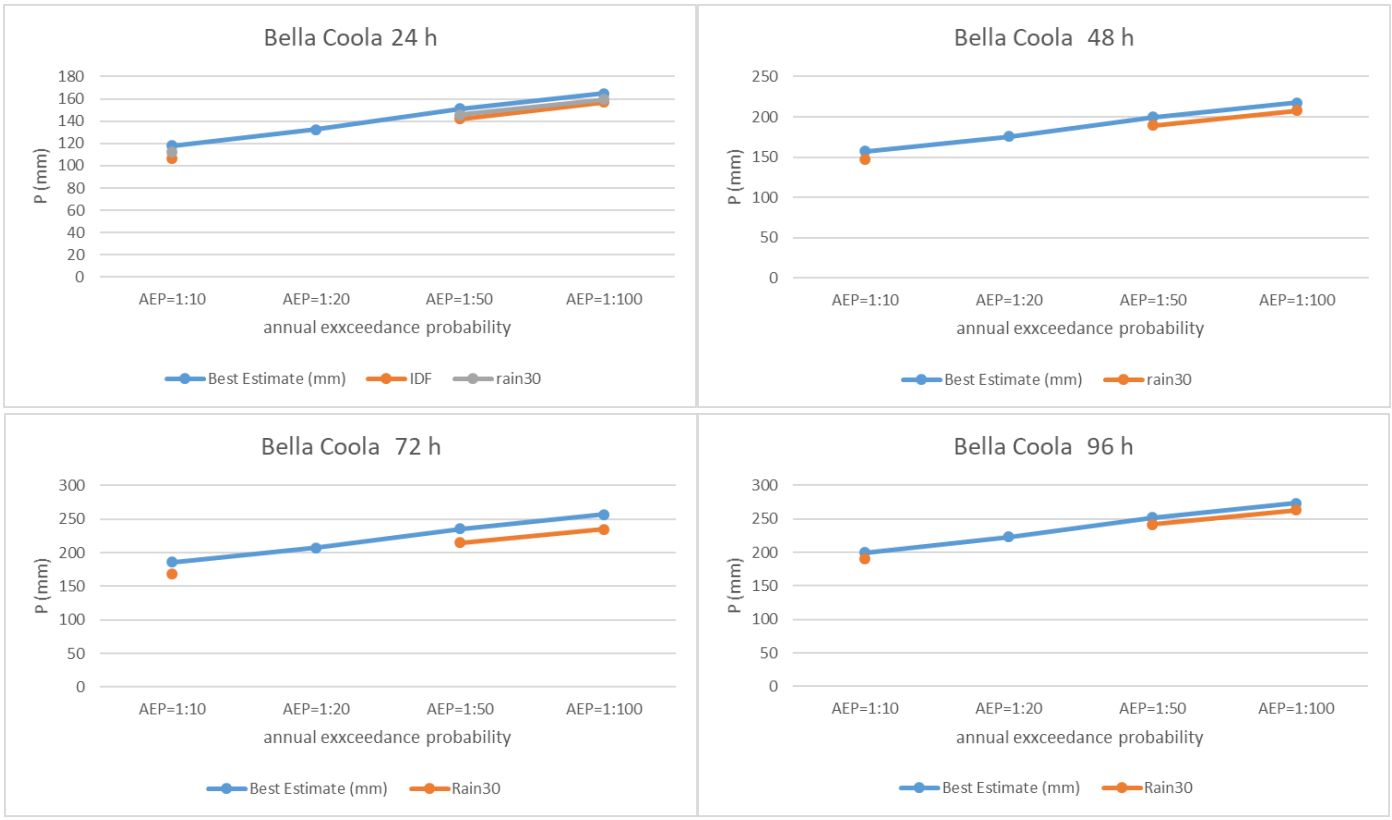

Figure 77: Comparison of point precipitation magnitudes for 1:10, 1:50, and 1:100 AEPs at the four durations of interest at Bella Coola (52.366°N, 126.692°W).

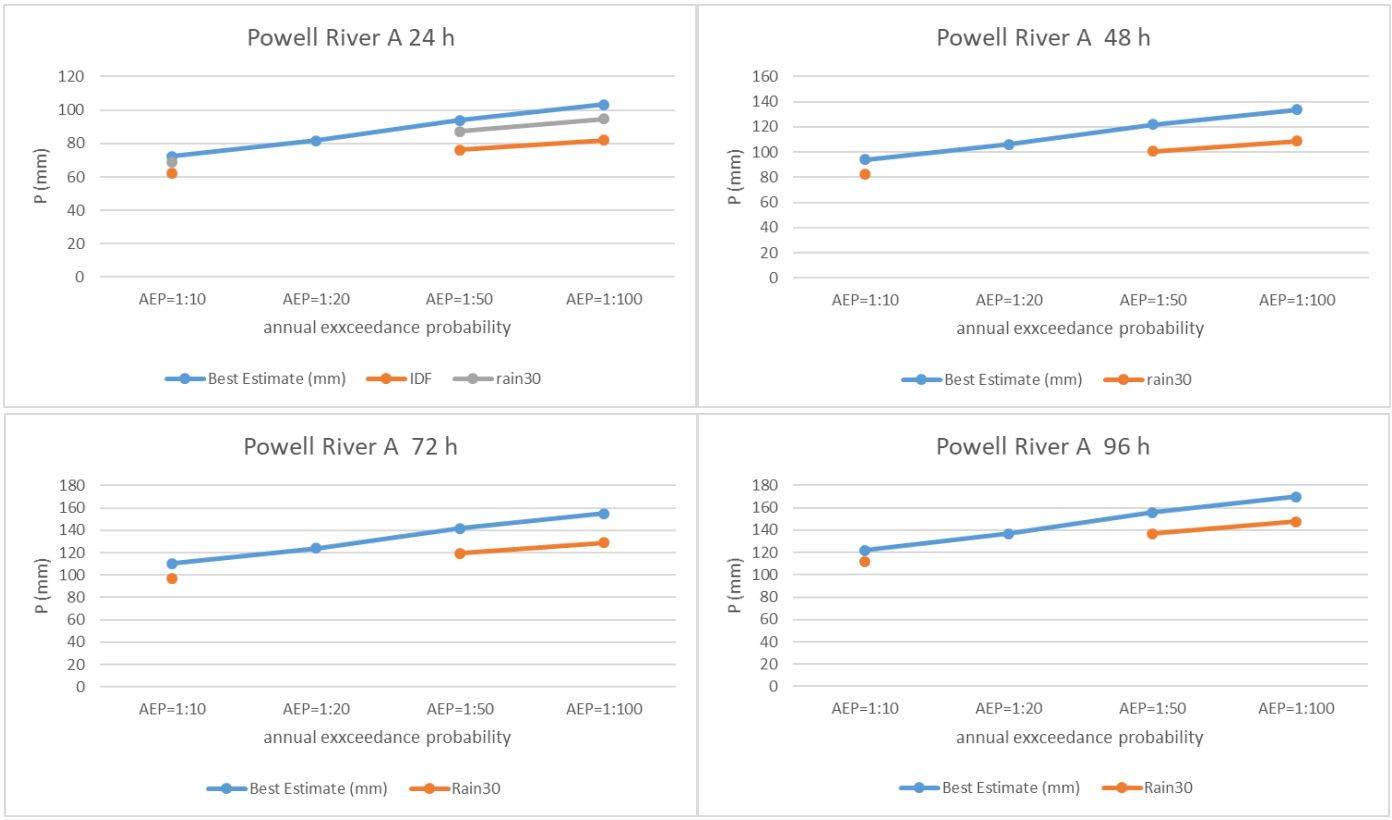

Figure 78: Comparison of point precipitation magnitudes for 1:10, 1:50, and 1:100 AEPs at the four durations of interest at Powell River (49.835°N, 124.501°W).

Figure 79: Comparison of point precipitation magnitudes for 1:10, 1:50, and 1:100 AEPs at the four durations of interest at Stewart (55.936°N, 129.982°W).

Figure 80: Comparison of point precipitation magnitudes for 1:10, 1:50, and 1:100 AEPs at the four durations of interest at Terrace (54.466°N, 128.579°W).

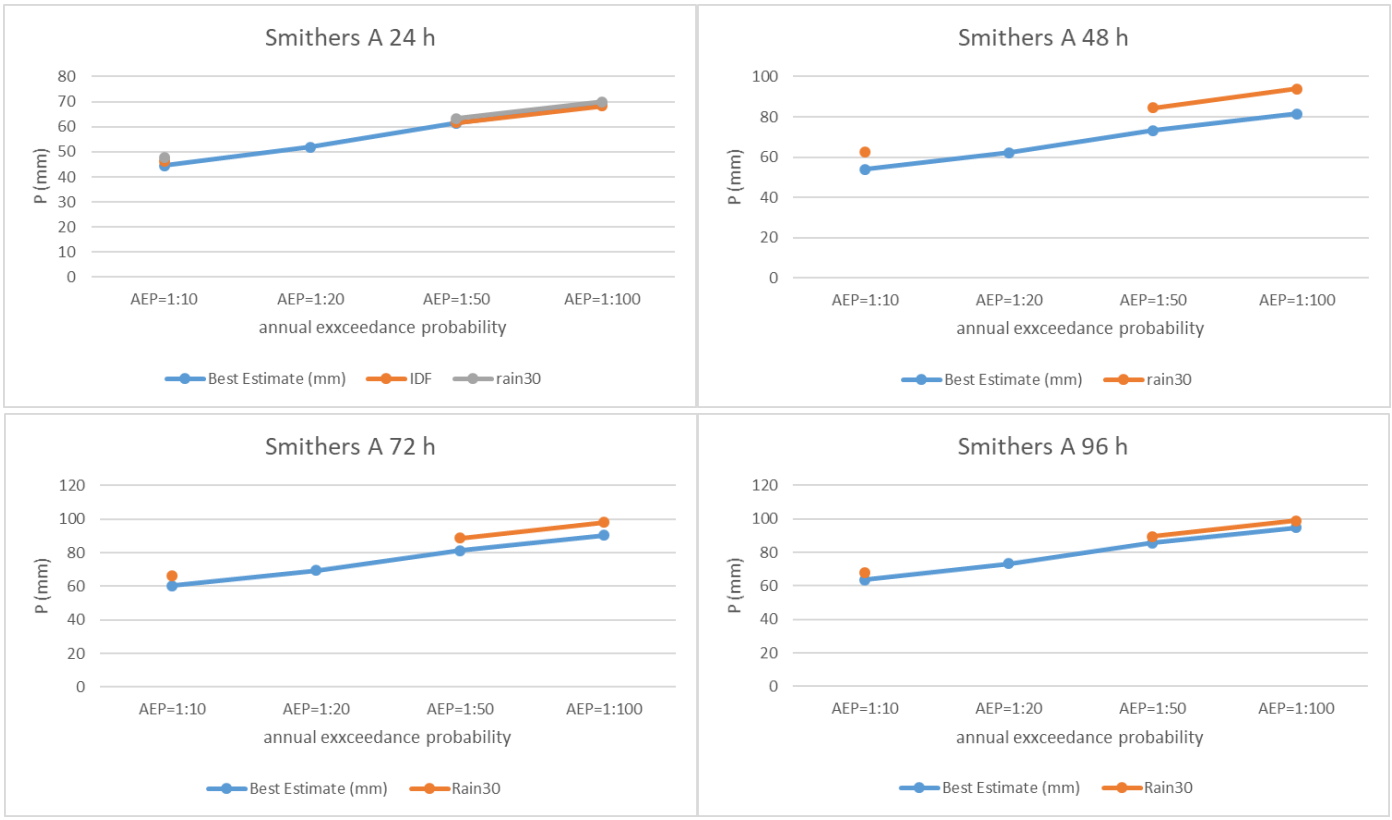

Figure 81: Comparison of point precipitation magnitudes for 1:10, 1:50, and 1:100 AEPs at the four durations of interest at Smithers (54.823°N, 127.184°W).

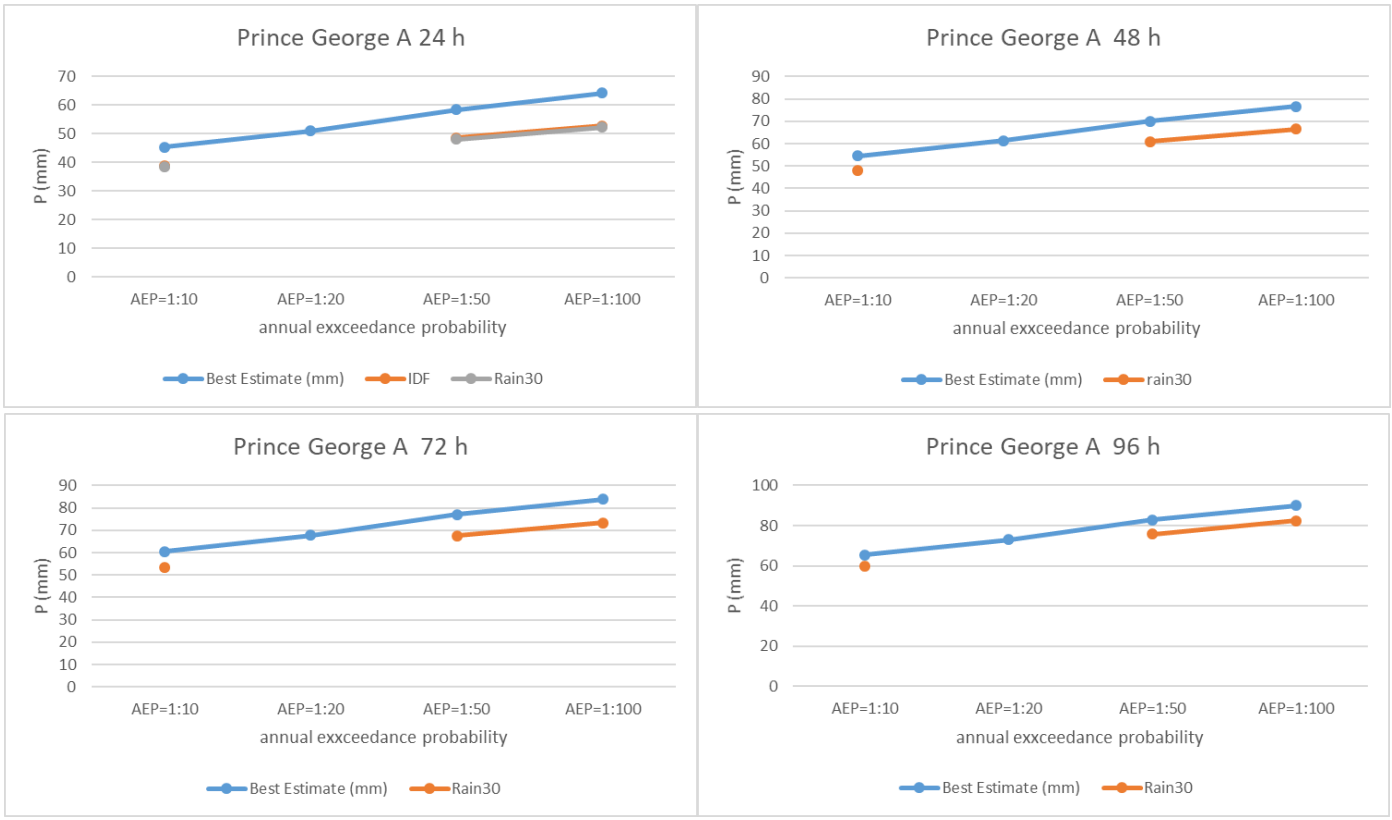

Figure 82: Comparison of point precipitation magnitudes for 1:10, 1:50, and 1:100 AEPs at the four durations of interest at Prince George (53.885°N, 122.678°W).

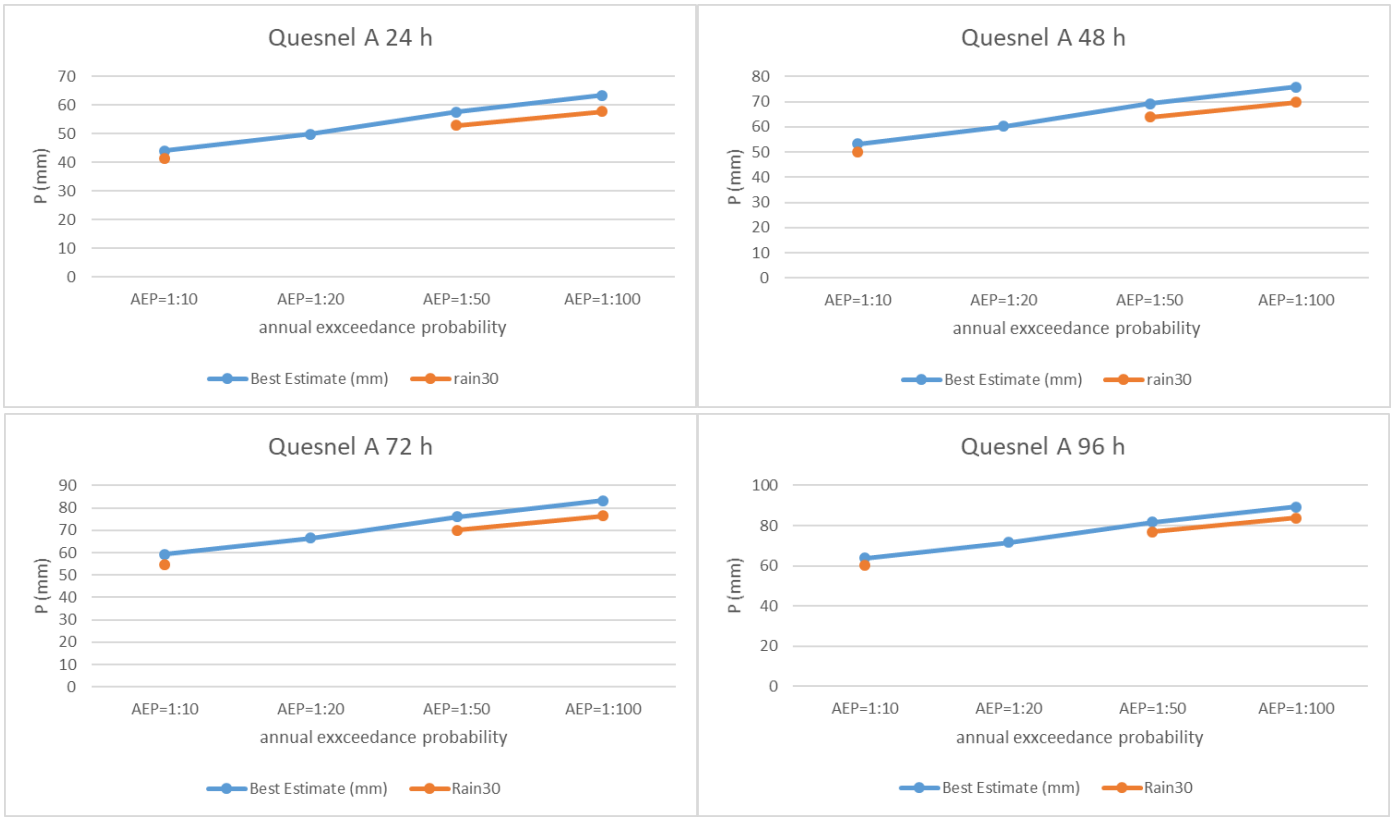

Figure 83: Comparison of point precipitation magnitudes for 1:10, 1:50, and 1:100 AEPs at the four durations of interest at Quesnel (53.025°N, 122.507°W).

Figure 84: Comparison of point precipitation magnitudes for 1:10, 1:50, and 1:100 AEPs at the four durations of interest at Williams Lake (52.186°N, 122.062°W).

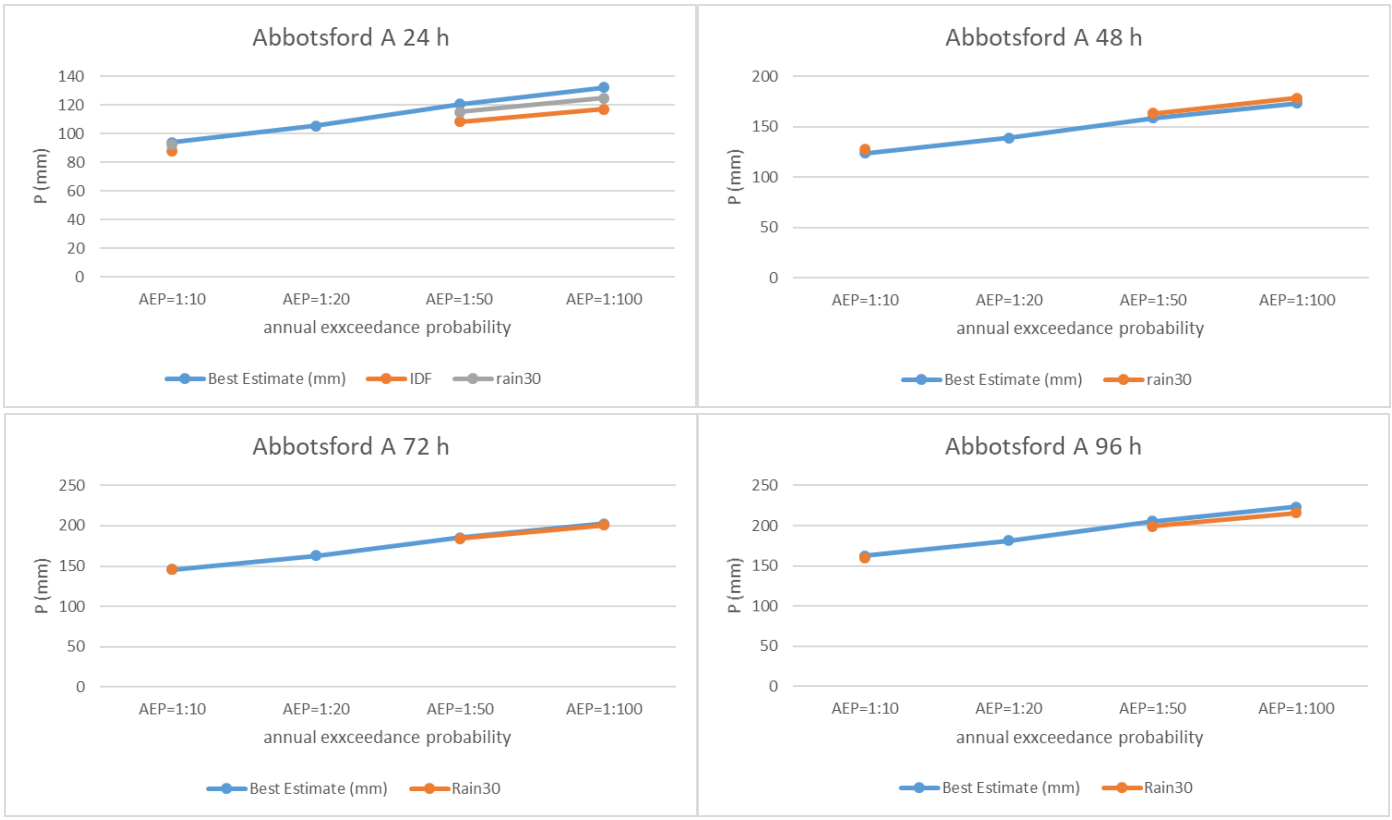

Figure 85: Comparison of point precipitation magnitudes for 1:10, 1:50, and 1:100 AEPs at the four durations of interest at Abbotsford (49.025°N, 122.372°W).

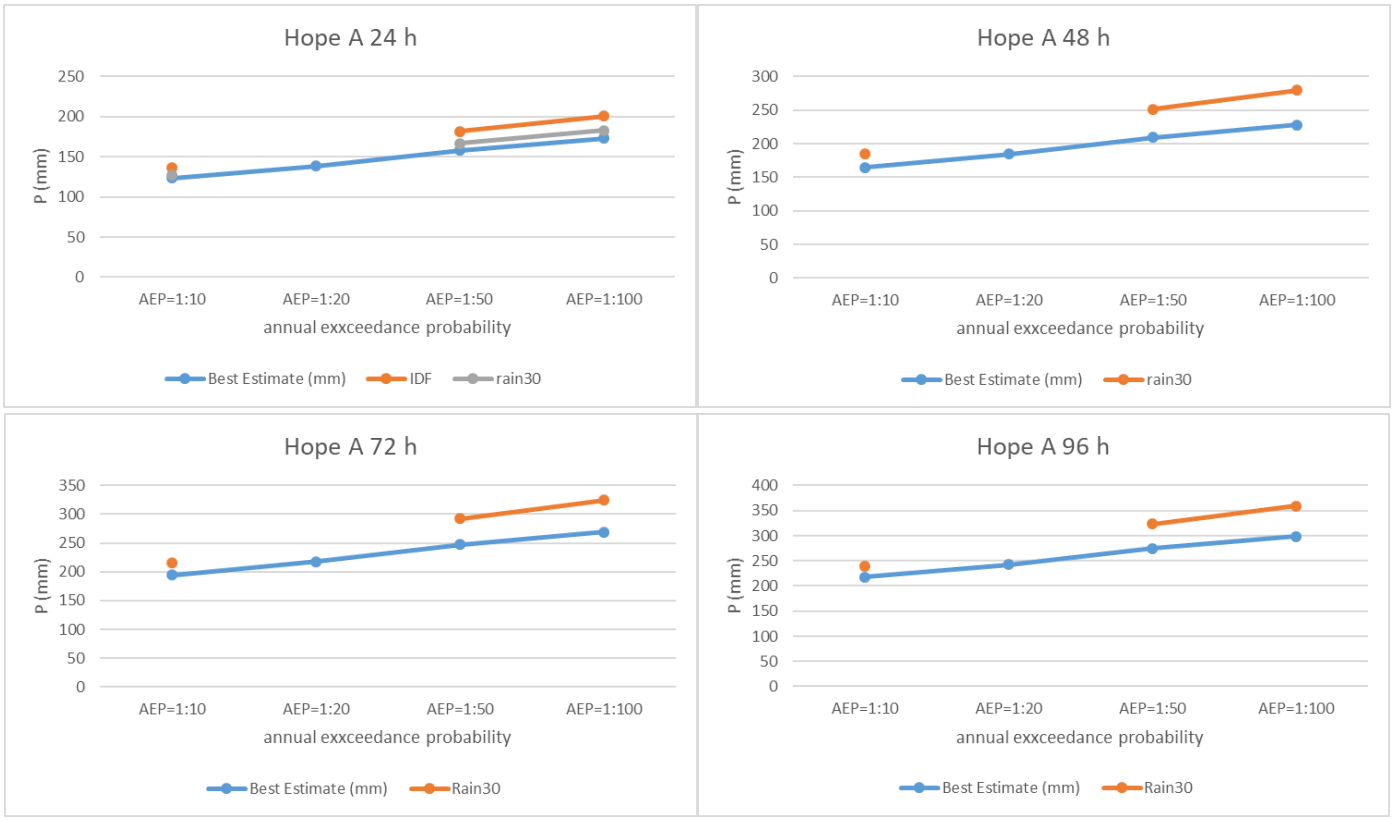

Figure 86: Comparison of point precipitation magnitudes for 1:10, 1:50, and 1:100 AEPs at the four durations of interest at Hope (49.369°N, 121.497°W).

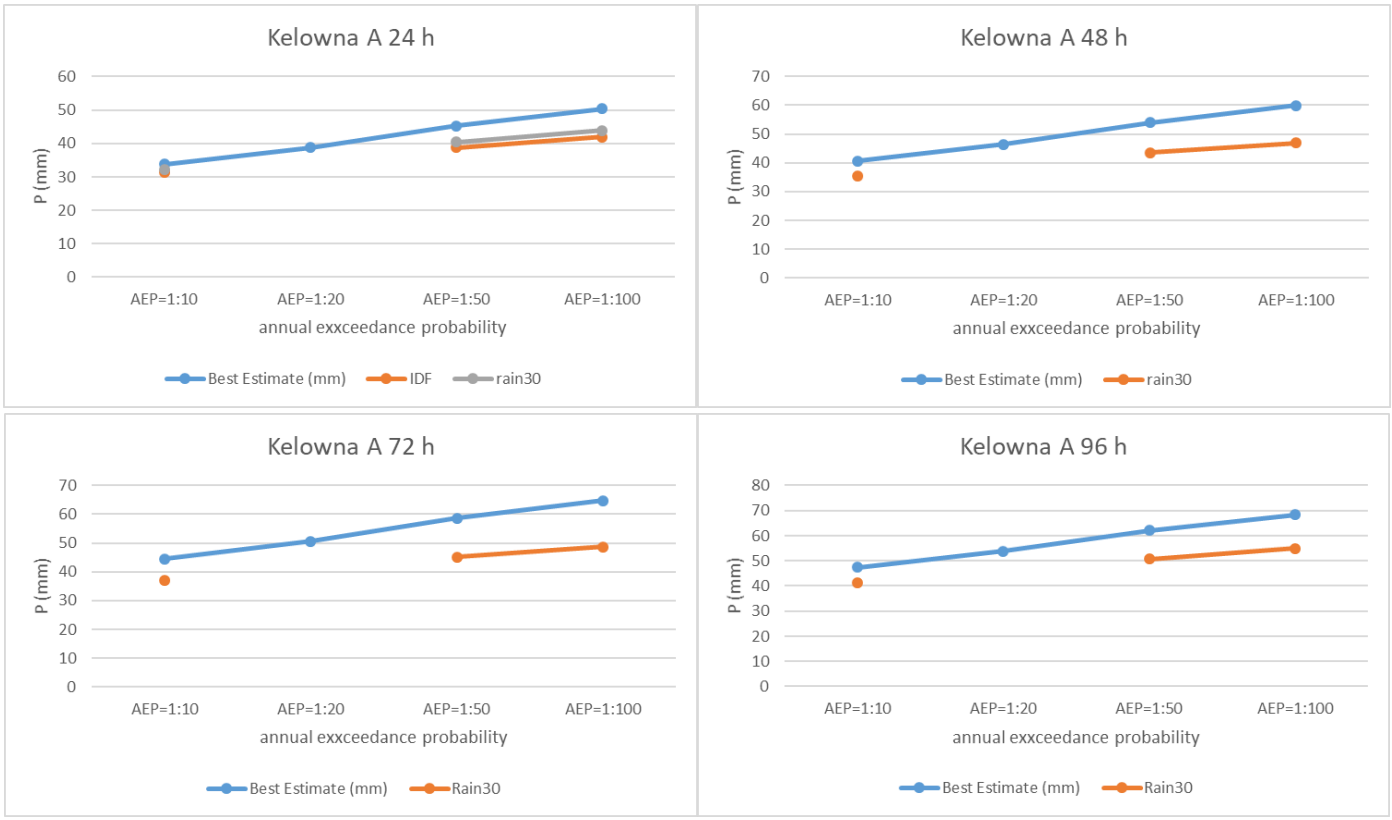

Figure 87: Comparison of point precipitation magnitudes for 1:10, 1:50, and 1:100 AEPs at the four durations of interest at Kelowna (49.951°N, 119.378°W).

Figure 88: Comparison of point precipitation magnitudes for 1:10, 1:50, and 1:100 AEPs at the four durations of interest at Penticton (49.460°N, 119.603°W).

Figure 89: Comparison of point precipitation magnitudes for 1:10, 1:50, and 1:100 AEPs at the four durations of interest at Princeton (49.468°N, 120.514°W).

Figure 90: Comparison of point precipitation magnitudes for 1:10, 1:50, and 1:100 AEPs at the four durations of interest at Castlegar (49.297°N, 117.634°W).

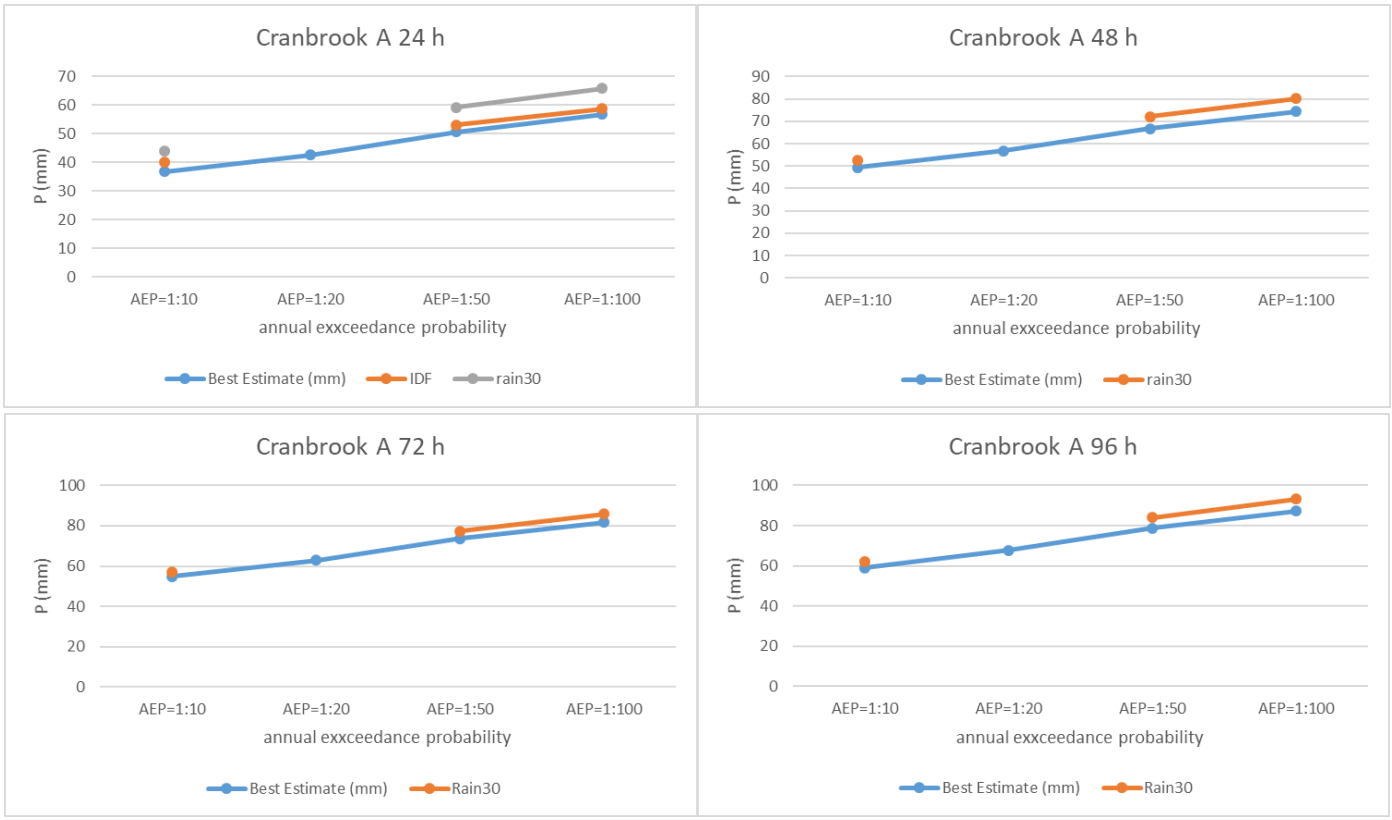

Figure 91: Comparison of point precipitation magnitudes for 1:10, 1:50, and 1:100 AEPs at the four durations of interest at Cranbrook (49.613°N, 115.784°W).

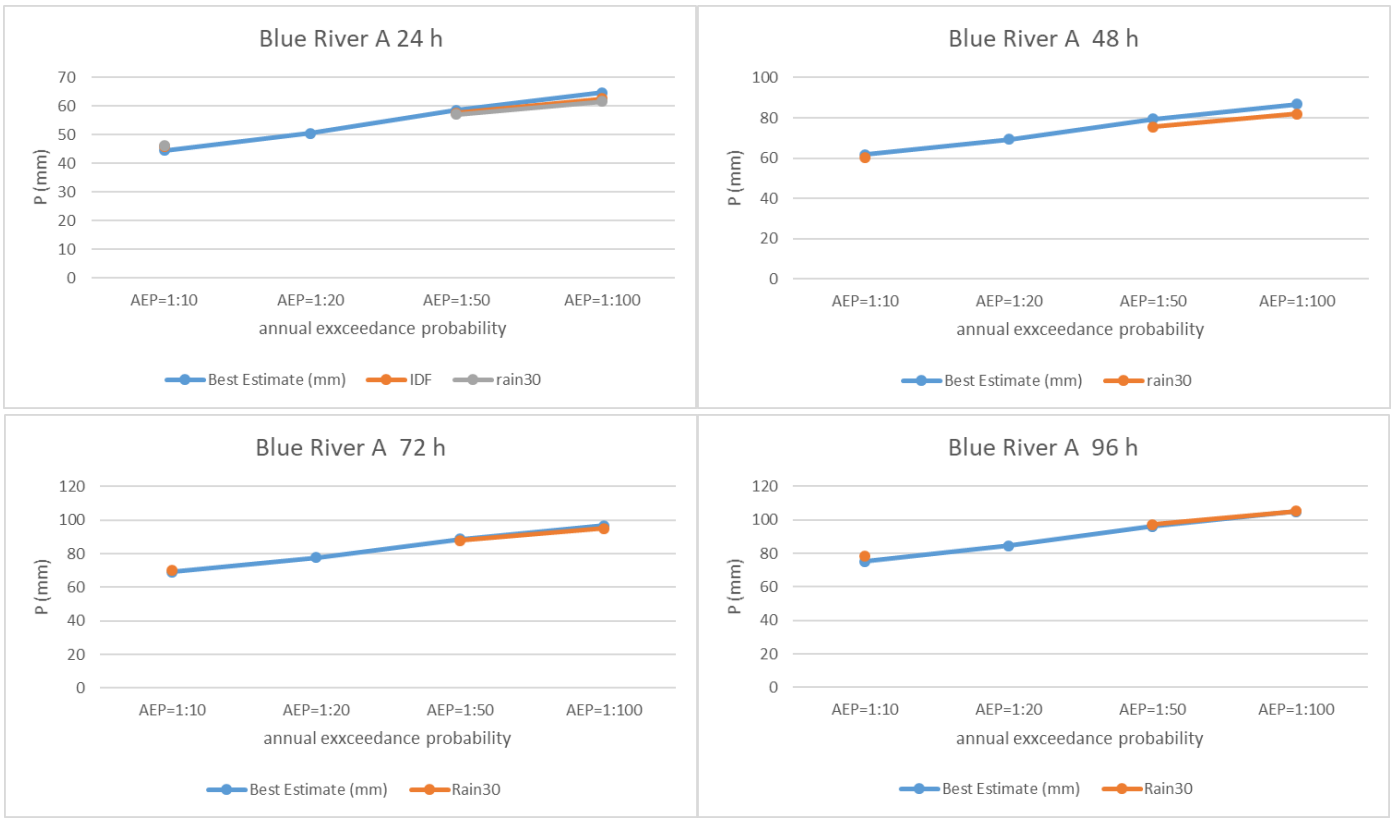

Figure 92: Comparison of point precipitation magnitudes for 1:10, 1:50, and 1:100 AEPs at the four durations of interest at Blue River (52.126°N, 119.292°W).

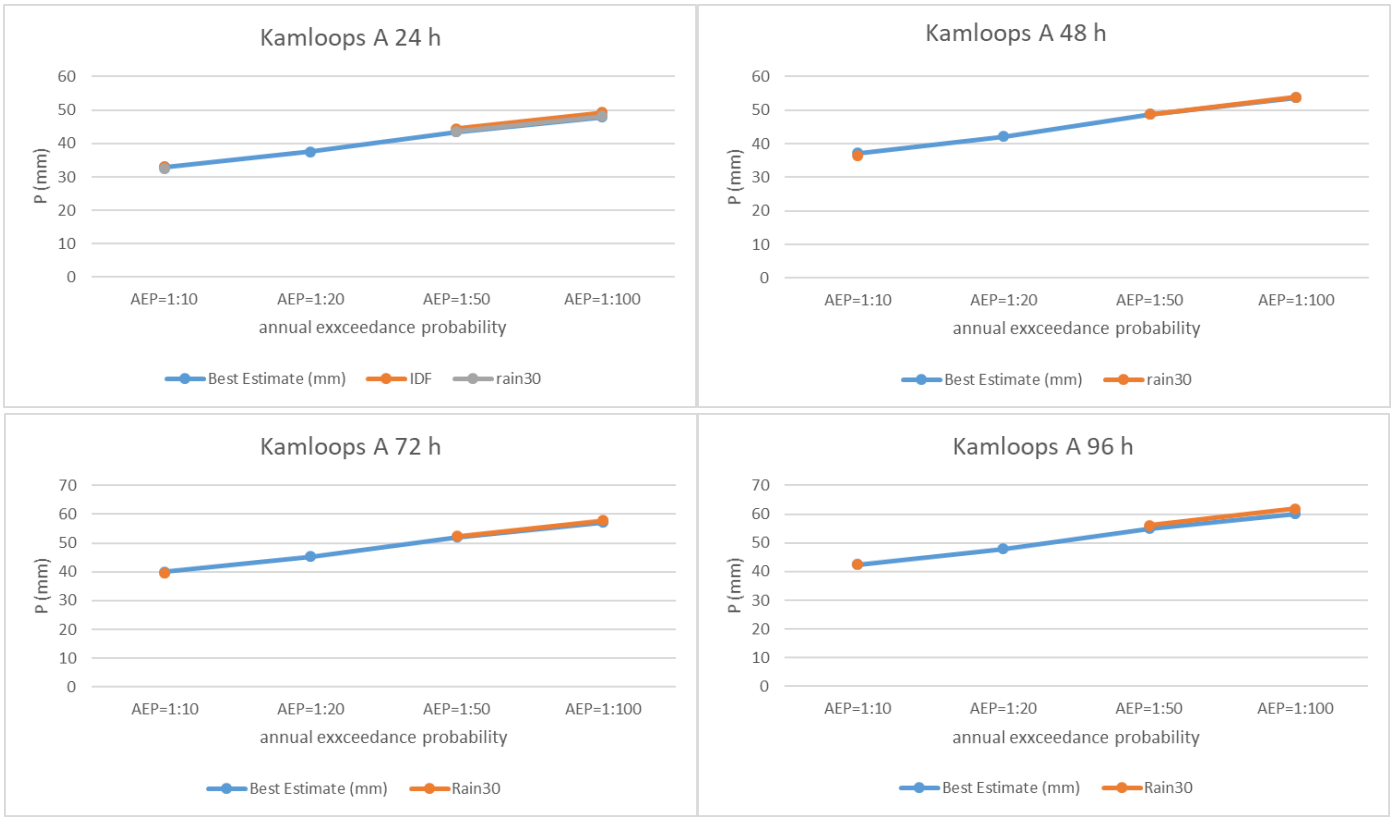

Figure 93: Comparison of point precipitation magnitudes for 1:10, 1:50, and 1:100 AEPs at the four durations of interest at Kamloops (50.703°N, 120.441°W).

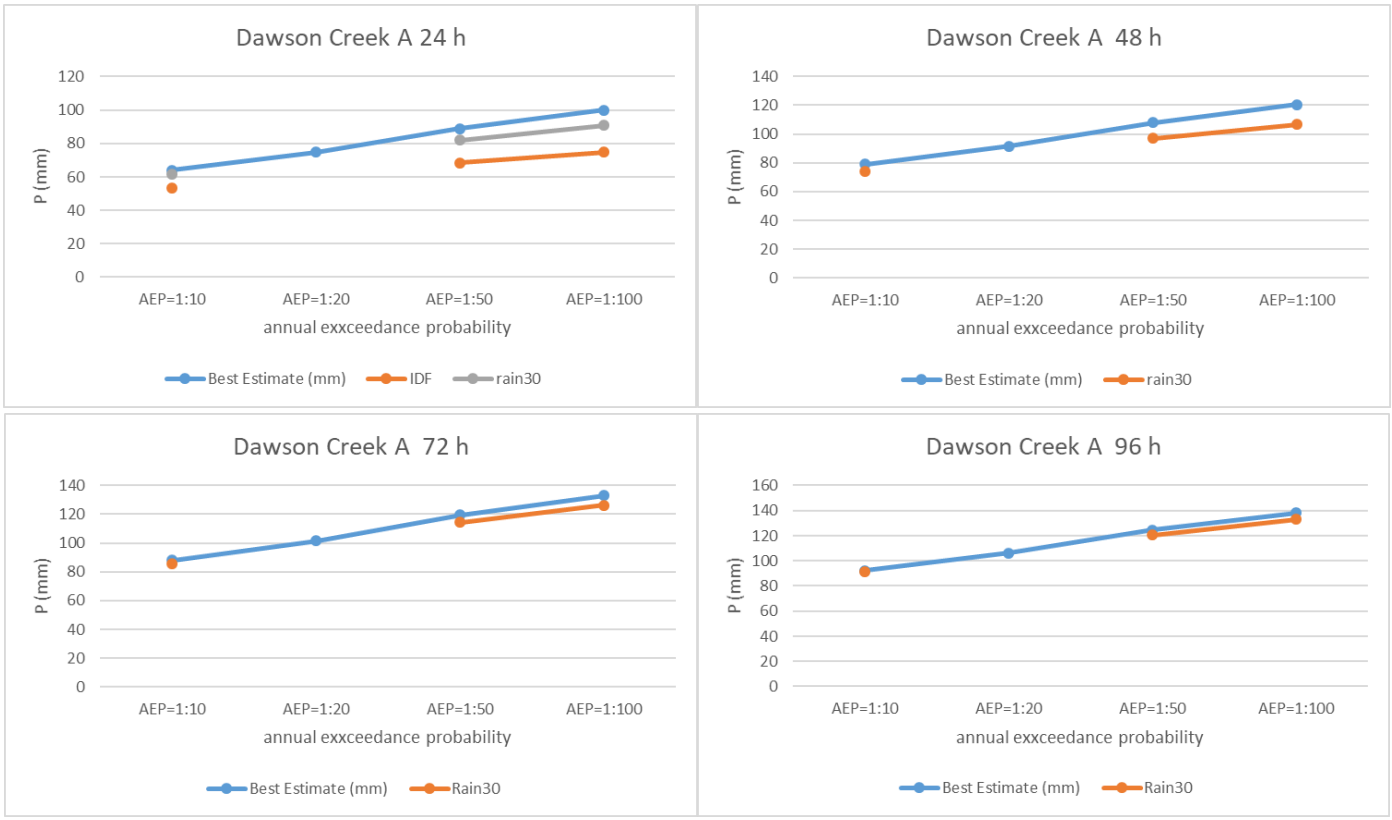

Figure 94: Comparison of point precipitation magnitudes for 1:10, 1:50, and 1:100 AEPs at the four durations of interest at Dawson Creek (55.742°N, 120.185°W).

Figure 95: Comparison of point precipitation magnitudes for 1:10, 1:50, and 1:100 AEPs at the four durations of interest at Fort St. John (56.244°N, 120.736°W).

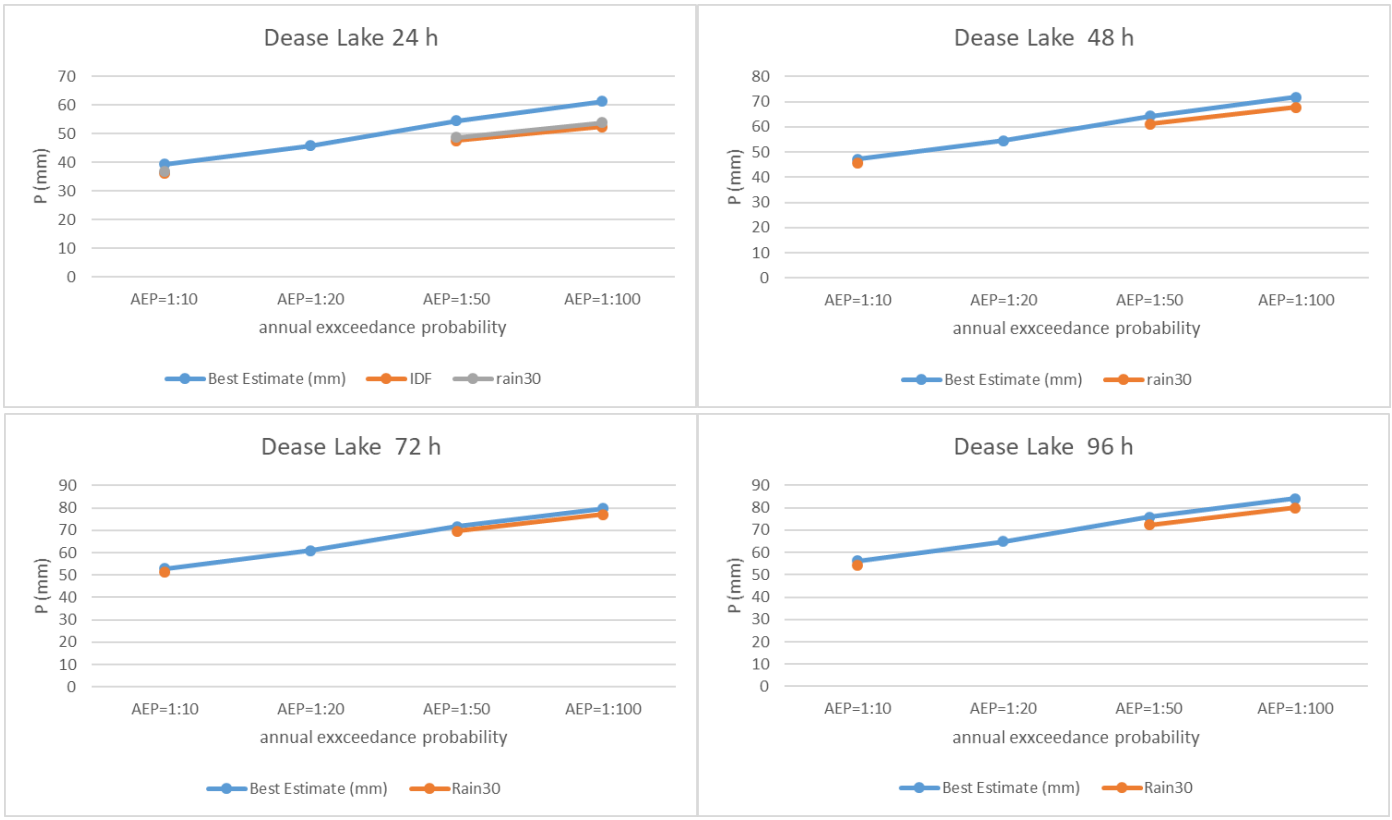

Figure 96: Comparison of point precipitation magnitudes for 1:10, 1:50, and 1:100 AEPs at the four durations of interest at Dease Lake (58.422°N, 130.028°W).

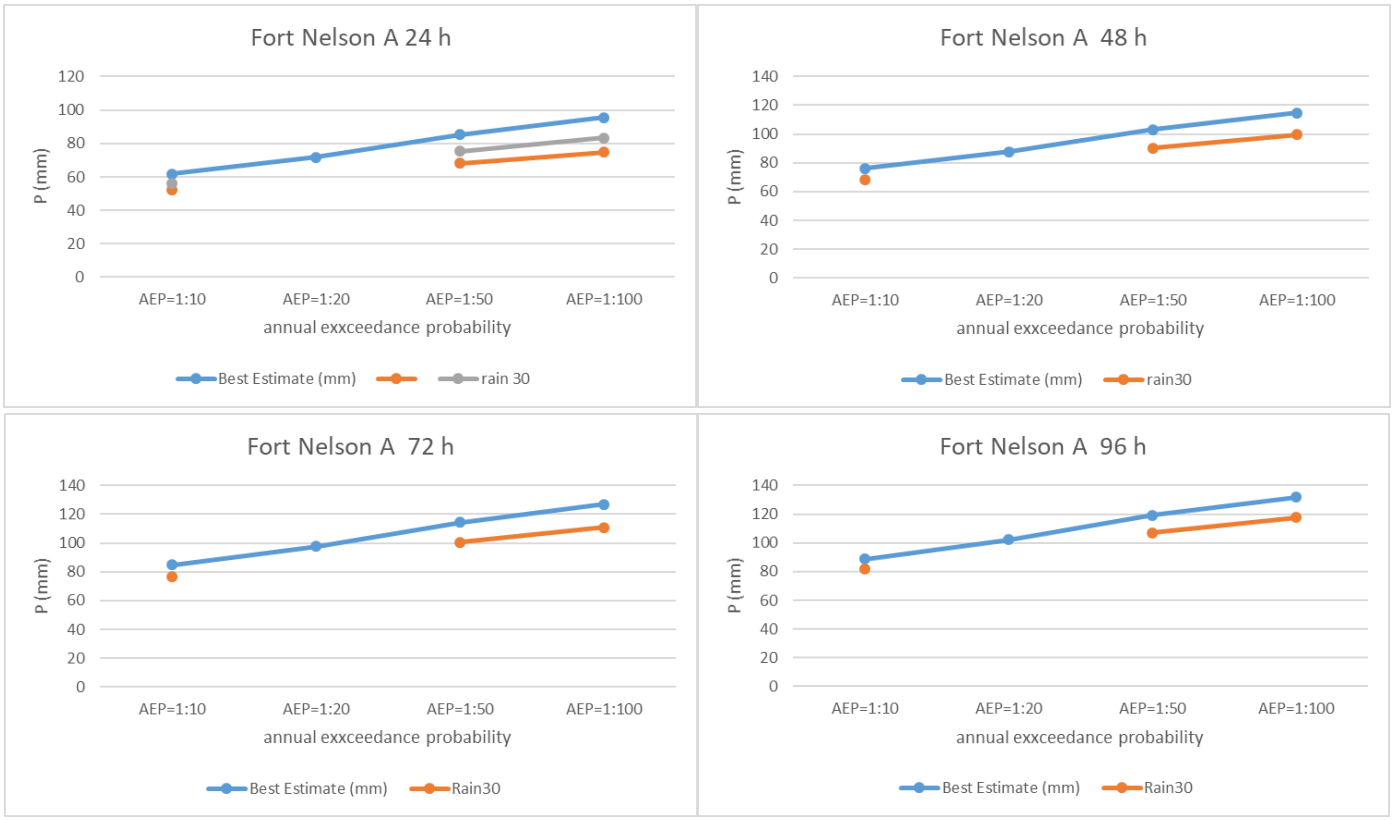

Figure 97: Comparison of point precipitation magnitudes for 1:10, 1:50, and 1:100 AEPs at the four durations of interest at Fort Nelson (58.838°N, 122.584°W).

Figure 98: Comparison of point precipitation magnitudes for 1:10, 1:50, and 1:100 AEPs at the four durations of interest at Revelstoke (50.962°N, 118.183°W).

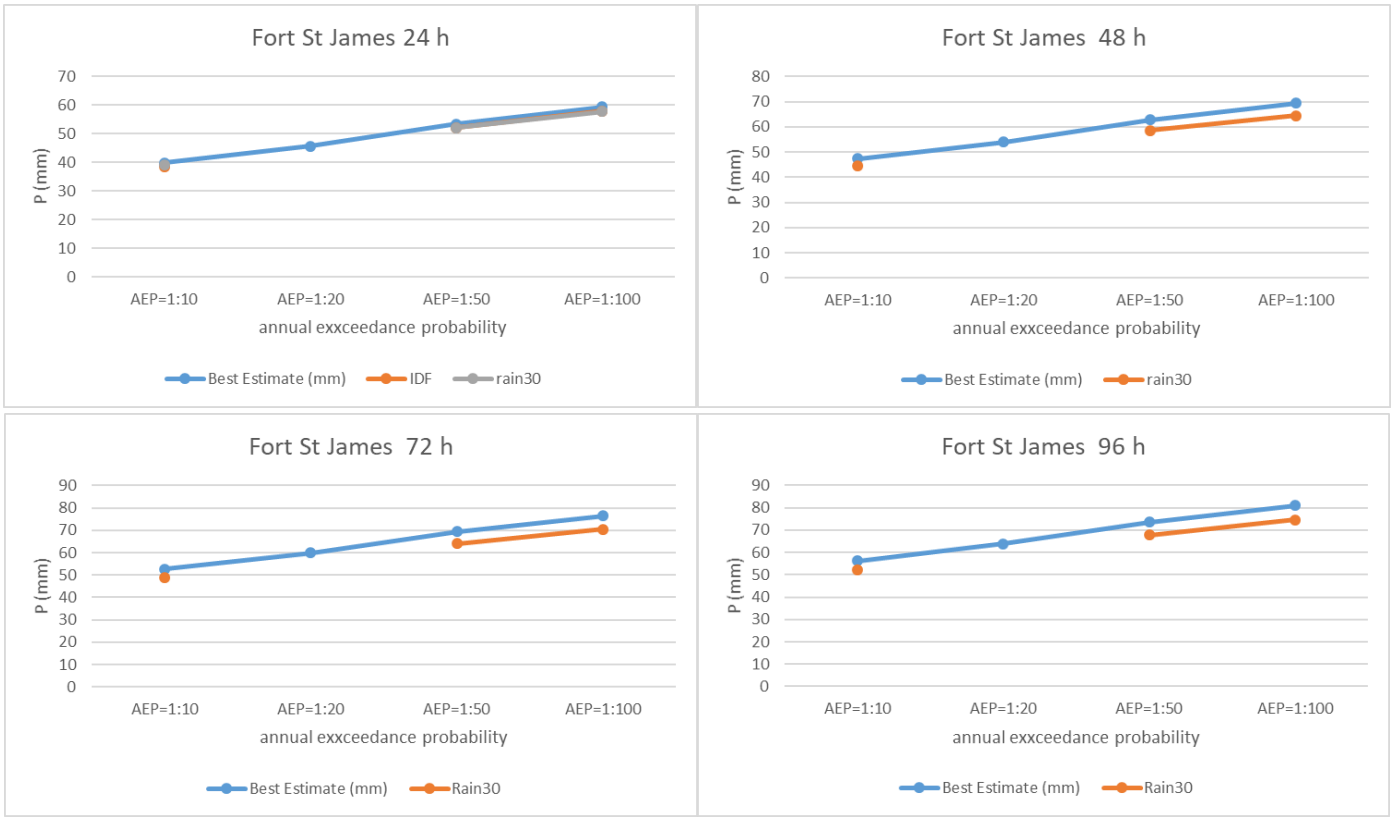

Figure 99: Comparison of point precipitation magnitudes for 1:10, 1:50, and 1:100 AEPs at the four durations of interest at Fort St. James (54.440°N, 124.254°W).

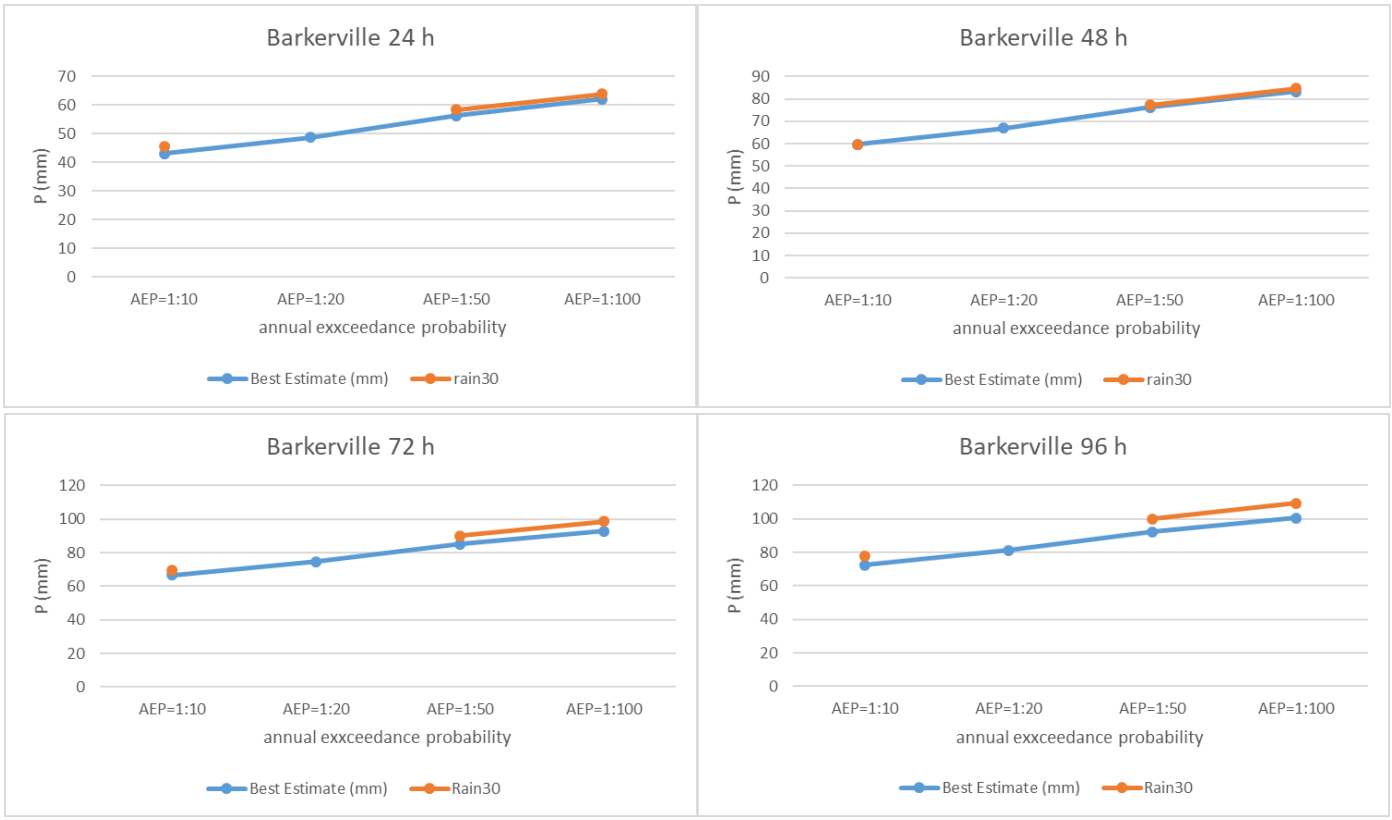

Figure 100: Comparison of point precipitation magnitudes for 1:10, 1:50, and 1:100 AEPs at the four durations of interest at Bakerville (53.067°N, 121.516°W).

Figure 101: Comparison of point precipitation magnitudes for 1:10, 1:50, and 1:100 AEPs at the four durations of interest at Fernie (49.505°N, 115.069°W).

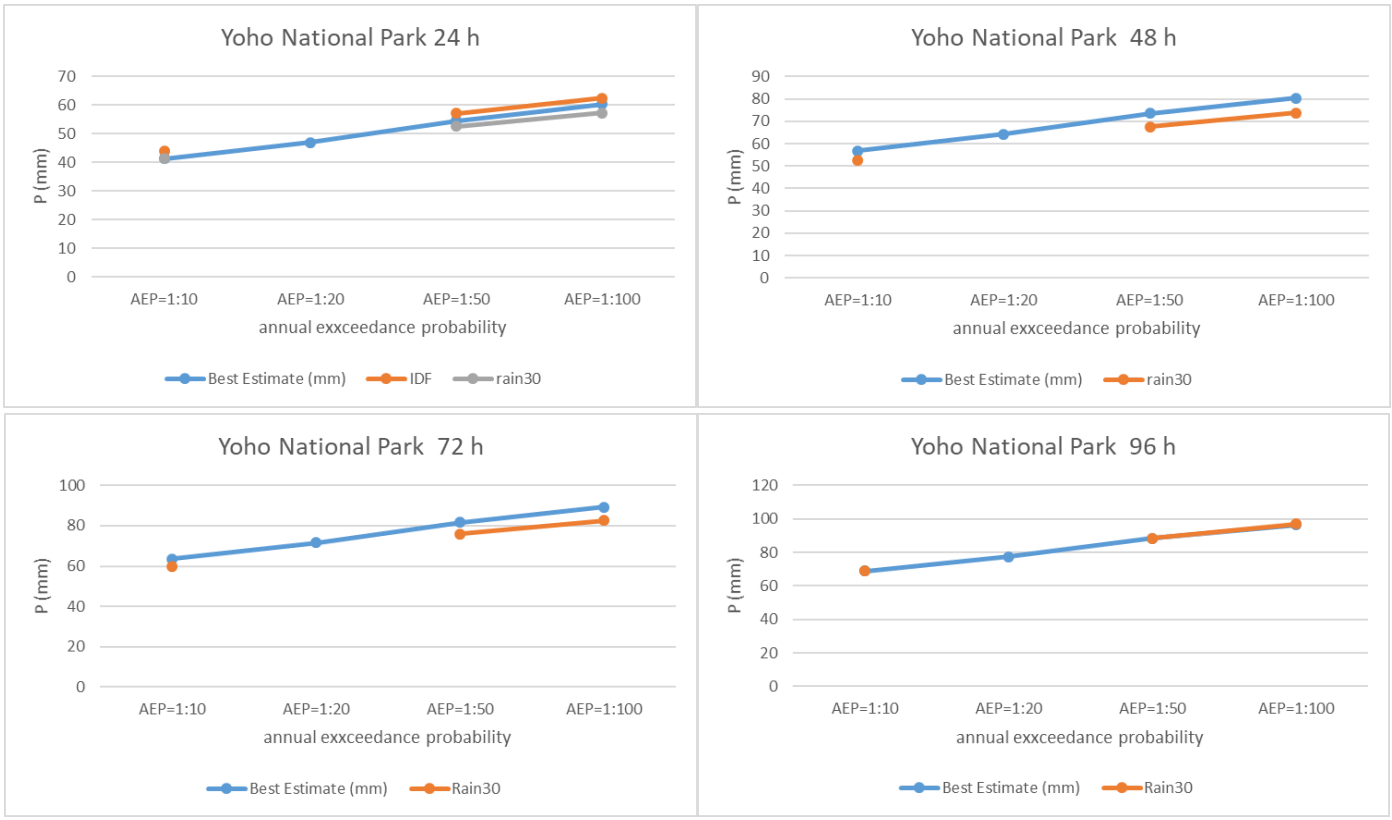

Figure 102: Comparison of point precipitation magnitudes for 1:10, 1:50, and 1:100 AEPs at the four durations of interest at Yoho National Park (51.361°N, 116.526°W).